

John F. Kennedy Space Center



**Research and Technology
2003 Annual Report**

Human Exploration and Development of Space



NASA-TM-2003-211190

Research and Technology 2003 Annual Report

John F. Kennedy Space Center

Foreword

When one visits the Kennedy Space Center (KSC) Home Page, the words “Launching the NASA Vision” immediately appear at the top of the screen. This phrase was never more true or applicable as the Agency works diligently to return to flight safely and implement the new vision for space exploration. The KSC team will play a major role in these Agency endeavors. KSC continues to emphasize programmatic excellence as we work toward becoming a truly great spaceport operations and technology Center. We remain committed to bringing our customers the greatest value in reaching their objectives by working toward a common set of priorities. Our technology development activities encompass the entire KSC team, consisting of Government and contractor personnel working in partnership with academic institutions and commercial industry. In 2002, KSC celebrated 40 years of pioneering the future. This year, NASA exceeded 1,000 days of permanent human habitation of the International Space Station. To continue our exploration of space and the development of the frontiers of the universe, we must be true to our vision, inspire the next generation of explorers, and partner with our customers and suppliers to make space travel safer and more accessible. This KSC Research and Technology 2003 Annual Report demonstrates some of these contributions to NASA’s mission.



Dr. Dave Bartine, KSC Chief Technologist, 321-867-7069, is responsible for publication of this report and is the point of contact for any desired information.

James W. Kennedy
Director
John F. Kennedy Space Center

CONTENTS

Command, Control, and Monitoring Technologies	1
<i>Command, Control, and Monitoring Technologies Roadmap</i>	<i>3</i>
<i>Multisensor Array Pressure Transducer</i>	<i>4</i>
<i>Color-Indicating Patch for Shuttle Auxiliary Power Unit Hydrazine Transfer Line</i>	<i>6</i>
<i>A Study of Hail Monitoring Strategies for Shuttle Launch Safety.....</i>	<i>8</i>
<i>Mass Sensor for Cryogenic Fluids.....</i>	<i>10</i>
<i>Shuttle Tile Moisture Sensor</i>	<i>12</i>
<i>New Gas Polarographic Hydrogen Sensor</i>	<i>14</i>
<i>Improved Fiber-Optic Pressure Block Connector</i>	<i>16</i>
<i>Common Application Framework (CAF)</i>	<i>18</i>
<i>Automated Test Tool</i>	<i>20</i>
<i>Digital Image Lens Distortion Correction Algorithm.....</i>	<i>22</i>
<i>Real-Time Detection and Tracking of Multiple Moving Objects in Complex Image Background.....</i>	<i>24</i>
<i>A Digital Signal Processing (DSP) Filter Tuned To Detect Diurnal Signals.....</i>	<i>26</i>
<i>Image Edge Extraction via Fuzzy Reasoning.....</i>	<i>28</i>
<i>Noniterative Optimal Image Binarization via Fuzzy Reasoning.....</i>	<i>30</i>
<i>Converting Analog Test Data to Audio Wave Files</i>	<i>32</i>
<i>Small Mass Spectrometer System Onboard High-Altitude Research Aircraft WB-57.....</i>	<i>34</i>
<i>Advanced Data Acquisition System (ADAS)</i>	<i>36</i>
<i>Visual Anomaly Detection System Prototype</i>	<i>38</i>
<i>Wireless Inclinometer</i>	<i>40</i>
<i>Enhanced Wireless Vacuum-Jacketed Line Sensor Network</i>	<i>42</i>
<i>A Field Prototype System for Vacuum-Drying Shuttle Tiles.....</i>	<i>44</i>
<i>Shuttle Tire Pressure Monitor Calibration Station.....</i>	<i>46</i>
<i>Vacuum-Jacketed (VJ) Thermocouple Calibration Station</i>	<i>48</i>
<i>Fast, Time-of-Flight Mass Spectrometer for Rugged Aerospace Applications.....</i>	<i>50</i>
<i>Inspection Tool for the Reaction Control System (RCS) Nozzles.....</i>	<i>52</i>
Fluid System Technologies	55
<i>Fluid System Technologies Roadmap.....</i>	<i>57</i>
<i>Modeling the RL10 Rocket Engine With Densified Liquid Hydrogen and Oxygen Propellants.....</i>	<i>58</i>
<i>On the Scaling Laws for Jet Noise in Subsonic and Supersonic Flow</i>	<i>60</i>
<i>Advanced Umbilical Development Automation Testbed.....</i>	<i>62</i>
<i>Advanced Umbilical Location System (AULS).....</i>	<i>64</i>
<i>Advanced Cold-Mate Cryogenic Fluid Quick Disconnect (QD)</i>	<i>66</i>
<i>Collapsible Cryogenic Vacuum-Jacketed (CCVJ) Fluid Transfer Lines.....</i>	<i>68</i>
<i>Fiber-Optic Quick Disconnect (QD).....</i>	<i>70</i>
<i>Ice Suppression Technologies</i>	<i>72</i>
<i>Automated Latching Systems.....</i>	<i>74</i>
<i>Umbilical Ice Suppression and Mitigation System (ISMS) and Cleanliness Verification System (CVS)</i>	<i>76</i>

CONTENTS (continued)

<i>Testing of Space Shuttle Spray-On Foam Insulation Under Cryogenic Vacuum Conditions</i>	78
<i>Glass Microspheres for Cryogenic Insulation Applications</i>	80
<i>Standardized Testing of Experimental Thermal Insulation Materials for Low-Temperature Applications</i>	82
<i>Thermal Performance Testing of Cryogenic Piping Systems</i>	84
<i>Piping System Repair Using Cryogenic Freeze Plug Technology</i>	86
<i>Automated Thruster Bench Test (ATBT) System</i>	88
<i>Venturi Off-Set Technology Cryogenic Valve</i>	90
Range Technologies	93
<i>Range Technologies Roadmap</i>	95
<i>Space-Based Telemetry and Range Safety (STARS)</i>	96
<i>Iridium Flight Modem</i>	98
<i>Autonomous Flight Safety System (AFSS) – Phase II</i>	100
<i>Range Simulator</i>	102
<i>Range Information System Management</i>	104
<i>Accurate Location of Lightning Strikes</i>	106
<i>Transient Voltage Recorder</i>	108
<i>Passive Millimeter Wave Imaging</i>	110
Spaceport Structures and Materials	113
<i>Spaceport Structures and Materials Roadmap</i>	115
<i>Electronic Single-Particle Aerodynamic Relaxation Time Analyzer for Mars Robotic Missions</i>	116
<i>Paschen Breakdown in the Martian Atmosphere</i>	118
<i>Wheel Electrometer Technology</i>	120
<i>Development of a Physical Model of Insulator-Insulator Triboelectric Charging To Understand Surface Charging of Materials on Earth and on Planetary Surfaces</i>	122
<i>Comparison of Surface Resistivity and Triboelectric Charge Generation Characteristics of Materials</i>	124
<i>Method for Measuring Charge Buildup on Materials</i>	126
<i>Electrostatics Testing of Materials at Low Pressures</i>	128
<i>Spacecraft Charge Monitor</i>	130
<i>Antistatic, Field-Emitting, Nanoparticle Coatings</i>	132
<i>Corrosion-Resistant Tubing for Space Shuttle Launch Sites</i>	134
<i>Electrochemical Characterization of Tubing Alloys in Simulated Space Shuttle Launch Pad Conditions</i>	136
<i>Advanced Multisensor for Electrolytic Characterization</i>	138
<i>Chromate Coating Replacement for Military Aircraft</i>	140
<i>Army Aircraft Alloys – Corrosion-Retardant Additive Testing</i>	142
<i>Electrochemical Analysis of Chloride Rinse Agents on Aircraft Alloys</i>	144
<i>Development of Liquid Applied Coatings for Protection of Steel in Concrete</i>	146
<i>Noise Mitigation of Ducted Supersonic Jets for Launch Exhaust Management Systems</i>	148

CONTENTS (continued)

<i>Development of a Robust Finite-Element Method for Rocket Acoustics Problems</i>	150
<i>Tape Adhesion Testing Software</i>	152
Process and Human Factors Engineering Technologies	155
<i>Process and Human Factors Engineering Technologies Roadmap</i>	157
<i>A Simulator Study of the KSC Shuttle Landing Facility Air Traffic Control Tower Design</i>	158
<i>Assessing Space Shuttle Launch Dates With Advanced Discrete-Event Simulation Technologies</i>	160
<i>Virtual Reality Simulations of Orbiter Temporary-Access Improvements</i>	162
<i>Range Process Simulation Tool (RPST)</i>	164
<i>Spaceport Safety Modeling and Optimization</i>	166
<i>Advanced Process for Developing and Balancing Quantitative Safety, Reliability, and Maintainability Requirements</i>	168
<i>Human Engineering in Design and Modifications</i>	170
<i>Task Analysis Technologies</i>	172
<i>Human Factors-Process Failure Modes and Effects Analysis (HF-PFMEA) Software Tool</i>	174
<i>Task Analysis of the Payload Test and Checkout System (PTCS)</i>	176
<i>Toolkit for Enabling Adaptive Modeling and Simulation (TEAMS)</i>	178
<i>Activity-Based Costing and Simulation for the Operational Assessment of Future Space Transportation Systems</i> ...	180
<i>Artificial Intelligence Techniques for Payload and Vehicle Processing Scheduling</i>	182
<i>Design Root-Cause Analysis Knowledge Base</i>	184
<i>Project Management Integration System (PMIS)</i>	186
<i>Portfolio Analysis Tool (PAT)</i>	188
Biological Sciences	191
<i>Biological Sciences Roadmap</i>	193
<i>Demonstration of a Porous Tube Hydroponic System To Control Plant Moisture and Growth</i>	194
<i>Atmospheric Management in Variable-Pressure Environments: A Step Toward Martian Greenhouses</i>	196
<i>Advanced Life Support (ALS) Crop Testing</i>	198
<i>Photosynthesis and Metabolism of Wheat in Microgravity</i>	200
<i>Plant Lighting System</i>	202
<i>Effect of Microgravity on <i>Raphanus Sativus</i> L.</i>	204
Index	207

KSC Technology Development



Shuttle Processing



Launch Services Program



**International Space Station/
Payload Processing**

Major Stakeholders



**Next Generation
Launch Technologies**



Robotic/Human Exploration



**Future Spaceports
and Ranges**



Orbital Space Plane Concepts

Technology Transfer Office

Introduction

The John F. Kennedy Space Center's (KSC) outstanding record of achievements has earned it an honored place in history and an essential role in Space Transportation Systems of today and tomorrow. KSC is increasing the momentum in technology development for current and future spaceports. KSC's dual mission includes space launch operations and spaceport and range technology development. The Spaceport Technology Center (STC) initiative carries out KSC's role within NASA to meet the goals of increased safety, reduced cost of space access, and rapid expansion of commercial markets by infusing spaceport technologies into all facets of current and future Space Transportation Systems.

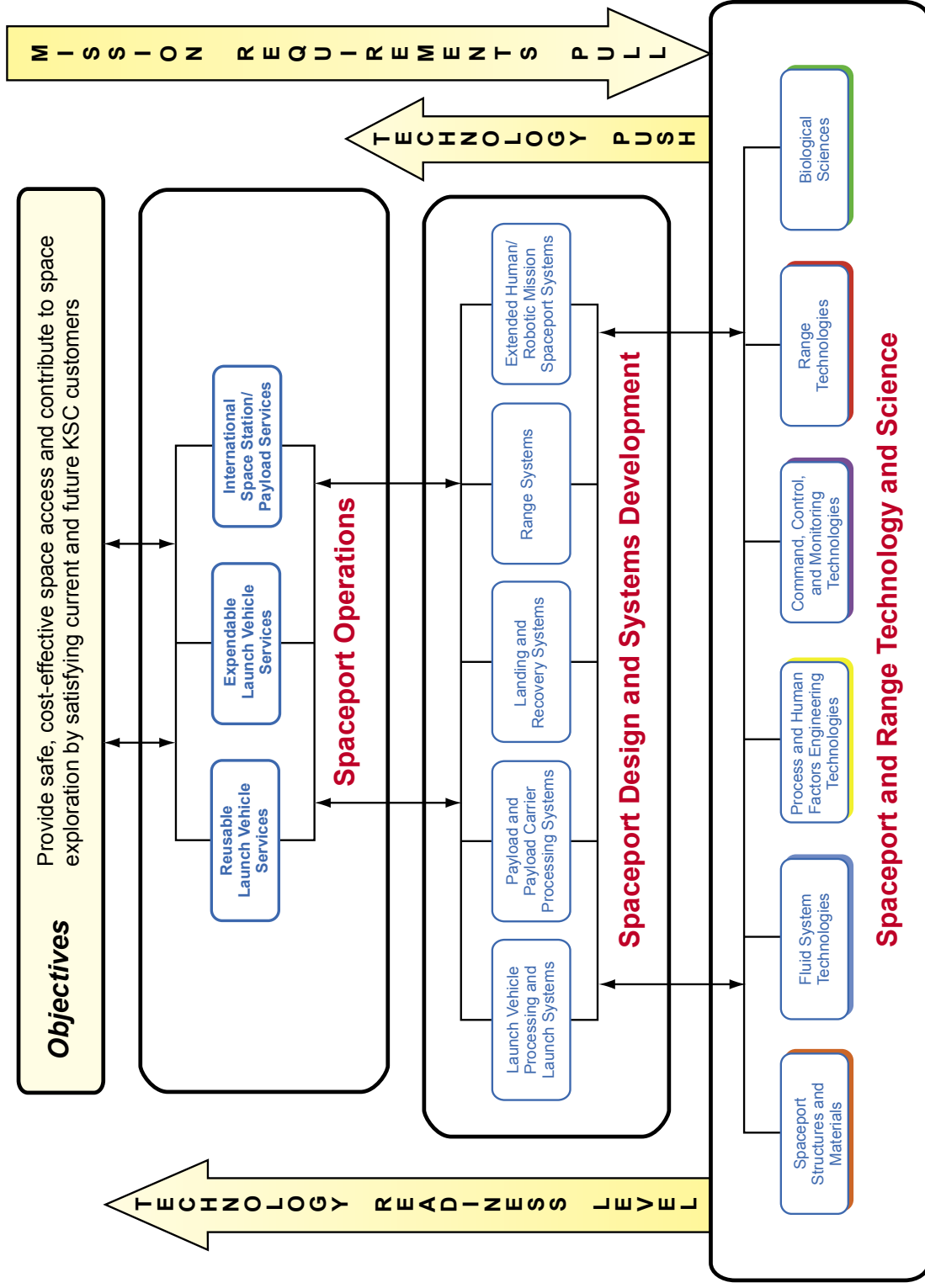
KSC's background as the nation's premier launch site creates an ideal environment for the STC. The STC's knowledge, expertise, facilities, and equipment provide technologies and processes to customers who propose to build and operate spaceports on Earth, in orbit, and beyond. KSC has three strategic lines of business: Spaceport Operations, Spaceport Design and Systems Development, and Spaceport and Range Technology and Science. KSC has unparalleled expertise in designing, building, and operating a spaceport with all of its complex technologies and systems.

STC technology development activities are concentrated in six Spaceport Technology and Science Product Lines – Fluid System Technologies; Spaceport Structures and Materials; Process and Human Factors Engineering Technologies; Command, Control, and Monitoring Technologies; Range Technologies; and Biological Sciences. KSC's leadership in producing safer, faster, cheaper, and more robust systems by developing and infusing technologies will pave the way for the future of the space industry. This report is organized by these six Spaceport Technology and Science Product Lines.

The primary stakeholders and customers for spaceport and range technologies are the programs and initiatives supporting current and future Space Transportation Systems and enabling technical programs. KSC aggressively seeks industry participation and collaboration in its research and technology development initiatives. KSC also seeks to transfer its expertise and technology to the commercial sector and academic community. Programs and commercialization opportunities available to American industries and other institutional organizations are described in the Technology Transfer Office Internet Web site at <http://technology.ksc.nasa.gov>. Additional information on KSC's Spaceport Technology Center can be found on KSC's home page at www.ksc.nasa.gov.

KSC External

Lines of Business and Product/Service Lines



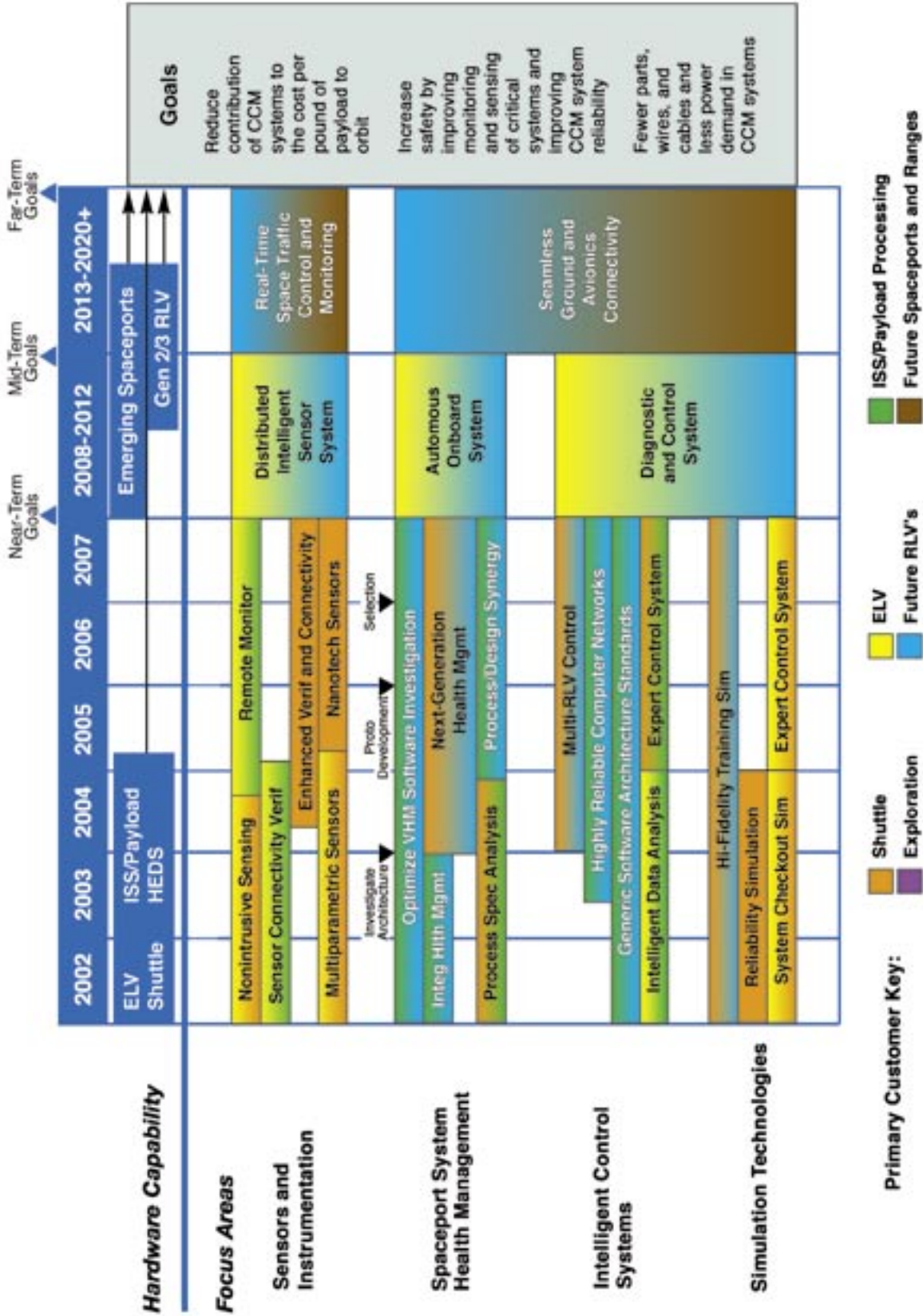
Command, Control, and Monitoring Technologies

The vision of Command, Control, and Monitoring (CCM) Technologies is to develop technology that enables future affordable, responsive, and safe spaceports. These spaceports can be Government-owned, commercial, orbital, or nonterrestrial. The goal is to reduce the cost of access to space while increasing safety. CCM Technologies can help in this role through the reduction and elimination of unique interface and infrastructure requirements. As we move away from a one-for-one cardinality between launch vehicle and ground infrastructure toward a truly many-to-many paradigm, we must shift our thinking about how we process and launch spacecraft. Spacecraft will have to become smarter and be in control of their spaceport processing, requesting needed services from the spaceport, as opposed to the smart spaceport telling the vehicle that it is now OK to fly. We must strive to remove complexity not only in the design but also in how information is presented to humans, wherever they may be in the loop, and provide decision support. Increases in processing requirements throughout the spaceport will drive advancements in the communication infrastructure, capability, and security. Finally, when dealing with human spaceflight, we need to support robust, fault-tolerant designs in both the software and hardware systems. The technology focus areas that will drive the roadmap toward that ultimate vision include the following:

- Sensors and Data Acquisition
- Spaceport Processing and Health Maintenance
- Advanced Software and Computing Architectures
- Simulation and Situational Awareness

For more information regarding Command, Control, and Monitoring Technologies, please contact Robert Waterman (Robert.D.Waterman@nasa.gov), YA, (321) 867-6680; Gregory Clements (Gregory.R.Clements@nasa.gov), YA-D8, (321) 867-8992; or David Kruhm (David.A.Kruhm@nasa.gov), YA-D5, (321) 867-6742.

Command, Control, and Monitoring Technologies Roadmap



Rev. Basic Oct. 2002

Multisensor Array Pressure Transducer

Multisensor array (MSA) transducers have been under development for the last few years, and recent achievements may make commercialization of such devices a reality in the near future. A prototype MSA pressure transducer was developed and demonstrated a measurable increase in transducer reliability and expanded transducer calibration cycles.

Common sense suggests that multiple sensors are better than one and, if so, how much better? Past experimentation focused on designing and implementing tests to answer this question and to quantify the relationship between the number of sensors and the associated improvement in sensor life and reliability (see KSC Research and Technology 2000/2001 Report, "Multisensor Array – Are More Sensors Better Than One?").

Multiple sensors can be implemented in numerous ways. The previously discussed method took advantage of the reduced size of microelectronic sensors and packaged several sensors onto a single circuit board. The result was a fully integrated multisensor array pressure transducer.

The pressure-sensing portion of the device consists of eight individual integrated-circuit (IC) pressure sensors mounted on a custom printed circuit board. These sensors, coupled with in-house-developed signal conditioning electronics, compose the electronics hardware of the device. Using knowledge gained from previous sensor characterizations and pressure calibrations, a microcontroller within the signal conditioning electronics was programmed with the in-house-developed multisensor array algorithm (MSAA). This algorithm compares the measurement error of each individual sensor and resembles the statistical process used in the Monte Carlo simulation. To provide a calculated output, a polling logic, combined with a sensor-



Multisensor Array Pressure Transducer

weighting algorithm and a sensor exclusion algorithm (to eliminate outliers from the decisionmaking process), is embedded in these sensor electronics.

To calculate the necessary single-pressure output value, the embedded software performs several functions and has unique characteristics. First, it allows the user to select target error/failure criteria. These are values that define acceptable overall measurement error and the acceptable error of any one sensor element. Once these are defined, the software utilizes complex sensor voting and measurement weighting schemes. When compared to defined error/failure criteria, this analysis provides the determination of valid sensor measurements as well as elimination of outlier values from the decisionmaking process; the transducer's single measurement output value is based on the voting and weighting results. Last, the availability of information pertaining to individual sensor element measurements allows for the real-time assessment of individual sensor element health. Internal tracking of this information will allow for trending and ultimately element and transducer failure prediction.

Key accomplishments:

- Paired the developed signal conditioning electronics with a commercially developed, eight-element, multiple-strain-gage sensor. Successfully demonstrated the coupled system.
- Began discussions for commercialization partnerships with transducer manufacturers.

Contact: J.M. Perotti (Jose.M.Perotti@nasa.gov), YA-D5-E, (321) 867-6746

Participating Organization: USTDC (N.N. Blalock, R.T. Deyoe, A.J. Eckhoff, Dr. C.D. Immer, and J.J. Randazzo)

Color-Indicating Patch for Shuttle Auxiliary Power Unit Hydrazine Transfer Line

The Auxiliary Power Unit (APU) is a hydrazine-fueled power unit in the Shuttle hydraulic system. The APU transfer line consists of 1/2-inch-outside-diameter stainless-steel tubing encased in a coaxial heater. An insulating glass fiber layer wraps around the tube heater assembly and is itself covered with LT-100 tape. Kapton tape is the outer layer wrapped around the LT-100 cover of the fibrous insulation. During routine maintenance of the APU system, evidence of microleaks was observed, as indicated by slight degradation of the glass fiber material. Although the leaks in the APU were small, it was essential to identify their location. Hydrazine is a highly corrosive and toxic substance, and it is a suspected human carcinogen. Currently, hydrazine leaks are monitored using the Interscan Hydrazine Monitor and/or Draeger tubes. To perform these tests, slits must be cut through the Kapton and LT-100 layers into the glass fiber insulation to extract air samples from the annular space for analyses. Both methods have major drawbacks. First, both methods are intrusive and require compromising the covering and insulation material of the APU transfer line. Second, both methods use an air pump to draw the sample, thus causing reduction of detection capability due to dilution of the hydrazine vapor by surrounding air. Third, it is labor-intensive to measure all potential leak locations since each location needs several minutes of analysis to accurately determine if there is a leak. Also, because of tight space, it is difficult to get to the location for a reliable measurement. A sensitive, easy-to-use, nonintrusive, in situ monitoring device of the colorimetric type could alleviate all of these difficulties.

The purpose of the project is to develop a monitoring device for the identification of both the presence and location of microleaks of hydrazine in the Shuttle APU system. The device is a colorimetric indicator patch that can be incorporated into the APU system. The patch changes from pale yellow to purplish gray upon exposure to hydrazine liquid or vapor. The active ingredient of the indicator, potassium tetrachloroaurate (III), is loaded onto a porous 3/8-inch-diameter glass fiber or cellulose substrate. Loading levels are controlled by pipetting precise volumes of an aqueous solution of the indicator reagent onto the substrate. The loaded substrate is dried and attached to the



Side-by-Side Photographs of 3/8-Inch-Diameter Cellulose Disks Coated With the Colorimetric Reagent Potassium Tetrachloroaurate (III) (The left side shows the color prior to exposure to hydrazine; the right side shows the color following exposure to hydrazine.)



Color Indicator Patch on a Mock APU Transfer Line

sticky side of a 1-inch-by-3-inch piece of LT-100 adhesive tape and covered by a protective layer of waxy paper to form a “band-aid.” After removing the protective wax paper cover, the “band-aid” can be easily applied to the glass fiber insulation of the APU system. Once applied, it needs only periodic visual inspection to determine if there is a color change. The color change induced on the indicator patch is readily seen, even through the Kapton covering. If the color is unchanged, the patch does not need to be replaced. These colorimetric patches are a precise monitoring system to identify the presence and location of hydrazine leaks. In addition, since the patch assembly also uses the LT-100 tape, deployment should not result in significant disruption to the integrity of the system or major redesign. To date, tests conducted in the lab showed the color developed is irreversible and stable for at least 2 months. Tests also indicated the patch is stable when stored in 40 degrees Celsius and under a vacuum of 10^{-7} torr for at least 4 weeks. The evaluation of the patch for shelf life is ongoing.

Key accomplishments:

- Developed the colorimetric chemistry for the detection of hydrazine.
- Verified the color developed is irreversible and stable for at least 2 months.
- Verified the indicator patch is stable at 40 degrees Celsius and under vacuum of 10^{-7} torr.
- Designed the “band-aid” for application.

Key milestones:

- Determine the shelf life of the indicator patch.
- Start using the colorimetric indicator patch in the Shuttle APU system.

Contact: R.C. Young (Rebecca.C.Young@nasa.gov), YA-C3, (321) 867-8765

Participating Organization: Dynacs (Dr. W.J. Buttner)

A Study of Hail Monitoring Strategies for Shuttle Launch Safety

In Florida most precipitation reaches the ground in the form of raindrops, with drop diameters ranging from less than 1 millimeter (mm) up to 5 or 6 mm. Occasionally, these hydrometeors are solid rather than liquid. Solid ice or hail occurs in diameters ranging from 0.5 centimeter (cm) or less up to 2 or 3 cm or more. Hail is a rare event at the Kennedy Space Center, but it does occasionally occur.

The example of hail damage on the surface of the External Tank (ET) shown in figure 1 was likely caused by a pea-size (0.5 cm) hailstone. Because of the potential of hail damage to the ET while exposed to the weather, it is desirable to remotely monitor hailfall in the vicinity of the Shuttle pad. If hail of sufficient size and quantity is detected by a hail monitoring system while the Shuttle is at the launch complex, the ET is thoroughly inspected for damage.

For over 40 years, meteorologists have used simple, inexpensive pads of Styrofoam for recording hail dents and estimating hailstone sizes. "Hailpads" have a proven record of reliably recording hail impacts down to the smallest size, while not recording raindrop impacts.

A hailpad calibration method developed during the 1978 Alberta Hail Project relates the pad dent diameter d to the hailstone diameter D , as an empirical second-order polynomial:

$$D = 0.38 + 1.11d - 0.04d^2 \quad (1)$$

where D and d are expressed in centimeters. Figure 2 shows a Colorado State University hailpad after impact with three 1.6-cm-diameter ice balls, fired by a paintball gun at the KSC Fire Training area.

Even though the hailpad is the "gold standard" in measuring hailfall, it was desirable to implement a remote hail monitoring system at the Shuttle launch pad. Imaging hailpads with a video camera system was one method considered. Another approach investigated by KSC used a single piezoelectric ceramic disc mounted under a 1-square-foot flat metal plate. The initial concept was subsequently improved by forming a shallow pyramid structure (see figure 3) that encouraged hailstones to bounce away from the sensor so they would not be counted more than once. In addition, the final prototype included a mounting box for the piezoelectric ceramic disc, which was offset from the pyramid apex, thus improving response uniformity.

One notable characteristic of this design is the potential to utilize frequency differences between the spectrums created from a raindrop impact and a hailstone impact. In other words, the sound of hail hitting a metal plate is distinctly different from the sound of rain impacting the same plate. This fortuitous behavior of the pyramid sensor may lead to a signal processing strategy that is inherently more reliable than one depending on amplitude processing only.



Figure 1. Example of Hail Damage on External Tank



Figure 2. Colorado State Hailpad After Ice Ball Test

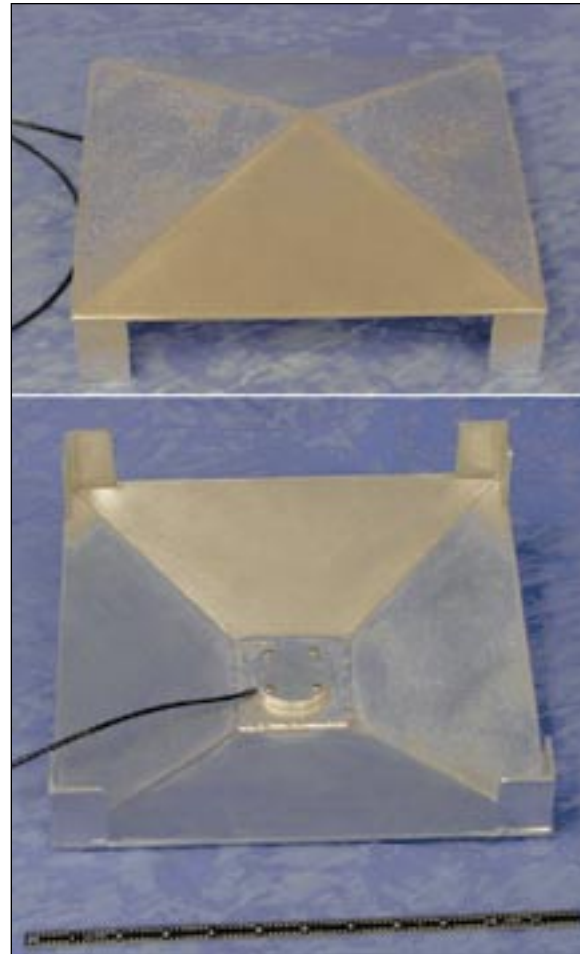


Figure 3. Prototype "Pyramid" Hail Monitor

Key accomplishments:

- Developed and characterized a hail monitor prototype – the “pyramid” sensor.
- Developed a hail simulation and testing procedure based on firing ice balls from a paintball gun monitored by a LabVIEW data acquisition system.

Key milestone:

- Plan to implement a hail monitoring system for Shuttle launch safety based on the pyramid sensor with collocated hailpads for in situ calibration and verification.

Contact: Dr. R.C. Youngquist (Robert.C.Youngquist@nasa.gov), YA-C3-E, (321) 867-1829

Participating Organizations: USTDC (W.D. Haskell, Dr. J.E. Lane, Dr. C.D. Immer, and R.B. Cox) and Colorado State University (Dr. N. Doesken)

Mass Sensor for Cryogenic Fluids

Next-generation launch vehicles will likely utilize densified cryogenic propellants so greater amounts of fuel and oxidizer can be placed into onboard tanks. This will improve the performance of future vehicles by allowing them to fly farther or carry heavier payloads. However, much of this enhancement will be lost if the total mass of propellant cannot be accurately measured. Current limitations on measurement technologies require that tanks be filled well over the level calculated as necessary, resulting in a loss of payload capacity. Ideally, an accurate and robust total mass sensor is needed for future launch vehicles so the proper amount of fuel and oxidizer can be loaded to match a given mission's needs.

One mass sensing method uses an extended capacitor reaching from the bottom to the top of the tank. Instead of determining the liquid height with such a device, as is commonly done, a judicious choice of parameters and design is made to obtain a total liquid mass measurement. The resultant device (shown in figure 1), demonstrated experimentally for liquid nitrogen and theoretically for liquid nitrogen, hydrogen, and oxygen, achieves a mass measurement more accurate than ± 1.0 percent (over a selected temperature and pressure range of interest).



Figure 1. Cryogenic Fluid Mass Sensor

The sensor is unique in that only a single measurement is needed to find the total mass of cryogenic liquid in a tank. Most cryogenic tanks do not have uniform cross sections, so normal capacitance-level sensors do not provide mass information. As illustrated in figure 2, the sensor is designed to compensate for noncylindrical tank shapes by varying the capacitance as a function of height. This is accomplished by physically shaping the inner conductor of a cylindrical capacitor so the capacitance is high where the tank area is large and low where the tank area is small. Also, the sensor produces a correct mass reading even if the cryogenic fluids stratify (i.e., if colder, denser fluid drifts to the bottom of the tank). This heavier fluid has a correspondingly higher dielectric constant and therefore yields a higher capacitance. Finally, if the tank contracts or expands thermally, the sensor output can be corrected easily by a simple multiplication. While a cylindrical capacitor was used to confirm the theory, other capacitive geometries could also be used to meet specific application requirements.

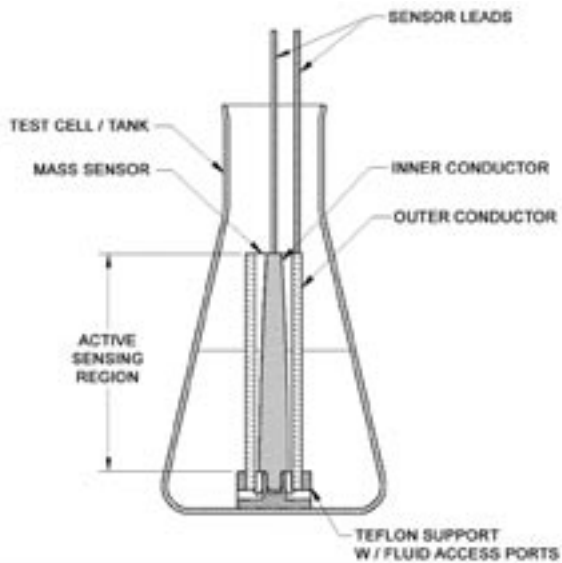


Figure 2. Mass Sensor Schematic



Figure 3. Experimental Setup

Key accomplishments:

- Designed and executed a proof-of-concept experiment where an insulated test cell was filled with liquid nitrogen and set on a scale (figure 3). A LabVIEW program was used to acquire data from the sensor and from the scale at 1-second intervals as the liquid nitrogen boiled off (figure 4). Theoretical development is continuing and matches the experiment to within 2 percent with the expectation of improved accuracy.

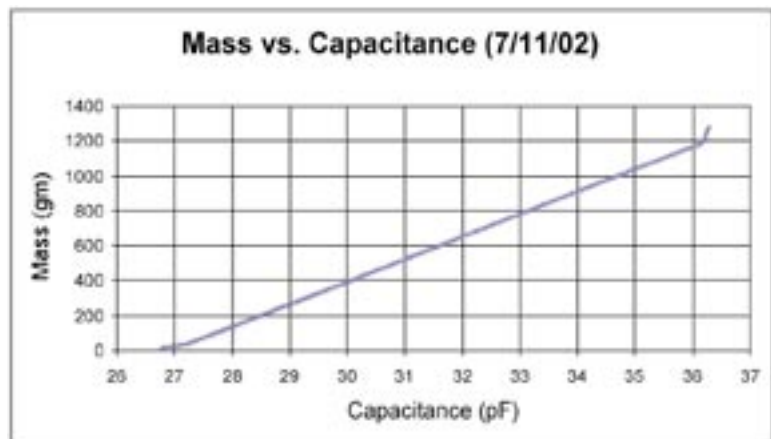


Figure 4. Comparison of Mass to Capacitance
(The plot shows more than 14,000 unprocessed data points taken as the liquid nitrogen boiled off. Note the nonlinearities at the ends of the capacitor and the exceptional linearity over the bulk of the tank mass range.)

Contacts: M.A. Nurge (Mark.A.Nurge@nasa.gov), YA-C3-E, (321) 861-9068; and Dr. R.C. Youngquist, YA-C3-E, (321) 867-1829

Shuttle Tile Moisture Sensor

Much of the surface of each Space Shuttle is protected from the heat of reentry by a high-temperature, reusable insulation commonly known as Shuttle tiles. These tiles are composed of 99.7-percent pure silica fibers that form a strong material with extremely low thermal conductivity. Each Orbiter has more than 20,000 tiles attached to it forming a thermal protection system that can withstand not only temperatures as high as 2,400 degrees Fahrenheit but also the acoustic levels (up to 166 decibels) common during launch. In particular, the tiles across the bottom of the Orbiter experience the greatest temperatures and are coated with a thin (about 0.01-inch) layer of borosilicate glass mixed with a silicon tetraboride emittance agent (i.e., black glass). This black glass coating raises the emittance of the tile above 0.8, allowing the majority of the heat of reentry to be radiated away from rather than conducted down to the skin of the Orbiter.

The tiles are lightweight because the silica fibers only fill 7 percent of the tile's volume. This is an advantage for a launch vehicle but raises an operational difficulty in that the fibers act as extremely absorbent sponges. Efforts are made to minimize the amount of water in the tiles on an Orbiter because water not only adds to the launch weight but can also freeze in space, possibly leading to serious tile damage and Orbiter damage on reentry.

During fabrication, every tile is treated with the waterproofing agent dimethylethoxsilane (DMES). This material coats the silica fibers, making them hydrophobic instead of hydrophilic (i.e., causing the fibers to repel water rather than absorb it). This waterproofing system is effective, but the DMES burns out of the tile during Orbiter reentry. During Orbiter processing, each tile is injected with replacement DMES through a small hole (about 1 millimeter in diameter) in the black glass coating, effectively rewaterproofing the tiles.

From reentry until the Orbiter is inside the Orbiter Processing Facility (OPF), the tiles are susceptible to water intrusion. Cracks are common in the black glass coating and are believed to provide a primary route for water to be drawn into the tiles. Rapidly protecting a recently returned Orbiter from adverse weather and other sources of water is a top priority.

However, it is not always possible to protect the Shuttle from these adverse conditions, and water has entered the tiles on several occasions. During vehicle processing, the water in the tiles is removed using heat lamps. An infrared camera is used to determine whether the water was sufficiently removed. The disadvantage of using an infrared camera to evaluate the presence of water is that the technicians have to wait several hours after the heat lamps have been disconnected before they can take readings. Furthermore, water must be close to the tile's surface for the infrared camera to detect it.

To overcome the limitations of the infrared camera, an alternative method of water detection based



Tile Moisture Sensor

on capacitance measurements was developed. The objective of designing the Shuttle Tile Moisture Sensor was to develop a tool capable of detecting small amounts of water in a tile. This was accomplished by taking advantage of the differences in permittivity (dielectric constant) of the materials involved. The permittivity of a material determines the amount of charge needed to create a voltage across the material; therefore, the capacitance presented by a material of a certain geometrical configuration will increase as the permittivity of the dielectric increases. Air has a permittivity close to unity, while freshwater has a permittivity of about 80, although it depends on temperature to some extent. Most nonconducting materials have relatively small dielectric constants with values typically less than 10. Oils, for example, have a value of about 2.0, silica glass about 4.0, Teflon about 2.0, and cryogenic fluids around 1.5. An accurate measurement of capacitance can be used to determine the presence of dielectric materials affected by the electric field generated by the capacitor's electrodes. The effect that a dielectric has on the measured capacitance depends on various factors, such as the geometrical configuration of the dielectric, its distance from the capacitor's plates, and the presence of other dielectrics or conductors nearby.

The operation of the new Shuttle Tile Moisture Sensor is based on the application of a small and fixed current to the electrodes composing the capacitive element. The duration of the current application is selected to prevent overvoltage saturation of the analog circuitry and the analog-to-digital converter due to the charge injected into the capacitor. Following the application of the current, the voltage at the capacitor is read. The resolution of the voltage measurement is increased by taking multiple readings (256 in this case) with different durations of the charge current (typically 125-nanosecond difference between readings) to remove the effects of the quantization noise at the analog-to-digital converter. This ensures that the voltage applied to the analog-to-digital converter is not identical for every measurement. Otherwise, the quantization noise would still be present and would limit the resolution of the capacitance measurements.

The Shuttle Tile Moisture Sensor is calibrated to remove the effects of known dielectrics, such as the Space Shuttle tiles themselves. Since the permittivity of the material used in the tiles is not unity, the moisture sensor detects a change in capacitance as the probe is placed against a tile. Preset calibration values are loaded in the sensor for various tile depths against the metal frame of the Orbiter.

To achieve the resolution and accuracy required, several features were implemented. Variable charging times were incorporated for successive measurements of the voltage developed due to the charging of the capacitive elements. An autozero was built in to remove the effects of the capacitance introduced by the wiring, circuit board, and active elements. A very stable active-current source capable of sourcing a submicroamp current was developed.

The prototype Shuttle Tile Moisture Sensor has several features that make it easy to use. A liquid crystal display allows the operator to select the thickness of the tile being tested (adjustable range) as well as to display the result of the capacitance measurement. Audible and visible alarms with preset thresholds make the device easier to operate. A 9-volt battery powers the tool.

Key accomplishments:

- Developed an advanced prototype Shuttle Tile Moisture Sensor in conjunction with Shuttle Operations.
- Currently field-testing the device in the OPF.

Contact: Dr. R.C. Youngquist (Robert.C.Youngquist@nasa.gov), YA-C3-E, (321) 867-1829

Participating Organization: USTDC (Dr. P.J. Medelius, J.D. Taylor, J.J. Randazzo, and J.A. Rees)

New Gas Polarographic Hydrogen Sensor

Polarography is the measurement of the current that flows in solution as a function of an applied voltage. The actual form of the observed polarographic current depends on how the voltage is applied and on the characteristics of the working electrode. The new gas polarographic hydrogen (H_2) sensor shows a current-level increment with concentration of the gaseous H_2 similar to those relating to metal ions in liquid electrolytes in well-known polarography. This phenomenon occurs because the diffusion of gaseous H_2 through a gas diffusion hole in the sensor is a rate-determining step in the gaseous hydrogen sensing mechanism. The diffusion hole artificially limits the diffusion of the gaseous H_2 toward the electrode located at the sensor cavity.

This gas polarographic H_2 sensor is actually an electrochemical pumping cell since the gaseous H_2 is pumped via the electrochemical driving force generated between the electrodes. Gaseous H_2 enters the diffusion hole, reaches the first electrode (anode) located in the sensor cavity, and is transformed into H^+ ions or protons. The H^+ ions pass through the electrolyte and reach the second electrode (cathode) to be reformed into gaseous H_2 .

Having a gas binary system and assuming steady-state conditions, no reaction, stagnant background gas, and mass transfer in only one direction and rate-limited at the diffusion hole, the limiting output current is predicted to be a linear function of the logarithm of the background gas concentration. This linear relation between the output-limiting current and the logarithm of the background molar fraction has a slope that includes the area and the length of the gas diffusion hole, the gas pressure, the gas temperature, the diffusion coefficient of the gaseous specie in the binary gas mixture, the Faraday constant, and the number of electrons per mole of the gaseous specie transferred between electrodes (this number is 4 for oxygen [O_2] and 2 for H_2 as indicated in figures 1 and 2, respectively).

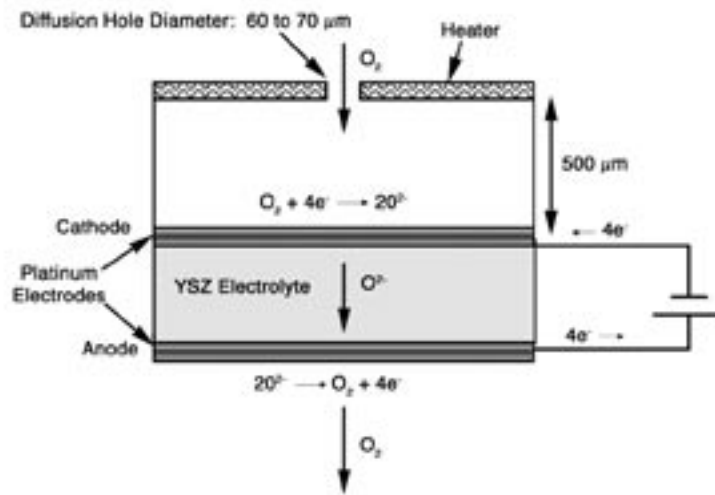


Figure 1. Schematic Diagram of Electrovac Gas Polarographic O_2 Sensor

Gas polarographic O₂ sensors are commercially available. A commercial gas polarographic O₂ sensor was used to prove the feasibility of building a new gas polarographic H₂ sensor. As expected, the output-limiting current proved to be dependent on H₂ composition; the output-limiting current is increased as the gaseous H₂ concentration increases. As in the case of gas polarographic O₂ sensing, a linear relation between the output-limiting current and the logarithm of the mole fraction of the background gas was also observed for gas polarographic H₂ sensing, as shown in figure 3. Further test runs and precise measurements of the diameter and the length of the diffusion hole are required to corroborate this linear relation.

Key accomplishments:

- Sensor was presented at the 2nd Institute of Electrical and Electronics Engineers (IEEE) International Conference on Sensors.
- Experimental tests fulfilled gaseous hydrogen sensing criteria, very fast response, good accuracy, and reasonable repeatability.
- Sensor's similarity to existing and commercially available oxygen sensors led to the potential use of both sensors to enhance performance of both sensors when the gas has both components — oxygen and hydrogen.

Contact: R.P. Mueller
 (Rob.Mueller@nasa.gov), YA-D1, (321)
 867-2557

Participating Organization: USTDC (J.A. Dominguez and Dr. R.G. Barile)

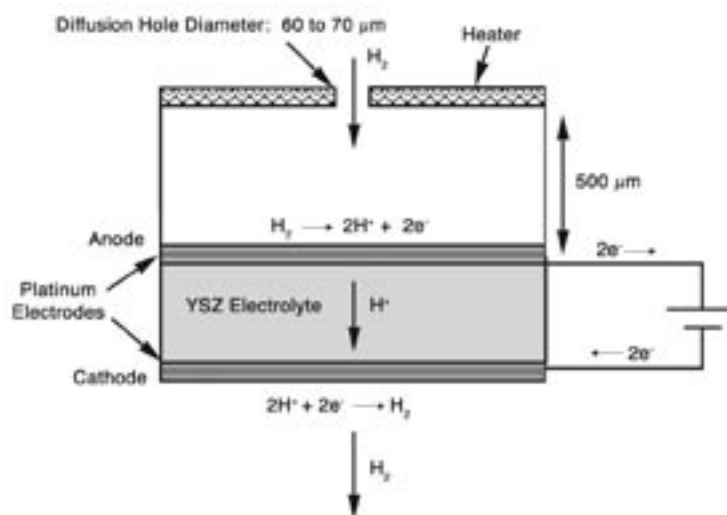


Figure 2. Schematic Diagram of a New Gas Polarographic H₂ Sensor

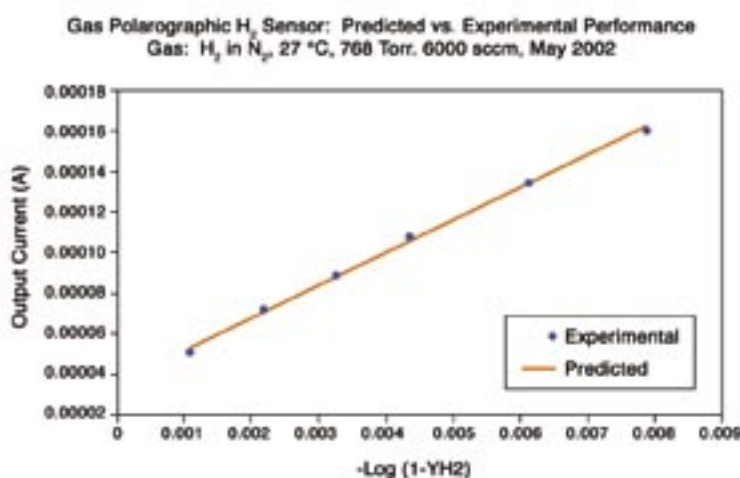


Figure 3. Polarographic H₂ Sensor Output Current Compared Against Predicted Values

Improved Fiber-Optic Pressure Block Connector

When using fiber-optic cable for transmitting video signals from a positively pressurized camera housing, it is necessary to use a leaktight fiber-optic connector to prevent loss of pressure from the housing.

A search for a commercially available connector to meet this requirement found very expensive items designed for high-vacuum service and bulkhead feed-through items that were not suitable because of the requirement to disconnect the fiber-optic cable from the camera housing. The search turned toward developing a simple low-cost connector using commercially available components that can be easily modified or used as is.

The main component selected was a \$15 standard part, KC-124-K10 bulkhead fitting, modified to accept a potting boot on one end and a standard FC-type adapter/connector on the other end. To block a leakage path from inside the cable jacket, a 3/8-inch section of the jacket is stripped, exposing the cladding inside the potting boot before filling the boot with polyurethane.

An adapter ring is required to mount an FC-type adapter/connector on the outside end of the KC-124-K10 bulkhead fitting. A stainless-steel inverted nut is welded to the potting boot end and, with a brass ferrule and a 1/8-inch "B" nut, provides a slight compression to the fiber-optic cable to prevent the polyurethane from leaking into the body of the KC-124-K10 bulkhead fitting.

These fiber-optic pressure block connectors are used in the Operational Television (OTV) Modernization Camera Housings. The complete design is documented on KSC Drawing 79K31859, Fiber-Optic Pressure Block.

Contact: R.A. Stute (Robert.A.Stute@nasa.gov), YA-E2, (321) 867-3985

Participating Organizations: USTDC (T.D. Greenfield, C.G. Hallberg, and J.D. Polk) and United Space Alliance (R.D. Gibbons)

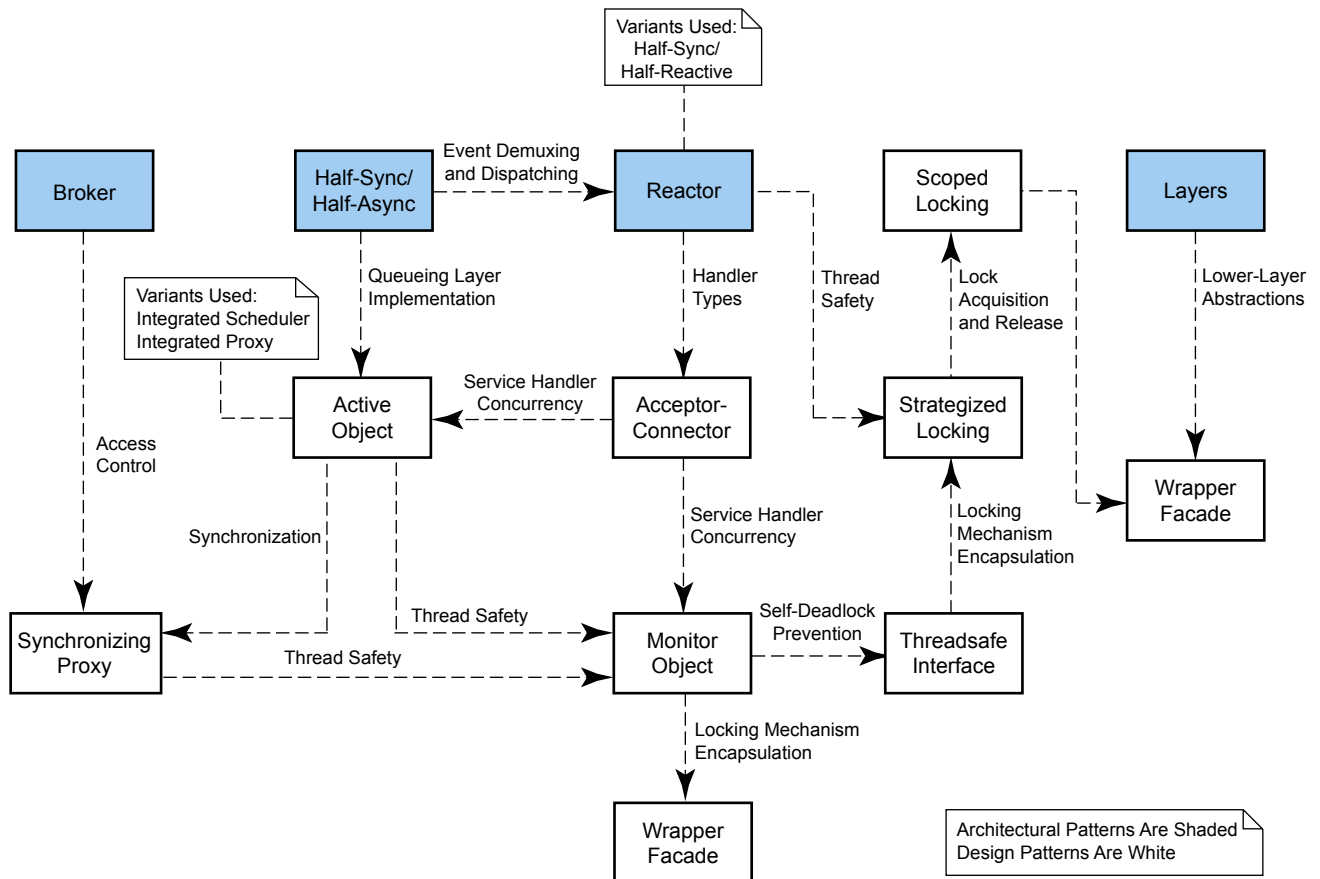


Improved Fiber-Optic Pressure Block Connector

Common Application Framework (CAF)

The Common Application Framework provides both common services and a layer of abstraction that insulates the applications developer from the platform details. The CAF accomplished this goal with a set of object-oriented components, base classes, abstract patterns, and concrete behaviors/services implemented using C++. The CAF allows the application developer to focus on the requirements and business logic necessary for the application. In addition, the framework makes extensive use of generic programming concepts (i.e., templates), mature open-source software packages, and industry-standard interfaces that make the framework easy to use and easy to extend.

One of the most significant features of the CAF is the embedded concurrency model. The CAF concurrency model insulates the application developer from the rigors of making an application threadsafe by enforcing serialization at an object level instead of an attribute level. This allows an object to be created as either an active or passive object to determine the thread of execution associated with the object. To support the concurrency model, the framework provides a pool of managed threads and an event-driven model. The combined functionality of the managed threads and the event processing means that one thread of execution can block waiting on an event, without fragmenting the application code to provide the multiplexing capability (i.e., signal handlers and switch statements). The CAF solution provides a threadsafe run-time environment and the means to produce software more quickly, with fewer experienced developers in a shorter time.



Common Application Framework (CAF) Architecture

The CAF also supports a data-driven initialization model. This means that the object composition, initial values, and associations can be derived from instance data when the application is initialized as opposed to hard-coded.

The features of the CAF provide abstraction, commonality, reliability, and increased code reuse that lead to enhanced software quality and safety.

The following are benefits of the Common Application Framework:

- Provides an embedded concurrency solution with serialization at the object level and managed threads of execution.
- Automatically detects deadlock and race conditions.
- Minimizes the time required to design and implement applications.
- Provides the concept of cancellation points (points in the software where a check is performed to determine if the application should continue processing in the current thread of execution).
- Provides an event-driven model.
- Supports both client and server applications.
- Provides a number of easy-to-use patterns for both monolithic and distributed applications (e.g., publisher subscriber, command, active object, singleton).
- Provides built-in IPC interfaces for CORBA, POSIX, SV5, and Sockets.
- Uses industry standards (CORBA, SQL, ODBC, POSIX, and C++).
- Makes extensive use of open-source packages (ACE, TAO, M4, Flex, and Bison [TAO can be replaced with any CORBA-compliant ORB and Name-service]). No licensing is required and documentation is readily available on the Web and in many books.
- Supports multiple platforms (e.g., Solaris – SPARC and Intel, Linux) and can be built with an ANSI/ISO-compliant C++ compiler.
- Promotes consistency within a development project.
- Provides a high-level syntax for procedural control within a thread of execution:
 - Read: Reads the value of a specific data point.
 - Write: Modifies the value of a data point.
 - Verify: Checks a list of data points for a specific value or list of values.
 - Verify Within: Checks a list of measurements for a specific value within a specific time range.
 - Delay: Pauses execution for a specified time.
 - Delay Until: Pauses execution until the specified condition is met.
- Minimizes the risk associated with inexperienced developers building concurrent applications.

Key accomplishments:

- Validated Common Application Framework's support of hundreds of requirements.
- Framework used by Hazard Warning System CSCI to validate software that performs the Orbiter Processing Facility checkout against a math model.
- Framework software used in test of Flight Controls CSCI to perform end-to-end performance tests at Shuttle Avionics Integration Laboratory.

Contact: D.A. Nieten (Daniel.A.Nieten@nasa.gov), YA-D8, (321) 861-2233

Participating Organizations: USTDC (R. Nieves, A. Crikis, and G. Poveda) and United Space Alliance (A.A. Ciavarella)

Automated Test Tool

The Automated Test Tool for C++ automates the execution and evaluation of software tests, including the logging of pass/fail results. In addition, test driver and script templates are automatically generated from C++ header files that are readily extensible to other languages. Since the tool encourages a data-driven test design combined with scripting languages, changes to test cases can be made easily without the need to recompile the application under test (AUT). Also, the AUT can continue executing while the test scripts are modified and debugged on the fly. If a repository or database is available containing information about the data under test (e.g., minimum/maximum values, enumerated values), the Automated Test Tool can readily interface with that data store and automatically incorporate the data directly into the test cases.

The Automated Test Tool provides a library of test procedures that enable the automatic execution and termination of AUTs along with many other predefined methods. Furthermore, the Automated Test Tool is able to wrap other test tools, such as performance test tools, and launch and drive those tools during execution.

Benefits of the Automated Test Tool include the following:

- Minimizes the time required to test software.
- Allows testing to be run incrementally.
- Removes drudgery of building the test scaffolding associated with the AUT.
- Allows for a rapid buildup of a test suite that can then be used for regression testing.
- Built on top of TCL and Expect – two mature, freely available computer languages. No licensing is necessary and documentation is readily available on the Web and in many books.
- Eliminates the monotony associated with testing.

Key accomplishments and milestones:

- Automatic validation of hundreds of requirements for an advanced real-time control framework completed in 20 minutes.
- Identification of errors in framework during regression testing of the real-time control framework.

Contact: G.S. Semmel (Glenn.S.Semmel@nasa.gov), YA-D8, (321) 861-2267

Participating Organizations: United Space Alliance (K.A. Vo and M.C. Michel), USTDC (B. Pelakh), IT-D2 (T.W. Merrill), and Aerospace Design and Development

```

...
Now testing use case parseStlString...
SRS Name -->
parseStlStringTokenize
Enter a delimiter character:
B
Enter a string that contains no more than one instance
of delimiter
character:
ABC
AC
Enter a delimiter string:
<delimiter>
Enter a string that contains no more than one instance
of delimiter string:
A<delimiter>Z
AZ
SRS Name -->
    PASS: svpParseStlStringTokenize
parseStlStringCombine
Enter the first string:
CLCS
Enter the second string:
World
combineStringToken: CLCSXWorld
SRS Name -->
    PASS: svpParseStlStringCombine
...

```

Screen Shot of Tool Running

```

Test Run By cma on Wed Jun 12 15:22:56 2002.
Hostname is ide2ccp2.ksc.nasa.gov. CCWS host
is ide2hci2.

```

```

    PASS: setup spawn_remote_shell.
Now testing use case logging...
    PASS: setup launch_application
    PASS: svpLogging
    PASS: setup shutdown_Eim
Now testing use case publishState...
    PASS: svpPublishStateInitializing
    PASS: svpPublishStateIdleAtEndInit
    PASS: svpPublishStateSupporting
Now testing use case initiateDisplay...
    FAIL: svpInitiateDisplay
    Now testing use case parseStlString...

    PASS: svpParseStlStringTokenize
    PASS: svpParseStlStringCombine
Now testing use case concurrency...
    PASS: svpConcurrencySingleEntryPoint
    PASS: svpConcurrencyMultipleEntryPoint
...

    === Summary ===

# of expected passes    284
# of unexpected failures 1

```

Sample of Summary Log Output

Digital Image Lens Distortion Correction Algorithm

Photogrammetry is defined by webster.com as “the science of making reliable measurements by the use of photographs and especially aerial photographs (as in surveying).” Two or more cameras are generally used to image objects, such that multiple views provide information on depth of terrain, for example, or any other three-dimensional (3-D) position feature of interest. In these cases, the distance from the cameras to the object (range) is much greater than the size of the object (field of view [FOV]). The cameras, which may be flying onboard an airplane or satellite, use long-focal-length lenses (or telescopic lenses). Under these conditions, the image in each camera appears flat, so all rays connecting the camera lens to parts of the imaged object are essentially parallel in the vicinity of the object. This is described by the so-called affine camera model.

Another form of photogrammetry, developed at KSC to make accurate 3-D position measurements, uses a single camera and high-contrast target (see “Surveying With a Digital Camera System,” KSC Research and Technology 2002 Annual Report). In this case, the rays connecting the target to the camera focal point are not parallel. Complete 3-D position coordinates, including depth information, are derived from the imaged target by means of the perspective (pin hole) camera model. In this application, the target range is comparable to the camera’s FOV. This comes about by a short-focal-length (f) lens.



Figure 1 (top) shows an outdoor scene taken with a commercial digital camera, using a short-focal-length setting (wide FOV). On close examination, a noticeable curvature can be seen along the horizon as well as the pole to the left (the pole is actually straight and perpendicular to the ground). This “fish-eye” effect is a common occurrence in camera images and worsens as the FOV increases (f decreases). Note that the pole does not appear perpendicular to the ground. This can be explained by the perspective camera model. The farther a point is from the camera, the closer to the center of the image the object will appear. In the case of the pole, the top is farther from the camera than the bottom, thus giving the appearance of a leaning pole.

The curvature of the pole, as well as the curvature of the horizon, is a consequence of lens distortion. Lens distortion can be thought of as the error produced in a camera imaging system that results in deviations from that expected from the ideal perspective camera model. As can be expected, lens distortion causes severe degradation of position measurement accuracy in single-camera photogrammetry.

Figure 1. Before (top) and After (bottom) Application of Lens Correction Algorithm

A simple empirical lens distortion model considers the distortion effect as proportional to the square of the distance from the center of the image, where the image center is coincident with the camera optical axis. A lens correction formula is then based on modifying the k th image pixel position \mathbf{p}_k of the original image, using the following formula:

$$\mathbf{p}'_k = \mathbf{p}_k \left(1 - \frac{\beta}{\alpha} \mathbf{p}_k \cdot \mathbf{p}_k \right)^{-1} \quad (1)$$

where $\alpha \equiv f / d_c$ (f is the lens focal length and d_c is the charge-coupled device [CCD] pixel width), and \mathbf{p}'_k is the new pixel coordinate in the corrected image.

The lens distortion correction factor β can be found by either trial and error or a calibration procedure using an xy table. By plotting uncorrected camera data versus the xz -table coordinates as shown in figure 2, where the subscript m denotes measured coordinates (from camera photogrammetry) and the subscript t denotes xz -table coordinates, β is determined by the slope of the resulting linear fit.

Key accomplishments:

- Developed a simple lens distortion correction algorithm for single-camera photogrammetry applications.
- Devised a lens calibration method using an xy table to determine lens correction factor for any given lens.

Key milestone:

- Plan to integrate lens correction algorithm in Payload Ground Handling Mechanism (PGHM) position measurement photogrammetry system.

Contact: Dr. R.C. Youngquist (Robert.C.Youngquist@nasa.gov), YA-C3-E, (321) 867-1829

Participating Organization: USTDC (Dr. C.D. Immer, Dr. J.E. Lane, and B.M. Burns)

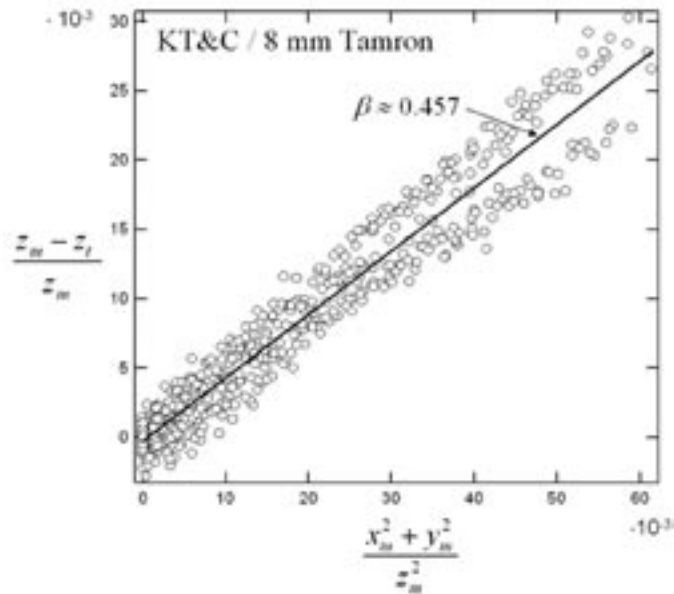


Figure 2. Determining Empirical Lens Calibration Factor β From xy -Table Data

Real-Time Detection and Tracking of Multiple Moving Objects in Complex Image Background

Motion detection is an important process for many machine vision systems. Systems that analyze aerial images, design special correlation chips for real-time applications, track moving objects, perform robot vision, detect moving targets, analyze traffic flow, or guide autonomous vehicles are examples of machine vision systems. The main goal of a motion detection system is to detect and track only structural changes in the scene. For machine vision to operate successfully, fast, accurate, and robust motion detection algorithms are needed. In the past, little work was directed toward solving this problem for time-varying outdoor scenes.

Motion detection is generally performed at the pixel level, at the edge level, or even at higher feature levels. Existing feature-level algorithms for time-varying outdoor backgrounds require more computational efforts than those working at the pixel level, but they provide more accurate information for higher system modules. We have implemented an innovative motion detection system that performs above the pixel level, provides accurate information, and surpasses the robustness of the existing high-feature-level algorithms while requiring less computation time.

The system was originally tested to detect potential foreign object debris (FOD) during the Space Shuttle liftoff. The image background during the Space Shuttle liftoff is quite complex because moving objects that are not FOD (ice flakes, fume clouds, external fuel line connections, etc.) constantly appear in the scene that is taped in black-and-white format. The system was able not only to detect two FOD items observed in the tape images but also to keep close track of both items (see figures 1 and 2). Figure 3 shows the trajectory for both items; this trajectory was drawn in real time as the FOD was detected. In regard to the computation time, the system was also able to process and execute motion detection features on every one of the 30 frames per second generated by the image acquisition system.

This real-time moving-object detection system is currently in its preliminary stage. The system concept and algorithm have proven to be robust. Implementation and validation are still needed. The current system works using a black-and-white image format. Images acquired in color will lead to an even more

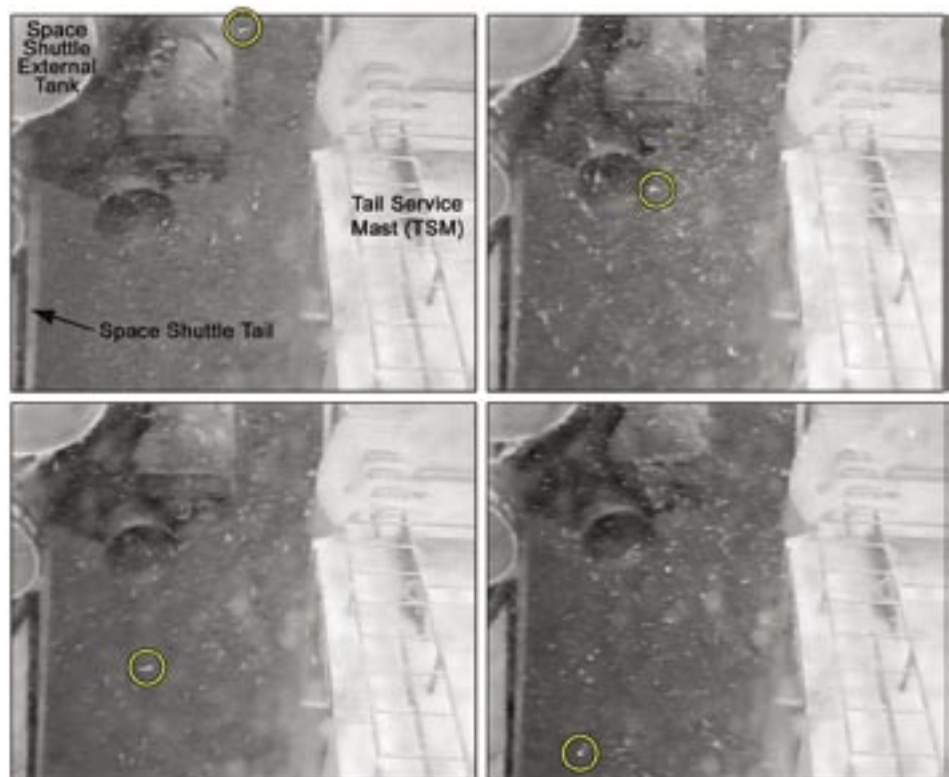


Figure 1. Image Sequence Showing an Object Moving From Top Center (Close to the Shuttle's External Tank) Toward the Bottom Left (Close to the Shuttle's Tail)

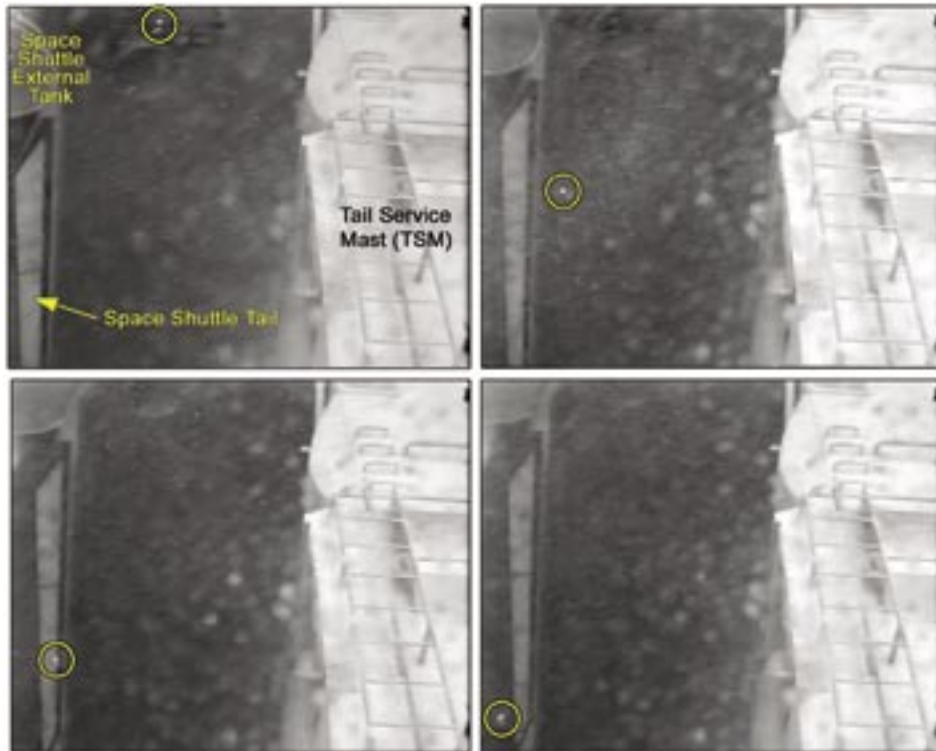


Figure 2. Image Sequence Showing an Object Moving From Top Left (Close to the Shuttle's Engine Exhaust) Toward the Bottom Left (Close to the Shuttle's Tail)

robust system that is not necessarily slower because a multiprocessing CPU approach, where individual CPUs would independently process each primary color, is quite feasible.

The potential applications for real-time moving-object detection and tracking objects in complex image backgrounds include analysis of aerial images, dynamic surveillance, robot vision, detection of moving targets, analysis of traffic flow, and guidance of autonomous vehicles.

Key accomplishments:

- Used as a tool to support the STS-107 investigation.
- Nominated to represent KSC during the 2003 NASA Software of the Year competition.
- Patent submission currently being considered.
- Two of NASA's support contractors (Research Triangle Institute and Southeast Regional Tech Transfer Center) are showing this software as an actual application of image technologies that are being currently marketed.
- Accepted for publication in *NASA Tech Briefs*.

Contact: C.K. Davis (Christopher.K.Davis@nasa.gov), YA-E2, (321) 867-8804

Participating Organization: USTDC (J.A. Dominguez and S.J. Klinko)



Figure 3. Real-Time Tracking Path of the Two Moving Objects (Figures 1 and 2)

A Digital Signal Processing (DSP) Filter Tuned To Detect Diurnal Signals

The predominant mesoscale feature across the Florida peninsula during the summer months is the land-sea breeze oscillation (LSBO). Intense solar heating during the day creates a thermal contrast between the temperature of the air over land (T_a) and the temperature of the air over water (T_w). When T_a sufficiently exceeds T_w , a thermally induced direct circulation occurs in the lowest few kilometers of the atmosphere. Near the surface, air flows from the cooler air mass over water to the warmer air mass over land, whereas a return circulation aloft flows from land to water. As the day progresses, a boundary interface or sea breeze (SB) “front” often develops at the leading edge of this circulation and advances inland. Air rises along this leading edge while air descends above the water, completing the direct circulation. At night, the land breeze (LB) completes this diurnal cycle.

The processing strategy behind an SB detector is based on the diurnal periodicity of the signal. Using a high-order band-pass (BP) filter, based on cascading second-order quadratic sections of figure 1, and coefficients corresponding to a maximally flat Butterworth response, an SB detection time filter is constructed as illustrated in figure 2. The BP filter provides an SB transition time predictor, which is compared with the low-pass (LP)-filtered wind direction signal at every spatial grid point. If the difference between the predicted BP-SB time and the LP-SB time exceeds 6 hours, no SB for that day is assumed.

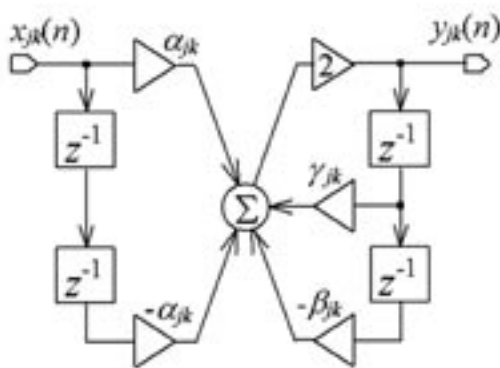


Figure 1. DSP IIR Filter, Second-Order Section Network Diagram

The LP filter is implemented as a moving average filter. The BP filter is a zero-phase recursive filter with $Q = 2$, made up of four second-order sections (i.e., an eighth-order filter). The center frequency f_0 is set to match the 24-hour LSBO period. The zero-phase infinite impulse response (IIR) filter is implemented by summing the outputs of two filters with identical characteristics, where one filter processes a block of data forward in time, and the other filter processes the data backward in time from the end of the block.

Figure 3 shows sample output using 5-minute-duration data samples for July 2000 at grid location $x = 53, y = 47$. Note that the SB filter algorithm fills in missing data by performing a linear interpolation

between end points around the missing data before the LP and BP sections.

Figure 4 displays the SB filter outputs for all grid points on July 6, 2000.

Figure 5 shows the contour of the transition time plot; its gradient is inversely proportional to the SB front-propagation (advection) velocity.

Key accomplishments:

- Completed processing of 5-minute-duration samples of tower data observed in a continuous 24-hour period to develop a time-filtering technique.
- Developed an the SB prediction filter using a recursive BP and nonrecursive LP filter.

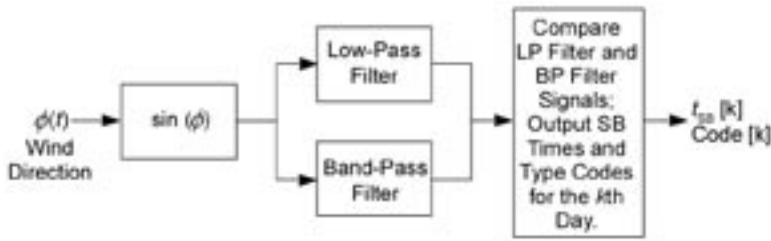
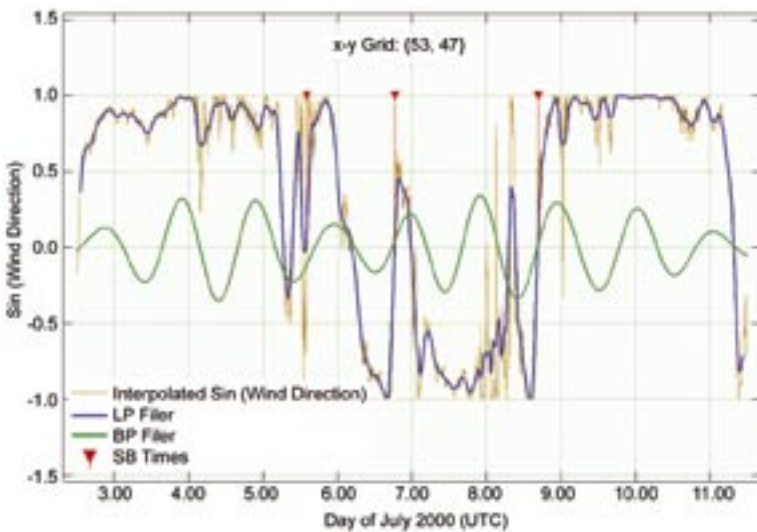


Figure 2. Sea Breeze/Land Breeze Detection Algorithm

- Examined output of SB filter for all days in July and August 2000 and compared to analysis of daily SB transition times; agreement between the SB prediction filter and subjective SB identification was excellent.



Contact: Dr. F.J. Merceret ([Francis J.Merceret@nasa.gov](mailto:Francis.J.Merceret@nasa.gov)), YA-D, (321) 867-0818

Participating Organizations: USTDC (Dr. J.E. Lane and Dr. C.D. Immer) and ENSCO (J.L. Case and Dr. J.T. Manobianco)

Figure 3. Sea Breeze Transition Times, Based on Algorithm From Figure 2

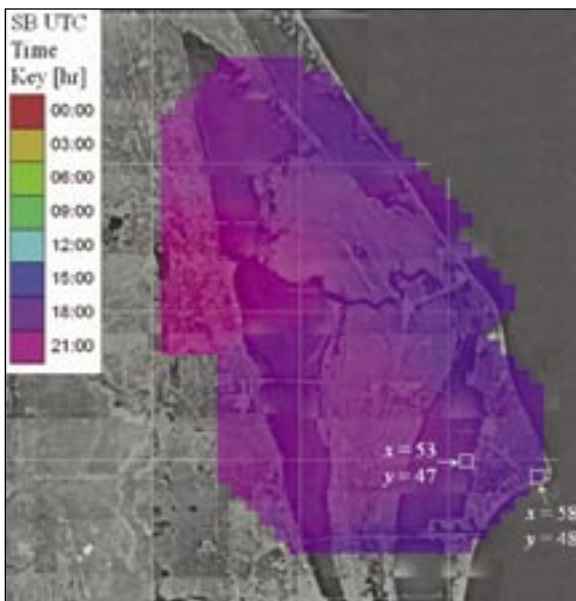


Figure 4. SB Transition Times Spatial Plot From Wind Tower Data

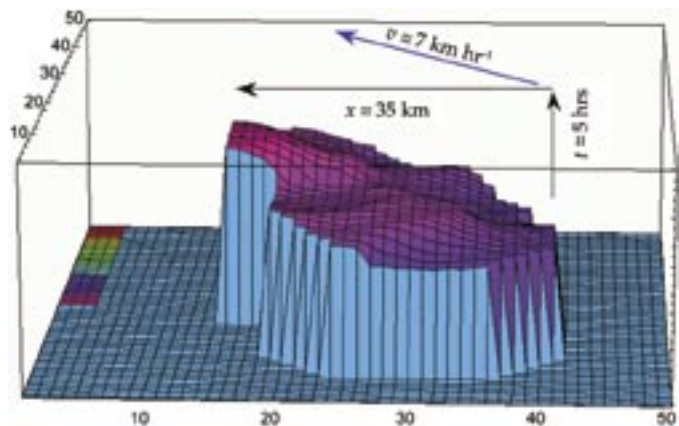


Figure 5. SB Advection Velocity

Image Edge Extraction via Fuzzy Reasoning

Edges carry the most important information in images, and accurate edge detection is vital to perform advanced image processing and analysis. Images of real scenes frequently contain ambiguous and incomplete data. In particular, the problem of determining what is and what is not an edge is compounded by the fact that edges are often partially hidden or distorted by various effects such as uneven lighting and image acquisition noise. Furthermore, images frequently contain data with edgelike characteristics, but a confident classification of this data can be best solved when high-level constraints are imposed on the interpretation of an image.

The fuzzy reasoning approach we implemented to detect image edges significantly surpasses current and widely used edge detection methods. An image of a CD was taken as a sample to compare the methods; the fuzzy reasoning approach shows edges with tiny details that are not detected or properly weighted by other methods. Figure 1 shows the original CD image; figure 2 shows the edge detection performed on the CD image (figure 1) using this new edge detection technique. The technique clearly detects a scratch in the center of the CD and hidden inner circles; it also provides the appropriate weight values to the generated edge map.

Potential uses for this edge detection approach are wide open. It has potential to be a key part of many computer vision applications, including but not limited to pattern recognition, anomaly or defect detection, tumor detection via medical imaging, surveillance, visual motion control, face recognition, object tracking, handwriting recognition, and robotic vision.

Key accomplishments:

- Patent submission being considered.
- Working with two of NASA's support contractors (Research Triangle Institute and Southeast Regional Tech Transfer Center) to market this image technology and generate leads for licensing. Companies in the medical, remote sensing, and biometrics industries will be contacted about the technologies.
- Accepted for publication in *NASA Tech Briefs*.
- Successfully used to preprocess images required by an image analysis application, an automated visual anomaly detection system.

Contact: C.K. Davis (Christopher.K.Davis@nasa.gov), YA-E2, (321) 867-8804

Participating Organization: USTDC (J.A. Dominguez and S.J. Klinko)

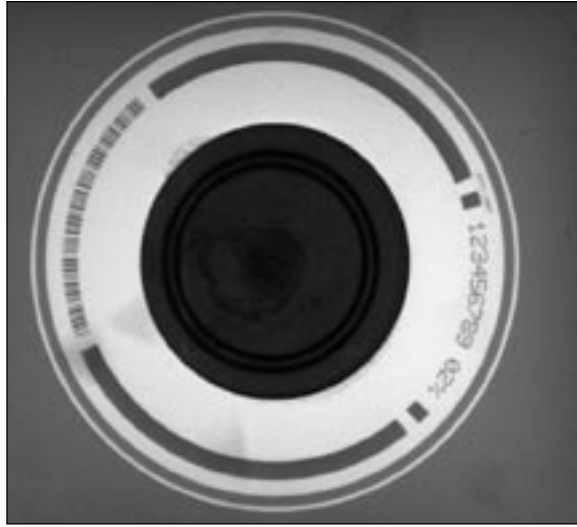


Figure 1. Original CD Image

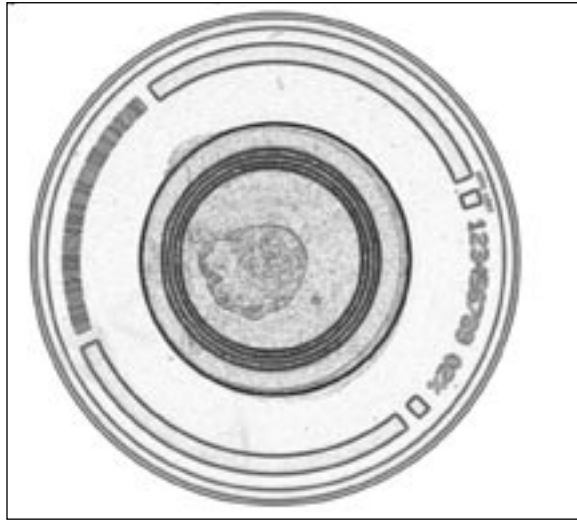


Figure 2. Edge Extraction Based on Fuzzy Reasoning Reveals a Hidden Scratch on the Center of the CD

Noniterative Optimal Image Binarization via Fuzzy Reasoning

Binary image processing is of special interest because an image with binary format can be processed with very fast logical (Boolean) operators. Since most image display systems and software assume images of 8 or more bits per pixel, the binarization of these images usually takes the two extreme gray tones, black and white, which are ordinarily represented by 0 and 255, respectively, in an 8-bit gray-scale display environment.

Usually a binary image is obtained from an 8-bit gray-level image by determining a threshold and assigning the low (0) and high (255) binary values to all gray levels based on the chosen threshold. Obviously, the threshold chosen is critically important since it controls the binary-based pattern classification obtained from the gray-level image. The key issue is to choose an optimal threshold so the number of misclassified image pixels is kept as low as possible.

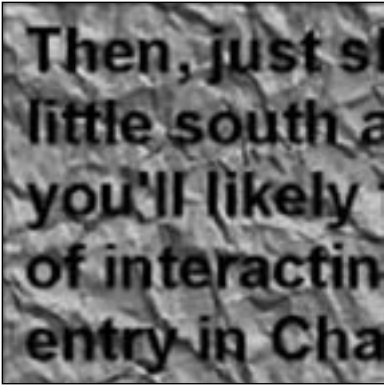
A new fast-computational technique based on fuzzy entropy was developed to find an optimal binary image threshold. In this method, the image pixel membership functions are dependent on the threshold value and reflect the distribution of pixel values in two classes; thus, this technique minimizes the classification error. The proposed method of choosing a threshold surpasses the Huang-Wang and Otsu methods, previously the most reliable and fastest thresholding methods, when the image contains textured background and poor printing quality (see the figures). The new technique provides a much simpler, faster, and more reliable binary segmentation tool for optical character recognition (OCR) application and texture analysis. Since the proposed method requires relatively little computation time (compared with Huang-Wang and Otsu methods), it might be used as a binarization operator within real-time image analysis systems.

Key accomplishments:

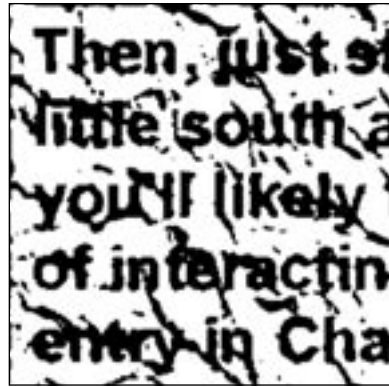
- Patent submission currently being considered.
- Currently working with Research Triangle Institute and Southeast Regional Tech Transfer Center to market this image technology and generate leads for licensing, targeting companies in the medical, remote sensing, and biometrics industries.
- Accepted for publication in *NASA Tech Briefs*.
- Successfully used to preprocess images required by two different image analysis applications, a moving object detection/tracking system and an automated visual anomaly detection system.
- Received Space Act Award granted by NASA Inventions and Contributions Board.

Contact: C.K. Davis (Christopher.K.Davis@nasa.gov), YA-E2, (321) 867-8804

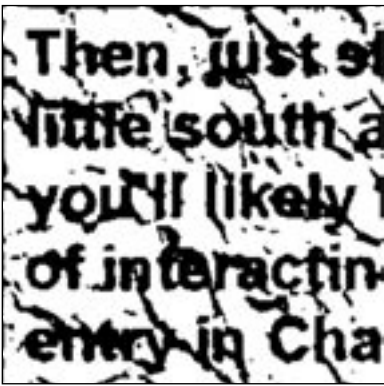
Participating Organization: USTDC (J.A. Dominguez and S.J. Klinko)



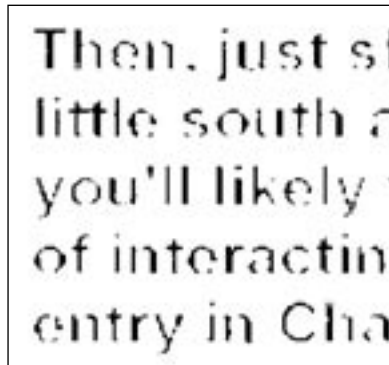
Original Image



Otsu Binarization



Huang-Wang Binarization



Fuzzy-Reasoning-Based Binarization

Converting Analog Test Data to Audio Wave Files

One common method of analyzing any type of data is to first plot the raw data to view its general characteristics and prominent features. Following that initial investigation, the data analyst may implement standard data evaluation algorithms, such as linear or polynomial regressions, data smoothing or filtering, and Fourier transforms to view data features in the frequency domain. All of these data analysis methods have one thing in common – they use our vision analysis system (eyes) to subjectively evaluate data by examining a graphical plot. An automated computer image processing system can be devised to perform a similar type of analysis, without actually creating a plot image.

Another investigative technique that may be equally useful to the data analyst uses our audio analysis system (ears). However, most computer utilities (such as those based on PC office software and spreadsheets) have little capability to perform audio analysis or to create audio from data contained in a data file or spreadsheet.

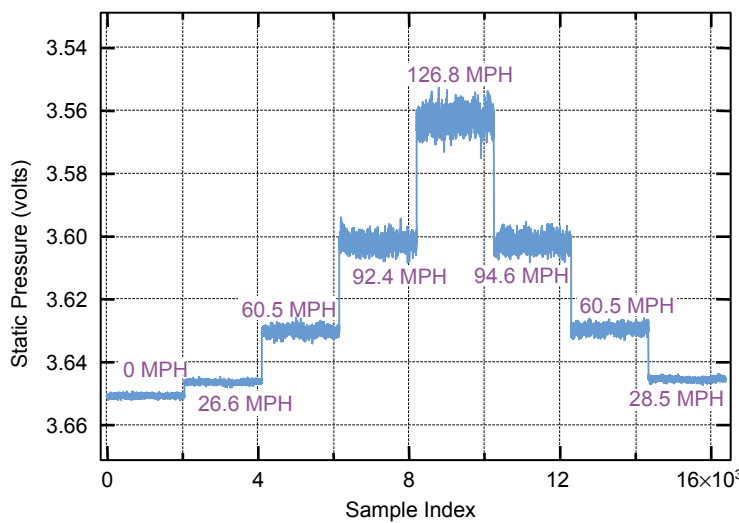


Figure 1. Wind Speed Test Data

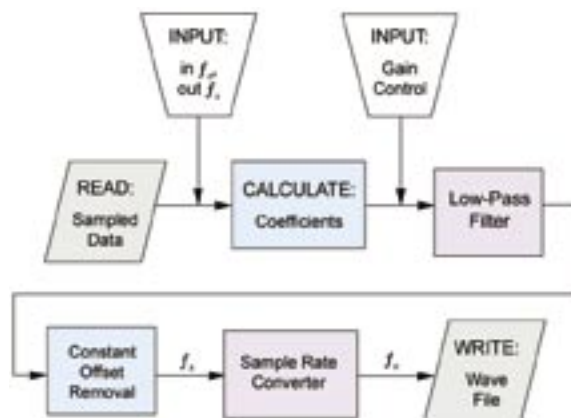


Figure 2. Block Diagram of Data-to-Wave-File Conversion

Figure 1 is a plot of static pressure data acquired from a wind tunnel test of an experimental NASA hurricane wind sensor (see “Extreme-Velocity Wind Measuring System: 3-D Venturi,” KSC Research and Technology 2002 Annual Report). The vertical axis of the plot shows raw pressure sensor output voltage (inversely proportional to the square of wind velocity), while the horizontal axis represents the sample index corresponding to a sample frequency of 100 hertz.

Figure 2 is a block diagram of a system developed at KSC that converts any type of data into a standard audio wave file that can then be played using a standard PC sound utility. The most important processing block in this algorithm is the sample rate converter (SRC). The primary function of the SRC is to generate N output samples for every M input samples. Figure 3 illustrates the effect on a set of 8 input samples for the particular case of $M = 1$ and $N = 20$. The ideal goal of any SRC is to change the number of output samples compared to the number of input

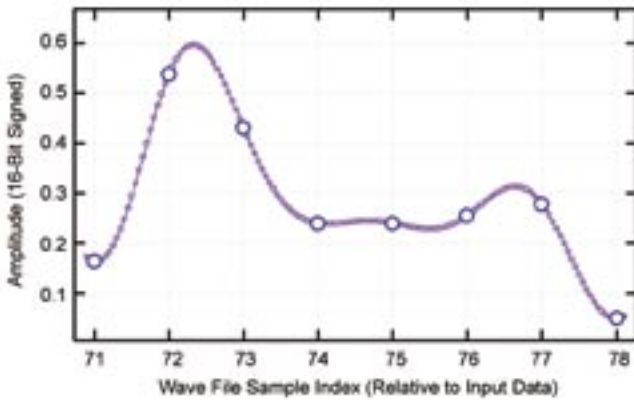


Figure 3. Sample Rate Conversion Example:
20 Output Samples for Each Input Sample

samples without altering the frequency characteristics of the data.

Figure 4a illustrates the result of performing the algorithm represented in figure 2 on the raw data from figure 1, with the gain control suppressed. Figure 4b shows similar data converted to wave file format where the gain control was used to normalize the amplitude as an additional investigative tool. Note that gaps of silence were inserted to audibly segregate the wind speeds.

Key accomplishments:

- Developed a procedure to convert arbitrary data (usually sampled data) to standard audio wave file format.
- Can increase or decrease the pitch (frequency scaling) by a specified amount during the sample rate conversion process.
- Accomplished optional amplitude normalization by amplitude scaling of consecutive frames of data.

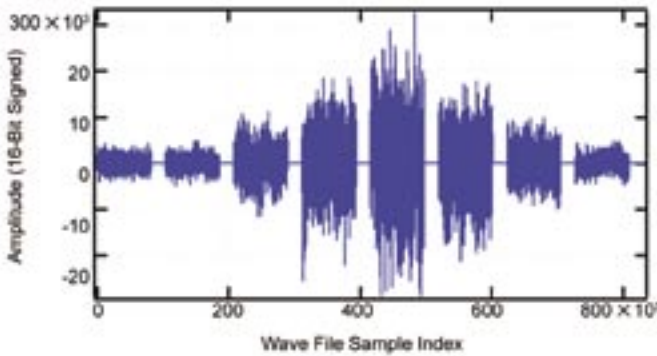


Figure 4a. Audio Wave File of Static Pressure Data

Contact: J.A. Zysko (Jan.A.Zysko@nasa.gov), YA-C3-F, (321) 867-8433

Participating Organization: USTDC (Dr. J.E. Lane)

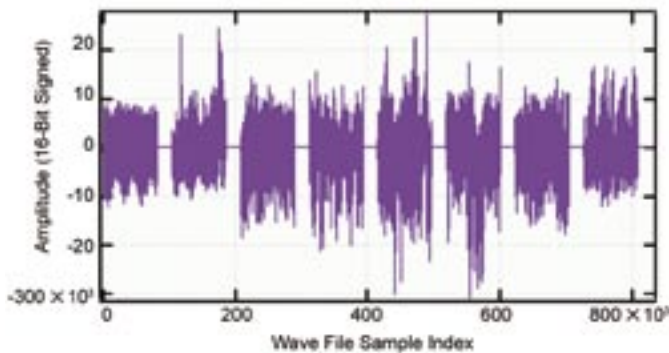


Figure 4b. Wave File of Normalized
Differential Pressure Data

Small Mass Spectrometer System Onboard High-Altitude Research Aircraft WB-57

The KSC Hazardous Gas Detection Laboratory is developing small mass spectrometer (MS) systems for various applications, including leak detection for the Shuttle, possible air quality analysis within the Mini-Payload Logistics Modules from the International Space Station, and automated environmental analysis. To meet these goals, it is necessary to research, design, and develop mass analyzers, sample transport systems, low- and high-vacuum pumps, and control circuitry that are small, lightweight, and rugged and provide rapid, accurate, and component-specific information.

The Aircraft-Based Volcanic Emissions Mass Spectrometer (AVEMS) is the first system developed under the Advanced Hazardous Gas Detection System plan. The goal of this multiyear plan is to develop small, lightweight, portable, and power-efficient MS systems for various types of gas analysis. Developing the AVEMS instrument had two specific goals: (1) to determine the Hazardous Gas Detection Laboratory's current ability to build small, lightweight systems capable of high-altitude flight and (2) to monitor volcanic emissions. The first goal was met by integrating the system into a WB-57 high-altitude research plane (figure 1). AVEMS has a total weight of 104 pounds and a volume of 3 cubic feet. It requires 350 watts of power at steady state, can operate at a temperature range of +25 degrees Celsius ($^{\circ}\text{C}$) to -65°C , and has a pressure range of 760 to 50 torr. Within this range, the system operated properly up to an altitude of 41,000 feet above sea level (asl).

The second goal was met in various ways. First, the system was mounted in the WB-57 and flown over several Costa Rican volcanoes at a typical altitude of 5,000 feet above ground level (agl). At this altitude, it was difficult to quantify components characteristic of volcanic emissions, such as helium (He), carbon dioxide (CO_2), sulfur dioxide (SO_2), hydrogen sulfide (H_2S), and various organic compounds. However, as the WB-57 flew through the volcanic plume, the instrument clearly showed a concentration rise for water, CO_2 , H_2S , and organic compounds.



Figure 1. AVEMS in the WB-57 Payload Bay



Figure 2. Operation of AVEMS at Turrialba Volcano in Costa Rica

It was also desirable to demonstrate the portability of the system. For this, two people carried the AVEMS into Turrialba volcano (10,960 feet asl) where several fumaroles were analyzed (figure 2) and compared with the air just 30 feet away. Figure 3 shows a significant difference between the gas evolved from four separate fumaroles and the ambient air around the fumaroles. Fumaroles 1 through 4 have significant amounts of CO₂, SO₂, and H₂S, with minimal amounts of nitrogen (N₂) and oxygen (O₂). A mere 30 feet away, the concentrations are similar to normal air. Each compound has a different sensitivity. AVEMS will not only enable scientists to better understand volcanoes but will also help in the development of smaller, more robust systems for many different applications.

Key accomplishments:

- Reduced size of quantitative MS system.
- Reduced system weight.
- Improved system ruggedness.
- Detected components over/in volcanoes.
- Achieved autonomous operation.

Key milestones:

- Further reduce size and weight.
- Improve detection limits.
- Explore other applications such as air quality monitoring, hazard warning, and mobile leak detection.

Contacts: F.W. Adams (Frederick.W.Adams@nasa.gov), YA-D7-E1, (321) 867-6671; Dr. T.P. Griffin, YA-F2-C, (321) 867-6755; and D.W. Follistein, YA-D7-E1, (321) 867-6747

Participating Organizations: USTDC (Dr. CR. Arkin, G.R. Naylor, W.D. Haskell, D.P. Floyd, C. Curley, and N.N. Blalock), University of Costa Rica (Dr. J.A. Diaz), Costa Rica Center for High Technology (CENAT) (Dr. J. Azofiefa), JSC CB/ASPL (Dr. F. Chang-Diaz), YA-D1 (P.G. Henderson), and PH (J.J. Edelman, S.K. Czaban, and R.J. Beil)

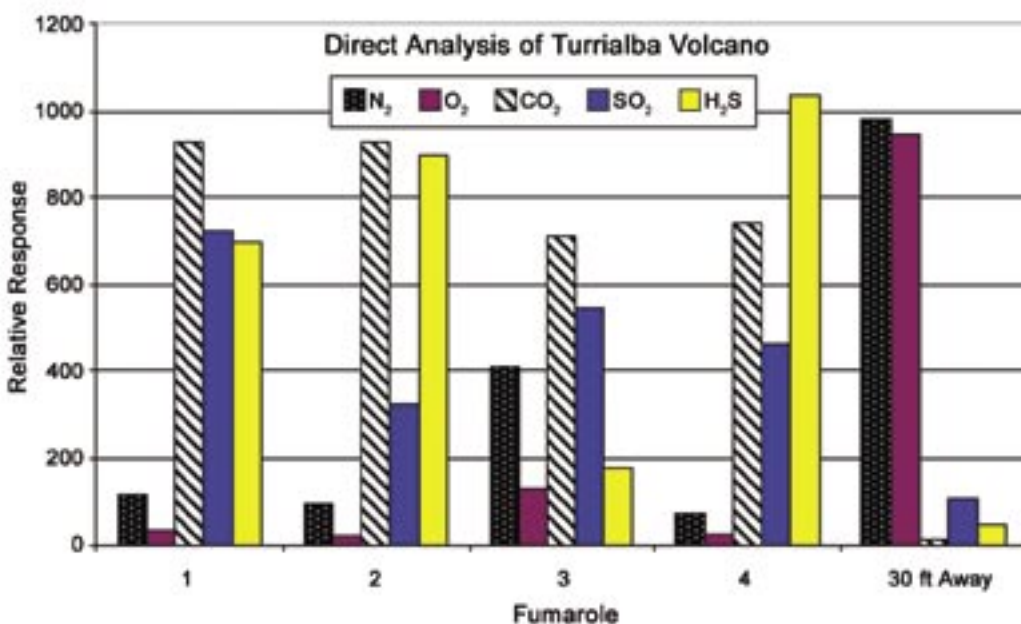


Figure 3. Analysis of Fumaroles at Turrialba Volcano in Costa Rica

Advanced Data Acquisition System (ADAS)

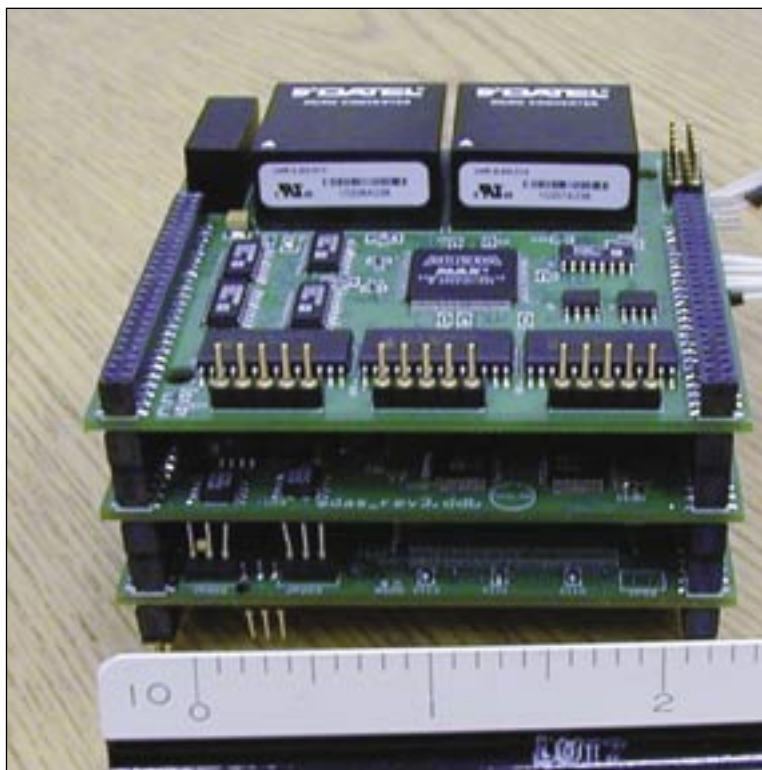
Current and future requirements of the aerospace sensors and transducers field call for the design and development of highly reliable, cost-effective data acquisition devices and instrumentation systems. New designs that incorporate self-health, self-calibration, and self-repair capabilities allow for greater measurement reliability and extended calibration cycles. With the addition of power management designs and components, state-of-the-art data acquisition systems allow data to be processed and presented with increased efficiency and accuracy.

A smart signal conditioning amplifier was designed incorporating these requirements. This device provides increased reliability by automatically rerouting signals through different paths when the processor identifies a component malfunction. It addresses the issues of signal redundancy and signal integrity without taking the traditional and costly approach of providing total hardware redundancy for every channel and every function block of a data acquisition system.

In addition to signal redundancy issues, the need for self-calibration verification played a defining role in the architectural approach. Data acquisition systems such as those used in spacecraft need the ability to calibrate automatically without external intervention. Furthermore, the quality of the measurement provided by the system is directly related to the system's ability to ensure a proper calibration through the life of the process being monitored. Finally, the data acquisition system's ability to check the system's health, detect and predict failure, and repair itself is critically important in systems where operator intervention is not possible.

Enhancements to the Advanced Data Acquisition System (ADAS) include the incorporation of new, commercially available components such as field-programmable gate arrays (FPGAs), field-programmable analog arrays (FPAAs), and digital signal processing (DSP) electronic/system controls. The ADAS architecture has been divided into three main components: Analog Signal Module, Digital Signal/Control Module, and Power Management Module.

The Analog Signal Module provides signal redundancy and signal integrity without costly, total hardware redundancy. It also provides self-calibration verification and the ability to perform system health checks, failure detection and prediction, and automated self-repair that is critical for inaccessible systems such as those in deep space. The Analog Signal Module employs an innovative concept called "spare parts – toolbox." Based on the reliability ratings given to the different areas of the system, the design provides the toolbox with n number of spare parts (components) necessary to ensure continued operation. The number of each type of spare part in the toolbox is related to its probability of failure. Areas with higher failure probabilities (because of user interaction and/or environment) are stocked with a greater number of spare parts than areas well protected by the system (lower probability of failure). The number of spare parts contained in the toolbox will diminish deeper into the system, where external factors have less effect.



ADAS Prototype Modules

The Digital Signal/Control Module controls, monitors, and processes analog signals. It also monitors the health of the system by processing defined measurements and/or trends. The Digital Signal/Control Module also implements the “spare parts – toolbox.” The architecture consists of one or more processors and FPGAs. Mean time between failure and redundancy requirements determine the final number of processors and FPGAs used in the design.

The Power Management Module (PMM) monitors, controls, and manages the power supply to the different sections of the system. To monitor and control the various functions, the PMM uses several processors, each with an associated watchdog circuitry that resets the processor if a problem is detected. Since processors operate in parallel under the same set of rules, control is handed off following the failure of one of the processors without power disruption. The processors can also decide whether circuitry must be powered down following the detection of an anomaly.

The ADAS firmware monitors input signals, controls the output lines, and performs signal processing. It detects signal path failures and performs self-repairs and periodic calibrations on the Analog Signal Module.

ADAS provides innovative solutions to problems associated with traditional data acquisition methods. It has been awarded a U.S. patent, and Circuit Avenue Netrepreneurs, LLC, has licensed rights to this technology.

Contacts: J.M. Perotti (Jose.M.Perotti@nasa.gov), YA-D5-E, (321) 867-6746; and A.R. Lucena, YA-D5-E, (321) 867-6743

Participating Organization: USTDC (Dr. P.J. Medelius, Dr. C.T. Mata, B.M. Burns, and A.J. Eckhoff)

Visual Anomaly Detection System Prototype

The Visual Anomaly Detection System finds anomalies or defects in real time under normal lighting operating conditions. The application is basically a learning machine that integrates the three elements of soft computing (fuzzy logic [FL], artificial neural network [ANN], and generic network [GA] schemes) to process the image, run the learning process, and finally detect the anomalies or defects. The system acquires the image, performs segmentation to separate the object being tested from the background, preprocesses the image using fuzzy reasoning, performs the final segmentation using fuzzy reasoning techniques to retrieve regions with potential anomalies or defects, and finally retrieves them using a learning model built via artificial neural and generic network techniques.

Fuzzy logic provides a powerful framework for knowledge representation and overcomes uncertainty and vagueness typically found on image analysis. ANN provides learning capabilities, and the GA approach leads to robust learning results. The system may run on either a regular PC under Windows NT or as an embedded version for portability.

The system acquires the images from a video camera via either an analog or digital image grabber. Using fuzzy reasoning, the image undergoes preprocessing including primary segmentation, object extraction, enhancement, filtering, and edginess detection. An adaptive fuzzy threshold converts the preprocessed image to binary code, and a selective blob detector picks image regions with high edginess activity. The system computes morphological, geometrical, and fuzzy edginess grading values for each region and uses them as inputs of the learning feature via GA-ANN schemes.

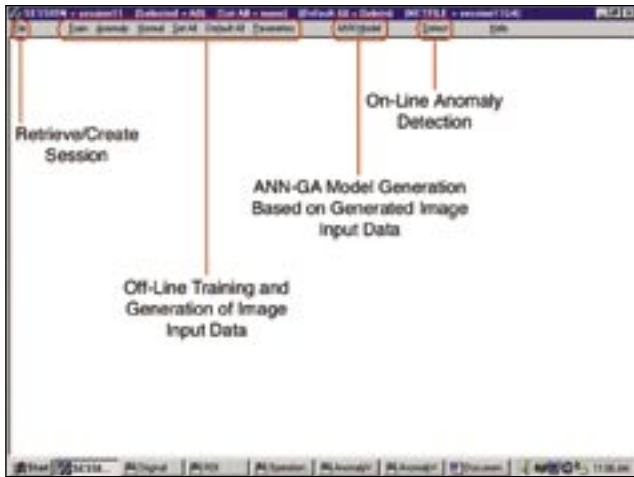
NASA built the Cable and Line Inspection Mechanism (CLIM) to automate image acquisition of the fourteen 1,000-foot slidewires used in the emergency egress system for the Space Shuttle at KSC. CLIM eliminates the hazardous, manpower-intensive, and time-consuming methods previously required to manually maintain the emergency egress system at peak performance. Inspecting the emergency egress system using CLIM still requires a person to continuously watch cable images for more than 48 hours.

The intelligent Visual Anomaly Detection System will be integrated into CLIM to completely eliminate the need for human involvement in detecting anomalies; the system will not only detect the anomaly but also document it. Images acquired by CLIM are being used to test the intelligent Visual Anomaly Detection System. Preliminary tests, using images recorded from a slide basket cable mounted in the laboratory, show promising results.

Because there is no need for special lighting, the potential applications of this anomaly detection system in an open environment are quite wide. One immediate application at KSC is the detection of anomalies on the Space Shuttle Orbiter's radiator panels. Potential applications include automated visual inspection of spacecraft, ground, and flight equipment. The embedded portable version of this system could make visually inspecting this type of



CLIM Being Tested at KSC Space Shuttle Launch Pad



Software Main Menu Holding All the Options Used To Run the Anomaly Detection System



On-Line Anomaly Detection Performed by the System and Displayed on the Screen

equipment (including spacecraft fuselage) quite feasible in an open environment.

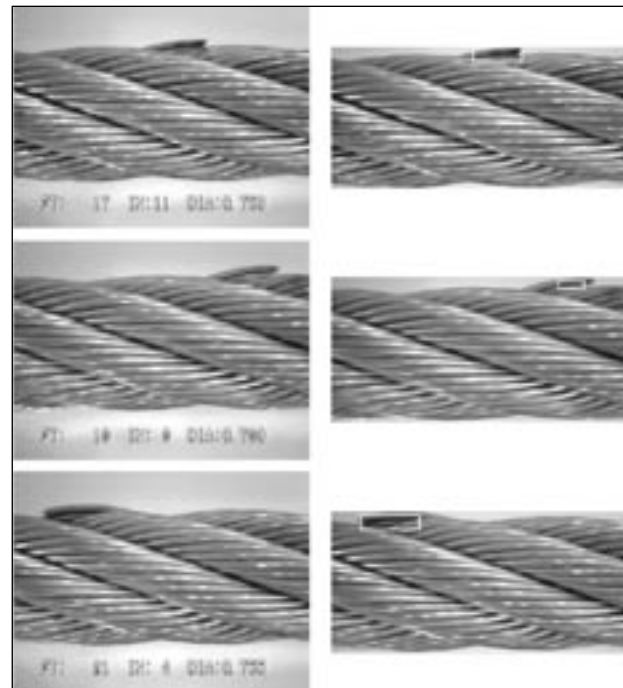
The fuzzy operators built to preprocess the image can be incorporated into other computer vision systems. Adaptive image thresholding via fuzzy reasoning, one of the image analysis features used to build this anomaly system prototype, plays a key role in a system prototype currently being implemented at KSC to detect foreign object debris (FOD) in real time during the Space Shuttle liftoff.

Key accomplishments:

- Patent submission currently being considered.
- Research Triangle Institute and Southeast Regional Tech Transfer Center are demonstrating this system as an application of currently marketed image technologies.
- Accepted for publication in *NASA Tech Briefs*.
- Presented at the Institute of Electrical and Electronics Engineers (IEEE) International Conference on Fuzzy Systems and Soft Computing.

Contact: C.K. Davis (Christopher.K.Davis@nasa.gov),
YA-E2, (321) 867-8804

Participating Organization: USTDC (J.A. Dominguez and S.J. Klinko)



Three Different Anomalies Detected and Displayed Under the Same Anomaly Class

Wireless Inclinometer

The Shuttle Orbiter hang angle operation is performed at every processing flow to ensure the Orbiter is within a specified range of inclination prior to transfer and mating with the External Tank-Solid Rocket Booster assembly. The current methodology uses a mechanical vernier inclinometer and processes that are both time- and labor-intensive. With so few cost-effective technological advances available in the field of angular measurement, these methods remained the best choice.

After an Orbiter has been processed for flight but before it leaves the Orbiter Processing Facility, the current operations require an angular measurement while the Orbiter is still in the horizontal position. Upon the Orbiter's arrival in the Vehicle Assembly Building and prior to being mated with the External Tank, another measurement is taken in the vertical position. If the angle is within required specifications, the Orbiter is ready to be mated. The present method requires two technicians to carefully maneuver a hydraulically operated mobile man-lift into a predetermined location along the payload bay doors and use a mechanical vernier measuring device to obtain the required measurement. This method not only introduces several potential sources of error but can also put flight hardware and personnel in danger.

Recently, economical high-precision measurement devices were joined with a very successful, proven wireless design to provide a complete, all-in-one, dependable measurement system. The Wireless Inclinometer System is composed of two main sections: the Wireless Inclinometer Module (WIM) and the handheld Central Station Data Collection Console (CSDCC). WIM involves the construction of an adapter plate that will mate with the Orbiter aft fuselage compartment access door. This section is composed of the following:

- A commercial off-the-shelf inclinometer.
- A wireless radio frequency (RF) transceiver module.
- A power management module.
- A power supply for the unit, currently composed of four C batteries.
- Embedded smart software algorithms.
- Other components necessary for the proper functionality of the system (antenna, etc.).

The design ensures proper and consistent location of the interface plate and minimizes measurement uncertainties caused by the plate-Orbiter interface and plate-inclinometer interface. The overall uncertainty of the measurement is anticipated to be 0.1 degree of inclination or less to meet the customer's requirements.

The handheld CSDCC consists of a portable ac/dc-powered display console that houses:

- A low-power single-board computer.
- Wireless RF transceiver module.
- Application-specific power management and distribution module.
- Embedded smart software algorithms.
- Other components necessary for the proper functionality of the system (antenna, etc).

The software algorithm configures the Wireless Inclinometer System for operation, acquires the information required by the user, displays and stores the information required by the user, and performs RF communication health checks of the system. Both the WIM and the handheld CSDCC contain the embedded software of the system.

General system software requirements include the ability to calculate and display the inclination accurately to within 1.0 degree, calculate and display actual inclination and relative (or offset) inclination, indicate mode of display (actual/relative), and display battery status of both the WIM and the handheld CSDCC.

The CSDCC can retrieve measurements, calculate averages, and display the inclinations. The CSDCC can also select a measurement to be used as a future reference value; check the remaining battery life, RF signal strength, and remote-unit temperature; and time-stamp and log data for later retrieval.

Incorporated in the WIM is an innovative power management system designed to keep power consumption to a minimum and extend battery life. Communications receivers operate on a low percentage of the duty cycle, and the transmitter power does not exceed 10 milliwatts. The wireless communications network has been incorporated into numerous recent designs and has a proven track record for reliability and robustness.

The new wireless inclinometer will provide an improved method of data acquisition. Measurements will be recorded from high-accuracy digital readouts. The equipment can be mounted and left in place during Orbiter moves and conveniently checked without additional manpower and equipment such as the mobile man-lift.

Key accomplishment:

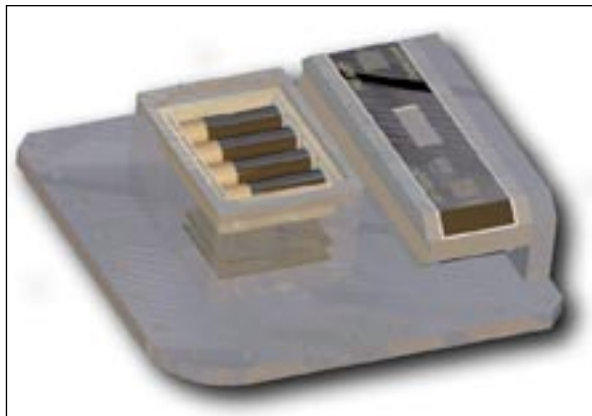
- Developed, fabricated, and preliminarily tested the prototype sensing unit and handheld CSDCC.

Key milestones:

- October 2003: Testing of integrated system.
- December 2003: System ready for operational testing within an Orbiter process flow.

Contacts: J.M. Perotti (Jose.M.Perotti@nasa.gov), YA-D5-E, (321) 867-6746; and A.R. Lucena, YA-D5-E, (321) 867-6743

Participating Organization: USTDC (A.J. Eckhoff, N.N. Blalock, B.M. Burns, Dr. C.T. Mata, and J.J. Randazzo)



Wireless Inclinometer Module (Rendition)



Handheld Central Station Data Collection Console

Enhanced Wireless Vacuum-Jacketed Line Sensor Network

The Space Shuttle launch pads and Mobile Launcher Platforms (MLPs) have several hundred feet of transfer lines for liquid oxygen (LO₂) and liquid hydrogen (LH₂) systems. The lines are used to transfer LO₂ and LH₂ to the Space Shuttle External Tank to be used as propellants for the main engines. The transfer lines consist of sections that are kept insulated using vacuum-jacketed (VJ) lines. This helps the LO₂ and LH₂ keep their liquid form and prevents boiloff.

In the transfer lines, sensors are installed for detecting vacuum within the VJ line. When vacuum is lost, this section of the transfer line is pumped down to the desired level. Currently, United Space Alliance (USA) personnel measure the vacuum level of the transfer lines manually. This requires connecting a special gage to a vacuum sensor, recording the reading, and disconnecting the gage. This is performed for each sensor in the transfer lines.

The Wireless Vacuum-Jacketed Sensor Network is designed to eliminate manual measurements of all VJ sensors installed in the transfer lines. The system will consist of a central station (CS), base station, and numerous remote stations. The only hardware interface required for each remote station is the connection to the already-installed vacuum sensor. Due to restrictions on electromagnetic interference (EMC) around some Space Shuttle systems, the radio frequency (RF) power output was kept to a minimum (10 milliwatts).

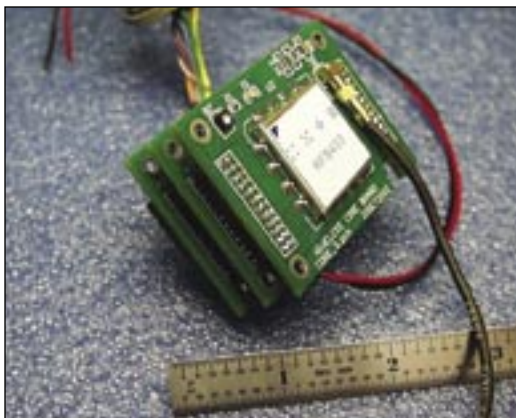
The CS is a rack-mountable industrial computer with a touch screen. The CS automatically performs the following tasks:

- Provides a direct wireless interface to the remote stations.
- Polls active remote stations for data and health status, coordinates frequency assignments, and performs trending analysis.
- Provides data collection and storage for VJ sensor measurements.
- Automatically provides system health data to selected users via e-mail.
- Offers remote data access via Ethernet for valid users.

Each remote station consists of a battery pack, antenna, small enclosure, power board, RF/core board, and analog board. The remote station boards are integrated into one stack. These electronics will be installed in an extreme environment and flammable commodities. It is important to protect them against the harsh environment with an intrinsically safe design.



Central Station Front Panel Display



Remote Station Boards

The power board manages the use of battery power. It cycles the power of the RF/core board and provides power to the analog board only when required. This minimizes battery pack replacement to once every 2 years when acquiring and transmitting data twice a day. Unlike the RF/core board, the power board is always on. It has a low-power microcontroller that manages the power cycles and stores the remote station configuration data. It performs a limited health check by tracking successful communications between the remote station and the CS. It automatically reconfigures the remote station to use an alternate frequency if communication errors persist.

The RF/core board contains a microcontroller and the RF module. Its main functions are to control the RF module and acquire data from the VJ sensor. It detects incoming transmission packets from the CS and validates the remote-station ID number. Once a valid command is received, the RF/core board coordinates with the power board for power requirements, executes the command, and transmits a formatted response to the CS. In addition, the RF/core board digitizes analog signals, contains calibration data used for compensating temperature effects, provides data acquisition and control of the analog board, and provides the communication protocol. The analog board supplies the excitation signal to the sensor, performs signal conditioning, and contains an analog-to-digital converter.

Each remote station is designed with a robust RF communication scheme. Each remote station can operate on alternate multiple preprogrammed frequencies assigned by the CS. A remote station is also capable of serving as a relay station from the CS to another remote station. This may be necessary when direct communication between the CS and a remote station cannot be achieved due to an out-of-range condition or when a structure is in the way.

Key accomplishments:

- 2002: Designed and tested the CS and remote station including hardware and software.
- 2003: Incorporated a health monitoring scheme, out-of-bounds notification to the user via e-mail, and an intrinsically safe design for the remote stations.

Key milestone:

- Install 40 field-rated remote stations and a CS for the LO₂ transfer line.

Contacts: J.M. Perotti (Jose.M.Perotti@nasa.gov), YA-D5-E, (321) 867-6746; and A.R. Lucena, YA-D5-E, (321) 867-6743

Participating Organization: USTDC (Dr. P.J. Medelius, Dr. C.T. Mata, B.M. Burns, N.N. Blalock, A.J. Eckhoff, and J.J. Randazzo)



Field-Rated Remote Station

A Field Prototype System for Vacuum-Drying Shuttle Tiles

Removing water from the thermal protection system tiles is a common Orbiter processing problem. The heat of reentry burns out some of the waterproofing in these tiles, and if the Orbiter is exposed to water before new waterproofing can be applied, the tiles will absorb and hold water, which must be removed. This is currently done by heating the tiles with heat lamps to boil the water out and using infrared (IR) cameras to determine if moisture is still present once the tile returns to thermal equilibrium. A new method of vacuuming air and water out of the tile appears to be faster, to remove more water, and to have fewer adverse side effects than the heating technique.

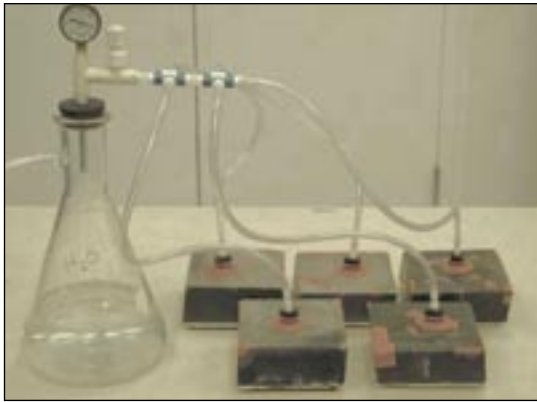


Figure 1. In-Lab Vacuum System (The vacuum line comes in from the left to a flask acting as a water separator. Attached to the flask is a one-to-five splitter allowing the vacuum to be routed to five tiles. Connection to the tiles is made via soft, silicon rubber suction cups placed over the waterproofing holes on each tile.)

A field prototype is capable of pumping multiple tiles at once from a single vacuum source (figure 1). Leading from an in-house vacuum system, 1/4-inch Tygon tubes ending in 2-inch-diameter silicon suction cups are fitted over the waterproofing holes of five Shuttle tiles and the water trapped in the tile is pulled out. The lines from the five tiles are combined in a manifold and sent into a water separator flask. The flask is maintained at vacuum.

The five-tile test was successful and well received by Operations, and the approach was scaled up to a full field prototype system. To quiet the operation, the vacuum system in the Orbiter Processing Facility (OPF) was used. This system pulls up to 750 standard cubic feet per minute (scfm) at a vacuum of 8 conventional inches of mercury (inHg). In testing, a vacuum pressure of 5 to 6 inHg was used and 1 scfm was pulled through each tile. Therefore, the OPF system may be capable of pulling water out of hundreds of tiles at the same time, but this may be limited by in-line pressure drops. Measurements were taken in the OPF and over 30 scfm could be pulled at about 7.5 inHg at any one of the 1-1/2-inch-diameter access ports into the vacuum system. It was decided to develop a system capable of drying 25 tiles simultaneously from any one access port in the OPF.



Figure 2. Water Separator Attached to the OPF In-House Vacuum System Through a 1-1/2-Inch-Diameter Vacuum Line

Figure 2 shows a water separator attached via a grounded vacuum line to one of the OPF vacuum ports. The vacuum line from the tank is connected to a five-to-one manifold (figure 3) where gray lines can be split off from the primary vacuum hose. Each gray line splits further into five 1/4-inch-diameter Tygon lines ending in a suction cup. This system can draw a vacuum of about 6 to 7 inHg at each of 25 suction cups, each with a flow rate of over 1 scfm. Figure 4 shows all 25 lines attached to a Plexiglas panel with holes simulating the tile waterproofing holes. Figure 5



Figure 3. Vacuum Line From the Water Separator Entering a Manifold

shows 10 lines drawing water from individual Shuttle tiles. Shuttle Operations personnel have been very pleased about the prospect of using the new vacuum system. Benefits of vacuum drying include:

- Time: Running eight vacuum systems simultaneously for 1 hour per tile, about a third of the Shuttle tiles can be dried in a standard workweek. Pulling the majority of the water from the tile allows evaporative drying to complete the moisture removal.
- Electricity Use: The vacuum system uses the OPF in-house vacuum that operates continuously, requiring no additional electrical power.
- Quantification: The vacuum system captures and measures the water pulled out of the Orbiter.
- Use of IR Camera: Recovery to ambient temperature should be faster.
- Access to Tiles: The vacuum system allows access to any tile on the Orbiter.
- Visibility: The clear Tygon tubing makes the water flow visible.



Figure 4. All 25 Lines Attached to a Plexiglas Sheet Into Which Small Holes Were Drilled Simulating the Waterproofing Hole on the Shuttle Tiles (There is sufficient vacuum through the system for the lines to easily carry their own weight.)

Contact: Dr. R.C. Youngquist (Robert.C.Youngquist@nasa.gov), YA-C3-E, (321) 867-1829

Participating Organization: USTDC (J.M. Surma, T.R. Hodge, and S.L. Parks)



Figure 5. Ten of the Possible 25 Lines Pulling Water Out of Shuttle Tiles

Shuttle Tire Pressure Monitor Calibration Station

While traditional calibration methods acquire sensor voltages using digital multimeters, the new Tire and Strut Pressure Monitor (TPM) calibration procedure acquires voltage readings directly from the analog-to-digital (A/D) converter of the device. This is achieved after calibrating the A/D converter with an in-house-developed linearization algorithm. These voltages are then sent to a computer for processing. A multinomial curve-fitting algorithm is then applied to generate the calibration coefficients of the TPM. This procedure provides better curve fitting and significantly reduces uncertainties and the cost of the calibration station since no digital multimeters are needed. Furthermore, the calibration station is automated, so highly skilled personnel are not needed to perform routine calibrations.

The TPM is a handheld system to accurately measure Orbiter tire and strut pressures and temperatures over wide temperature ranges, as well as to improve personnel safety by reducing the pressurized volumes in the measuring device. The design places a highly accurate pressure sensor (also used as a temperature sensor) as close to the tire or strut measurement location as possible, allowing the user to make accurate measurements rapidly, minimizing the amount of high-pressure volumes, and allowing a reasonable distance between the tire or strut and the operator. The stringent requirements of the TPM made calibrating it a challenge.

The original TPM calibration station consisted of a pressure standard, an environmental chamber, a precision voltage source, two digital multimeters, and a computer. Reflecting the traditional approach, the calibration algorithm created a table of several pressures and temperatures for which sensor voltages were recorded using the digital multimeters. These voltages were then used to calculate the coefficients of a multinomial that would fit the gathered data. The procedure was implemented, and through several data verification tests, it was found that the TPM did not meet the desired accuracy (although it was within the requirements). Measurement uncertainties included nonlinearities and hysteresis of the temperature and pressure sensors and A/D errors (integral linearity error, differential linearity error, transition noise, full-scale error, full-scale error drift, etc.) of the TPM. The calibration station also required expensive laboratory equipment and too many man-hours of highly skilled personnel, making its implementation very costly.

To eliminate some uncertainties and to improve the accuracy of the TPM, the pressure and temperature sensor voltage readings were taken directly from its A/D converter. This procedure was performed by first calibrating the analog circuitry of the TPM, which brought the voltages from the A/D converter within acceptable error limits. As a result, the digital multimeters were no longer needed and were removed from the calibration station. The voltages read by the A/D converter were transmitted to a computer and used to calculate the calibration coefficients. The new approach resulted in approximately half the uncertainties of the traditional approach, and the cost of the calibration station was reduced by about half.

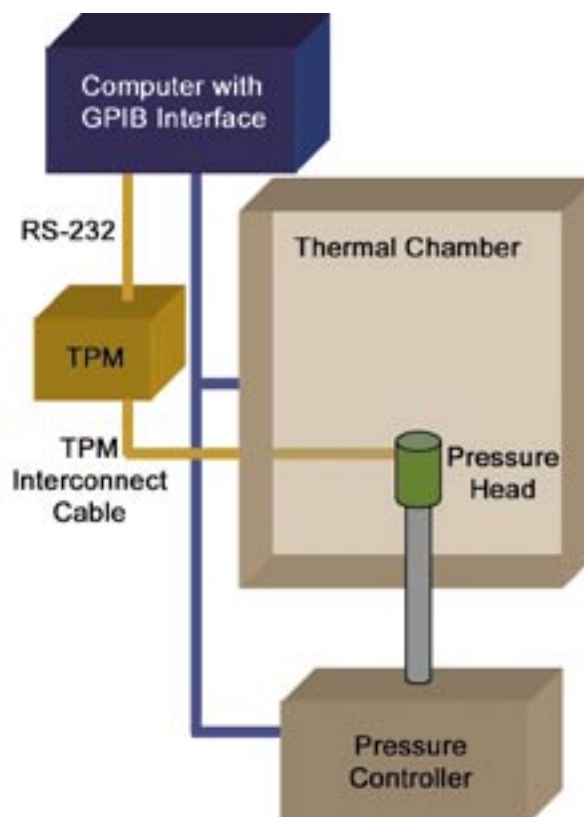
The calibration station now consists of a pressure standard, an environmental chamber, a precision voltage source, and a computer with custom software to control the calibration process.

The following are novel features of the calibration station:

- Sensor voltages are taken directly from the TPM A/D converter, avoiding the use of costly multimeters.
- Uncertainties of traditional calibration stations are reduced by half.
- Reduction in equipment use results in significant savings on the cost of the calibration station.
- Automated calibration process requires fewer highly skilled personnel and results in significant man-hour savings.

Contact: J.M. Perotti (Jose.M.Perotti@nasa.gov), YA-D5-E, (321) 867-6746

Participating Organization: USTDC (Dr. C.T. Mata, B.M. Burns, and R.T. Deyoe)



Block Diagram of the TPM Calibration Station

is composed of a vacuum pump, a single-board computer, power supply modules, a pressure standard, communication ports, and a VJ thermocouple gage signal conditioner (see the block diagram in figure 1). If the pressure read by a VJ thermocouple is higher than allowed, that section of the line is pumped down using the VJ calibration station in line with the vacuum pump. The pressure of the line is measured by a pressure standard, and the VJ thermocouple output is monitored as the line is pumped down. The readouts are stored in the single-board computer and used to characterize that particular VJ thermocouple sensor. As a result, a characterization curve is obtained and the sensor is calibrated. This in situ calibration method is extremely practical because the regular pumpdown procedure is not altered; yet the calibration of the sensors is realized. The uncertainties of wrong measurements are now minimized because sensor degradation can be identified as long as calibration is performed within certain periods.

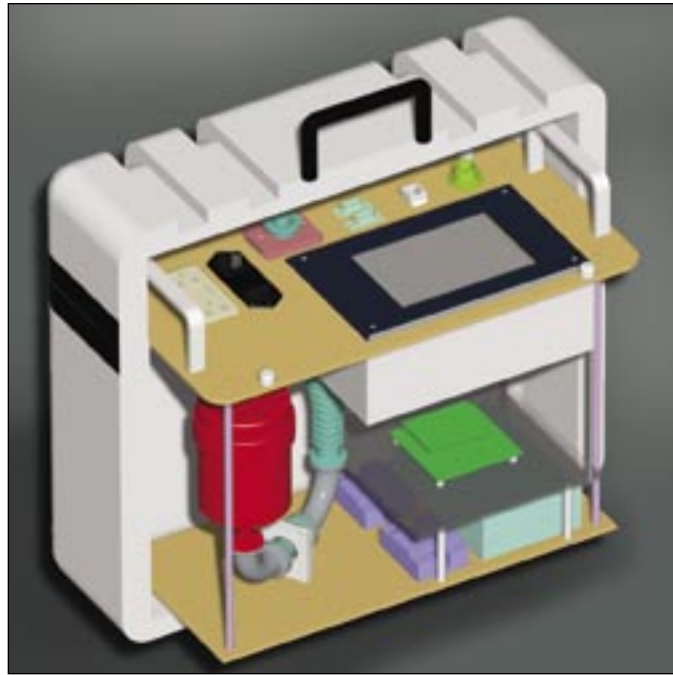


Figure 2. A View of the VJ Calibration Station in Its Conceptual Stage

The VJ calibration station (except for the vacuum pump) is enclosed in a light, weatherproof case that can easily be taken anywhere along the cross-country VJ line (see figure 2).

The following features are considered novel improvements to the existing system:

- The calibration station is used in-line with the existing vacuum pump without altering the pumpdown procedure.
- Readout uncertainties due to out-of-calibration or degraded sensors are minimized by calibrating the thermocouple sensors when the VJ line sections are pumped down. In situ calibration is achieved by characterizing the VJ thermocouple sensor with a pressure standard as the line is being pumped down.

The VJ calibration station is expected to be finished by the end of FY 2003 and to be used with the new VJ wireless sensor network during FY 2004 to provide an automated data acquisition system with in situ calibration capabilities for VJ thermocouples.

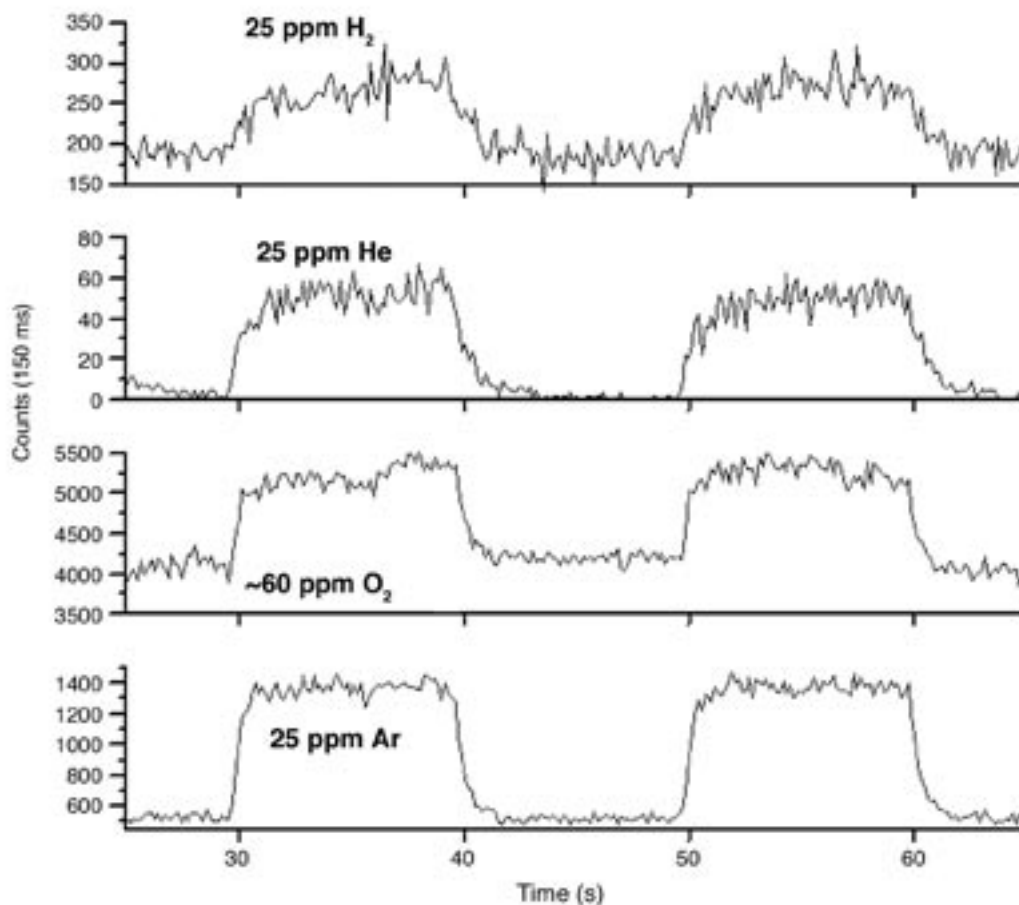
Contact: J.M. Perotti (Jose.M.Perotti@nasa.gov), YA-D5-E, (321) 867-6746

Participating Organization: USTDC (Dr. C.T. Mata, A.J. Eckhoff, B.M. Burns, J.J. Randazzo, and S.J. Stout)

Fast, Time-of-Flight Mass Spectrometer for Rugged Aerospace Applications

Time-of-flight (TOF) mass spectrometry is designed around the properties of molecular matter, Newton's first law, and the forces imparted to charged particles by electric fields. At the beginning of a measurement cycle, pulsed electron beams form ions from neutral molecules. Immediately after these ions are created, they are accelerated by pulsed electric fields into a drift region where they are separated into groups by their differences in velocity, an inverse function of their mass. These groups arrive at the detector inversely according to their mass; lightest first, heaviest last. When the ions strike a detector plate, their time of arrival and quantity are measured. When the last ion group in the sample has arrived, a new cycle can be initiated. For the gas molecules of interest to the aerospace community, the time to complete a measurement cycle is about 30 microseconds. At this rate, approximately 30,000 measurement cycles can be made in 1 second.

A compact TOF mass spectrometer, developed earlier on a Small Business Innovation Research (SBIR) contract and delivered in CY 2000, was modified to incorporate an ionizer that does not rely on thermionic emission for operation. The original instrument was designed as a fast sensor for use as a propellant (hydrogen, helium, oxygen, and argon) leak detector during the first few seconds of a space vehicle launch cycle, after main engine ignition and prior to release from the ground. The major NASA-defined benchmarks for this application of sensitivity, accuracy, dynamic range, response time, and (to a degree) ruggedness were



Calibration Gas Data Acquired in 150-Millisecond Sample Timeframes

designed into the current prototype using the new ionizer technology. The test article is located at the vendor's facility, and NASA personnel plan to evaluate the instrument under controlled laboratory conditions at KSC.

A conventional time-to-digital converter was used for data acquisition. This has the advantage of high sensitivity (low detection limits) but has limited dynamic range. The dynamic range of a TOF mass spectrometer is principally limited by saturation of the microchannel plate detector, which can handle only a few million counts per second. An approach to overcome that limitation for this application is being worked through a third SBIR Phase I contract with the vendor. A detector scheme is under development using a special form of the time-to-digital converter, which will increase the dynamic range by 2 orders of magnitude to 10^5 counts per second. Patent application PCT/US99/13965 explains this unique approach.

Low part-per-million detection limits were achieved for all species of interest (hydrogen, helium, oxygen, and argon) in a nitrogen background within an acquisition time of 150 milliseconds. A fast interface allows response times below 1 second for air sampling with an 8-inch, 128-micron capillary and a rise time of 200 to 300 milliseconds. Identical mass spectra were achieved by direct comparison of the filament and surface desorption (SD) ionizer schemes.

The ionizer used in this prototype is based on a spontaneous SD process and does not require a hot-wire filament for operation. Compared to thermionic emission, the classical method of creating free electrons in a vacuum, this electron source provides advantages in efficient use of power. Rugged construction leads to a reliable instrument that can acquire gas concentration data in an extremely harsh operational environment, typical of what might be found in the aft compartment of a spaceflight vehicle or autonomous ground vehicle.

Electron emission stability and current density are similar to that achieved with the electron filament used in the first prototype. Adequate performance of the SD ionizer in the TOF mass spectrometer has been demonstrated. Various

geometries of the ionizer were tested during the development process. Electron currents up to 100 nanoamperes were registered. This limit is imposed by the electrical properties of the electron multiplier. Increased currents can be obtained by using channel electron multipliers that provide currents up to several microamperes. More current might be possible but has been limited by device lifetime.

The electron current density of this ionizer would satisfy most time-of-flight mass spectrometer applications but at the cost of a bulkier mechanical structure. The new design is more robust than the filament-based version, but it ultimately suffers from degradation due to reduced gain in the channel electron multiplier as a function of extracted current and time. The major limitation to this SD technique is identical to that of the channel electron-plate-based ion detector – only 1 coulomb can be extracted over the usable lifetime of these channel plate structures.

Work remaining includes the miniaturization of control and data acquisition electronics, overall ruggedization and test, rugged pump development, and advanced detector and ionizer development to improve operational lifetime.

Key accomplishments:

- Developed a small, fast, aerospace-gas-specific, potentially rugged, time-of-flight mass spectrometer.
- Demonstrated filamentless ionizer.

Contacts: F.W. Adams (Frederick.W.Adams@nasa.gov), YA-D7-E1, (321) 867-6671; D.W. Follistein, YA-D7-E1, (321) 867-6747; and Dr. T.P. Griffin, YA-F2-C, (321) 867-6755

Participating Organizations: USTDC (Dr. CR. Arkin, W.D. Haskell, and G.R. Naylor) and Ionwerks (Dr. J.A. Schultz)

Inspection Tool for the Reaction Control System (RCS) Nozzles



Figure 1. Version 1 Composed of an Inner Teflon Cylinder Holding a Mirror and an Outer Centering Plug



Figure 2. Version 2 Shown Completed (top) and in Use (bottom) (The centering plug was dropped, the cylinder was opened up, and a handle and tether were added.)

The Space Shuttle Orbiter maneuvers in space using the RCS, which is composed of small hypergol thrusters located around the vehicle. These thrusters consist of an elaborate hydrazine and nitrogen tetroxide delivery system attached to the small end of a rocket nozzle. The rocket nozzle contains a combustion chamber where the fuel and oxidizer mix and explode, followed by a throat that constricts the explosion, followed by a parabolic expansion region that funnels the expanding gases away from the vehicle. The nozzles are made of niobium (also known as columbium) coated with an oxide layer designed to survive the high temperatures within the combustion chamber. After each mission, the nozzles are checked for defects, usually small divots caused by a section of the oxide layer coming off. These defects are serious if the underlying niobium is exposed because the metal can melt from the heat of the hypergol reaction. However, if some of the oxide layer remains, then the nozzle may be safe to fly.

In 2001 a defect was found in a rocket nozzle while the Shuttle was at the pad, and it was unclear if the underlying metal was exposed. After significant effort, it was determined that sufficient oxide was present and that it was safe to fly. However, had this defect exposed the niobium, not only would the Shuttle have been brought back to the Vehicle Assembly Building but the Orbiter would have been demated and brought back to the Orbiter Processing Facility for repair – an enormous expense of both time and labor. Consequently, the decision was made to put more resources into defect detection, measurement, and in situ repair. The result was the evolution of a rigidly mounted device into a handheld, illuminated inspection tool that allows users to look inside the throat of a rocket nozzle on the Space Shuttle to search for defects.

The original motivation was to create a tool that could evolve into a defect measurement system. Consequently, a two-part inspection tool was designed to hold a mirror at a known depth and centricity within the nozzle. This first-generation tool is shown in figure 1 and consists of a Teflon sleeve and a Teflon mirror assembly. Only Teflon was permitted to contact the oxide layer within the nozzles. If this design proved acceptable to the users, then a microscope system could be attached to the mirror assembly, allowing a user to scan the throat and combustion regions of the nozzle and to measure the size and depth of a defect. Upon delivery, though, the inspectors were more interested in just the mirror portion of the device. Previously, they had been using a rather small, low-quality mirror, and the large mirror mounted in Teflon provided better visibility of defects within



the nozzle. So, the design direction was altered to concentrate on a better handheld inspection tool.

Figure 2 shows the resulting next-generation device. The sleeve was removed, the design was opened up to make the mirror more visible, and a handle and tether were added. This unit was well received by Operations and used successfully in the field, but it had a significant limitation – the inspector had to hold a flashlight to see inside the nozzle.



Figure 3. Version 3 With Illumination

Figure 3 shows the illuminated version of the inspection mirror. Small, high-efficiency, white light-emitting diodes (LEDs) were added, and circuitry was designed to drive them from a set of three AA batteries. These LEDs provided significant light as seen in the figure, eliminating the need for a separate flashlight. The batteries were located in the handle of the unit, which was designed to turn on and off by twisting the handle. Field testing by Operations indicated that a shorter handle was the only modification necessary. In the final design (shown in figure 4), the battery was moved back in line with the mirror mount to avoid interference with the nozzle. This allowed the inspector more reach into the nozzle and permitted a thumb-operated on/off switch.



Figure 4. Version 4 With Improved Reach, Access, and Operation

This iterative design process emphasizing user involvement yielded a tool that makes rocket nozzle inspections easier to perform while minimizing the risk of damaging the nozzle coatings.

Contacts: Dr. R.C. Youngquist (Robert.C.Youngquist@nasa.gov), YA-C3-E, (321) 867-1829; D.E. Willard, YA-C3-E, (321) 867-8578; and J.W. Peters, PH-G2, (321) 867-4431

Participating Organization: USTDC (W.D. Haskell and R.B. Cox)

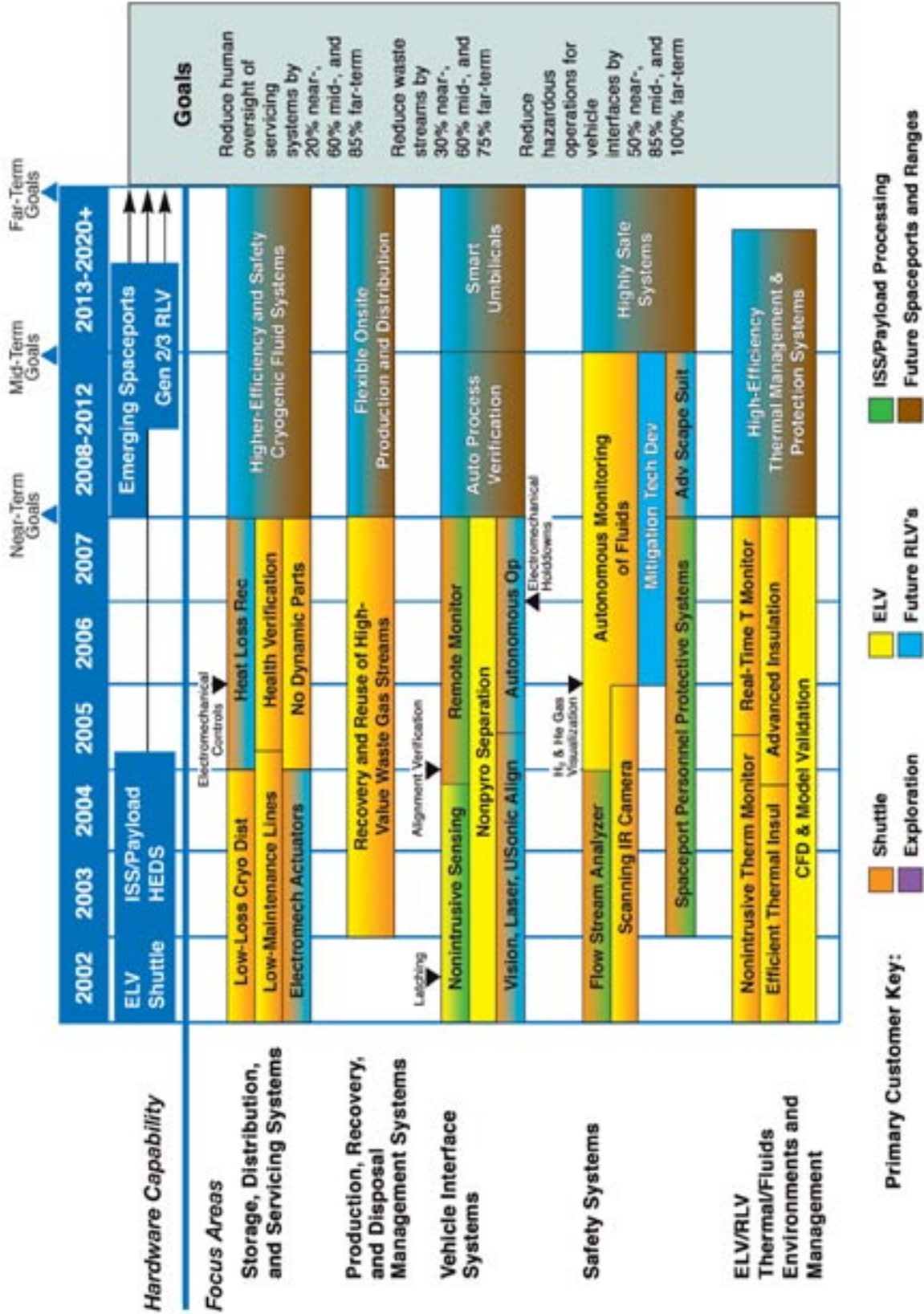
Fluid System Technologies

The vision of Fluid System Technologies is to develop technology that enables future affordable spaceports. These spaceports can be Government-owned, commercial, orbital, or nonterrestrial. The goal is to reduce the cost of access to space and increase safety. Fluid System Technologies can help in this role through reducing the human oversight of servicing, reducing the waste streams, and reducing the number of hazardous operations and vehicle interfaces. Fluid System Technologies will support developing a better understanding of the fluid environment in all areas of spaceport activity through analysis and simulation. In addition, Fluid System Technologies will seek to develop the means to reduce thermal losses associated with cryogenic fuels, minimize maintenance and process monitoring costs, and provide for safe operation of the spaceport. A major goal of this technology product line is to create efficient technologies that can be quickly adapted to the changing fluid needs of future space vehicle elements and systems residing at the spaceport. The technology focus areas of the roadmap that drive technology development toward the ultimate vision include the following:

- Storage, Distribution, and Servicing Systems
- Production, Recovery, and Disposal Management Systems
- Vehicle Interface Systems
- Safety Systems
- Expendable Launch Vehicle (ELV)/ Reuseable Launch Vehicle (RLV) Thermal/ Fluids Environments and Management

For more information regarding Fluid System Technologies, please contact Jack Fox (Jack.J.Fox@nasa.gov), YA-E6, (321) 867-4413; or Russel Rhodes (Russel.E.Rhodes@nasa.gov), YA-D4-A, (321) 867-6298.

Fluid System Technologies Roadmap



Modeling the RL10 Rocket Engine With Densified Liquid Hydrogen and Oxygen Propellants

There are many benefits to using densified propellants on launch and space vehicles. The increase in propellant density translates into smaller propellant tanks that result in lower lift-off weights and larger vehicle payload capacities. The subcooling of densified propellants also allows lower system operating pressures in propellant tanks that extend tank life in reusable systems. The increased cooling capacity is a potentially vital heat sink for leading edges and shock wave regions subjected to aerodynamic heating and for rockets or rocket-based combined-cycle engine combustion chambers and nozzles.

Analysis of rocket engine performance using densified propellants is a key component of the research necessary to optimize engine design and is necessary to advance the maturity of densified propellant technology. To further understand the effects of densified propellants on rocket engine systems, an RL10 engine was analytically modeled with densified propellants using the Rocket Engine Transient Simulation (ROCETS) mathematical modeling code. A validated model of the RL10A-3-3A rocket engine was modified to simulate densified propellant inlet conditions and was used to determine the effects on overall system operating conditions. The nominal operating conditions of the RL10A-3-3A were compared with operating conditions obtained at various levels of densified propellant inlet conditions.

The ROCETS code was developed by Pratt & Whitney for NASA in 1990. The program simulates a complete rocket engine system and calculates the values for all flow, pressure, temperature, and state variables at various locations within the engine system components. The code enables a number of study types to be conducted, including parametric, dynamic response, component geometry changes, and overall system characterization. The code has been used at Pratt & Whitney and several NASA Centers to model rocket engines and rocket engine test facilities.

The ROCETS model was used to study the effects of densified propellants on rocket engine performance, which was the ultimate goal of this work. In this study, the model input parameters (such as engine thrust, oxidizer/fuel mixing ratio, combustion chamber pressure, and liquid oxygen [LOX] and hydrogen fuel inlet pressures) were fixed. Other inputs, such as LOX and hydrogen fuel inlet temperatures, were varied from normal boiling point at ambient pressure down to near triple point. The behavior of a number of different engine system components as a function of the thermodynamic state of the LOX and hydrogen propellants was predicted. In general, as propellant inlet temperatures decrease, the RL10A-3-3A model shows

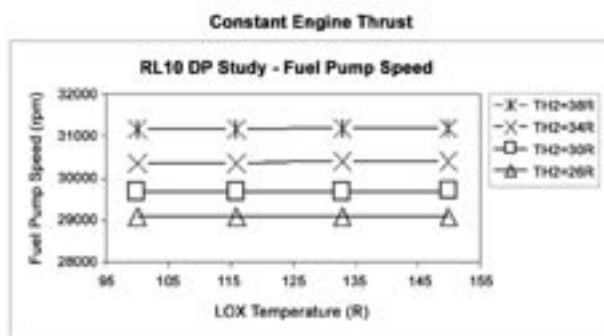


Figure 1. Fuel Pump Speed Performance

a significant decrease in fuel and LOX pump speeds. This reduces engine system failure probability and prolongs engine life. Pressure drops across the injectors and cooling jacket are smaller due to a smaller volume of flow rate for densified fuel and LOX. Inlet temperatures at the injectors are reduced as engine inlet propellant temperatures decrease. Turbine inlet temperature, torque, and power decrease with decreasing propellant temperatures. Figures 1 through 5 illustrate the behavior of several system components.

The research results quantified some of the key benefits of densified propellants in engine systems, including pressure drop reduction and decreased turbine/pump speeds. In general, the results show a reduction in pressure drop and turbo-machinery rotational speed as liquid propellant inlet temperatures decrease and fluid densities increase. The advantages of these effects on the engine and vehicle include increased reliability and engine life. The data generated in this study can be used for optimizing current engine system configurations for densified propellants or for designing new lighter-weight engines that take advantage of the increased density of the propellants.

Key accomplishments:

- Modified a ROCETS model of the RL10A-3-3A cryogenic hydrogen and oxygen expander-cycle rocket engine to simulate the use of densified propellants.
- Performed validation of the mathematical model with existing engine test data.
- Developed methodologies for assessment of engine systems optimization methods for densified propellants.

Key milestones:

- Conduct a detailed experimental study on engine combustion stability and ignitability.
- Research the effects of densified propellants on increased engine thrust.
- Conduct further detailed analyses of key engine components.
- Conduct testing of an existing RL10 engine with densified liquid hydrogen and LOX.

Contact: L.K. Walls (Laurie.K.Walls@nasa.gov), VA-F3, (321) 476-3637

Participating Organization: Sierra Lobo, Inc. (M.S. Haberbusch, C.T. Nguyen, and A.F. Skaff)

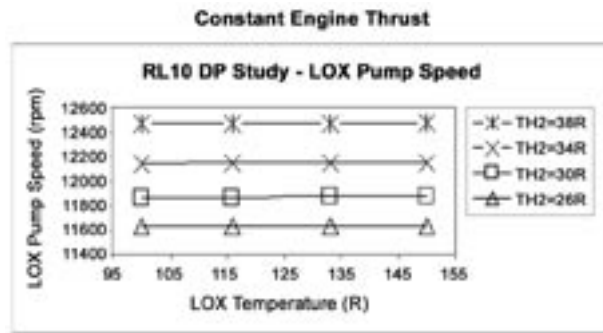


Figure 2. LOX Pump Speed Performance

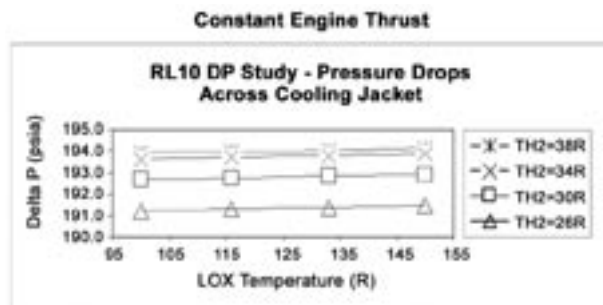


Figure 3. Pressure Drop Across Cooling Jacket

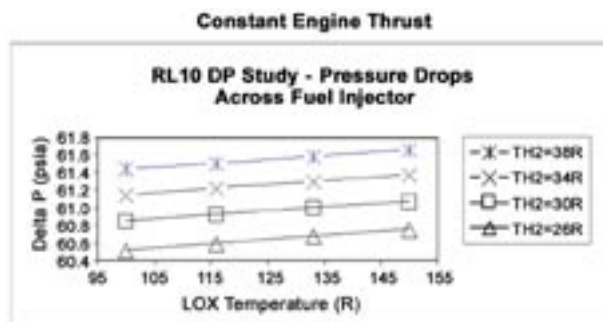


Figure 4. Pressure Drop Across Fuel Injector

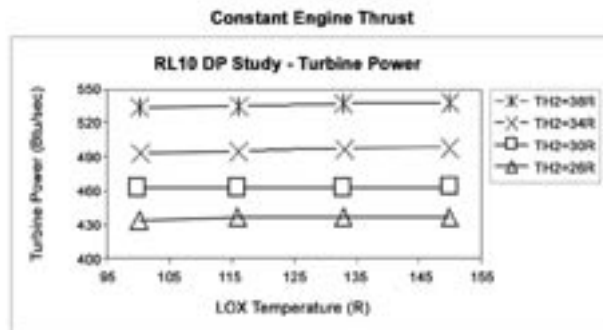


Figure 5. Turbine Power

On the Scaling Laws for Jet Noise in Subsonic and Supersonic Flow

Noise generation by turbulent jets is of great practical interest in the design of jet engines (subsonic and supersonic civil transport) and the study of launch vehicle acoustics. Acoustic loads in a launch vehicle environment induce structural vibration of vehicle components, ground support structures, and equipment in the immediate vicinity of the launch pad. In designing launch vehicles, it is highly desirable to generate data on acoustic loads (near-field and far-field noise levels) both analytically and from testing small-scale and full-scale models. Since full-scale acoustic and vibration testing is often cost-prohibitive, the option of small-scale testing combined with analysis methods remains a practical alternative.

Noise from subsonic jets is caused by turbulent mixing, composed of the contributions of large-scale and fine-scale structures. The turbulent mixing noise is mainly broadband. In perfectly expanded supersonic jets (nozzle exit plane pressure equals the ambient pressure), the large-scale mixing noise manifests itself primarily as Mach wave radiation caused by the supersonic convection of turbulent eddies with respect to the ambient fluid. In imperfectly expanded supersonic jets, additional noise is generated by broadband shock noise and screech tones.

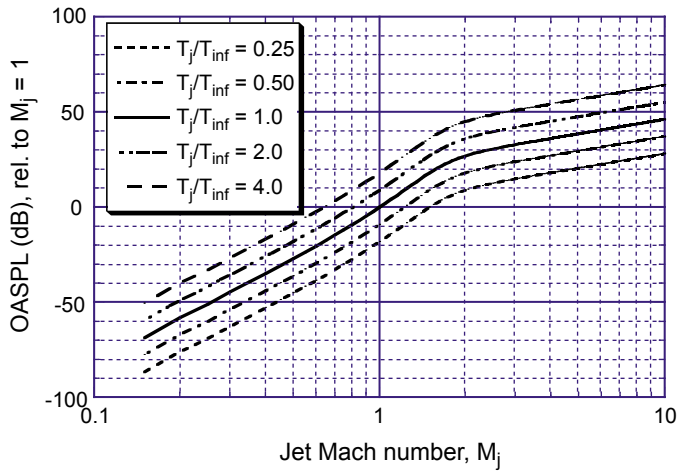
In early design stages, scale models are often used to predict the acoustic environment associated with flight vehicles. A detailed knowledge of the mechanisms of noise generation and noise radiation by jets is essential in designing a scale model of the noise source. To ensure complete similarity between model and full scale, we need to ensure similarity of flow, noise generation, and noise propagation.

In practice, it is generally difficult to duplicate (simulate) all the characteristic parameters in the scale model. Model testing with even small rocket engines requires extensive safety precautions. Heated jet facilities also involve considerable complexity and cost. The use of less expensive facilities or lower gas temperatures, for example, would considerably simplify model testing. The ability to conduct a scale-model test with a substitute gas (air, nitrogen, helium, etc.) results in considerable savings (reduced costs of test facilities, test time) and advantages. For example, helium-air-mixture jets for simulating high-temperature effects have been studied. These substitute gas tests require some compromise of the actual physics of the hot jet.

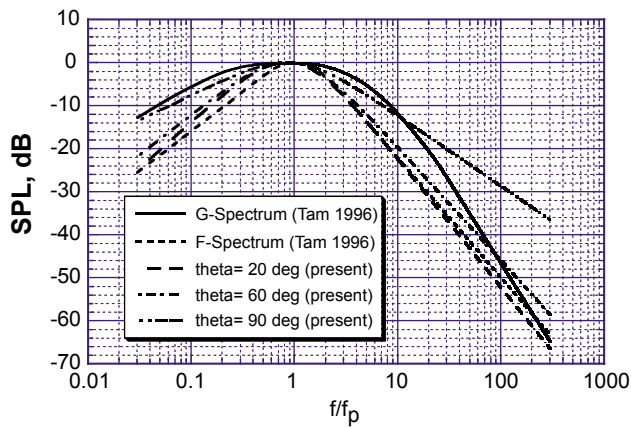
In the absence of an exact match between the dimensionless parameters of the scale model and the full scale, a detailed knowledge of the functional relationship with respect to the various parameters is essential to aid in the interpretation of scale-model data to predict the full-scale environment.

Key accomplishments:

- Reviewed the scaling and similarity laws applied to jet noises.
- Studied the effect of jet temperature in supersonic jets.
- Proposed a similarity spectrum for sound power level for both subsonic and supersonic flows.



Effect of Temperature Ratio on Overall Sound Power Level



Similarity Spectra for Jet Noise at Mj=2

Key milestones:

- Perform cold-jet acoustic testing.
- Present the study at the American Institute of Aeronautics and Astronautics (AIAA) Aero-acoustic conference.
- Begin the development of hot-jet facility.

Contact: Dr. B.T. Vu (Bruce.T.Vu@nasa.gov), YA-C2-T, (321) 867-2376

Participating Organization: USTDC (Dr. M. Kandula)

Advanced Umbilical Development Automation Testbed

Numerous launch vehicles, planetary exploration systems, and rovers require umbilical systems for fluid flow and electrical connections. Simple, reliable, autonomous mating is required to make certain missions and systems feasible (e.g., Mars methane-fueled rovers) and to provide low-cost and safe launch operations. The environment for mating (temperature, humidity, dust, cost, weight, and power) varies drastically from system to system. However, a common core technology and numerous sensor and mating techniques are needed to provide low-cost, common solutions for all systems.

The Smart Umbilical Mating System (SUMS) is a general-purpose, fully automatic, extend-and-retract umbilical system that can be used in a multitude of applications. It was built to demonstrate the latest in control technology. SUMS incorporates a fault-tolerant, fail-operational control architecture and utilizes linear motors for passive compliance. In addition, SUMS will be used as a technology testbed to integrate component-level mechanical, instrumentation, and other umbilical technologies into a working proof-of-concept prototype. The intent of this system is to provide a platform to allow multiple technologies to be evaluated from a system perspective. System design is generic for use with a wide variety of launch vehicles and the development of enabling technologies, such as quick disconnect connectors, sensors, location/alignment systems, latching/actuation systems, deicing/decontamination systems, control systems, and verification systems.

SUMS is capable of extensive application of redundancy and alternate modes of operation. These capabilities are demonstrated in the application of techniques to enhance operational reliability. For example:

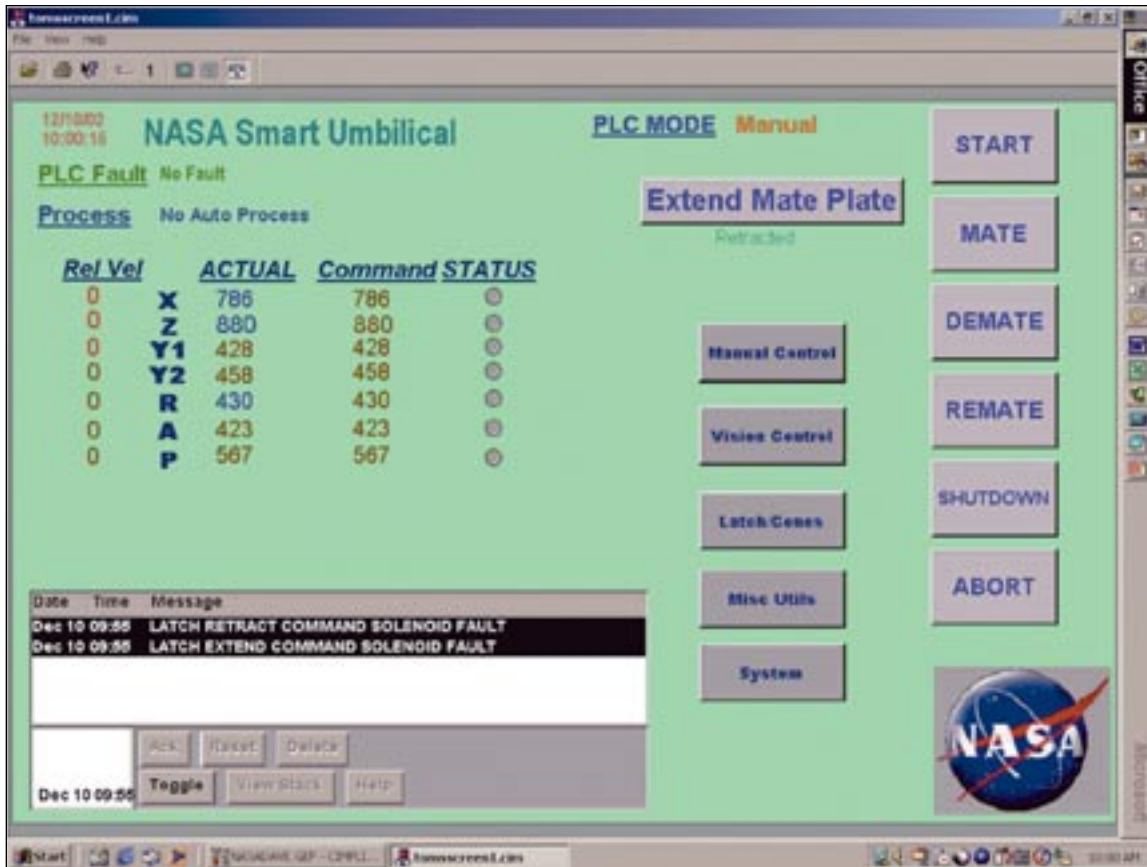
- The control system uses a fault-tolerant, voting algorithm for critical controls.
- A redundant vision system that utilizes two cameras is employed to align the mating cones to receptacles on the flight half of the umbilical plate.
- Linear motors are used on all axes, and the pitch actuator incorporates a redundant motor to demonstrate the system's fault tolerance.



Smart Umbilical Hardware (right side) and Simulated Flight-Side Plate (left side)



Control Station Consisting of Redundant Control Architecture



Main Operator's Screen

Technology areas include redundant system control, autonomous operation and automated mating, location control and reconnect capability, ice suppression technology, and man-machine interface. SUMS increases the umbilical technology readiness level by demonstrating that the umbilical connect, disconnect, and reconnect capability at any point in the countdown process improves safety of launch operations; the autonomous mating operation reduces costs and improves reliability of ground processing operations; and the umbilical system integrates system health management to verify the system operational status.

Key accomplishments:

- Developed a remotely controlled graphical user interface for the SUMS hardware.
- Performed liquid nitrogen cryogenic mate, demate, and remate testing.
- Demonstrated a potential ice mitigation solution.

Contacts: T.C. Lippitt (Thomas.Lippitt@nasa.gov), YA-D1, (321) 867-1391; and R.P. Mueller, YA-D1, (321) 867-2557

Participating Organizations: USTDC (R.A. Gordie and J.K. Trautwein) and Rohwedder, Inc. (T. Adams)

Advanced Umbilical Location System (AULS)

Automated umbilicals are being developed at KSC that will dramatically reduce the time required to mate an umbilical system to the launch vehicle interface. To do so, the ground umbilical plate must have a positioning mechanism with an associated control system that will locate the ground umbilical plate with respect to the flight umbilical plate. The flight umbilical plate has six degrees of freedom since it is mounted onto a launch vehicle that is positioned on the launch pad and is subject to installation tolerances and wind load excursion movements. The ground plate also has six degrees of freedom and must be accurately positioned in terms of location and orientation to within 0.125 inch, and it must be parallel to the flight plate to within ± 1 degree. The orientation and parallelism can be achieved with a mechanical pin/spring mechanism, but the location to within 0.125 inch must be provided by a separate system. The location system must be able to remotely find a target on the launch vehicle flight plate and then advance and position itself over a gap of 6 feet. An AULS proof-of-concept prototype was developed to test functionality.

The AULS uses a modulated light-emitting diode (LED) light source mounted on the ground flight plate that shines onto a prismatic reflector on the flight-side plate. The light is reflected back to the ground side and is detected by a photovoltaic sensor that is divided into four quadrants. The electric signal generated is fed into an analog electronics feedback logic circuit, which then powers positioning stepper electric motors on lead screw mechanisms corresponding to each quadrant on the light sensor. The net result is that the ground flight plate travels toward the target location on the flight plate represented by the reflector. In this way, the umbilical ground plate is able to track the flight plate in real time as the ground plate is extended out toward the flight plate in the umbilical mate operation. The AULS constantly adjusts the position of the ground plate so it tracks the flight plate even if the flight plate is moving or vibrating. The modulated light is used to distinguish between the signal light and any stray sources of ambient light. The whole assembly has been mounted on a cart.



AULS Proof-of-Concept Prototype (front view)



AULS Proof-of-Concept Prototype (side view)



AULS Proof-of-Concept Prototype Analog Electronics Control System

Testing shows the AULS is capable of real-time tracking of a moving target and is accurate to within 0.125 inch for final location and orientation.

Key accomplishments:

- Developed AULS prototype concept.
- Designed and fabricated AULS proof-of-concept prototype.
- Tested location capabilities of AULS to within 0.125-inch accuracy.
- Tested real-time response of AULS in ambient light conditions.

Contact: R.P. Mueller (Rob.Mueller@nasa.gov), YA-D1, (321) 867-2557

Participating Organization: American Remote Vision Co. (S. Gleman)

Advanced Cold-Mate Cryogenic Fluid Quick Disconnect (QD)

Loading propellant onto launch vehicles requires using cryogenic fluid quick disconnect (QD) fittings. The QD fittings, which are mounted onto umbilical systems with related mechanisms, mate or demate the QDs to the launch vehicle ground-to-flight interface. Cryogenic propellants such as liquid hydrogen and liquid oxygen are then loaded onto the launch vehicle through the QDs and related fluid lines. At launch, the umbilical systems must be retracted from the launch vehicle and stored in a protective housing to avoid damage from the launch blast and to allow reuse of the umbilical system. If a launch is scrubbed or aborted, the propellants may be drained from the launch vehicle. If the umbilical has been retracted prior to T-0, as is anticipated with the use of automated umbilicals, then the QDs must be capable of a cold mate while the QDs are still at cryogenic temperatures. The problem that arises during cold mates is that the humidity in the air condenses onto the cold QD surfaces and forms a layer of frost or ice, which compromises the integrity of the sealing surface on the QDs. The frost/ice prevents a good mate from taking place between the male and female halves of the QD, resulting in a ground-to-flight fluid interface that may leak. Fuel or oxidizer leaks at the launch pad may cause dangerous explosive conditions, which are a Criticality 1 Hazard that may cause loss of vehicle and crew.

A specification titled “Operating Parameter Goals for Advanced Cryogenic Fluids Disconnect” was developed and released to private industry in a solicitation for proposals. NASA selected VACCO Industries, Inc. Space Products, of El Monte, California, to develop the Cold-Mate QD. VACCO owns a design that was used on the Shuttle Centaur upper stage planned for installation in the Space Shuttle Orbiter payload bay. The Centaur design has a shroud that encapsulates the QD to prevent the accumulation of any propellants leaked in the Orbiter payload bay. The Centaur design was used as a baseline to further develop the Cold-Mate QD design (figure 1).

Ice formation can be prevented by isolating all cold QD surfaces from moist atmospheric air. The typical method for achieving this in a spaceport launch pad environment is to use a dry, inert-gas purge such as helium or nitrogen. Because the respective liquefaction-phase-change temperatures are lower than liquid hydrogen and liquid oxygen, the purge gas does not liquefy and is an effective isolation medium.

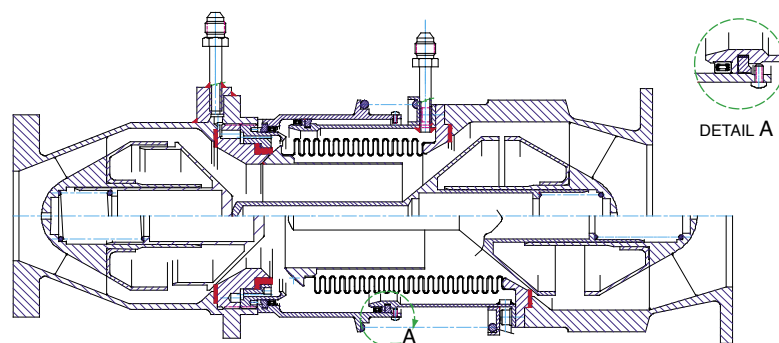


Figure 1. Cross Section View of Cold-Mate QD Design



Figure 2. Mated QD in Test Fixture at LN₂ Temperature



Figure 3. Male QD Half Showing Ice Prevention on Sealing Surface

An inert-gas purge method was selected for ice prevention on the QDs. To contain the gas purge, a spring-loaded telescoping-tube shroud mechanism was designed and installed around an existing VACCO cryogenic fluid QD coupling. A test fixture was built (figure 2) to simulate the ground-to-flight interface mating of the two QD halves under liquid-nitrogen (LN₂) temperature conditions. The LN₂ test was performed and showed that the inert-gas purge was effective in keeping the QD sealing surfaces free of frost or ice (figure 3). The QD was pressurized to 50 pounds per square inch gage (psig) at a temperature of -290 degrees Fahrenheit (°F) and showed favorable results.

Tests demonstrated the capability of the advanced Cold-Mate QD concepts to mate and demate after a separated cold soak simulating a T-0 launch abort. In addition, the prototype QD demonstrated the capability to verify leakage at various stages of engagement. Further development work is desired to make a production version of the prototype QD for use in future automated umbilicals.

Key accomplishments:

- Developed viable inert-gas purge concept for ice prevention on a cryogenic QD design.
- Designed and fabricated a prototype Cold-Mate QD.
- Successfully tested the Cold-Mate QD prototype at a temperature of -290 °F and a pressure of 50 psig.

Contact: R.P. Mueller (Rob.Mueller@nasa.gov), YA-D1, (321) 867-2557

Participating Organization: VACCO Industries, Inc. (W. Stalnecker and D. Wicke)

Collapsible Cryogenic Vacuum-Jacketed (CCVJ) Fluid Transfer Lines

Launch vehicle umbilical systems require vacuum-jacketed (VJ) fluid transfer lines to load cryogenic propellants at the launch pad. Since umbilical systems consist of mechanisms that extend and retract the umbilical plates to and from the ground to flight interface, these VJ lines must have flexibility or a degree of freedom of motion. Typically, this has been accomplished by using VJ flex lines. These flex lines may be as large as 8 inches in diameter, and the corresponding minimum bend radius is as large as 3 feet with corresponding reaction forces that must be controlled. These reaction forces are typically restrained by a large energy chain device such as the one shown in figure 1, which was used for the Atlas V Autocoupler umbilical system.

The VJ flex lines are effective but require significant overhead in terms of additional mechanisms, structure, and space occupied. Clean launch pad concepts and other desired efficiencies require that the automated umbilical should have a better packaging ratio.

To make more compact and efficient umbilical systems, a collapsible cryogenic VJ line was developed as a proof-of-concept model. The model shows that the VJ flex line can be replaced by a VJ hard line that contains one or more cryogenic swivel joints at critical points that then allow the VJ line to be folded up or collapsed. A VJ hard line is more thermally efficient than a VJ flex line, and it has a far better packaging ratio since the minimum bend radius is avoided. This is demonstrated in the proof-of-concept model and is shown in figures 2 and 3 in the extended and retracted positions, respectively.

Key accomplishments:

- Developed CCVJ prototype concept.
- Researched and located unique CCVJ swivel joint.
- Designed and fabricated CCVJ proof-of-concept prototype.

Contact: R.P. Mueller (Rob.Mueller@nasa.gov), YA-D1, (321) 867-2557

Participating Organization: Chart Industries, Inc. (B. Appleton)



Figure 1. Atlas V Autocoupler Umbilical With Energy Chain for Large-Bend-Radius VJ Flex Lines



Figure 2. CCVJ Line Proof of Concept With Swivel Joint (Extended)



Figure 3. CCVJ Line Proof of Concept With Swivel Joint (Retracted)

Fiber-Optic Quick Disconnect (QD)

Launch vehicles require data transmission from the ground to the flight hardware. Typically the electrical signals used in the data transmission are conducted across traditional shell-and-pin connectors that rely on physical contact of the pin with a corresponding receptacle hole. These pins are often subject to corrosion, which causes a malfunction of the electrical connector. In addition, there are precise alignment and mating force requirements to make the connection. If the alignment is not achieved, then the result is a bent pin condition, which also causes a malfunction of the electrical connector. Furthermore, vibrations during a T-0 disconnect in the launch environment may cause damage to the pins and prevent reuse of the connector.

To address these issues, an engineering evaluation was performed to identify viable solutions and concepts. The results indicated that using fiber-optic light signals to transmit data across the ground-to-flight interface would meet all the requirements.

A fiber-optic QD can transmit data signals across the ground-to-flight interface with no physical contact. The light source is transmitted across a fiber-optic interconnect/cable assembly using expanded-beam technology, which physically expands and collimates transmission signals into an optical beam over 14 times its original diameter. It is then refocused back down into the core of the receiving fiber. This concept provides ease of alignment and low sensitivity to thermal changes and contamination. High-strength, precision connector housings enhance a durable connection, optimizing low loss and repeatable performance. Vibration effects are avoided because of the expanded-beam footprint.

Such a fiber-optic QD is manufactured by Amp/Tyco Electronics. It is a Fiber-Optic Cable Assembly (insert) part number P00-3691-16-1 and an Arinc 404 Single-Cavity Fiber-Optic Receptacle Assembly (shell) part number P00-3690-26-1.

Spaceport launch pad environments are unique and not typical of most industrial applications. Compatibility with cryogenic temperatures, vibrations, and salt fog is required. Such tests were conducted at the KSC Materials Science Laboratory. The fiber-optic QD was tested in accordance with the vibration requirements contained in KSC MSL-325-2001. The power spectral density (PSD) was defined in 79K31824, Revision A, as $28.2 \text{ g}_{\text{rms}}$. All vibration tests showed acceptable levels of transmittance during the vibration application.

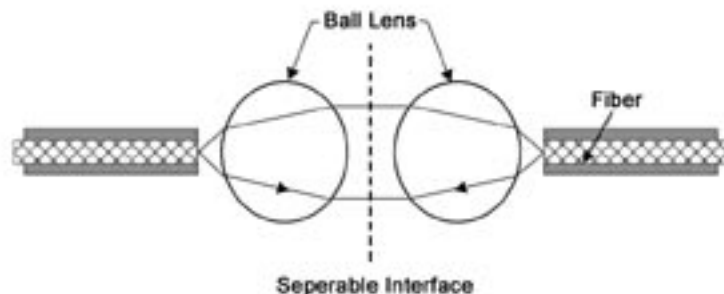
Expanded Beam Principle



From left to right: Pro beam, Pro Beam Jr., and Mini-Expanded Beam

Product Facts

- Light is expanded, collimated, and transmitted across an air gap
- Ball lens expands cross-sectional area of light over 200 times for multimode and over 2000 times for singlemode



Amp/Tyco Electronics Fiber-Optic Interconnect/Cable Assembly

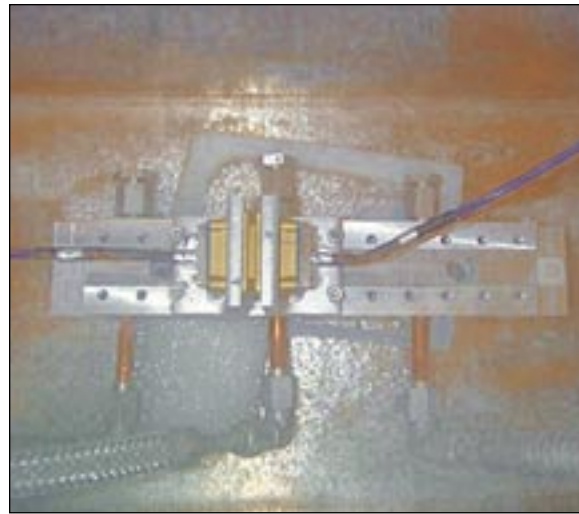
Cryogenic temperature testing was performed at the Launch Equipment Test Facility (LETF) Cryogenics Testbed to liquid-nitrogen cryogenic temperatures (-320 degrees Fahrenheit [°F]). All cryogenic testing showed that signal loss was within acceptable limits as the temperature was lowered.

The salt fog tests simulated the effects of being in a seacoast environment for 30 days. The testing was conducted in a salt fog test chamber at the Materials Science Laboratory at KSC. During the 1,200-hour test, the fiber-optic QD performance did not degrade substantially, and the only effect noted was a buildup of salt on the housing.

The results of environmental testing of the Amp/Tyco Electronics Fiber-Optic Cable Assembly (insert) part number P00-3691-16-1 and an Arinc 404 Single-Cavity Fiber-Optic Receptacle Assembly (shell) part number P00-3690-26-1 indicate that this fiber-optic QD is acceptable for use in a typical launch pad environment. It is anticipated that this fiber-optic QD will be used in future launch vehicle ground-to-flight-interface umbilical systems, and it is a candidate for other ground-to-ground interface connections in a launch pad environment as well.

Key accomplishments:

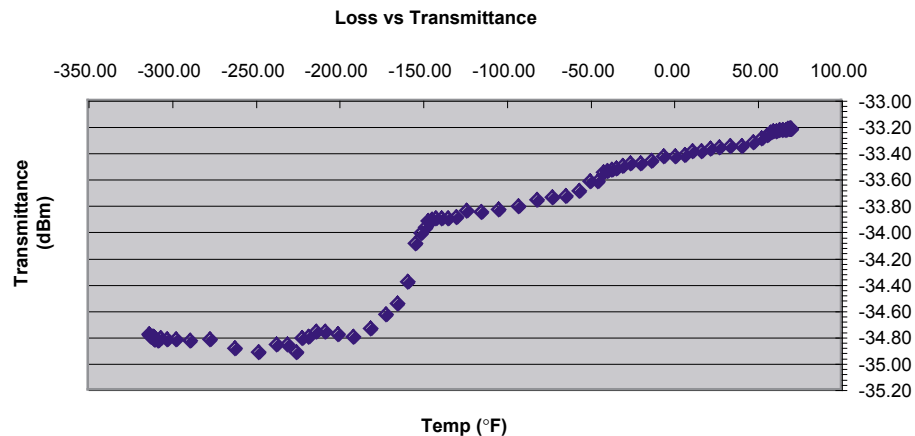
- Performed liquid-nitrogen cryogenic thermal environment performance testing.
- Performed launch pad vibrations environment performance testing.
- Performed seacoast salt fog environment performance testing.
- Identified Tyco/ Amp Electronics Fiber-Optic QD as a viable candidate for use in ground-to-flight-interface applications.



Fiber-Optic QD in Cryogenic Test Fixture

Contacts: R.P. Mueller (Rob.Mueller@nasa.gov), YA-D1, (321) 867-2557; E.C. Smith, YA-G, (321) 867-8785; and L.G. MacDowell, YA-C2-T

Participating Organization: USTDC (J.J. Curran, Z.F. Nagy, and R. Grier)



Expanded Fiber-Optic Beam Assembly Change in Transmission of -1.70 Decibels per Milliwatt (dBm) QD Temperature From 70.38 °F to -312.67 °F

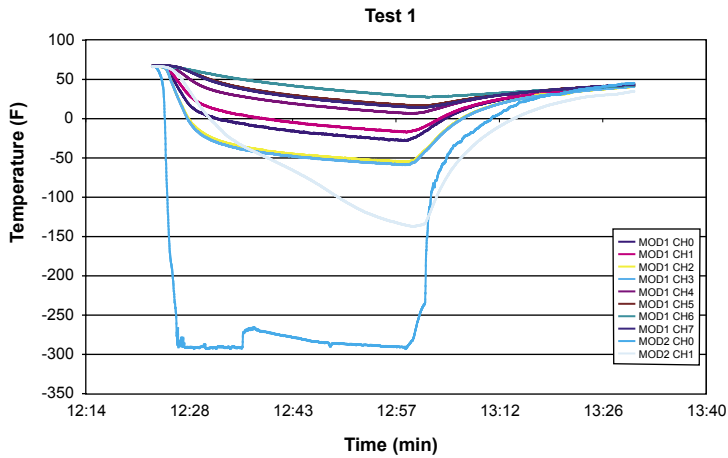
Ice Suppression Technologies

At cryogenic temperatures, ice forms on chilled equipment because of the condensation and subsequent solidification of moisture that is present in Earth's humid atmosphere. The ice can become foreign object debris (FOD) and can interfere with mechanisms and motion or can compromise the sealing surfaces of launch pad umbilical systems. An effort was made to identify potential solutions to the icing problem that have specific applications to spacecraft umbilical systems and generic applications to launch pad cryogenic systems.

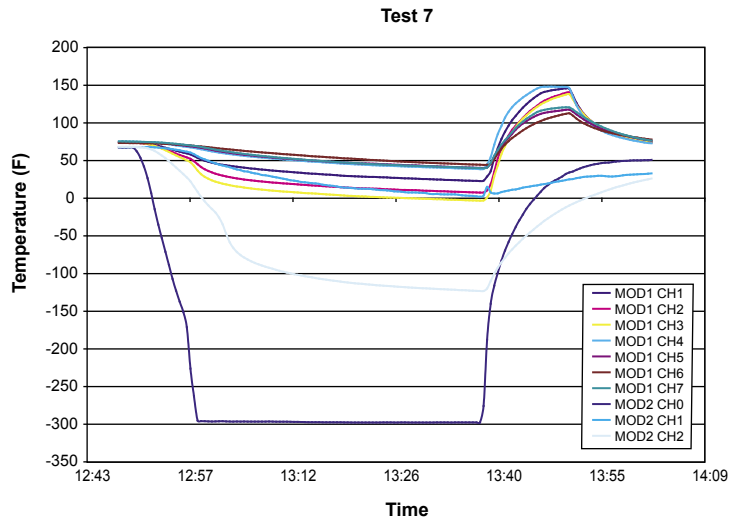
A team of NASA and contractor design and operations engineers compiled a list of 38 potential solutions whose technology readiness levels (TRLs) ranged from very low (such as biological agents) to mid (such as piezo-electric vibration methods) to high (such as inert dry gas purges).

The process yielded the following three methods of ice suppression for umbilical systems:

1. **Split Purge Shroud:** The shroud encapsulates both halves of the umbilical system (ground and flight plates), which mate to form a common purge cavity. This approach was pursued with a proof-of-concept prototype and is documented separately as the Ice Suppression and Mitigation System (ISMS).
2. **Expandable Ice Suppression and Cleanliness Preservation (EIS-CP) Chamber:** This apparatus is designed to encapsulate an individual quick disconnect (QD). The EIS-CP chamber is a donut-shaped device designed to create a contaminate- and moisture-free cavity around a subject quick disconnect. The device is 1-inch thick when compressed. It can be attached to an umbilical plate holding a subject QD. As the umbilical plates are demated, the EIS-CP chamber will expand and follow the moving umbilical plate to a height of approximately 6 inches. At this point, the upper part of the EIS-CP chamber will narrow to form a nearly sealed configuration, thus reducing the amount of purge gas needed and preventing contaminants from reaching the QD sealing surfaces. Once the EIS-CP chamber has performed its function and is ready to be retracted into its compressed position, the flow pressure to the inner bladder can be stopped. The gas pressure keeping the outer bladder expanded can be closed and the vacuum pump started, evacuating the air from the inside of the chamber causing a negative pressure. This will collapse the chamber and pull it down into its housing. The chamber would then be out of the way and cause no constraint to the umbilical plate remate operation.
3. **Infrared (IR) Heat and Gaseous Nitrogen (GN₂) Air Knife:** These two methods were used to prevent and mitigate ice buildup and were combined in various ways to provide information on the effectiveness of these methods. The IR lamps were powered by 480 volts (V) ac and cooled using an open-loop water line. They were mounted on a stand that held them vertical and parallel with a 1/2-inch gap between them. The air knife was mounted on top of the flight plate so the stream would flow in a laminar sheet down the front of the plate. The GN₂ heaters were mounted on both ends of the air knife to provide enough heated gas to the knife. The results



Baseline Test (Deicing equipment was not used. It took 30 minutes for the ice on the QD to melt and over 2 hours to dry.)



Test With Two IR Lamps and an Air Knife With Heated GN₂ (It took 6 minutes for the ice to melt and 10 minutes to dry.)

show that the IR heaters are very effective at deicing the QDs. The more difficult problem is removing the water from the QDs. Using these two methods, it should be possible to get the melting time below 2 minutes and the drying time below 5 minutes.

Contacts: R.P. Mueller (Rob.Mueller@nasa.gov), YA-D1, (321) 867-2557; and T.C. Lippitt, YA-D1, (321) 867-1391

Participating Organizations: USTDC (J.K. Trautwein and I.I. Townsend) and American Remote Vision Co. (S. Gleman)

Automated Latching Systems

Automated latching systems are required for remote latching and preloading of ground umbilical plates to flight umbilical plates in spacecraft vehicle ground-to-flight fluid interface systems. Two such devices were developed at KSC.

The Non-Pyrotechnic Automated Latch/Lock System (NPALLS) is a highly innovative latching mechanism that can be remotely operated. It is based on an in-line gripper wire rope device shown in figure 1.

The in-line gripper was used in a mechanism that pulls on a rod inserted into the in-line gripper. As the separation force is increased, then the gripping force increases proportionately with a multiplier effect on the force. This results in exceptionally high gripping loads for relatively low actuation forces. The actuation will be provided by a pneumatically actuated cylinder that will surround the in-line gripper mechanism. As a proof of concept, a scissors-type mechanism was used to actuate the in-line gripper, and it was demonstrated that a separation of 1,000 pound-force could be sustained by the in-line gripper device. This proof-of-concept apparatus is shown in figure 2.

Another automated latching system developed at KSC is the Automated Pneumatic Collet Latch (APCL). An existing, manually operated collet latch design with flight heritage dating back to the Apollo and Space Shuttle programs was used as a baseline for the APCL. The collet latch was redesigned so that a pneumatic cylinder mechanism actuates the locking pin, which then spreads the fingers of the collet inside a receptacle housing on the flight-side plate. This results in a latching of the ground-side umbilical plate to the flight-side umbilical plate with the additional advantage of included preload forces. The pneumatic cylinder can be actuated by a remote signal command to a pneumatic valve, therefore achieving automation capabilities. Figure 3 shows an expanded view and an assembly view of the APCL.

Key accomplishments:

- Developed NPALLS and APCL prototype concepts.
- Designed and fabricated NPALLS proof-of-concept prototype.
- Created fabrication drawings for APCL.

Contact: R.P. Mueller (Rob.Mueller@nasa.gov), YA-D1, (321) 867-2557

Participating Organizations: American Remote Vision Co. (S. Gleman) and YA-D1 (A.C. Littlefield and T. Bonner)



Figure 1. In-Line Gripper Wire Rope Device

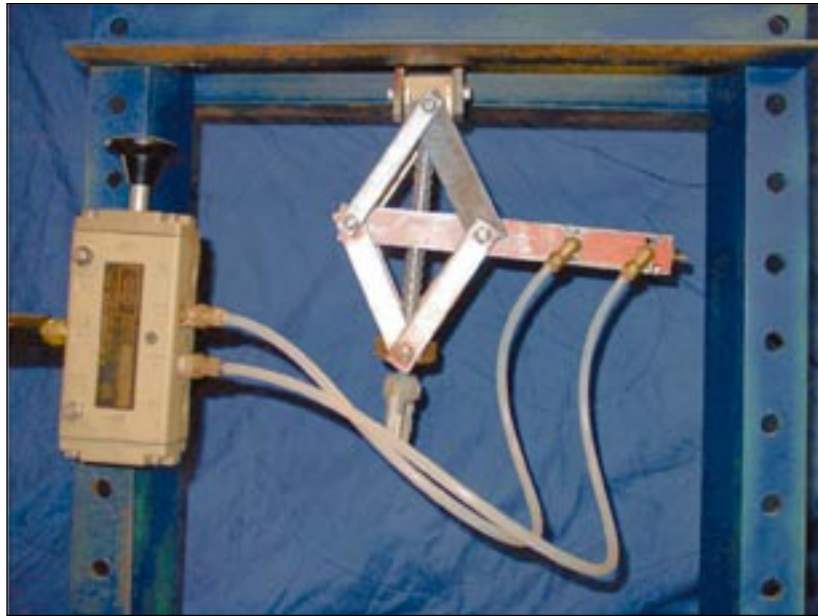


Figure 2. In-Line Gripper Proof-of-Concept Apparatus

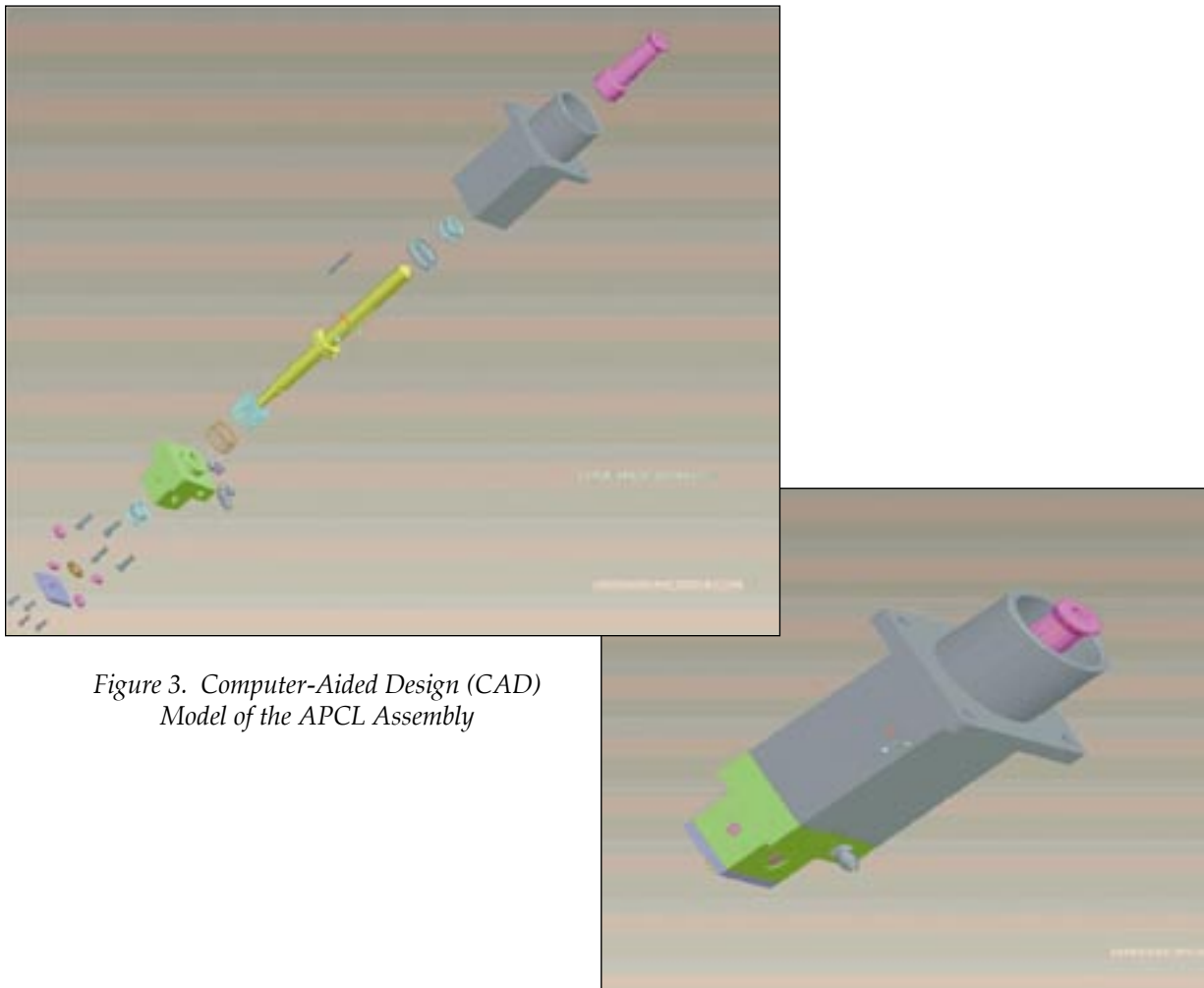


Figure 3. Computer-Aided Design (CAD) Model of the APCL Assembly

Umbilical Ice Suppression and Mitigation System (ISMS) and Cleanliness Verification System (CVS)

Critical automated umbilical systems are retracted from the launch vehicle interface shortly before T-0 to ensure reliability of release and to protect the umbilical system from launch blast damage. In the event of a launch abort, the umbilical system must be reconnected to the launch vehicle interface to safe the vehicle and to drain hazardous cryogenic propellants for reuse. A chilled umbilical system that is retracted and exposed to humidity in the atmospheric air will instantly form a layer of frost, which can turn into ice. The frost/ice can compromise sealing surfaces and can inhibit correct functioning of the umbilical system's mechanisms and dynamics. Therefore, to enable automated umbilicals, ice must be suppressed from forming, or if that is unavoidable, then its presence must be mitigated.

In addition, the umbilical and all sealing surfaces must be clean and free of any contamination. Debris or other contamination in the quick disconnects (QDs) can cause improper sealing, resulting in a hazardous propellant leak, or may cause impurities to be introduced into the main propulsion system.

These factors dictate that an automated umbilical system employs an Ice Suppression and Mitigation System (ISMS) and a Cleanliness Verification System (CVS). A proof-of-concept prototype incorporating an ISMS and a CVS was conceptualized, designed, built, and tested.

The ISMS consists of a spring-loaded, dry, inert-gas purge shroud that surrounds the entire QD umbilical plate on both the flight side and the ground side. A sliding door keeps the purge contained on each umbilical plate when they are separate. The gaseous-helium or gaseous-nitrogen purge prevents ice from forming since the humid atmospheric air is kept away by the positive-pressure purge gas. When the umbilical plates are mated, the shroud retracts with a spring-loaded mechanism, and the purge shroud doors open after the two halves of the purge shroud have mated. The umbilical continues to move forward until the actual QDs have mated. During the entire operation, the QDs are continually purged so there is no chance of any frost/ice formation.

To verify there is no contamination present on the QD, the CVS employs a video camera that transmits a digital image to an electronic image analysis device. As long as there is no change in the digital image, the alarm does not sound. As soon as a piece of foreign object debris (FOD) lands on the QD, there will be a change in the digital image, which causes an alarm to sound with a corresponding signal. Once the FOD is identified visually on a display monitor, the operator can remotely operate a pulsating pressurized gaseous-nitrogen jet nozzle, which is aimed at the FOD on the QD. The pulsating gaseous-nitrogen jet blows the FOD off the QD, and a visual inspection verifies the QD is clean.

The purge shroud prevents ice/frost formation and also maintains a clean environment. The CVS allows for a final inspection and corrective action by blowing the FOD off the QD.

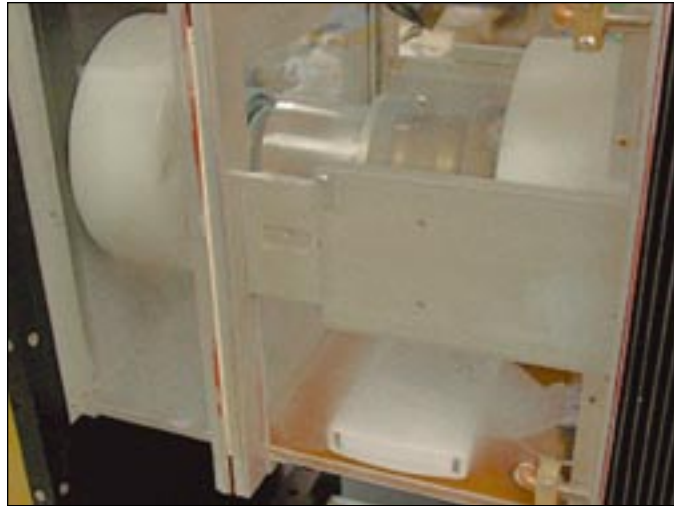
The ISMS and CVS prototypes were tested at liquid-nitrogen temperatures with very positive results. There was no ice formation and the CVS was demonstrated to be an effective concept.

Key accomplishments:

- Developed ISMS and CVS prototype concepts.
- Designed and fabricated ISMS and CVS prototypes.
- Successfully tested the ISMS and CVS prototypes at liquid-nitrogen temperature.

Contact: R.P. Mueller (Rob.Mueller@nasa.gov), YA-D1, (321) 867-2557

Participating Organization: American Remote Vision Co. (S. Gleman)



Cryogenic Fluid Quick Disconnect Inside Ice Suppression Purge Shroud



Proof-of-Concept Prototype ISMS/ CVS Mounted on a Mobile Cart



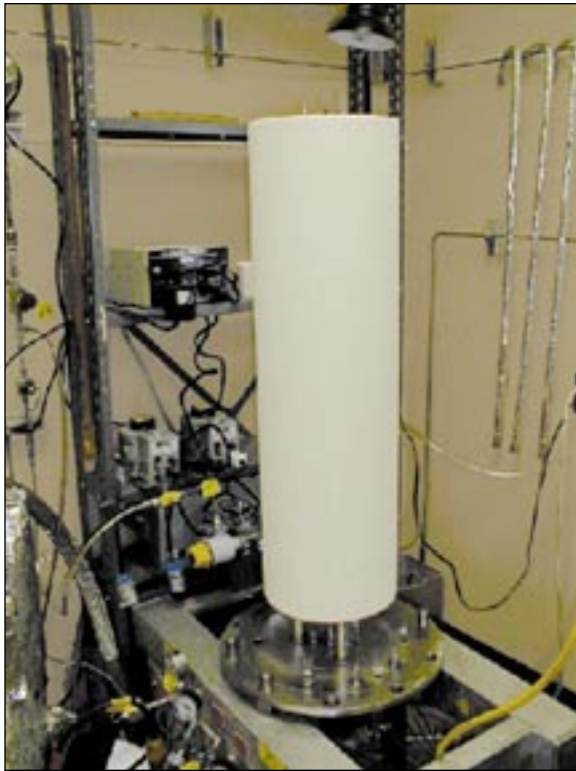
CVS Vision System Control Panel

Testing of Space Shuttle Spray-On Foam Insulation Under Cryogenic Vacuum Conditions

A key element of space launch vehicles is thermal insulation for cryogenic tanks, and the most commonly used thermal insulation material is Spray-On Foam Insulation (SOFI). This lightweight material, a Freon-blown polyurethane foam, provides an excellent combination of thermal and mechanical properties. However, this type of material is generally good only for a one-time-use tank due to problems with multiple thermal cycling and environmental degradation. The reusable launch vehicle of the future will require a fully reusable high-performance thermal insulation system for its cryogenic propellant tanks and feedlines. The cryogenic tank insulation must perform well in all phases of ground servicing, ascent, on-orbit, and reentry mission operations. A well-established reference point based on SOFI is therefore needed for the new materials technology development work. Thermal performance testing of SOFI under full-range cryogenic vacuum conditions was performed at the KSC Cryogenics Test Laboratory in 2002. The SOFI test specimens were sprayed by United Space Alliance personnel.

The steady-state liquid nitrogen boiloff (evaporation rate) calorimeter methods established by the Cryogenics Test Laboratory were used to determine apparent thermal conductivity (k-value) of the insulation material: Cryostat-1 (Cylindrical Test Apparatus) for absolute k-values and Cryostat-4 (Flat-Plate Test Apparatus) for comparative k-values. An overall view of the Cryostat-1 apparatus is shown in figure 1. A liquid nitrogen cold mass maintained the cold-boundary temperature (CBT) at approximately 78 kelvin (K) (-319 degrees Fahrenheit [$^{\circ}$ F]). The warm-boundary temperature (WBT) was maintained at approximately 293 K (+68 $^{\circ}$ F) using an external heater with electronic controller. The temperature difference was therefore 215 K (387 $^{\circ}$ F) while the mean temperature was about 186 K (-125 $^{\circ}$ F). Vacuum environments, or cold-vacuum pressures (CVPs), included the following three basic cases: high vacuum (HV) (below 1×10^{-4} torr), soft vacuum (SV) (1 torr), and no vacuum (NV) (760 torr). Additional tests were performed at cold-vacuum pressures from 1×10^{-5} torr to 760 torr. The key portion of a test from Cryostat-1 is shown in figure 2.

Thirty-three tests of three different specimens were performed. The combined run-time of steady-state liquid nitrogen evaporation was over 500 hours (not including the vacuum pumping and heating cycles). Each of the three test series included at least eight specific vacuum levels (eight tests) from high-vacuum to no-vacuum conditions. The test conditions were representative of the actual-use conditions for cryogenic insulation. The test measurements were made at the full temperature difference and included the full-vacuum pressure range. The results, in terms of k-value and mean heat flux, are currently being used as a calibration reference and as a benchmark of comparison with new materials for next-generation thermal insulation systems. Plans for further work include the experimental study of environmental effects, such as aging and moisture intrusion, and the incorporation of low-temperature compatible coatings.



Contacts: J.E. Fesmire (James.E.Fesmire@nasa.gov), YA-C2-T, (321) 867-7557; and Dr. M.K. Williams, YA-C2-T, (321) 867-4554

Participating Organization: USTDC (K.W. Heckle, Sr. and Dr. S.D. Augustynowicz)

Figure 1. View of Cryostat-1, Cryogenic Insulation Test Apparatus for Cylindrical Specimens, With the Vacuum Can and Instrumentation Removed (The SOFI test article C136 is shown mounted on the cold mass of the cryostat.)

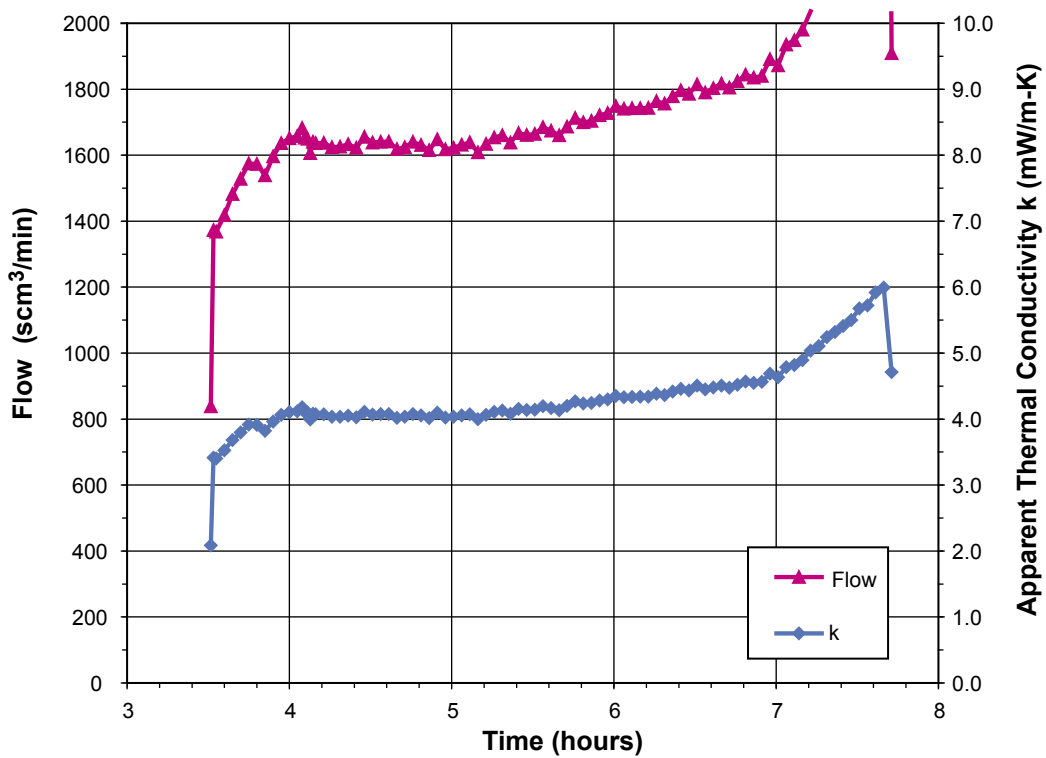


Figure 2. Example of Test Results From Cryostat-1, C136, Test 17: Variation of Liquid Nitrogen Boiloff Flow Rate and Apparent Thermal Conductivity (*k*-value) With Time (The cold-vacuum pressure is approximately 0.1 millitorr.)

Glass Microspheres for Cryogenic Insulation Applications

A common and critical element of space launch vehicles and systems is thermal insulation for cryogenic tanks and piping. Glass microspheres, also known as glass bubbles, represent an alternative insulation material for a number of applications. Commonly used materials, such as Spray-On Foam Insulation (SOFI) for vehicle tanks and perlite powder for ground storage tanks, are targeted for replacement with the new glass bubbles systems. Determining a complete thermal characterization of the glass bubbles was the first step in producing the engineering solutions required for the energy-efficient, low-maintenance cryogenic systems of the future. The testing was performed at the Cryogenics Test Laboratory at KSC in 2002.

The steady-state liquid nitrogen boiloff (evaporation rate) calorimeter methods established by the Cryogenics Test Laboratory were used to determine apparent thermal conductivity (k-value) of insulation material systems. The insulation test material was glass microspheres in bulk form. This economical material is manufactured by 3M. These glass bubbles are hollow and are formulated for a high strength-to-weight ratio. The target isostatic strength, or crush strength, of Type K1 glass bubbles is 1.7 megapascals (MPa) (250 pounds per square inch [psi]). The particle size distribution ranges from 30 to 110 microns with a mean particle size of 65 microns. The bulk density is typically around 0.060 gram per cubic centimeter (g/cm^3).

Fourteen tests were performed using the cryogenic insulation test apparatus for cylindrical specimens, Cryostat-1. The test measurements were made at the full temperature difference (typical boundary temperatures of 78 kelvin [K] and 293 K) and included the full vacuum pressure range. The results were calculated in terms of k-value and mean heat flux. The test conditions were representative of the actual-use conditions for cryogenic insulation. This research showed that a number of tests under different conditions are needed to understand and characterize the glass microsphere material for the full vacuum pressure range. These results will be applied to a number of different projects in energy-efficient cryogenics for space vehicles, space launch, and industry.



Different Cryogenic Insulation Materials in the Bulk Fill Form



LO₂ Storage Tank at Launch Complex 39B

Key accomplishments:

- Characterized material thermal performance under cryogenic vacuum conditions.
- Tested structural insulation panel system using glass microspheres.

Key milestones:

- Experimental study of vacuum and moisture properties of material.
- Testing cryogenic tank insulation system.

Contacts: J.E. Fesmire (James.E.Fesmire@nasa.gov), YA-C2-T, (321) 867-7557; R.A. Breakfield, YA-F2-P, (321) 867-1923; and B.E. Scholtens, YA-C2-C, (321) 867-9196

Participating Organizations: USTDC (Dr. S.D. Augustynowicz and K.W. Heckle, Sr.) and Technology Applications, Inc. (M. Allen)

Standardized Testing of Experimental Thermal Insulation Materials for Low-Temperature Applications

A major function of the Cryogenics Test Laboratory is to develop a world knowledge base for low-temperature thermal insulation systems, materials, and testing. The Cryogenics Testbed now has extensive data on the performance of a wide range of insulating materials at cryogenic temperatures. Ambient temperature data for well-established materials are often readily available from the literature, material vendors, or other Government agencies. However, many new or experimental insulation materials do not have any standard thermal performance characterization to compare with other materials. Furthermore, outside data sources are not consistent in listing test conditions, boundary temperatures, and other important testing details.

To meet the need for standardized testing of experimental thermal insulation materials under ambient conditions, a Netzsch Lambda 2300F Heat Flow Meter has been activated at the Cryogenics Test Laboratory. This in-house capability, using the American Society for Testing and Materials (ASTM) C-518 standard protocol, is being used to complement the extensive technology development work being performed using the family of five insulation research test cryostats currently in service. While the cryostats provide apparent thermal conductivity values for materials under the simulated actual-use conditions of cryogenic temperature and full vacuum, the heat flow meter provides calibrated thermal conductivity values for a material at ambient temperature and ambient pressure only. The new self-contained unit provides quick consistent results for material screening and baseline performance comparisons.

The operational techniques and procedures of the Heat Flow Meter were successfully demonstrated with the proper level of accuracy and consistency within the scope of its intended function. The results of the tests conducted on a standard reference material, Spray-On Foam Insulation (SOFI), were consistent with values obtained from the National Institute for Standards and Testing. Important data were also obtained for aerogel beads, aerogel blankets, glass microspheres, experimental composites, and a number of different types of polyimide foams. In addition, a device and procedure to accommodate "loose fill" and uniquely shaped materials in the test apparatus were successfully developed. This new capability will continue to support research projects for the development of next-generation thermal insulation systems.



Netzsch Lambda 2300F Heat Flow Meter With Typical Sample

Key accomplishments:

- Activation of standardized thermal insulation test machine.
- Development of new capability for experimental material screening.

Key milestones:

- Building insulation material thermal performance database.
- Testing support of next-generation thermal insulation systems research.

Contacts: J.E. Fesmire (James.E.Fesmire@nasa.gov), YA-C2-T, (321) 867-7557; M.A. Doctor, PH-P4-A, (321) 861-7090; B.E. Scholtens, YA-C2-C, (321) 867-9196; and Dr. M.K. Williams, YA-C2-T, (321) 867-4554

Thermal Performance Testing of Cryogenic Piping Systems

From food industry, transportation, energy, and medical applications to the International Space Station, cryogenic liquids must be stored, handled, and transferred from one point to another. The basic problem for any application of cryogenics is protection against heat transfer to minimize the evaporation ratio. This energy conservation translates into a lower cost of operation for the user. There are a number of scenarios for protecting storage tanks and transfer lines from heat. For example, short-term storage, using the cryogen to provide a source of gas, does not require a tank or piping system with an extremely low thermal conductivity factor. System process control is still important, and the thermal insulation systems must be designed accordingly. Applications in which long-term storage and maintaining the quality of the liquid are critical require high-performance materials that provide the most effective level of thermal isolation that can be justified by design and economics. Whatever the cryogenic application, knowledge of the system's operation from the heat transfer point of view is essential. That knowledge will prevent the higher-than-expected life cycle operating costs that often result from selecting the least expensive thermal insulation system, despite its initial cost savings.

The Cryogenics Test Laboratory has developed a new Cryogenic Pipeline Test Apparatus for testing pipelines under different temperature, vacuum pressure, and flow conditions. With cryogenic use more prevalent and with the requirements for higher and higher energy efficiencies, the total system design must be understood in light of its heat-load effects. Up to three different pipelines, in lengths of 18 meters or longer, can be tested simultaneously. The apparatus gives accurate heat leakage data for the test article under simulated conditions of an actual field installation.

The apparatus includes two cold boxes, one upstream and one downstream, between which the test articles are connected. The method of testing can be static (boiloff) or dynamic (flow-through). Figure 1 gives a simplified schematic of the apparatus configured for the static method of testing. An overall view of the upstream cold box, showing three different 18-meter-long cryogenic pipelines under test, is shown in figure 2. The cold boxes are generally oriented so the downstream end of the pipeline is slightly elevated. The cold boxes are mobile such that the apparatus can be reconfigured for different test requirements and a variety of test articles.

The apparatus and method of operation can provide the basis for a standardized test of the thermal performance of pipelines or piping systems. Existing standards have strict limitations, such as applicability for system operating temperatures above ambient. The pipeline test apparatus at the Cryogenics Test Laboratory is U.S. patent-pending and currently slated for use in a number of applied research projects supporting the development of energy-efficient space launch sites. Preliminary work on the insulation envelopes for flexible high-temperature superconducting (HTS) power cables has been completed in collaboration with the Department of Energy and Oak Ridge National Laboratory. Evacuated microsphere insulation panels for cryogenic piping systems are being developed in collaboration with Technology Applications, Inc., Boulder, Colorado. Another project, with AMAC International, Newport News, Virginia, is the development of a cryogenic transfer line with magnetic suspension.

This work was supported in part by the Center Director's Discretionary Fund (CDDF) project "Cryogenic Piping Networks for Energy-Efficient Launch Sites."

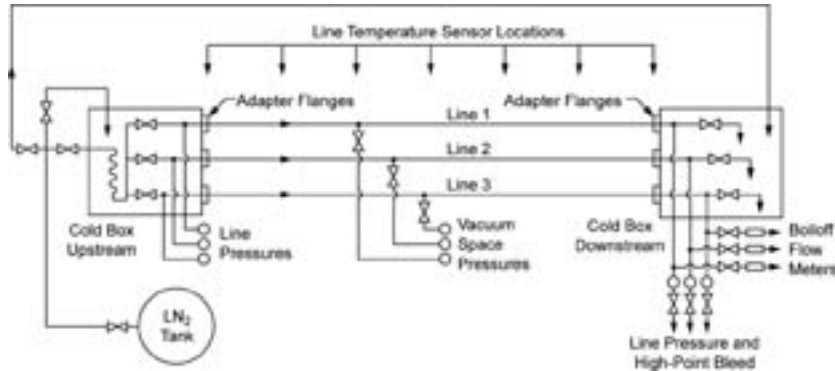


Figure 1. Simplified Mechanical Schematic of the Cryogenic Pipeline Test Apparatus

Key accomplishments:

- Developing a standardized method of static heat leak rate testing.
- U.S. patent application placed for test measurement system and method.
- Testing of state-of-the-art commercial vacuum-jacketed flexhose.

Key milestones:

- Produced prototype experimental pipeline for demonstrating new insulation technology.
- Generated paper and presentation for the International Congress of Refrigeration, Washington, D.C., in August 2003.
- Provided testing support for Small Business Innovation Research (SBIR) projects with Technology Applications, Inc., and AMAC International.



Figure 2. View of the Upstream Cold Box of the Cryogenic Pipeline Test Apparatus With Three 18-Meter-Long Test Articles Installed

Contacts: J.E. Fesmire (James.E.Fesmire@nasa.gov), YA-C2-T, (321) 867-7557; and R.A. Breakfield, YA-F2-P, (321) 867-1923

Participating Organization: USTDC (Dr. S.D. Augustynowicz, Z.F. Nagy, K.R. Cummings, and J.E. Gibson)

Piping System Repair Using Cryogenic Freeze Plug Technology

A safe and reliable method for isolating leaks in cryogenic systems has been developed by the Cryogenics Test Laboratory. In September 2002, a leak caused by a cracked gasket upstream of a liquid oxygen storage tank block (shutoff) valve at Pad 39A threatened to delay a Space Shuttle launch. The new cryogenic freeze plug technology was successfully applied and the cracked gasket was replaced without having to drain (and potential waste) many thousands of gallons of liquid oxygen. This significantly reduced the cost and amount of time needed for the repair and allowed the Shuttle to launch on time.

Previously, this type of repair required draining the 900,000-gallon liquid oxygen storage tank to permit replacement of the pipe sealing gasket. Thermal cycling due to draining/warmup induces stresses on the storage vessel and presents a safety consideration in that the number of drain/warmup cycles is limited.

Creating a freeze plug to isolate the failed gasket and to allow its changeout was discussed with lab personnel. Because liquid oxygen in its solid-state is unstable, freezing it was ruled out. The team investigated an alternative methodology, and an acceptable secondary fluid was introduced into the system downstream of the failed gasket. This secondary fluid was frozen within the cryogenic piping to create an effective plug in the line. This allowed the gasket to be safely replaced without draining the tank.

To accomplish this repair procedure, several technical issues had to be addressed: a dense liquid with acceptable thermal properties had to be found, and it needed to be compatible with liquid oxygen. In addition, it had to be easy to remove, down to a residual concentration level of less than 10 parts per million. A liquid precision cleaning agent was selected and successfully tested on a high-fidelity mockup at the Cryogenics Test Laboratory. These successful demonstration tests and the data obtained were presented to the Engineering Review Board. The repair procedure was then approved for implementation at the launch pad.

The cryogenic freeze plug technique for piping system repair is being further developed for use on larger line sizes and with different fluids.

Key accomplishments:

- The gasket was changed successfully in a liquid oxygen tank outlet pipe with no thermal cycle of the tank required and no commodity loss.
- U.S. patent pending.

Key milestones:

- Investigate using the technique on larger diameter piping systems.
- Investigate alternative secondary fluids.

Contact: C.E. McCaskey (Edward.McCaskey-1@nasa.gov), PH-G1, (321) 861-3754

Participating Organizations: USTDC (Z.F. Nagy, K.R. Cummings, and J.E. Gibson) and United Space Alliance (P.J. Klonowski)



*Cryogenic Freeze Plug Technique Being Applied on Piping at Launch Complex 39A
Liquid Storage Tank*

Automated Thruster Bench Test (ATBT) System

The objective of this effort is to develop a ground test system for Shuttle thrusters that will reduce the possibility of human error. In the past, test results were often recorded incorrectly due to errors in math, data interpretation, and data transcription from the test equipment to the procedure. While these errors have been greatly minimized in recent years, a backup system to the current test setup was still needed.

The system developed uses a commercial off-the-shelf data acquisition system, a standard office PC, and LabVIEW software to perform all thruster tests. Ground testing of thrusters includes solenoid valve timing and valve leak rates, heater checkout, and a three-point calibration of the chamber pressure transducer. The computer performs all data reduction, eliminating mathematical errors. All data is recorded directly onto the computer hard drive, eliminating transcription errors as well. The data is stored in a standard ASCII text format, allowing easy access by computers connected to the network.

The Shuttle primary thrusters use a solenoid valve with a pressure-assisted main stage and a magnetically actuated pilot stage. Requirements for these valves call for determining the valve opening and closing times. This can be determined for the solenoid primary stage from characteristic “peaks and valleys” in the voltage and current during valve opening and closing. These peaks and valleys correspond to movement of the magnetic pilot stage. Movement of the nonmagnetic primary stage is determined by output from an accelerometer. The accelerometer records vibrations through the valve body that occur when the primary stage contacts the valve stops.

The software also monitors the valve timing data for adverse trends and calculates statistical control limits from a database of over 100 previous thruster bench tests. A warning is sent to the user if any of the timing data matches the following criteria:

- Outside of the requirement limits.
- Outside of a 3 sigma control limit (mean ± 3 standard deviations).
- More than 5 data points trending up or down.
- More than 10 data points that do not vary by more than 1 standard deviation.

These control limits are particularly important in this application since the requirement limits are much larger than the typical spread of the data. Without trend monitoring and control limits, abnormal readings could go unnoticed.

Key ATBT features include a software test mode, which allows all the functions of the software to be tested; determination of valve timing data by the software by detection of peaks and valleys in the solenoid valve voltage, current, and accelerometer readings; and application of control limits and trend analysis to valve timing data.

Contact: A.O. Kelly (Andrew.O.Kelly@nasa.gov), PH-G2, (321) 861-3927



ATBT Prototype System



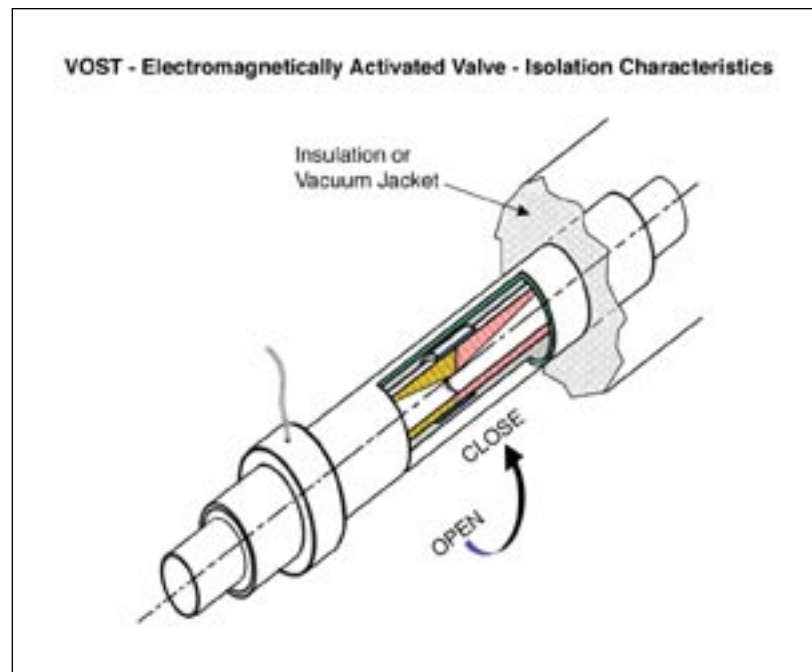
Software Detection of Thruster Valve Timing

Venturi Off-Set Technology Cryogenic Valve

KSC Spaceport Engineering and Technology Directorate is partnering with Big Horn Valve, Inc., Sierra Lobo, Inc., and the Florida State University (FSU) National High Magnetic-Field Laboratory to prototype and test an axially operated, high-efficiency, low-mass cryogenic valve. This valve design innovation, termed Venturi Off-Set Technology (VOST), addresses four critical needs for effective storage, transfer, and use of cryogenics in aerospace:

- Thermal isolation to minimize heat leakage.
- Low-pressure drop to accommodate high flows without cavitation.
- Minimal mass and space requirement due to low profile.
- Adaptability to electromechanical actuation (see the figure).

Existing cryogenic valves require elaborate insulation measures to mitigate heat leakage through actuator stems. They are also characterized by high-pressure drop at high flows, large mass-to-envelope ratio, and high actuation torques. VOST valves eliminate actuator contact with internal wetted parts, potentially improving thermal and fluid containment characteristics necessary for cryogenic propellants, while maintaining high flow. The VOST design is an axially actuated, high-flow, low-pressure-drop, low-mass, thermally isolated valve. The combination of high fluid flow, minimal pressure drop, and axial design envelope is unique and significant among cryogenic valves. The VOST design will eliminate perpendicular actuation devices that are



VOST Valve Cutaway

known, significant heat leak sources, minimize pressure drop under high-flow conditions, reduce device mass, and enable a device envelope that is suited for superior insulation and electromechanical actuation. Currently available cryogenic valves require complex and bulky insulation strategies to maintain safe and predictable fluid conditions, such as warm-gas barriers necessary for effective stem seal operations. VOST valves are ideally suited for electromechanical actuation because only low torque is required to open and close them. These features combine to improve valve safety and reliability necessary for use of cryogenics on Earth, in space, and in extraterrestrial environments.

Applications of this technology include storage and transfer of cryogenic fuel for testing facilities and spacecraft. Non-NASA applications include but are not limited to production facilities for cryogenic and toxic fluids, short- and long-distance transfer of cryogenic and toxic fluids, and the control of cryogenic and toxic fluids within process systems (such as refineries and tank farms).

Contact: W.U. Notardonato (Bill.Notardonato@nasa.gov), YA-D1, (321) 867-2613

Participating Organizations: Big Horn Valve, Inc. (J. Stender), USTDC (Z.F. Nagy and S.J. Sojourner), and Florida State University National High Magnetic-Field Laboratory (S. Van Sciver)

Range Technologies

Range Technologies consist of unique facilities and equipment technologies that provide the control and measurement data necessary to ensure the safety of launch and test operations for the range/spaceport. Examples of these technologies include (1) data processing equipment for range safety analysis, communications systems for telemetry processing, reception, and destruct command systems; (2) sensor and instrumentation systems for vehicle tracking, such as radar systems and optical tracking displays; and (3) data communications management, distribution, and recording systems. Significant capital investment is required to build and maintain this capability and as a result, these assets have traditionally been slow to modernize or have limited flexibility to accommodate new requirements and vehicles. In addition, the cost associated with range system infrastructure is difficult to quantify.

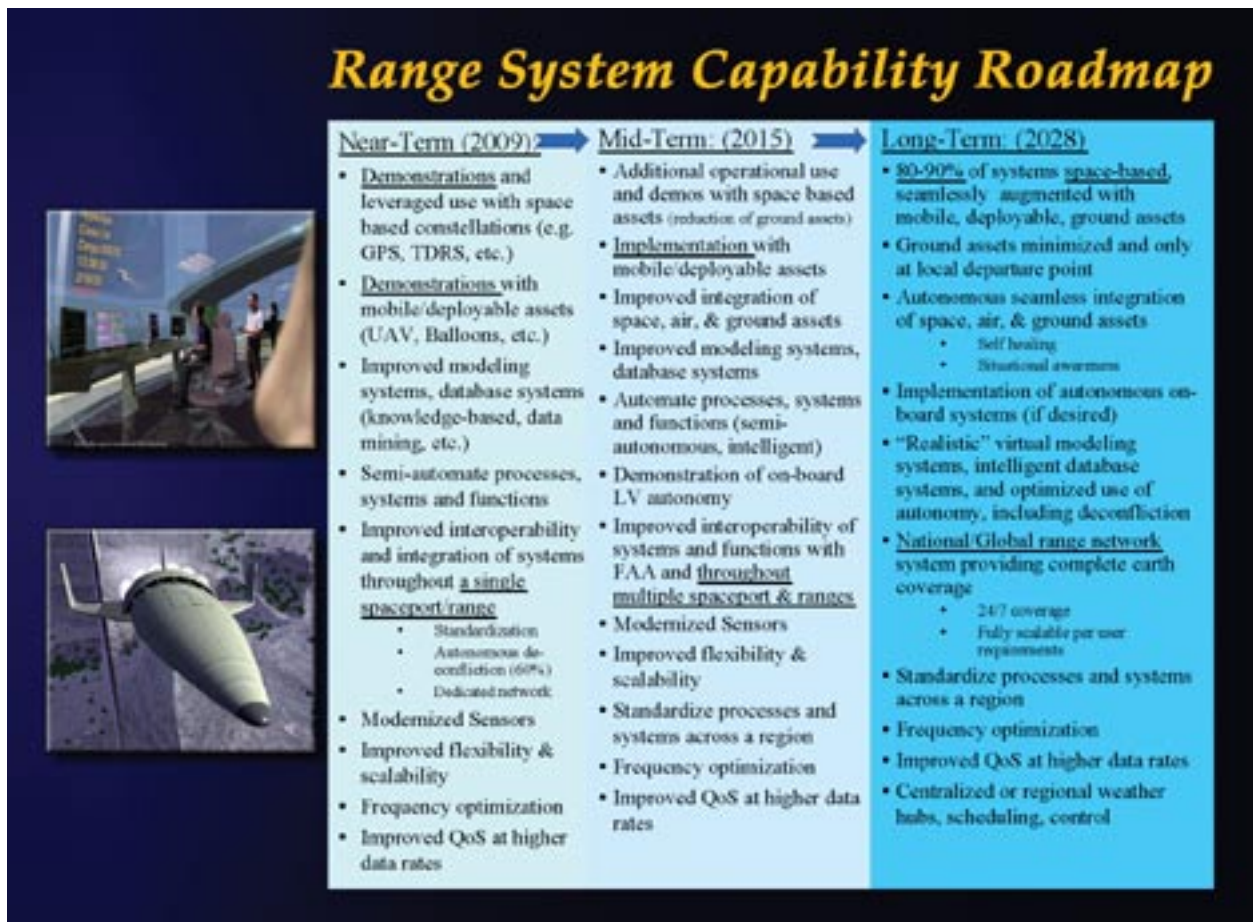
Future range operations will require flexible range technologies that can incorporate the latest technological advances. It is expected to be largely space-based and will be seamlessly augmented with mobile, deployable, and/or ground-based assets. Minimal ground infrastructure will be required and will primarily be located at the launch head, reducing the operational cost. Self-healing autonomous ground and flight systems will become the norm. Range systems will have situational awareness and be intelligent enough to reconfigure autonomously when individual systems “drop out” or are unavailable. A National/Global Range Network with regional hubs is envisioned, which provides 24/7 coverage, is scalable to user requirements, and is seamlessly integrated into the national and global air space. The modernization activities will also ensure that future technology improvements will be able to adapt to different space flight hardware designs, and the degree of customization or reconfiguration for specific launch vehicles operations will be minimized. Multiple simultaneous test and launch operations by multiple vehicles from multiple spaceports are also envisioned.

With the goals and objectives of improving safety, improving range responsiveness (support more launches, reduce lead and turnaround time, and reduce delays), reducing variable launch and range costs, reducing cost of fixed infrastructure, and improving capacity and flexibility, the KSC team has stepped up to colead, with the Air Force Space Command, a national coalition called Advanced Range Technologies Working Group (ARTWG), which is identifying the next-generation range technology roadmaps for the next 25 years.

The seven range technology areas of focus include:

- Weather Instrumentation and System Technologies
- Tracking and Surveillance Technologies
- Telemetry Technologies
- Decision Modeling and Analysis Technologies
- Planning, Scheduling, and Coordination-of-Assets Technologies
- Command and Control Technologies
- Communication Architecture Technologies

An overall system capability roadmap has been developed. In addition to the system roadmap, individual technology roadmaps have also been developed for each of the seven technology focus areas. The complete set of roadmaps is available at the ARTWG Web page at <http://ARTWG.KSC.NASA.GOV>.



ARTWG Range System Capability Roadmap

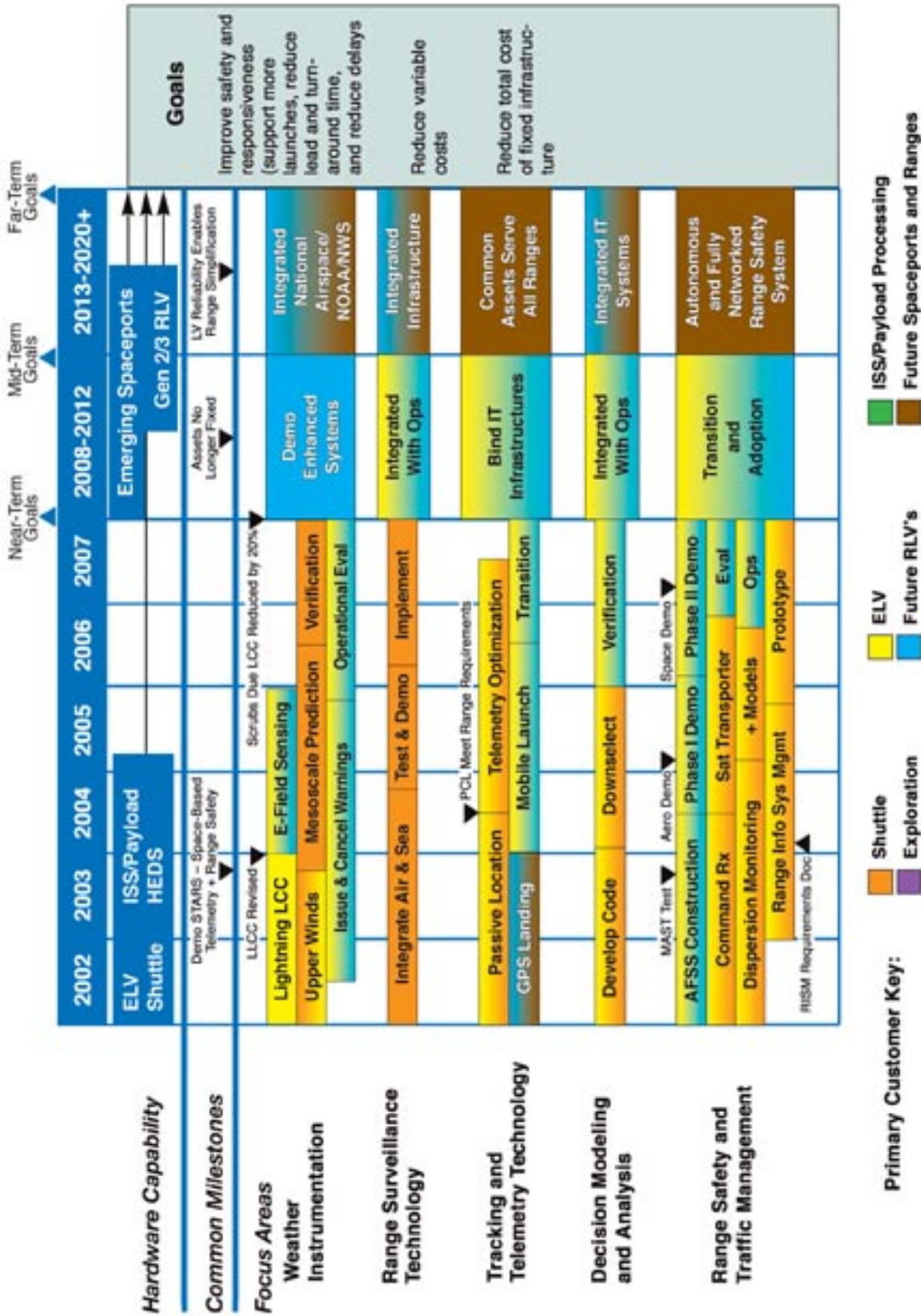
The national Advanced Range Technologies roadmaps and the KSC Range Technologies Roadmap are being used by KSC to help define our technology development plans and strategies.

The overall goals of both of these road-mapping activities are to identify technology improvement plans for future launch and test ranges that are more reliable, maintainable, available, and operable; more adaptable to fit the mission; more flexible and allow for more capacity; more integrated with other systems (range, spacecraft, launch vehicle); more customer- and user-friendly; and more economically viable.

The technology projects that follow provide a glimpse of some of the current technology development activities to allow for the significant improvement desired.

For more information regarding Range Technologies, please contact Richard Nelson, (Richard.A.Nelson@nasa.gov), YA-D7, (321) 867-3332, or Darin Skelly (Darin.M.Skelly@nasa.gov), YA-E, (321) 861-3639.

Range Technologies Roadmap



Space-Based Telemetry and Range Safety (STARS)

The goal of the Space-Based Telemetry and Range Safety (STARS) project is to determine the feasibility of using space-based assets, such as the Tracking and Data Relay Satellite System (TDRSS) and Global Positioning System (GPS), to increase flexibility and minimize range operation costs by reducing the need for ground-based range assets and infrastructure.

STARS is divided into the Range Safety (RS) and Range User (RU) subsystems. The RS subsystem provides GPS data for vehicle tracking and Flight Termination System (FTS) commanding, and the RU subsystem provides vehicle telemetry such as video, voice, and data. The core components for the RS subsystem for Flight Demonstration 1 include a versatile low-power transceiver (LPT) (figure 1) for bidirectional communications with TDRSS and ground-based facilities near the Launch Head, a state-of-the-art Command and Data Handler (C&DH) (figure 2) to process the FTS commands and format the return link telemetry, and a commercial high-dynamics GPS receiver. The RU subsystem uses a commercial multiplexer S-band transmitter and S-band antennas.

Data from the flight demonstrations will be distributed in real time to Dryden Flight Research Center (DFRC), KSC, and Wallops Flight Facility (WFF) via White Sands Complex (WSC) (see figure 2). KSC has integrated a “Range Simulator” using commercial off-the-shelf software and hardware to support STARS and other Range Technology projects. The simulator was used to support acceptance testing of STARS hardware and will be used to graphically display flight parameters and telemetry data in real time during flight and to aid in postflight analysis.

For Flight Demonstration 2, the LPT, GPS receiver, and the C&DH will be combined into a single box that will perform nearly all the Range Safety functions, and the FTS command link will be encrypted and encoded. The RU subsystem will use a Ku-band transmitter and a Ku-band phased-array antenna that is under development to support increased communications bandwidth requirements.



Figure 1. Low-Power Transceiver (LPT)



Figure 2. Command and Data Handler (C&DH)

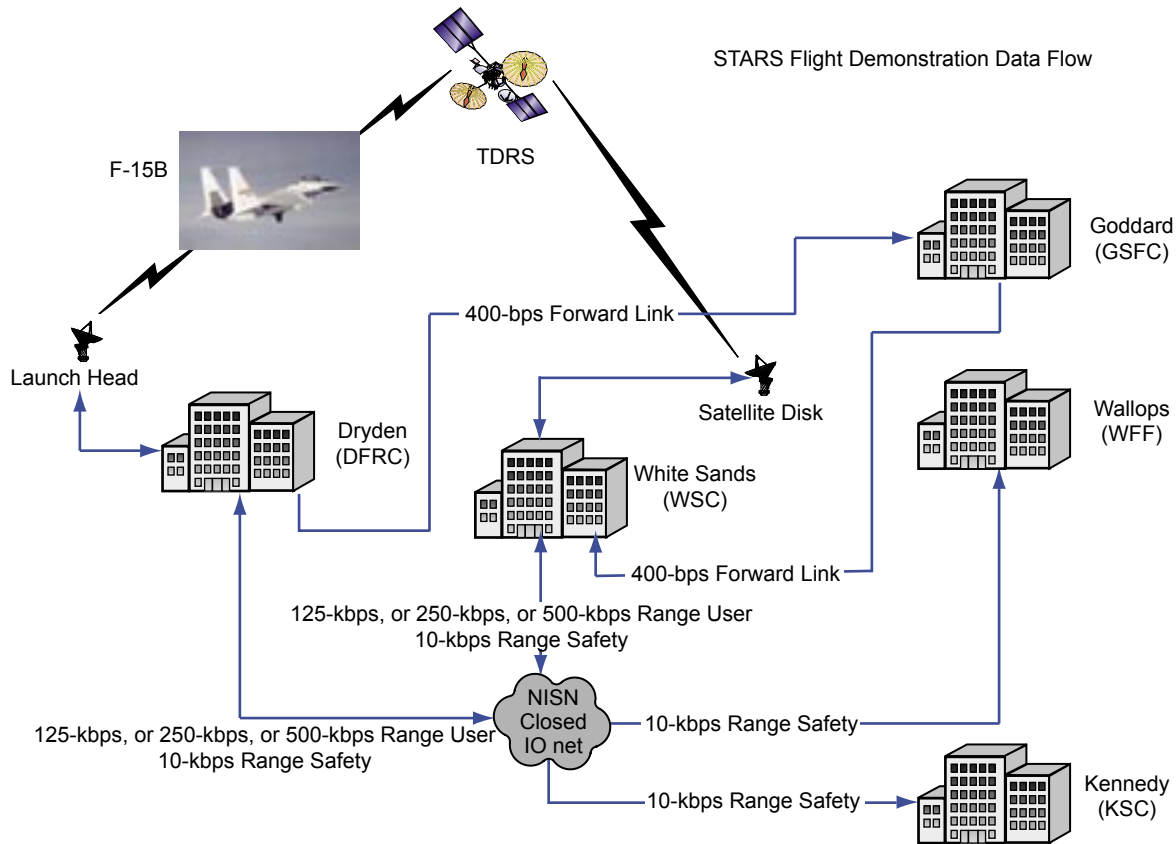


Figure 3. Data Distribution Diagram

STARS is truly a One NASA project. Eleven NASA facilities, as well as the Eastern and Western Ranges, are involved.

Key accomplishments:

- Developed and delivered RS and RU hardware to DFRC.
- Integrated STARS hardware on F-15B.
- Successfully completed Flight Demonstration 1, which consisted of a series of seven flight tests to prove the concept of a spaced-based range.

Key milestones:

- 2003: Flight Demonstration 1 on an F-15B at DFRC.
- 2004: Flight Demonstration 2 on an F-15B at DFRC.
- 2005: Flight Demonstration 3 on a hypersonic vehicle.

Contacts: R.A. Nelson (Richard.A.Nelson@nasa.gov), YA-D7, (321) 867-3332; L.M. Valencia, YA-E6, (321) 861-7682; and E.C. Denson, YA-D7, (321) 867-6537

Participating Organizations: USTDC (R.B. Birr), GSFC (T.C. Sobchak), DFRC (R.D. Sakahara and D.E. Whiteman) WFF (S.N. Bundick), WSC (J.M. Gavura), and ITT (M. Harlacher and S. Casteel)

Iridium Flight Modem

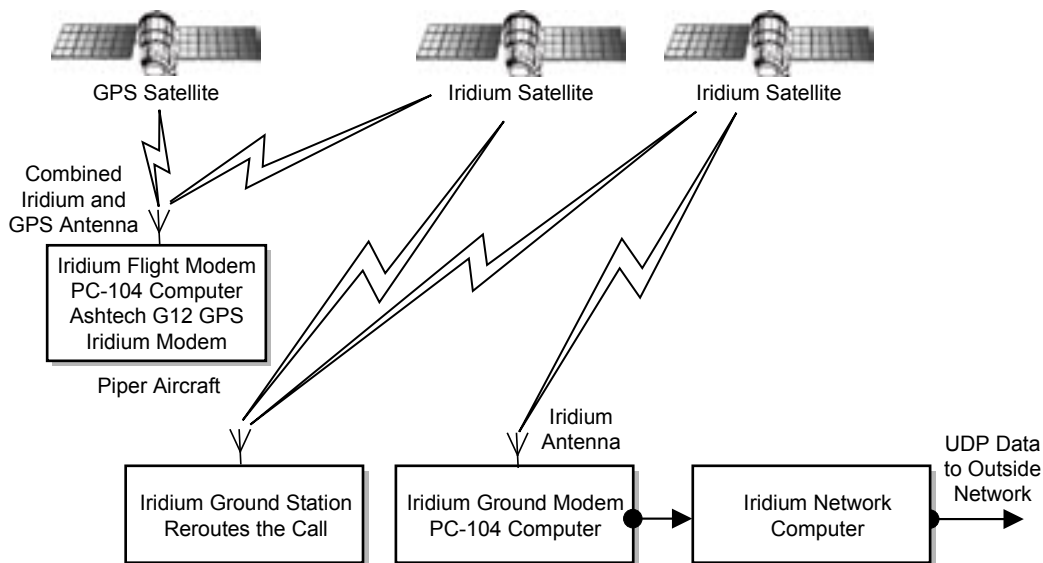
This has been a very successful second year for Iridium Flight Modem, a joint project at KSC and Wallops Flight Facility (WFF) to investigate the Iridium satellite system for low-rate, full-duplex aerospace-related communications (Global Positioning System [GPS] tracking data and commands). Flight Modem uses commercial off-the-shelf communications equipment, a high-dynamics Coarse Acquisition (C/A-Code) GPS receiver, and a PC-104 computer. The target applications for this project are tracking and telemetry for weather balloons, manned and unmanned aircraft tracking and commanding, and possibly two-way backup communications systems for rockets.

Iridium is a commercial global satellite cell phone system for voice and data. Worldwide coverage is provided by 66 low Earth orbit satellites equally spaced in 6 orbital planes at an altitude of 780 kilometers (km). Each satellite has 48 spot beams, and each spot beam has a diameter of 300 to 400 km on the Earth's surface. Because these beams overlap, each satellite can effectively cover a circular region on the ground with a diameter of 3,000 to 4,000 km.

L-band frequencies are used for the uplink/downlink segments, and the signaling is frequency division multiple access/time division multiple access. The guaranteed data rate is 2,400 bits per second (bps) with a 12-decibel link margin, although this can be increased to 3,800 bps with a smaller link margin. The primary gateway is in Tempe, Arizona, and a Department of Defense gateway is in Hawaii. The main satellite ground control station is in Leesburg, Virginia, and a backup facility is being added in Chandler, Arizona. The current cost of modems is about \$1,200 and is expected to drop to \$200. Airtime currently costs about \$0.80 per minute and may also decrease in the future.

Various types of connections are available, including mobile-to-PSTN (public switched telephone network), PSTN-to-mobile, mobile-to-mobile, and direct Internet, where Iridium is the Internet service provider. Short-burst messaging capability is in beta testing and mobile-to-direct Internet protocol is planned for the future.

Flight tests indicate that Iridium Flight Modem operates reasonably well for relatively slow moving aircraft, although the currently attainable reconnect times of 20 to 30 seconds may preclude



Configuration of Iridium Flight Modem During the First Two Test Flights



Integrated Iridium Flight Modem/Computer Box

its use as a primary Range Safety asset. Flight Modem's performance during high-dynamic and high-altitude (greater than 100,000 feet) maneuvers with large Doppler shifts and decreasing spot size will be tested on an upcoming sounding rocket flight.

A future weather-related project under consideration is using Iridium Flight Modem to transmit the current position of surveillance planes to an integrated weather display for pre-launch operations.

Key accomplishments:

- November 2001: Developed flight-ready prototype of Iridium Flight Modem.
- December 2001: Performed ground-based demonstration with GPS data sent from KSC to WFF via Iridium satellite system. WFF verified data originated from KSC with mapping software.
- March 2002: Conducted first aircraft flight test on a Piper Cherokee 140 flying in the KSC vicinity.

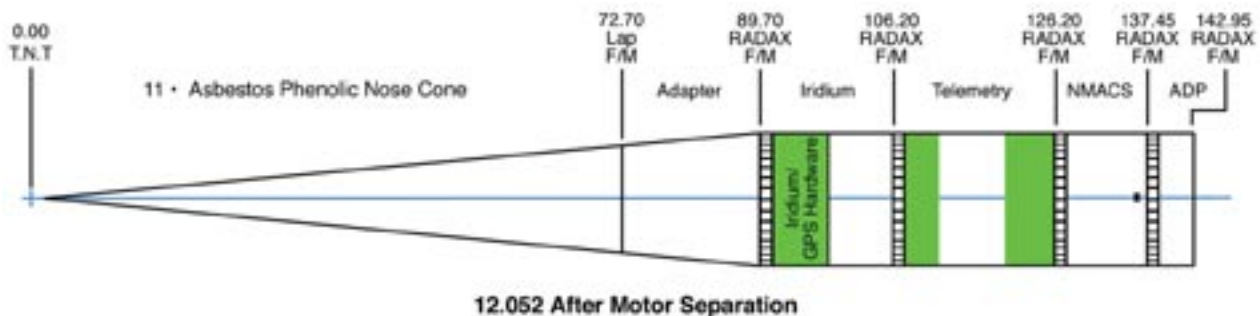
- May 2002: Conducted second flight test on a Piper Cherokee 140 flying a series of banked turns and spirals off the coast of KSC. Changed to a Linux operating system.
- June 2002: Conducted third and fourth flight tests on a P-3 Orion. These were flights of opportunity and consisted of a 3-hour round-trip training flight from WFF to Greensboro, North Carolina, and a 3-1/2-hour geophysical mapping operation from WFF to Iowa.
- July 2002: Developed prototype multiplexed dual modems.
- February 2003: Designed and built an integrated computer/modem box for quick installation on aerospace vehicles.
- March 2003: Conducted first unmanned aerial vehicle test on a large-model aircraft at KSC. Showed that antennas and modems could be mounted on such a vehicle and initial link could be established.

Key milestone:

- June 2003: Sounding rocket flight scheduled at WFF. This test will help determine the limits of this technology.

Contacts: Dr. J.C. Simpson (James.C.Simpson@nasa.gov), YA-D7, (321) 867-6937; E.C. Denson, YA-D7, (321) 867-6537; and A.J. Murray, YA-D7-E1, (321) 867-6673

Participating Organizations: USTDC (R.B. Birr and Dr. C.T. Mata), NAL Research Corporation (Dr. N. Hoang), and WFF (A.M. Coleman and R.L. Wessells)



Placement of Iridium Hardware on a Typical Sounding Rocket

Autonomous Flight Safety System (AFSS) – Phase II

The Autonomous Flight Safety System (AFSS) is a real-time onboard hardware and software system for tracking and possible flight termination. AFSS is designed primarily for small expendable vehicles at remote launch sites where providing traditional ground-based range safety infrastructure, including radio frequency (RF) communication and command links, radar stations, data processing, display facilities, and trained operators, would be extremely expensive. Advantages of using AFSS include global coverage and decreased costs during remote launch site operations. The system may also be useful as a training aid and as a backup system for other types of vehicles. It may also serve as a flight crew advisory system for manned vehicles. Global Positioning System (GPS) receivers provide tracking data. An onboard processor compares the current position, velocity, and attitude with the nominal trajectory and predetermined flight safety rules to autonomously terminate flights when appropriate. A feasibility study (Phase I) was completed in 2000, and a proof-of-concept hardware system (Phase II) was successfully tested in 2002.

This report covers AFSS Phase II testing and test results (see Research and Technology 2002 Annual Report for design information). A small team of NASA and contractor employees as identified below, along with major responsibilities, performed the Phase II work:

- NASA – KSC: flight hardware, real-time operating system (RTOS), and integration.
- NASA – Wallops Flight Facility (WFF): trajectory simulation.
- Lockheed Martin, prime contractor, supported by subcontractor KT Engineering: algorithm, decision logic, and display software.

The primary objective of the laboratory demonstration test was to evaluate the AFSS decision logic software installed in a fully integrated AFSS system, using WFF-generated flight trajectory simulations. Testing was conducted in the WFF GPS Simulation Laboratory in accordance with the AFSS Test Scenario Procedures document (developed by the WFF Guidance, Navigation, Control, and Systems Engineering Branch). Two baseline missions were utilized; the first was based on Kodiak Star, and the second was a custom-designed trajectory referred to as Wallops Express. Various failure scenarios created by WFF personnel based on these two missions were run and graded.

The AFSS Phase II flight configuration used for demonstration testing included Ashtech G12 GPS receivers in conjunction with a VME Radstone PPC4A-750 single-board computer (SBC) running VxWorks RTOS.

Although there were several failures of the AFSS system (both decision logic and SBC RTOS input/output [I/O]-based), the primary test objective of verifying this type of system's feasibility was met during the testing of 28 unique scenarios.

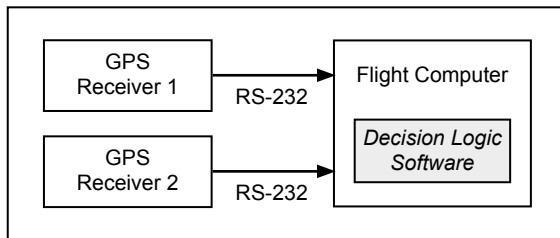
Many of the decision logic problems can be traced back to an attempt to emulate the human decision process exactly. Among the unique problems

encountered with the decision logic are “first motion of the flight vehicle” and divergence of redundant sensors. In addition, more robust I/O routines are needed on the SBC RTOS to ensure reliability of the AFSS.

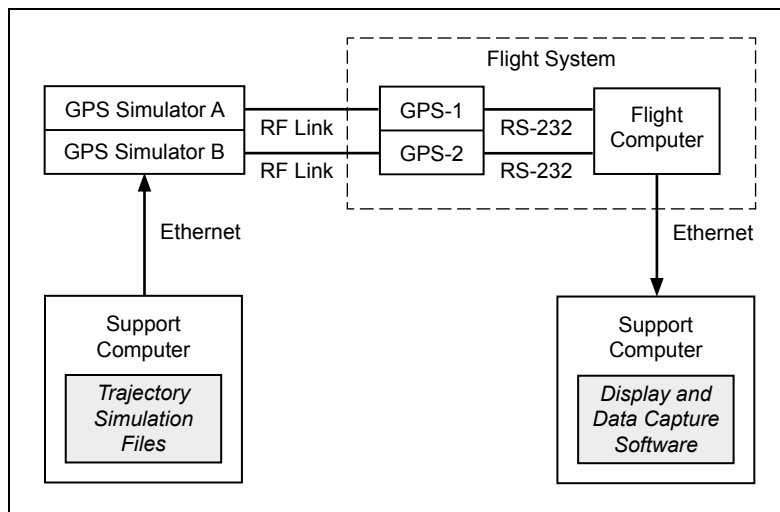
Currently, the potential of a Phase III to produce an integrated, flight-ready, and flight-tested system with improved nonmap-based algorithms is being studied, and use of onboard inertial measurement units is being examined.

Contacts: Dr. J.C. Simpson (James.C.Simpson@nasa.gov), YA-D7, (321) 867-6937; B.A. Ferrell, YA-D7, (321) 867-6678; and R.A. Nelson, YA-D7, (321) 867-3332

Participating Organizations: USTDC (J.A. Marin, R.D. Zoerner, and T. Erdogan); WFF (J.B. Bull, J.C. Hickman, R.J. Lanzi, M.S. Patterson, W.R. Powell, S.E. Kremer, and G.F. Robinson); and Lockheed Martin (S. Haley)



Phase II Flight Configuration



Laboratory Demonstration Test Configuration

Range Simulator

The KSC Advanced Range Technologies Laboratory has successfully integrated several different hardware and software packages into a versatile support environment that is used daily for a variety of projects. The core packages include a CAST Global Positioning System (GPS) simulator, high-dynamic GPS receivers, Satellite Tool Kit (STK), and Veridian telemetry decommutation boards and telemetry software. There are also real-time operating system development environments such as VxWorks and Linux for embedded processors; digital signal processors; and MATLAB, LabVIEW, and many custom programs for technical computing and visualization.

The GPS simulator produces a subset of the signals created by the GPS satellite constellation at specific places and times determined by either internal test scenarios or external trajectory files. These signals are then connected to a GPS receiver whose output can be used to test the GPS coverage and the receiver's performance. External files for antenna patterns can also be included. The simulator has been used for pre- and postflight analysis and acceptance testing.

STK is the leading commercial off-the-shelf software solution for the aerospace industry. Some of STK's basic applications include calculating and visualizing a vehicle's position and attitude in two or three dimensions using either internal test scenarios

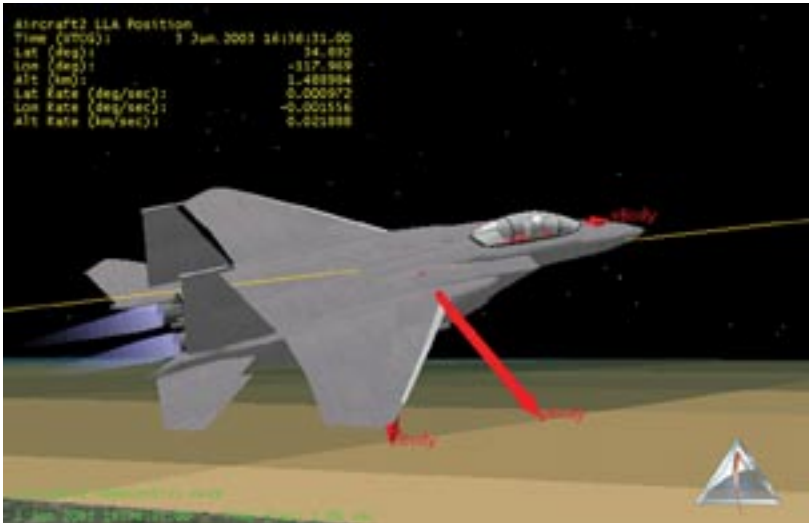
or external data files, determining acquisition times from space- or ground-based sites, analyzing the vehicle's field of view, and determining communications link margins. A large database of satellite orbits is also available.

Veridian hardware and software are widely used in the aerospace industry for real-time and post-test data processing and telemetry signal decommutation and reproduction. Data from a wide variety of archived and real-time sources can be displayed, manipulated, and easily reformatted for further analysis.

The support provided for the Space-Based Telemetry and Range Safety (STARS) project is an excellent example of the capabilities of the Range Simulator. STARS is a multifaceted and multicenter NASA project to determine the feasibility of using the NASA Tracking and Data Relay Satellite System (TDRSS) and GPS to provide reliable communication, telemetry, and tracking for launch vehicles. The GPS simulator was used to flow data through the custom-built Command and Data Handler (C&DH) flight processor with a real-time operating system during acceptance testing and was used to build a scenario to test predicted link margins. During the first series of flight tests with an F-15B at Dryden Flight Research Center (DFRC) in May 2003, KSC received the real-time Range Safety data over the NASA data network. The Veridian hardware decommutated and reformatted this data for display on a large video screen in a conference room at KSC. LabVIEW was used to display various health and status information, and STK/MATLAB showed the aircraft's posi-



LabVIEW Telemetry Interface Showing STARS Internal Processor Health and Status



STK Display of the F15 During the First STARS Test Flight Using Actual Flight Data

tion and heading on a 3-D animated map. Data was recorded and archived at DFRC for postflight analysis using Veridian's database, playback, and reformatting capabilities; STK's analysis and visualization tools; and many of the customized analysis programs.

Key accomplishments:

- STARS Support.
 - VxWorks real-time operating system on embedded computer.
 - Acceptance testing of the C&DH processor.
 - Trajectory and link margin analysis.
 - Real-time telemetry decommutation.
 - Data extraction/analysis for flight tests using archived files.
 - Real-time data displays and 3-D visualization during flight tests.
- Autonomous Flight Safety System Support.
 - VxWorks real-time operating system on embedded computer.
 - Interface development and testing using GPS receivers and simulated GPS data.
- Iridium Flight Modem Support.
 - Signal analysis.
 - Linux and VxWorks real-time operating system on embedded computers.
 - Trajectory and link margin analysis including use of actual antenna patterns.
 - Acceptance testing of miniaturized integrated modems/GPS receivers.

- Columbia Accident Investigation Support.
 - Trajectory and vehicle attitude analysis.

Key milestones:

- 2001: Conceptual design of the simulator.
- 2002: Integrated STK, MATLAB, and GPS simulator.
- 2003: Added Veridian hardware/software and LabVIEW capabilities. An upgrade is planned to the GPS simulator to include simulated inertial measurements capabilities.

Contacts: Dr. J.C. Simpson (James.C.Simpson@nasa.gov), YA-D7, (321) 867-6937; E.C. Denson, YA-D7, (321) 867-6537; and S.W. Boyd, YA-D7-E1, (321) 867-6741

Participating Organization: USTDC (T. Erdogan, R.B. Birr, J.A. Marin, R.D. Zoerner, Dr. C.T. Mata, and Dr. C.D. Immer)

Range Information System Management

Current Range Technology systems rely heavily on expensive networks of unique and costly ground-based communication assets to interconnect tracking, communications, and flight termination functions. Much of this aging infrastructure is interconnected through legacy-installed, nonmovable cables. A future vision of a more flexible Spaceport and Range is emerging, based on high-speed first mile/last mile communication technology arising from recently developed commercial technologies. These new technologies, seamlessly extending existing legacy Range infrastructure without wires and cables, hold great promise for preserving the utility of existing Range infrastructures while providing life cycle cost savings and increased operational flexibility.

The common theme needed to accomplish this future vision is a coherent Range Information System Management (RISM) plan. In FY 2002, the RISM project began work on this plan by surveying the Range and identifying the existing key communication functions. In addition, the RISM project investigated the leading candidate commercial technologies in which early involvement would likely provide the greatest returns on investment toward accomplishing future Range-related communication tasks. In FY 2003, the follow-on project, Emerging Communication Technology (ECT), continues this effort through a detailed investigation of the leading candidate technologies identified by RISM. Together, RISM and ECT provide a course of action for achieving a coherent vision for meeting future Range communication technology needs.

During FY 2002, the RISM project identified three key emerging technology candidates to be further investigated on ECT. These three technologies were Ultra-Wideband (UWB), Wireless Ethernet (Wi-Fi), and Free-Space Optical (FSO). The RISM project also released a report identifying the major communication trends and techniques being developed today in the private sector, as well as their likely contributions to meeting future Spaceport and Range needs.

The following are key aspects of the Range communication vision:

- Mobile, portable, fixed Range/Spaceport requirements.
- High bandwidth, high data-rate capability over three decades of data rates (10 megabits per second [Mb/s] to 10+ gigabits per second [Gb/s]).
- Seamless connections to today's wired communication infrastructure and future systems.
- Selectable features versus communication capability to best match future needs and flexible provisioning for quick turnaround.

The ECT project will procure UWB, Wi-Fi, and FSO exemplars and will collect measured results on various performance parameters using a specially instrumented advanced networking laboratory at KSC to determine the limits of these technologies. With this knowledge, the shortcomings of the commercial products will be identified, and it will be possible to influence the developments of the next generation of commercial products to meet specialized Range needs.

Comparison of Leading Candidate Communication Technologies

Key Range Communication Attributes	Medium Data Rates (10 Mb/s – 100+Mb/s)	High Data Rates (100 Mb/s – 1,000+Mb/s)	Highest Data Rates (1,000 Mb/s – 10,000+Mb/s)
Candidate Technology	Wireless Ethernet (Wi-Fi)	Ultra-Wideband (UWB)	Free-Space Optical (FSO)
Maximum Range	> 30 km	> 10 km	> 1.5 km
Typical Range	> 10 km	> 5 km	> 1 km
Minimum Range	< 1 m	< 2 m	< 100 m
Selectable Data Security	Yes	Yes	Yes
Portable, Mobile, Fixed	Yes	Yes	Yes
Regulatory Impacts	None	< 50 m Maximum Range at Present for UWB	None

The ultimate outcome will be to establish a set of criteria for best fitting the appropriate technology to the Range communications needs while achieving connectivity over at least three decades of data rates. Once the performance limits of these technologies are determined on ECT, it will be possible to enhance future Range capabilities while maintaining or even increasing Range safety and lowering life cycle costs.

Key accomplishments:

- Attended Advanced Range Technology Working Group (ARTWG) and Advanced Spaceport Technology Working Group (ASTWG) conferences at KSC and Colorado Springs, Colorado.
- Established the Future Integrated Range and Spaceport Technology Working Group (FIRSTWG) comprising more than 80 senior aerospace leaders and managers from Government, industry, and academia.
- Arranged technical seminars for FIRSTWG presentations in FY 2002 (continuing biweekly through FY 2003.)
- Arranged site briefings and familiarization visits for NASA and contractor personnel to the Eastern Range facilities.
- Supported ARTWG and ASTWG development efforts through participation in the following subgroup teams: Vision, Communication, Telemetry, Command and Control, and Tracking and Surveillance.

Key milestone:

- September 2002: Released RISM Phase I final report identifying Range communication infrastructure sites and links, existing commercial communications technologies, and three key technologies for further investigation.

Contact: R.A. Nelson (Richard.A.Nelson@nasa.gov), YA-D7, (321) 867-3332

Participating Organizations: USTDC (Dr. G.L. Bastin, W.G. Harris, C. Kerios, T. Erdogan, and E.H. Williams). More than 80 people from at least 14 organizations are also participating in this project in FIRSTWG telephone conferences. Major scientific contributors include Wallops Flight Facility, 45th Space Wing, KSC, FAA, NOTU, CCAFS, VAFB, SMC/CWP, ENSCO, DOC, DOD, Boeing, CSR, Lockheed-Martin, Harris Corporation, University of Central Florida, Florida Institute of Technology, and University of Florida.

Accurate Location of Lightning Strikes

Lightning strikes generate large electric and magnetic fields. These fields, when introduced into electrical conductors, can result in large voltage or current spikes. These large induced voltages can result in immediate damage to sensitive components, especially those containing semiconductor devices.

Following a lightning strike at the Space Shuttle launch pads, equipment and instrumentation are tested according to the test plan in KSC SWE-0018, Volume 2. Complete testing involves turning all the equipment on and is conducted when either of the following conditions is met:

- The voltages or currents recorded by the Lightning-Induced Voltage Instrumentation System (LIVIS) at the launch pads exceed the limits established by the operation and maintenance requirements.
- The lightning channel traveled past the mast and the catenary lightning protection wire and struck either the pad structure or the vehicle.

There have been instances when it was impossible to see the attachment

point of the lightning strike due to heavy rain. Without a clear attachment point, it is hard to know whether to conduct a complete test or waive the requirement. The accurate lightning location system can assist in determining the exact attachment point and can help assess whether additional testing is required.

The fast-varying electric current associated with lightning discharges generates large electric field variations, which propagate at the speed of light in a radial direction away from the striking point. At the same time, thunder is generated as a result of the sudden heating of the air caused by the large currents associated with the lightning discharge. For an observer located away from the striking point, the electric field waveform arrives earlier because it travels at a speed of 300 million meters per second (m/s), while the sonic wave travels at about 350 m/s depending on air temperature and humidity.

The Sonic Lightning Locator (SOLLO) consists of an electric field sensor and four sonic (thunder) recorders. Three of these sonic sensors are located in the perimeter of a 4-m-radius circle, 120 degrees apart from each other, with the electric field sensor placed in the center of the circle. The fourth sonic sensor is located 2 or 4 m above the plane formed by the other three sensors. Based on the differences in the time of arrival of the sonic wave at each sensor, a set of equations is solved to obtain the direction to the lightning strike. The differences in the times of arrival can be measured to better than 10 microseconds by performing real-time digital cross-correlations among the signals received by the four sonic sensors. The result consists of direction (azimuth and elevation) and distance to the lightning strike. The location accuracy is better than 5 meters for a strike within a 0.5-kilometer radius. Digital signal processing techniques are used to discriminate between thunder waveforms from a close lightning strike (within approximately a 1-mile radius) and thunder waveforms from a preceding but more distant strike. This process is important because during the active phase of a thunderstorm lightning activity could occur at a rate exceeding 10 strikes per minute.



SOLLO

Key accomplishment:

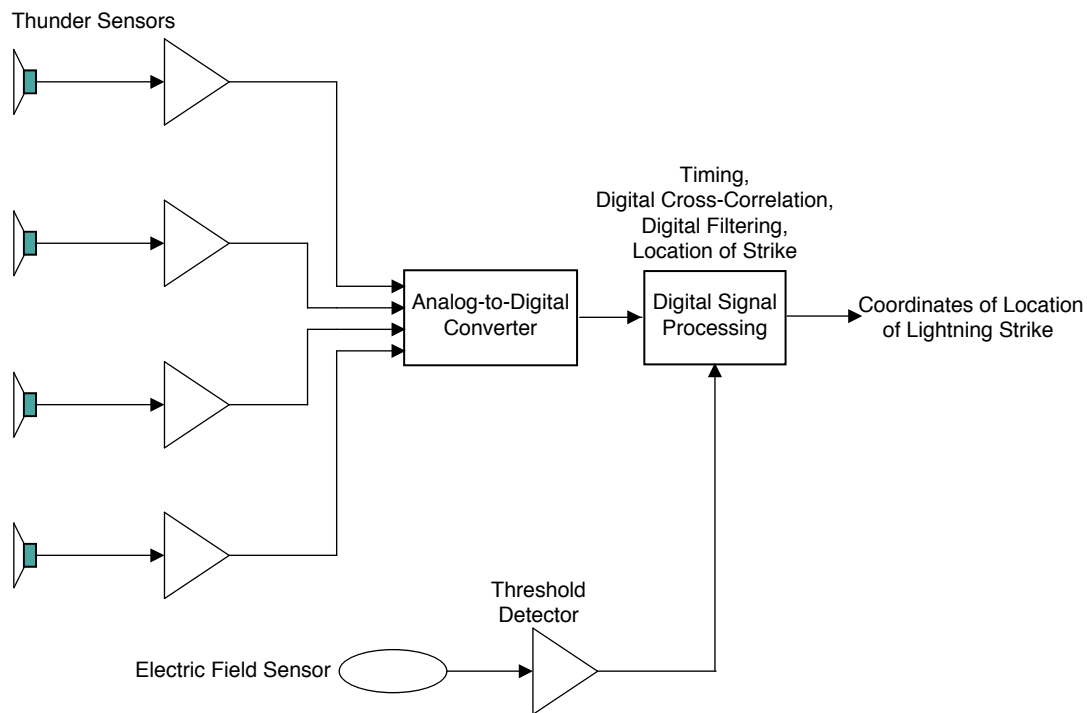
- The Sonic Lightning Locator was successfully tested during the thunderstorm season of 2002, recording 7 triggered lightning strikes and 29 natural lightning flashes. The sensitivity of the electric field sensor was adjusted for it to trigger on lightning strikes occurring within 1.5 miles of the recording station. The sensitivity calibration is based on the typical strength of the electric field generated by a lightning strike in Florida. Different calibration parameters can be applied when using the SOLLO at other geographical locations.

Key milestone:

- To measure the magnitude of the electric field and to provide an estimate of the lightning current, circuitry is being added to enable recording of the following main parameters of the electric field waveform:
 - Peak magnitude.
 - 10- to 90-percent rise time.
 - Mean duration.
 - Number of strokes.

Contact: J.T. Madura (John.T.Madura@nasa.gov), YA-D, (321) 867-0814

Participating Organization: USTDC (Dr. P.J. Medelius)



SOLLO Block Diagram

Transient Voltage Recorder

The Transient Voltage Recorder was designed for monitoring the effects of lightning-induced voltages on communication and power lines associated with Expendable Launch Vehicles at Cape Canaveral Air Force Station. Although electronic equipment and instrumentation usually have some form of transient protection, limitations exist on the maximum voltage and maximum duration of the transient voltages to which they can be exposed before permanent damage occurs. Electronic components and equipment can fail immediately when subjected to voltages larger than their maximum-rated values. Transient voltages can also alter the characteristics of an electronic component without any immediate sign of damage. Unless there is a way to determine transient voltages are present, such anomalies can remain undetected and eventually lead to a premature and unexpected failure of an electronic component or an instrument.

Transient voltage recorders have been used for many years to monitor voltage spikes in cables. Common sources of transient voltages include large electric motors, switching of power equipment, induced voltages from nearby lightning, and direct lightning strikes. The transients generated by sources other than lightning tend to have frequency components well below 1 megahertz (MHz), which most commercial transient recorders can detect and record. On the other hand, lightning-induced transients contain voltage peaks whose amplitude can rise from 10 to 90 percent in a fraction of a microsecond and can generate multiple transients within an few milliseconds of each other. It is therefore important to be able to record and characterize the impulsive nature of transients caused by lightning strikes.

Commercially available transient voltage recorders can sample multiple signals at fast rates (e.g., 20 megasamples per second [MS/s]) and measure voltage transients up to several hundred volts. However, the main disadvantage of many recorders is that data must be retrieved through a serial communication link, and depending on the amount of data being recorded, the onboard storage can be filled before data retrieval is completed. Large amounts of data are transmitted, although the users usually require only a relatively small part of the information.

The technology implemented for the new Transient Voltage Recorder overcomes the limitations of existing transient recorders and provides essential information regarding the transient



Transient Voltage Recorder

voltages without the overhead associated with the recording, storage, and transmission of a complete transient waveform. The technology consists of a transient voltage recorder that characterizes the transient waveform in real time. A fast-sampling analog-to-digital converter, operating at speeds up to 100 MS/s is used to sample the transient waveforms. Compared to traditional recorders that sample and store complete waveforms, the new recorder analyzes the data as it is being sampled and stores only the parameters of interest. A real-time comparator and peak detection circuit was implemented with the use of a fast Field-Programmable Gate Array (FPGA). Compared to the traditional

approach that requires thousands of bytes to store each waveform, the present technology requires less than 20 bytes of storage per waveform. In addition, the typical dead time between subsequent triggers is now reduced from hundreds of microseconds to about one-tenth of a microsecond.

This recorder calculates and stores the following parameters:

- Peak voltage value.
- Duration of transient at 25, 50, and 75 percent of peak (in 10-nanosecond increments).
- 10- to 90-percent rise time.
- 90- to 10-percent decay time.

The Transient Voltage Recorder can be configured for different input ranges, depending on the expected magnitude of the transient voltage being monitored. Typical input ranges include ± 10 , 50, and 100 volts. The termination can be either single-ended or differential and selectable among 50, 120, or 10 kilohms. A bipolar scheme is used so either a positive or negative transient can trigger the system and initiate the real-time waveform characterization. Depending on the implementation, multiple data channels could be analyzed simultaneously, with a trigger signal from any channel

determining the start of the waveform characterization process.

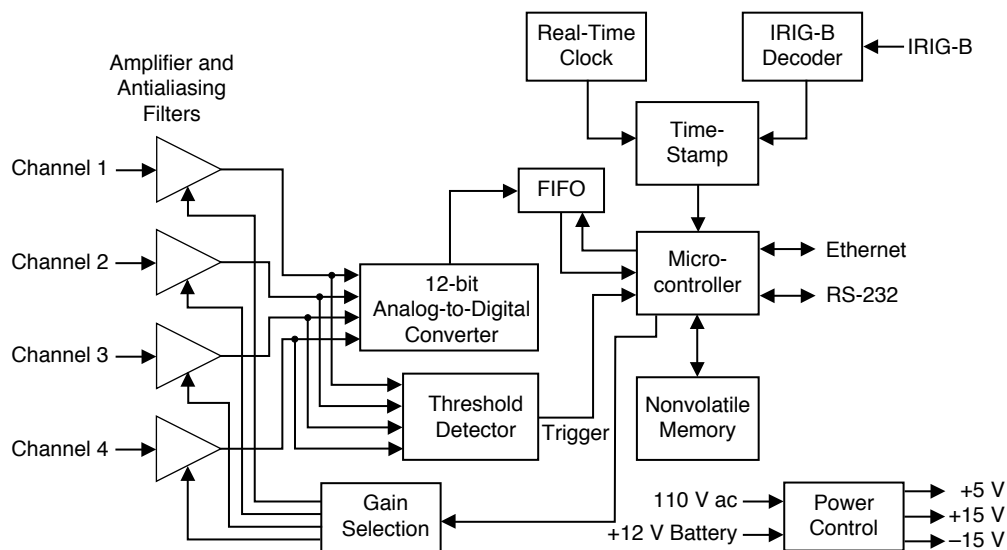
A real-time clock is included to accurately time-stamp any recorded waveform. This is important if it is necessary to correlate a transient with other measurements, such as those provided by a lightning location system. The power supply includes backup batteries that can maintain the transient voltage recorder operational for up to 15 days in case of main power loss. The batteries are automatically charged during normal operation.

Key milestone:

- The Transient Voltage Recorder was used to monitor transient voltages in support of the GALEX mission. Current measurements were conducted at four different power, communication, and ground lines.

Contact: D.H. Trout (Dawn.H.Trout@nasa.gov), VA-F3, (321) 476-3675

Participating Organization: USTDC (Dr. P.J. Medelius)



Transient Voltage Recorder Block Diagram

Passive Millimeter Wave Imaging

Current Range Safety launch requirements for missions carrying nuclear payload materials call for continuous observation by Range Safety officers from T-0 through tower clear. Historically, optical and laser scanning imaging systems have provided the bulk of the imaging equipment needed to meet this Range Safety observation requirement. However, with the advent of larger launch vehicles with ever increasing numbers of strap-on solid rocket motors (e.g., graphite epoxy motors), more capable water deluge systems are needed on launch pads to reduce potentially damaging acoustic energies during launch. The unintended consequence of building more capable pad deluge systems is an increase of obscuring clouds of plume exhaust and steam during launches. An updated method of viewing launch vehicles through these larger clouds during launch is needed.

The fundamental issue, relative to legacy optical and laser scanning systems, is the attenuation introduced by the clouds of plume exhaust at the wavelengths of both the visible imaging systems and the scanning laser beams. To increase the efficiency of solid rocket motors, exhaust particle size must be kept very small. Unfortunately, current particle sizes are now of such a small diameter that high attenuation occurs at both visible light wavelengths and scanning laser beam wavelengths. In short, the old viewing methods no longer can meet the imaging needs for maintaining Range Safety for larger launch vehicles.

One solution investigated this year on the Millimeter Wave Imaging project was passive millimeter wave imaging systems. These work because, at all temperatures above absolute zero, physical objects naturally emit millimeter wave energies passively. No millimeter wave energy illumination is required, and unlike radar beams, no energy must be radiated at the launch vehicle. Passive millimeter wave imaging systems therefore hold great promise for providing enhanced observation capabilities for the current generation of heavy launch vehicles while remaining inherently safe for use with launch ordnance devices and pyrotechnics.

The Millimeter Wave Imaging project extended the theoretical understanding of applying passive millimeter wave imaging technology to launch situations. The tasks accomplished on the project included modeling of expected attenuations versus wavelength at several millimeter wavelengths, resulting in the identification of optimal wavelengths that can best enhance Range Safety. This theoretical effort included developing models for estimating steam production, particle sizes, and total attenuation through plume exhaust launch clouds. The results of this theoretical investigation were released in a final report identifying the major limits of this technology.

Follow-on tasks anticipated for the coming year are to coordinate a vendor demonstration of a military millimeter wave imaging system to implement an initial proof of concept, followed by additional theoretical investigations to further determine the limits of applying this technology for enhancing Range and Spaceport Safety. A wide range of applications exists for passive millime-



Vehicle Obscuration During Launch

ter wave imaging technology, including the passive inspection of external Orbiter tanks during fueling on the launch pad and the passive inspection of cargo and container trucks at guard station checkpoints.

Key accomplishments:

- Arranged site briefings and familiarization visits to Innovative Science and Technology Experimentation Facility (ISTEF), Launch Complexes 17A and 17B.
- Researched key technical journals and papers.
- Developed theoretical models for estimating the performance limits of passive millimeter wave imaging in a launch environment.

Key milestones:

- October 2002: Commenced research.
- December 2002: Released final report to the Evolved Expendable Launch Vehicle (EELV) program identifying the major technical limits to applying passive millimeter wave imaging technology to launch environments.

Contact: Dr. R.C. Youngquist (Robert.C.Youngquist@nasa.gov), YA-C3-E, (321) 867-1829

Participating Organizations: USTDC (Dr. G.L. Bastin and T. Erdogan) and VA-C (A. Sierra)

Spaceport Structures and Materials

Advanced structures and materials are critical to achieving the goals of reduced costs, increased reliability, and higher flight rates for future spaceports. Spaceport structures and materials technology development areas include corrosion abatement, static charge dissipation, nondestructive evaluation (NDE), reduction of vibroacoustic loads during launch, and nonflammability. Sources of corrosion and material degradation include humid saltwater environments surrounding launch structures and aggressive ozone and hard radiation environments of Earth orbit. Static charge buildup on payloads, spacecraft, and launch structures can present significant safety issues for personnel and equipment. NDE technologies are critical to obtaining rapid status analysis of flight hardware. Passive sound mitigation techniques to replace active noise reduction methods such as water suppression systems are desirable for future launch vehicle pads. Advanced nonflammable materials are desirable to enhance the safety of crew and ground personnel during operations. Since materials are ubiquitous in spaceflight, the reach of this technology thrust area will encompass launch structures, payload processing, spacecraft design, and vehicle maintenance.

Technology focus areas include the following:

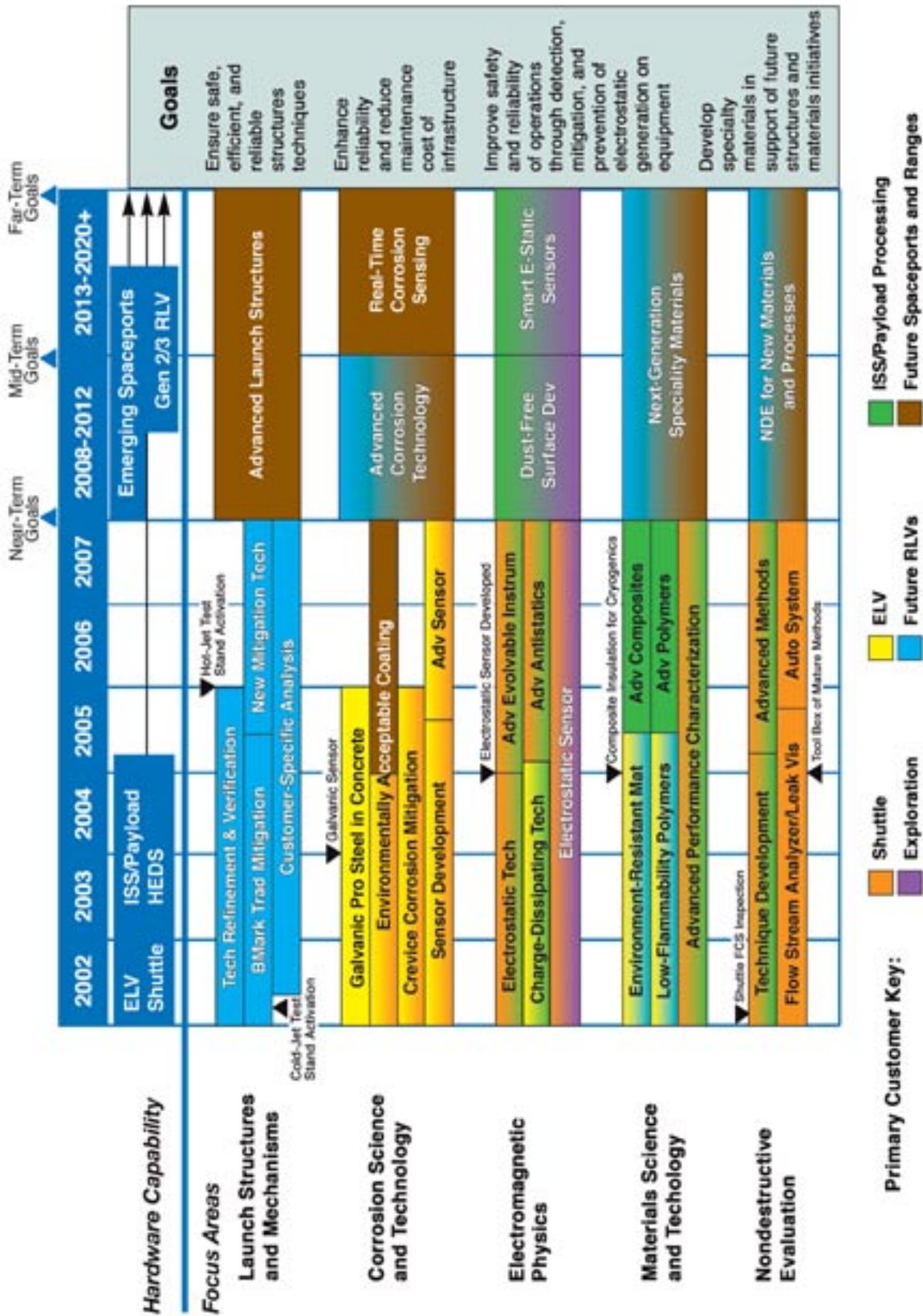
- Launch Structures and Mechanisms
- Corrosion Science and Technology
- Electromagnetic Physics
- Materials Science and Technology
- Nondestructive Evaluation

The goals and objectives of Spaceport Structures and Materials include the following:

- Ensure safe, efficient, and reliable structures techniques
- Enhance reliability and reduce maintenance cost of infrastructure
- Improve safety and reliability of operations through detection, mitigation, and prevention of electrostatic generation on equipment
- Develop specialty materials in support of future structures and materials initiatives

For more information regarding Spaceport Structures and Materials, please contact Karen Thompson, (321) 867-7555, Karen.L.Thompson@nasa.gov; or Dr. Carlos Calle, (321) 867-3274, Carlos.I.Calle@nasa.gov.

Spaceport Structures and Materials Roadmap



Electronic Single-Particle Aerodynamic Relaxation Time Analyzer for Mars Robotic Missions

With funding from NASA's Office of Space Science, under its Planetary Instrument Definition Program, KSC's Electrostatics and Surface Physics Laboratory and the University of Arkansas at Little Rock are currently designing and building an Electronic Single-Particle Aerodynamic Relaxation Time (E-SPART) analyzer that will perform real-time, simultaneous measurements of the aerodynamic diameter and the electrostatic charge distributions of dust particles in the Martian atmosphere (figure 1). To date, there have been no direct measurements on the surface of any planet (other than Earth) characterizing the concentration, distribution, size, or shape of suspended dust particles or the charge deposited on them.

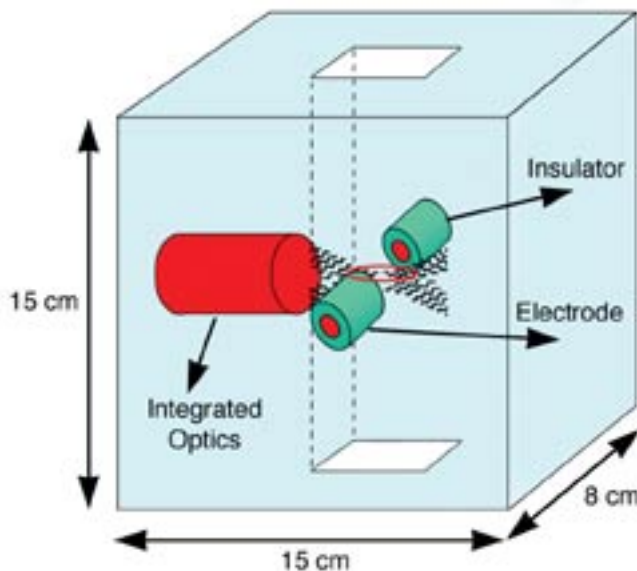


Figure 1. Schematic of the Electronic Single-Particle Aerodynamic Relaxation Time (E-SPART) Analyzer

The E-SPART analyzer consists of a dual-beam, frequency-biased laser Doppler velocimeter (LDV); a relaxation cell; and an electronic signal and data processing system. In the E-SPART analyzer, the LDV measures, in a non-invasive way, the particle velocity in its sensing volume. The sensing volume is located at the center of a relaxation chamber. The Mars dust particles flow vertically downward through the sensing volume. As the particles move through the sensing volume, in the direction normal to the plane containing the two converging laser beams, they experience an alternating current (ac) electric excitation that causes the particles to oscillate in a horizontal direction, parallel to the direction of LDV velocity measurements. The ac electric excitation

is generated using a pair of electrodes located inside the relaxation cell and positioned symmetrically across the LDV sensing volume.

The electronic signal and data processor analyzes the phase lag of the particle motion with respect to the ac electric field driving the particle. The gas dynamic diameter is derived from the phase lag value. The measurements of diameter and the direction and amplitude of the electrical migration velocity of the particles with respect to the electric field provide the polarity and magnitude of electrical charge of a particle.

Results of an example of particle sampling of a Martian regolith simulant charged against stainless-steel beads for 10 minutes at room temperature with 44-percent relative humidity are shown in figures 2 and 3. The simulant was ground down using a ball mill and measured with the E-SPART. The average particle diameter was 6.63 millimeters (mm) with a standard deviation of 1.91 mm. The total particle count was 5,039 with a total mass of 3,901.3 nanograms

and total charge of -311.02 femtocoulombs (fC). This gives a charge-to-mass ratio of -0.13 millicoulomb per gram (mC/g). The results are given as a three-dimensional view showing the number of particles versus the diameter and the percentage of maximum charge (figure 2) and as the charge-to-mass ratio (Q/M) of positively and negatively charged particles as a function of particle size (figure 3).

While the net charge-to-mass ratio (positive plus negative) for the Martian simulant dust in the size range 1 to 30 μm is -0.13 mC/g against stainless steel, the individual particles were found to be highly charged. For example, 1.06- μm -diameter particles showed Q/M of -27.83 mC/g for negatively charged particles and +20.16 mC/g for positively charged particles.

This technology will allow us to find the charge-to-mass ratio and concentration of particles suspended in the Martian atmosphere. The technology will also provide KSC with a future flight instrument for inclusion in the Mars 2009 mission.

Contact: Dr. C.I. Calle (Carlos.I.Calle@nasa.gov), YA-C2-T, (321) 867-3274

Participating Organizations: University of Arkansas at Little Rock (Dr. M.K. Mazumder) and Swales Aerospace (Dr. C.R. Buhler)

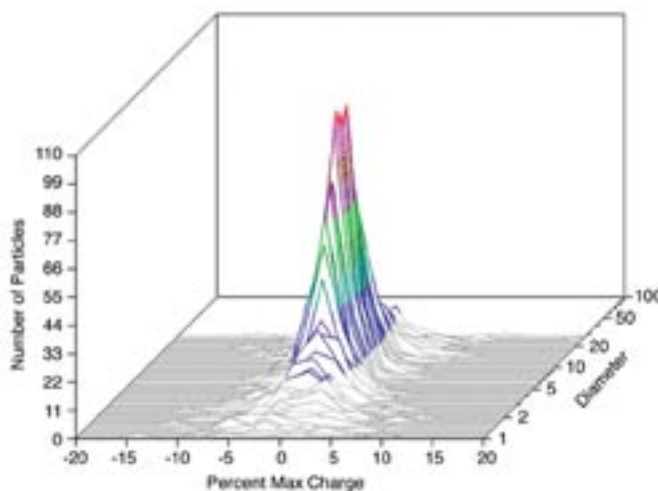


Figure 2. E-SPART Results for a Martian Soil Simulant Electrostatically Charged Against Stainless-Steel Beads for 10 Minutes at 72 Degrees Fahrenheit With 44-Percent Relative Humidity

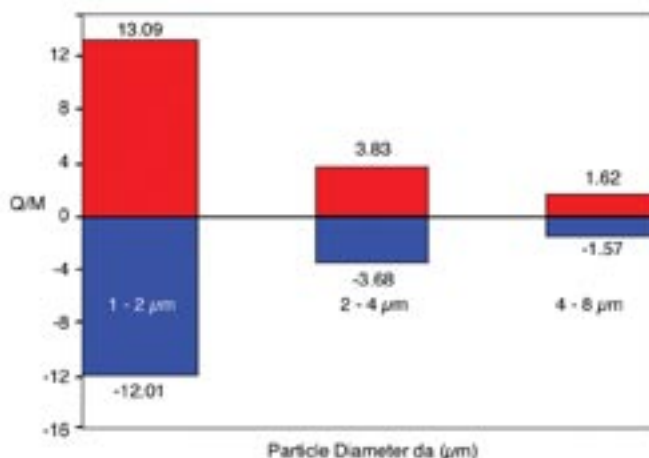


Figure 3. Charge-to-Mass Ratio Plotted as a Function of the Equivalent Aerodynamic Diameter of Dust Particles Charged Against Stainless-Steel Beads for 10 Minutes

Paschen Breakdown in the Martian Atmosphere

The high probability of dust interactions during Martian dust storms and dust devils, combined with the cold, dry climate of Mars, will most likely result in airborne dust that is highly charged. On Earth, potential gradients up to 5 kilovolts per meter have been recorded and in some cases resulted in lightning. Although the Martian atmosphere is not conducive to lightning generation, it is widely believed that an electrical discharge, in the form of a corona, occurs.

To understand the breakdown of gases, Paschen measurements are taken, which relate the minimum potential required to spark across a gap between two electrodes. The minimum potential is plotted versus the pressure-distance value for electrodes of a given geometry. For most gases, the potential decreases as the pressure decreases. For carbon dioxide (CO_2), the minimum in the curve happens to be at Mars atmospheric pressures (5 to 7 conventional millimeters of mercury [mm Hg]) for many distances and geometries. However, a very small amount (less than 0.1 percent) of mixing gases radically changes the curve, as noted by Leach (figure 1). Here, we present experimental results of a Paschen curve for a Mars gas mixture compared with 100-percent pure CO_2 .

Voltages of either positive or negative polarity were applied at one custom-made brass electrode, while the other was grounded. The cylindrical electrodes have a diameter of 5.059 centimeters (cm) with curved edges to eliminate edge effects that create strong electric fields. Thus the electrodes fixed 0.1 cm apart provided the parallel-plate geometry.

The chamber was pumped down to 104 mm Hg and backfilled to approximately 50 mm Hg with the atmospheric gas. It was pumped down again to remove residual gases and contaminants. The gases that were used are 100-percent CO_2 and a Mars gas mixture provided by Praxair, Inc., that consisted of 95.5-percent CO_2 , 2.7-percent nitrogen, 1.6-percent argon, 0.13-percent oxygen, and 0.07-percent carbon monoxide. Measurements were taken by simply increasing the voltage until the power supply shut off as a result of the current divergence during breakdown. Figure 2 shows the minimum voltage required for electrical breakdown of the two gases for both positive and negative polarities.

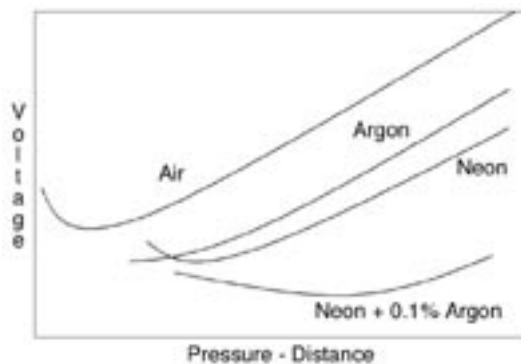


Figure 1. Leach Shows That Paschen Measurements Differ Greatly With Minimal Change in Atmospheric Gas Content

Clearly, as the pressure is lowered, less voltage is required for breakdown to occur for both gases. At the higher pressures, the spark potential does not seem to depend on the makeup of the gases.

At lower pressures, a clear difference in breakdown potentials can be seen. Figure 3 shows how the small concentrations of nitrogen, oxygen, argon, and carbon monoxide greatly alter the Paschen curve for pressures ranging between 1 and 10 mm Hg. We can see that the minimum in the CO₂ curve at around 4 to 5 mm Hg becomes shifted to 6 to 7 mm Hg once the other gases are added. This suggests that, even though breakdown occurs easily at Mars pressures, it may not occur at the minimum in the Paschen curve for CO₂. Instead, the results seem to indicate that there may actually be a local maximum near the minimum in the CO₂ curve. Once the pressure is lowered below 1 mm Hg (not shown), both the CO₂ and Mars gas mixture rise again since there are no molecules to ionize in a hard vacuum.

It is interesting to note that around Mars pressures the blue spark seen at higher pressures turns into a purple-blue corona. At pressures less than 2 mm Hg, there is no longer a well-defined spark between the cylinders; instead there is only the corona breakdown to the gas around the charged electrode.

This research yielded the following major conclusions:

- Paschen curves for a Mars gas mixture are not too different from pure CO₂, although differences can be seen.
- Knowledge of the electrical breakdown of the Martian atmosphere is crucial for future human and robotic exploration of Mars.

Contact: Dr. C.I. Calle (Carlos.I.Calle@nasa.gov), YA-C2-T, (321) 867-3274

Participating Organization: Swales Aerospace (Dr. C.R. Buhler)

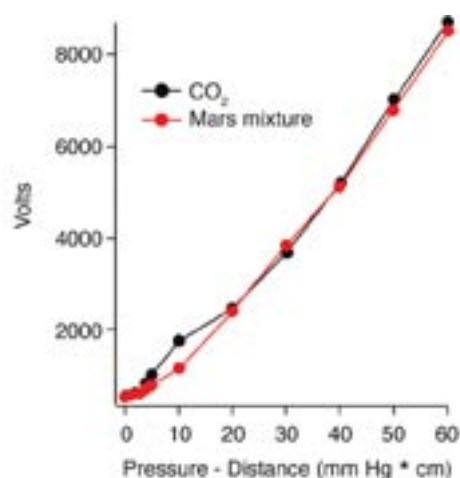


Figure 2. Minimum Voltage Required for Breakdown of CO₂ and Mars Gas Mixture as a Function of the Pressure-Distance Relationship (The error bars are smaller than the points.)

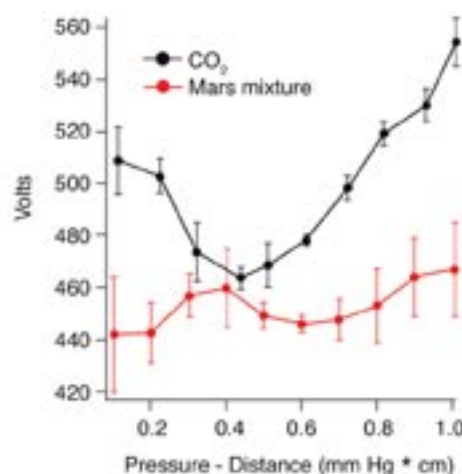


Figure 3. Minimum Spark Potential in the Range 1 to 10 mm Hg for Pure CO₂ and the Mars Gas Mixture Using Brass Electrodes at 0.1 cm Apart

Wheel Electrometer Technology

Surface sand and dust electrification is a highly probable phenomenon in the low-pressure, low-humidity environment of Mars. Surface soil and dust particles on Mars may become electrostatically charged due to incident ultraviolet (UV) radiation reaching the surface. Recent experiments have shown that this process can electrify the soil and provide a photoelectron sheath that levitates charged particles about 1 meter above the surface, a phenomenon that was possibly seen on the Moon and that may also exist on Mars. Contact charging may also occur because of collisions between wind-blown dust particles and stationary surface particulate matter. It has been suggested that the formation of soil agglomerates and sand dunes may be attributed to the electrostatic properties of the Martian soil. To date, no experiment on the surface of Mars has directly measured the amount of charge on the surface dust and soil particles.

A system of embedded sensors that can be incorporated into the wheel of any future mission rover would provide for a simple and fairly unobtrusive way to measure the distribution of electrostatic fields on the Martian surface and to measure variations in soil electrostatic response. The Wheel Electrometer Sensor (WES) consists of two types of sensor modules. These sensors will be attached just beneath the rover wheel so each sensor will be exposed to the Martian regolith either by line of sight through a small amount of Martian atmosphere or by direct contact with the regolith. A description of how the WES might be incorporated into one of the wheels of the Field-Integrated Design and Operations (FIDO) helps to illustrate the technology. FIDO is an advanced vehicle used in technology definition and field tests for future NASA Mars programs.

Figure 1 shows the FIDO wheel with both the electric field sensor (ELF) and triboelectric (TRIBO) sensor modules. The five TRIBO sensors use a different insulator material and are backed by independent miniature electrometers, while the ELF is a bare sensor recessed from the wheel surface. The ELF and TRIBO sensors are actually based on the same technology. Each type of sensor simply measures the amount of charge induced on a metal electrode that has been exposed to some external distribution of electrostatic charge, and both have sensitivities that are achieved by adjusting circuit component values and the sensor area.

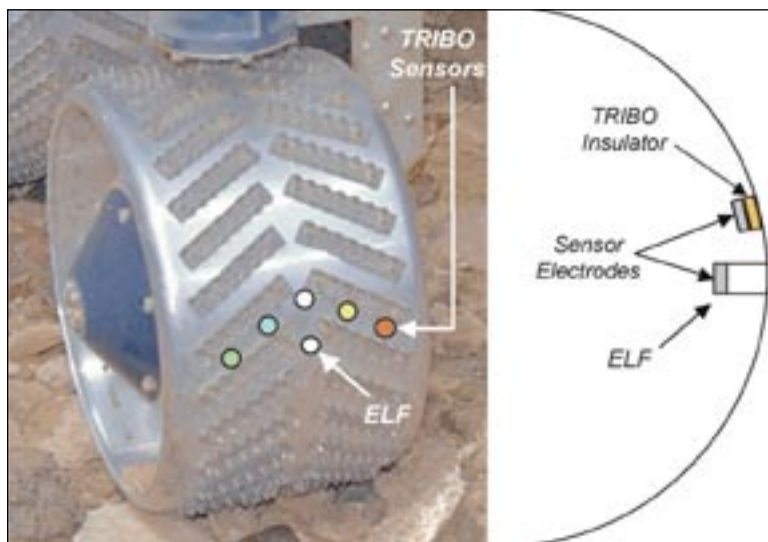


Figure 1. Wheel Electrometer System (WES) Shown on the FIDO Wheel (left) and Cross-Sectional View of the ELF and TRIBO Modules (right). (The ELF is recessed to allow measurement of an undisturbed soil plug that has not been compressed or rubbed by the wheel rim.)

In the case of the ELF sensor, the source of the charge would be any charged soil particles present on the Martian surface at the time the rover wheel rolls over it. The ELF sensor electrode will be recessed several centimeters radially inward from the outer surface of the wheel through a hole in the wheel. This will ensure the ELF directly measures any naturally occurring charge that may be present on a small patch of undisturbed Martian regolith as the wheel rolls forward. The ELF will provide an output voltage that is directly proportional to the amount of charged regolith that the sensor “sees” through the hole. The regolith’s surface charge density will be determined using the charge measurement and the known hole area. As the rover travels across

the Martian surface, the local surface charge density will be mapped using the ELF measurements. These data will provide direct measurements of the presence of electrically charged particles on the Martian surface.

The TRIBO sensor module will have five independent sensors. The electronic circuitry for each sensor is identical, but a different insulator material will cover the electrometer sensor electrode of each sensor. As the rover wheel rolls over the Martian regolith, each of the five different insulators will make contact with the surface. The electrostatic response to contact charging of each insulator with the regolith will provide data regarding how the regolith fits into the triboelectric series.

A prototype of the WES with four TRIBO sensors was built in the KSC Electrostatics and Surface Physics Laboratory to test the concept in a simulated Martian environment using Johnson Space Center (JSC) Mars-1 simulant soil (figure 2). The prototype wheel is 12.7 centimeters (cm) in diameter and 10.3 cm long. The four TRIBO sensors have a diameter of 1.84 cm with a concentric guard and a shield. The sensors are capped with Teflon, Lucite, fiberglass-epoxy G-10, and Lexan disks 2.0 cm in diameter and 0.7 cm thick. Figure 3 shows preliminary data obtained with the prototype WES in dry air at 9-percent relative humidity and at atmospheric pressure. The prototype wheel was rolled along a 60-cm tray containing JSC Mars-1 simulant. The four insulators acquire different electrostatic charges when in contact with this simulant. The sharp peaks observed in the graph are due to the initial contact with the soil. Repeated contacts show an increase in the charge exchanged between simulant and insulator. Several runs were



Figure 2. Prototype Wheel Electrometer System

taken prior to the one generating the data presented here. The insulators and simulant were exposed to an ionizer to neutralize their surface charges before this run but were not cleaned. Thus, this procedure is fairly close to an actual procedure that could be used on a flight instrument.

This research yielded the following major conclusions:

- A wheel electrometer could easily detect surface changes covered with fine dust that would be undetected visually.
- This wheel electrometer will map electrostatic fields while traversing surfaces.
- Determination of the electrostatic properties of the Martian regolith could help us understand several unsolved problems related to sand transport and the low erosion rate on Mars.

Contact: Dr. C.I. Calle (Carlos.I.Calle@nasa.gov), YA-C2-T, (321) 867-3274

Participating Organizations: USTDC (Dr. C.R. Buhler), Florida Institute of Technology, (Dr. J.G. Mantovani), YA-C2-T (E.E. Groop), Jet Propulsion Laboratory (Dr. M.G. Buehler), and USTDC (A.W. Nowicki)

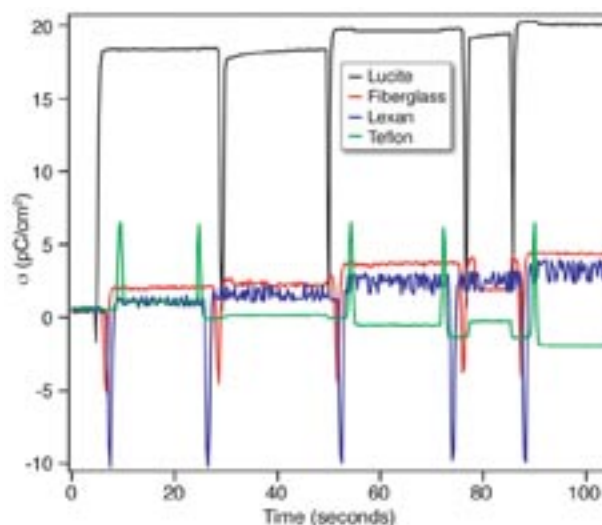


Figure 3. Charge Generated on the Four Polymers Capping the Electrometer Sensors on the Prototype WES

Development of a Physical Model of Insulator-Insulator Triboelectric Charging To Understand Surface Charging of Materials on Earth and on Planetary Surfaces

The electrostatic charging of materials by contact or rubbing is called triboelectric charging. It is a serious problem for materials on Earth and on dusty planetary surfaces, such as that of Mars. The least understood type of triboelectric charging occurs when insulators contact each other. A hypothesis being investigated to explain insulator-insulator charging is that an exchange of surface ions takes place upon material contact or rubbing. A physical model being developed is that ions are weakly attached to an insulator's surface either in a thin (about 100-angstrom) water layer and/or directly attached to the surface by intermolecular forces such as the van der Waals force. When the surfaces are in contact, there is ion exchange resulting (upon separation) in one surface being negatively charged and the other positively charged.

The surface charge can be viewed as n ions occupying n sites of N total sites on the surface. Using a thermodynamic relation for n and Gauss's law, an equation for the surface charge density can be found:

$$\sigma = \frac{q_e N}{A} \frac{P_v}{(k_B T)^{5/2} \left(\frac{m}{2\pi \hbar^2} \right)^{3/2} e^{-\xi_0/k_B T} + P_v} \quad (1)$$

where P_v is the vapor pressure, A is the surface area, q_e is the electron charge, m is the ion mass, T is temperature, k_B is Boltzmann's constant, \hbar is Planck's constant divided by 2π , and ξ_0 is the ion surface adsorption energy. Experiments were performed where surface charge was measured for insulator materials (polymers) that were charged up triboelectrically and then had the atmospheric pressure decreased. The curve fits to experimental data in the figure are from (1). The fitting parameters used in (1) provide values for the adsorption energies and number of occupiable charge sites per unit area at room temperature (300 kelvin [K]). Thus, it may be possible to determine the amount of charge deposited on insulators after insulator-insulator contact if these two parameters are known. The atomic species chosen was the sodium ion (Na^+ , $m = 3.82 \times 10^{-26}$ kilogram) because sodium chloride is one of the most common and easily solvated ionic compounds.

The values of ξ_0 developed by the curve fit correspond to the difference of the work functions for material A and material B , $(\phi_A - \phi_B)$, measured for metal-insulator contact. Conventionally, insulators are assigned "effective work functions" based on their charging properties against metals of known work function. Therefore, it is believed that charging of two insulators could be determined by comparing their effective work functions.

Thus, an alternative method for determining the amount of charge transferred between insulators is presented. Here the mechanism is that of ion transfer as opposed to electron transfer. Experiments indicate that surface properties, such as hydrophobicity, play a key role. The model focuses on identifying the source and meaning of the adsorption energies for insulators. Determination of insulator work functions by contact with a metal appears to be equivalent to our determination of the adsorption energy. Thus, charging an insulator and

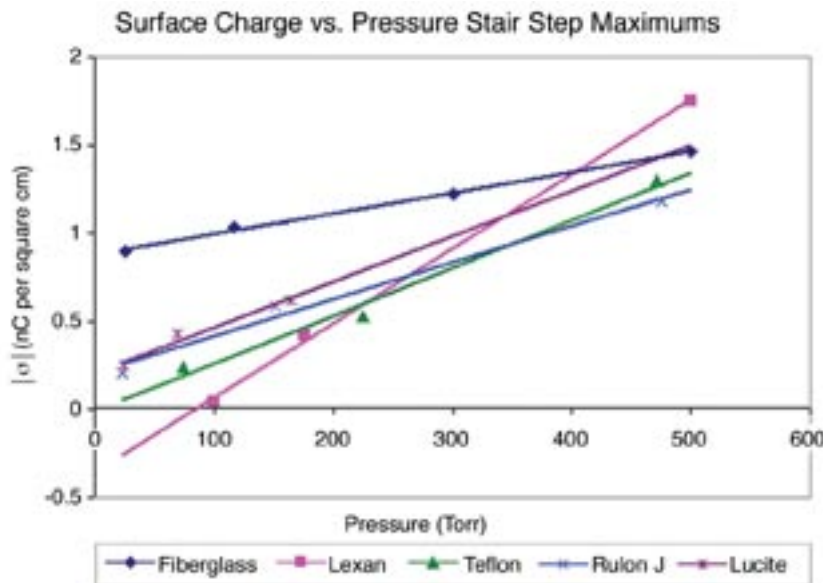
removing the vapor pressure may provide an alternative method for determining $(\phi_A - \phi_B)$, the difference of work functions. This interpretation may provide a clearer picture of the phenomenon.

Key milestones:

- 2002/2003: Development of a pressure-dependent physical model of insulator-insulator triboelectric charging.
- 2003: Refine physical model by developing realistic values for N/A , and ξ_0 and perform additional triboelectric experiments where surface charge is measured as a function of pressure for various insulator materials.
- 2003 and beyond: Use model and experimental data to develop methods or materials that will mitigate triboelectric surface charging.

Contacts: M.D. Hogue (Michael.D.Hogue@nasa.gov), YA-C2-T, (321) 867-7549; and Dr. C.I. Calle, YA-C2-T, (321) 867-3274

Participating Organizations: Swales Aerospace (Dr. C.R. Buhler) and University of Central Florida (Dr. W. Luo)



Maximum Surface Charge Data From Experimentation Showing Nature of Discharge With Decreasing Pressure

Comparison of Surface Resistivity and Triboelectric Charge Generation Characteristics of Materials

The Electrostatics and Surface Physics Laboratory at KSC has recently focused on providing test data that demonstrates the lack of correlation between the surface resistivity of materials and the materials' ability to generate charge due to contact. This research was undertaken to emphasize the need for contact or triboelectric charge generation testing when using materials in sensitive or hazardous environments.

When the threat of electrostatic discharge is a concern during an operation or application, the users need to be aware of the material's tendency to acquire large voltages that could lead to a spark. The majority of material testing concentrates on surface resistivity measurements. These measurements determine the material's ability to bleed off accumulated charge. However, resistivity measurements do not give an indication of the initial quantity of charge and therefore on the voltage that the material has a tendency to develop. This initial charge accumulation can pose a threat in hazardous environments.

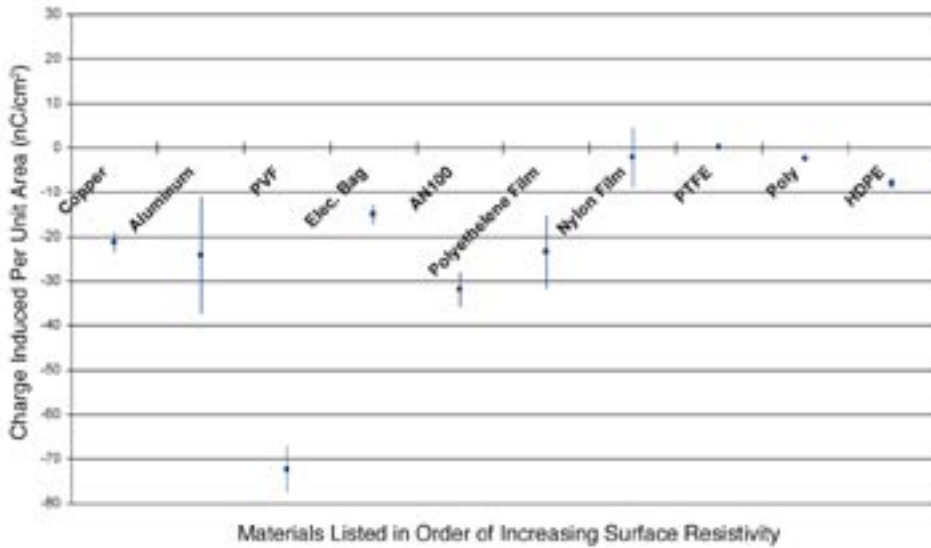
Dissipative or conductive materials can retain large amounts of charge and hence maintain hazardous voltages if the materials are not connected to a sink to which they can bleed the charge. This research concentrated on the importance of triboelectric charge generation tests for hazardous areas. Triboelectric testing can identify safer materials that have a low tendency to retain charge and therefore a low tendency to develop high voltages. A spark can pose a serious threat in areas with sensitive electronics or flammable materials. Areas where conductive and dissipative

materials cannot be adequately grounded or where insulating materials must be used pose an increased risk for dangerous charge accumulation.

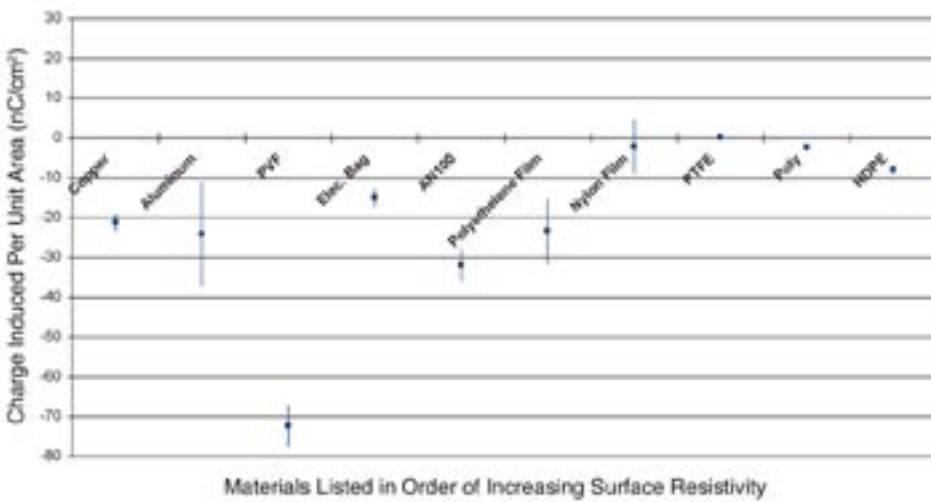
Analysis of the data emphasizes that there is no correlation between surface resistivity and charge accumulation tendencies of materials. The lack of this correlation points to the importance of developing a better understanding of the triboelectric charging tendency of materials and to the importance of developing a test method that can be used during operations to monitor charge accumulation.

List of Tested Materials in Order of Increasing Surface Resistivity

Material	Surface Resistivity (Ohms/Square)
Copper	<1
Aluminum	<1
PVF Film	10^7
Electronics Bag	10^{10}
AN100	10^{11}
Polyethylene Film	10^{12}
Antistatic Nylon Film	10^{13}
PTFE	$>10^{16}$
Polycarbonate	$>10^{16}$
HDPE	$>10^{16}$



Induced Charge per Unit Area on a Copper Plate When Contacted by the Listed Materials Whose Surface Resistivity Increases From Left to Right



Induced Charge per Unit Area on a PTFE Sheet When Contacted by the Listed Materials Whose Surface Resistivity Increases From Left to Right

Contacts: E.E. Groop (Ellen.E.Groop@nasa.gov), YA-C2-T, (321) 867-4861; and Dr. C.I. Calle, YA-C2-T, (321) 867-3274

Participating Organization: USTDC (A.W. Nowicki)

Method for Measuring Charge Buildup on Materials

The methods developed to test for the charge generation propensity of materials due to contact or triboelectric charging are not very reproducible. Triboelectric charge testing is highly dependent on the environment in which the testing is conducted and the type of contact that is made (rubbing, rolling, etc.). Research has been completed in the KSC Electrostatics and Surface Physics Laboratory that compares the current triboelectric testing method for electronic components developed by the Electrostatic Discharge Association to a new triboelectric testing method based on capacitive sensors for monitoring charge generation throughout a process or activity.

For the most part, triboelectric testing of materials has consisted of using the material or device as it is used in an application and then depositing the device into a Faraday pail. Figure 1 shows a histogram of 25 data points taken using the Faraday pail method. This test method gives only a limited amount of information since it only measures the charge that remains on the device after it is used.

The new device, shown in figure 2, is a rough prototype intended to be used to simulate a microchip. The charge that is generated on the pins of the chip is read as a voltage across a known capacitor (figure 3). The advantage of using this device to monitor charging is that the charge can be monitored throughout the process and not just at one point. This allows for the identification of electrostatic discharge hot-spots where high voltages are developed during an application or operation.

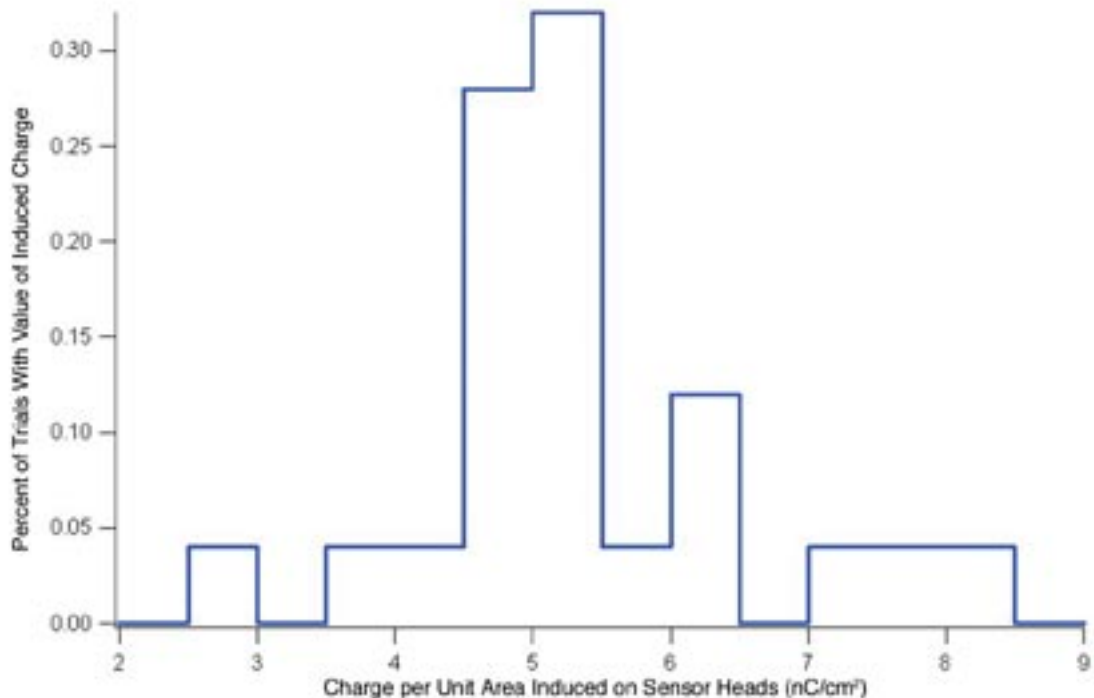
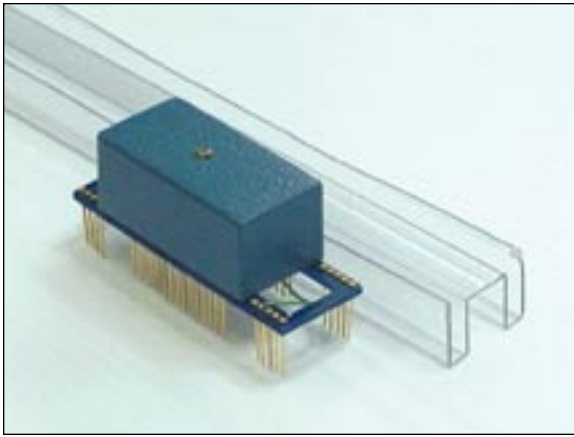


Figure 1. Histogram of the Charge Developed on the Pins of the Device During Testing Using a Faraday Pail



Contacts: E.E. Groop (Ellen.E.Groop@nasa.gov), YA-C2-T, (321) 867-4861; and Dr. C.I. Calle, YA-C2-T, (321) 867-4861

Participating Organization: USTDC (A.W. Nowicki)

Figure 2. Microchip Simulator Device for Measuring the Charge Induced on the Pins During an Operation

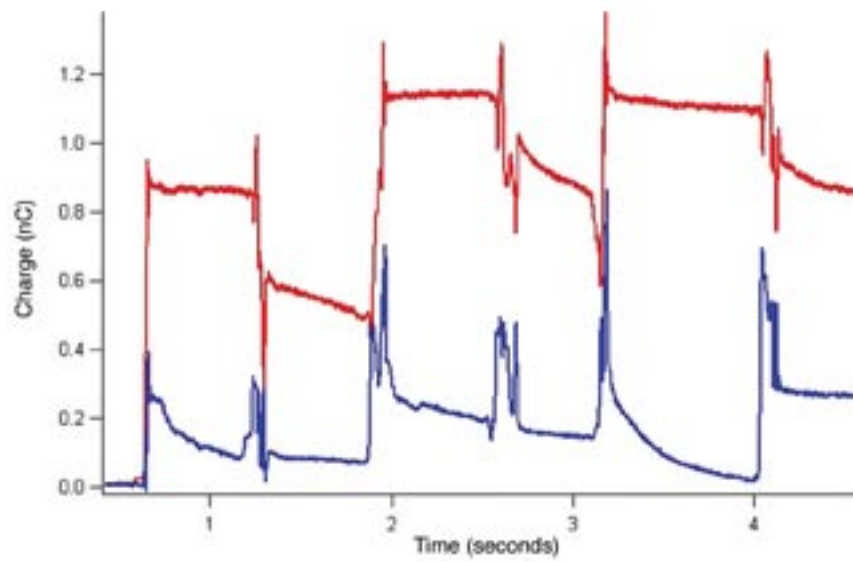


Figure 3. Charge Developed on Two Pins of the Microchip Simulator While Being Rocked Six Times in a Magazine

Electrostatics Testing of Materials at Low Pressures

The Electrostatics and Surface Physics Laboratory at KSC recently developed an Automated Electrostatics Test Device (figure 1) that operates in a chamber at KSC. With this device, it is now possible to perform electrostatics testing at atmospheric pressures down to 0.4 torr and at temperature ranges from -120 to 200 degrees Celsius ($^{\circ}\text{C}$). The gas environment in the chamber can also be selected to reproduce a variety of environments found not only on Earth but also on Mars.

Our laboratory has been testing the electrostatic charging and decay properties of materials for 40 years. Tests on thousands of materials during this time show the effects of relative humidity on the charging and decay properties. The new device allows us to test and identify the effects on electrostatic charging and decay under controlled humidity, temperature, low atmospheric pressures, and selected gas environments. Figures 2, 3, and 4 show typical test reports.

This laboratory can duplicate a wide variety of environments where materials are used. Materials can be tested in these simulated environments to select the best one for a given application. The Automated Electrostatics Test Device was designed to measure both the electrostatic-generating potential and the discharge time of the material under test. It can test films, clothing materials, space suits, solar panels, solid foams, gloves, paints, and coatings. The device operates in a laboratory test chamber (after proper material acclimation time) under the following environmental conditions:

- Atmospheric pressure: 0.4 to 760 torr (0.533 to 1010 millibars).
- Temperature: -123 to 200 $^{\circ}\text{C}$.
- Humidity: 0.5 to 100 percent.
- Various atmospheric gas combinations.

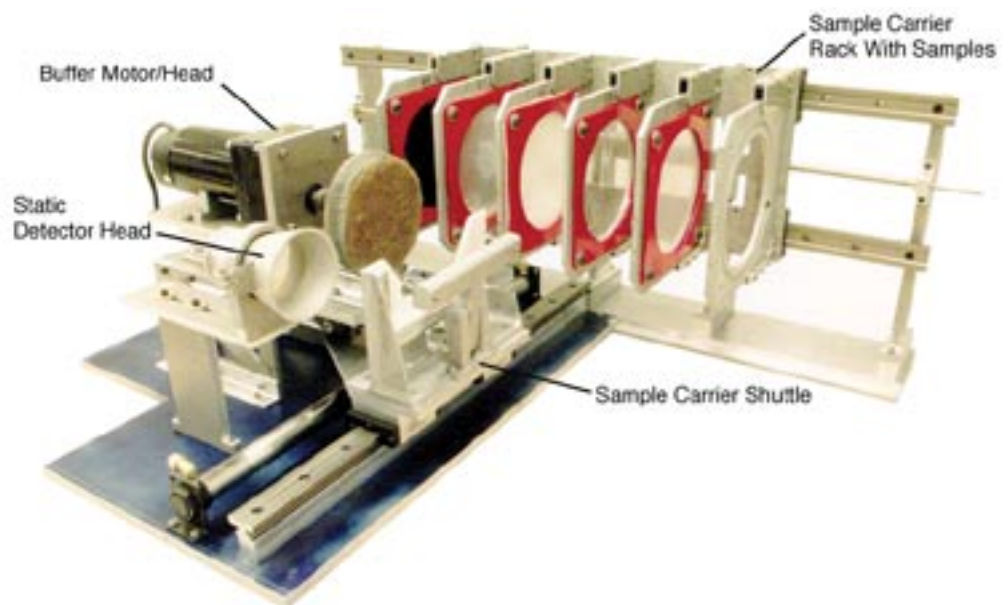


Figure 1. Automated Electrostatic Test Device

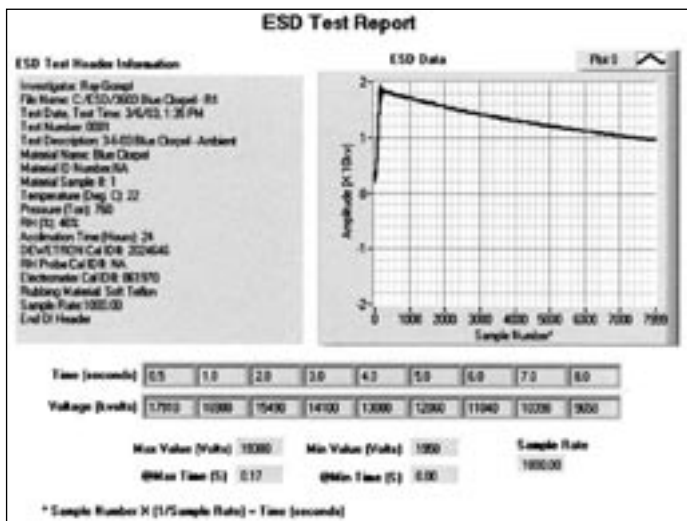


Figure 2. Material Test at Ambient Atmospheric Conditions

Contacts: Dr. C.I. Calle (Carlos.I.Calle@nasa.gov), YA-C2-T, (321) 867-3274; and Dr. R.H. Gompf, YA-C2-T, (321) 867-3267

Participating Organization: YA-F1 (P.F. Richiuso and J.A. Bayliss)

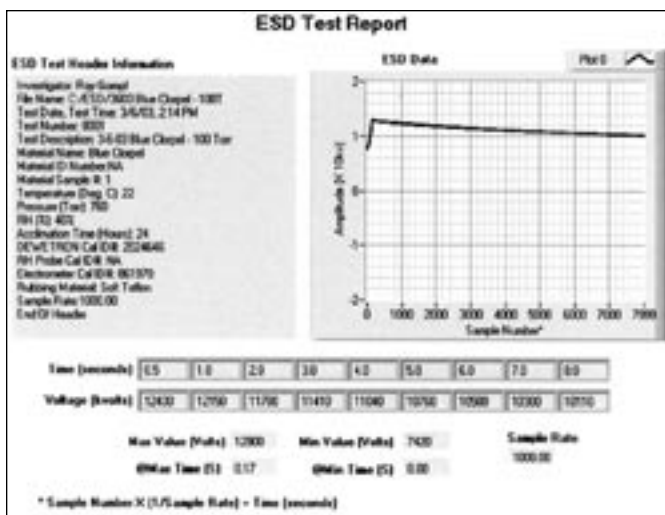


Figure 3. Material Shown in Figure 2 at 100 Torr

Number Of Materials: 8 Selected

Material ESD Test Comparison Table

Note: Table values must be at the same sample rate!

Sample Rate: 1000.00 Samples Per Second

Times & Volt (Volts), Times (Sec) Header test values are in seconds and vary with the sample rate. Times (Tns) in microseconds. The table values are the corresponding voltages (Volts).

Test Description	Time	@760	Time	@760	0	1	2	3	4	5	6	7	8
34-02 Blue Chapel - Ambient	1138	168	1250	0	17910	16380	15400	14700	13900	13200	12600	12000	9000
34-02 Blue Chapel - 100 Torr	1138	168	7420	1	12400	12750	11700	11410	11040	10750	10580	10300	10710
34-02 Blue Chapel - 50 Torr	3250	219	280	0	3000	2600	2410	2200	2100	2040	1960	1760	1470
34-02 Blue Chapel - 25 Torr	680	207	90	30	1070	1090	1480	1300	1200	1110	1020	1020	800
34-02 Blue Chapel - 10 Torr	1020	187	190	0	800	800	800	740	740	740	740	740	800
34-02 Blue Chapel - 1 Torr	400	187	660	1210	400	370	370	270	270	270	270	270	0

Figure 4. Material Shown in Figures 2 and 3 at a Variety of Pressures

Spacecraft Charge Monitor

Electrostatic charging can damage spacecraft, cause instrument biases that limit the accuracy of scientific measurements, and even pose a direct hazard to personnel during extravehicular activity. Currently, there are few options available for monitoring spacecraft charge. An inexpensive, compact, reliable, easily deployed spacecraft charge monitor is needed. Funded by a NASA Small Business Innovation Research (SBIR) Phase II grant, Goembel Instruments is developing the Spacecraft Charge Monitor (SCM) for KSC's Electrostatics and Surface Physics Laboratory.

Goembel Instruments has advanced the SCM from concept to the initial stages of a complete flight instrument (figures 1 and 2). An SCM test apparatus was built to test the different prototypes of the SCM (figure 3). The SCM will bring a substantial improvement to the field of spacecraft charge detection and will find a ready market in aerospace.

The SCM is based on electron spectroscopy. The method is dependent on a phenomenon known as photoionization. When sunlight strikes the Earth's upper atmosphere the molecules of nitrogen and oxygen eject electrons that travel with kinetic energies of only a few electronvolts (eV). A significant portion of the electrons produced in photoionization travel at four well-defined energies between 20 and 30 eV: 22.2, 23.9, 25.2, and 27.2. These electrons travel away from the lower altitudes where they are produced (approximately 150 to 250 kilometers [km]) to higher altitudes where they can be detected by spacecraft.

The SCM measures the spacecraft charge by measuring the energy of electrons produced by the photoionization of the Earth's upper atmosphere. The SCM's reference potential is spacecraft ground. Spacecraft charging is apparent if we see a shift in the energy location of the peaks that would appear at 22.2, 23.9, 25.2, and 27.2 eV on an uncharged spacecraft. If it

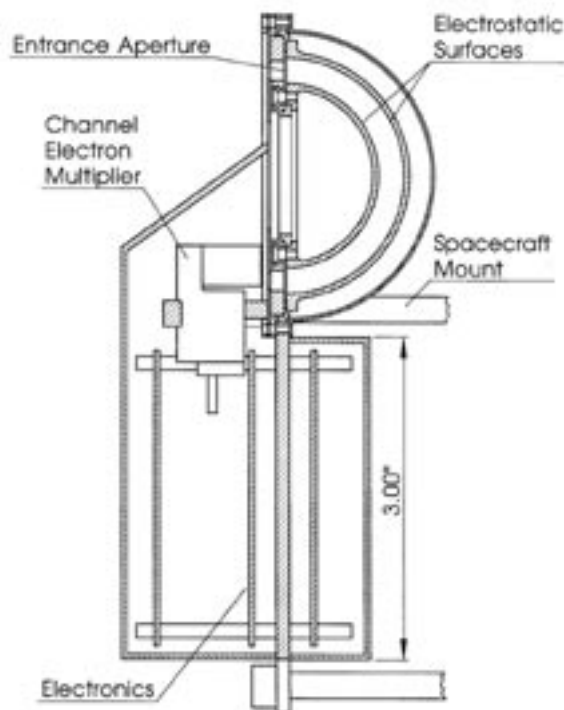


Figure 1. Cutaway Drawing of the Flight SCM

appears that the electrons have been slowed down as they approach the spacecraft, it is because the spacecraft is charged negatively, and the negative charge of the spacecraft repulses the negatively charged electrons. If the spacecraft has a negative floating potential of 10 volts relative to the space plasma where the photoelectrons were produced, the four photoionization peaks will appear at 12.2, 13.9, 15.2, and 17.2 eV. By the same mechanism, positively charged spacecraft will accelerate the electrons to higher speeds, and the peaks will appear shifted to higher energies. One of the outstanding features of this method of determining spacecraft floating potential is that there is a one-to-one correlation between the shift in the location of the photoionization peaks and the spacecraft floating potential. Thus, the data analysis for floating potential promises to be direct and accurate. The diagram in figure 4 illustrates this one-to-one correlation between spacecraft floating potential and a shift in the energy location

of the photoionization peaks in an electron energy spectrum.

In designing and building the flight SCM, the device will be configured so it can be easily accommodated on a wide variety of spacecraft. The SCM will weigh 500 grams and consume 1 watt of power. The device will fit within a space of 6.5 by 3 by 3 inches. In addition, the SCM will use an RS-422 interface, and it is likely that we will be able to build the flight prototype SCM with radiation-tolerant parts (rated to 12 kilorads). Because the Air Force Research Laboratory (Hanscom AFB, Massachusetts) has offered to recommend the flight of the SCM through the Air Force Space Test Program (STP), the device is being designed to meet or exceed standards for STP flights. Their standards include operation at a temperature range of -24 to +61 degrees Celsius, vibration tolerance to 9 g's, and the ability to operate with power from a 28 ±6-volt spacecraft power system.

The SCM has been included, for a second time, in a proposal to fly as a component of a suite of science instruments on a series of satellites. More information about the SCM can be found at www.goembel.biz.

The following tasks were completed under the SBIR Phase II grant:

- Converted an empty room into a state-of-the-art electron spectroscopy laboratory.
- Completely designed a flight-quality SCM sensor head.
- Completed a preliminary design for the flight electronics.
- Contracted Payload Systems, Inc. and Elf Electronics, Inc., to deliver flight-quality boards for the SCM.

Contact: Dr. C.I. Calle (Carlos.I.Calle@nasa.gov), YA-C2-T, (321) 867-3274

Participating Organization: Goembel Instruments (Dr. L. Goembel)

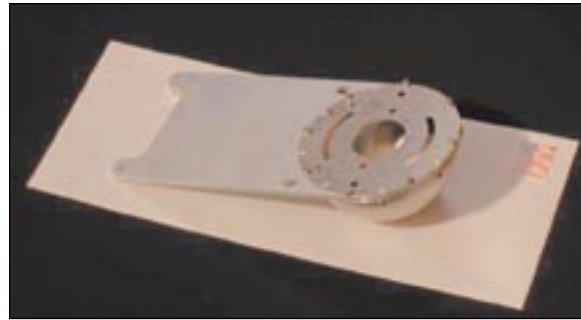


Figure 2. SCM (Incomplete Assembly) and Standard Business-Size Envelope for Scale



Figure 3. The SCM Test Apparatus in the Goembel Instruments Laboratory

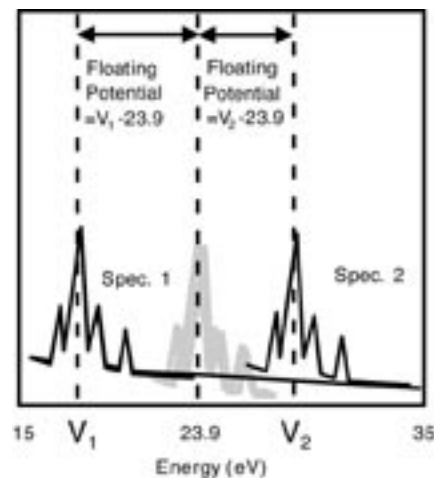


Figure 4. Spectra (Simulated) That Exhibit a Shift in the Energy Location of the Peaks

Antistatic, Field-Emitting, Nanoparticle Coatings

Production of antistatic, field-emitting coatings that can prevent destructive electric discharges is currently underway at Eltron Research Inc., funded by a Small Business Innovation Research (SBIR) Phase II contract with NASA KSC. The antistatic coatings are being designed to survive the atomic oxygen and intense ultraviolet light of low Earth orbit by using refractory electron-conducting ceramic oxides. To silently discharge a surface through electron field emission, it is necessary to produce local electrostatic fields in the range of 10^9 to 10^{10} volts per meter (V m^{-1}). To achieve such high fields at modest applied voltage, small, nano-sized particles are used in the coatings. Assuming as a first approximation that the electrostatic field E of an isolated spherical particle is given by $E = V/r$, where V is the applied potential in volts and r is the radius in meters, then the estimated required radius of the field emitters is given by $r = V/E$. For a modest applied potential of 500 V, the radii of the particles need to lie in the range between $r = 500 \text{ V}/10^9 \text{ V m}^{-1} = 5 \times 10^{-7} \text{ m}$ and $500 \text{ V}/10^{10} \text{ V m}^{-1} = 5 \times 10^{-8} \text{ m}$. In nanometers (nm), the particles must have radii between 50 and 500. Particle diameters, therefore, must be in the range of 100 to 1,000 nm.

Because of the extremely high surface free energy of finely divided matter, most base metals and semiconductors of nanometer size would rapidly oxidize in Earth's atmosphere or would react with atomic oxygen in orbit to form insulating surface layers. Therefore, electron-conducting ceramic oxides were chosen for the new coating materials. Since these materials are already stable oxides, there is little tendency for them to further oxidize. All but one of the compounds synthesized over the past year are stable to at least 900 degrees Celsius ($^{\circ}\text{C}$) (1173 kelvin [K]) in air. The figure is a scanning electron microscopy image of an electron-conducting coating showing the typical submicron particle size of the materials. The new materials compare favorably to conductive graphite and some of the conductive oxides used previously by NASA.

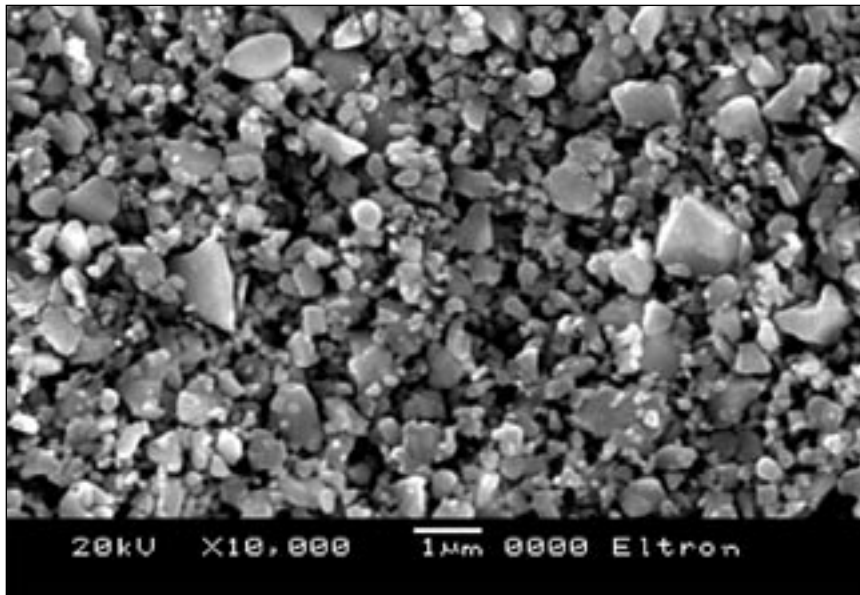
By varying the stoichiometry of the compounds, materials can be made that are either metallic conductors or semiconductors. Metallic conductors increase in resistivity with increase in temperature, whereas semiconductors increase in resistivity with decrease in temperature. Metallic conductors are preferred to avoid possible formation of insulators from semiconductors if coatings experience cryogenic temperatures in space.

Tests are currently under way to optimize the use of the new materials with inorganic binders that have been used successfully by NASA as binders for zinc orthotitanate and other coatings. Inorganic binders are preferred because, unlike organic binders, they are not degraded by atomic oxygen and vacuum ultraviolet light. Preparations have also been made for testing the stability

of materials in vacuum while exposed to atomic oxygen and ultraviolet radiation from a deuterium lamp equipped with magnesium fluoride windows with transmission down to 115 nm. Samples of three materials were accepted by NASA for the next long-duration exposure facility flight.

Contact: Dr. C.I. Calle (Carlos.I.Calle@nasa.gov), YA-C2-T, (321) 867-3274

Participating Organization: Eltron Research Inc. (Dr. M.V. Mundschau, Dr. X. Xie, Dr. J.S. Thompson, D.A. Gribble, and M.A. Taylor)



Scanning Electron Microscopy Image of an Antistatic Field-Emitting Coating of Small Particles of an Electron-Conducting Ceramic Oxide (Small particle size enhances local electrostatic fields, allowing electron field emission. Scale bar is 1 micrometer.)

Corrosion-Resistant Tubing for Space Shuttle Launch Sites

The existing 304 and 316 stainless-steel (SS) tubing and fittings at Launch Pads 39A and 39B are susceptible to pitting corrosion. This pitting corrosion can cause cracking and rupture of both high-pressure gas and fluid systems. The failures can be life-threatening to launch pad personnel and can influence schedules. Outages in the systems where the failures occur can affect the safety of Shuttle launches. Improved corrosion-resistant tubing systems will greatly enhance the safety of personnel and the Shuttle. These new materials will require less maintenance over their lifetime and significantly reduce costs associated with these systems.

A range of materials was selected for testing that includes stainless steels (austenitic, low-carbon, Mo-alloy, superaustenitic, duplex, and superferritic), Ni-Cr-Mo alloy, Ni-Cr-Mo-Fe-W alloy, and austenitic Ni-base superalloy. Each tubing test article contains a series of 90-degree bends, 37-degree tube flairs, and an orbital weld. Four environmental conditions are being tested on the same beach where the launch pads are located: seacoast (unsheltered and sheltered) and seacoast with acid rinse (unsheltered and sheltered).

Based on the 1-year exposure data of the materials tested, austenitic stainless steel AL6XN was found to be the most cost-effective tubing material to replace the existing 300-series stainless steel. AL6XN welded tube was determined to be in the same price range as seamless 300-series SS while offering much higher pitting corrosion resistance.

The 304L SS tubing is in the process of being replaced with AL6XN at the launch pad. The tubes are being installed using orbital welding. This welding process did not compromise the mechanical properties of AL6XN SS. During a pull test, a welded AL6XN tube failed far away from the orbital weld, proving the strength of the weld joint. Several tests were conducted to assess the integrity of the material's properties in the postwelded tube.

X-ray dot mapping was conducted to test for segregation of alloying elements. This test showed no anomalies with the microstructure of the material. X-ray photoelectron spectroscopy (XPS) was used to test the integrity of the protective oxide layer. The surface of the postwelded AL6XN tubing was restored by passivating it with nitric acid, which is the preferred passivating method for SS in industry.

Metallography of representative samples was performed to check for sensitization issues using American Society for Testing Materials (ASTM) standards as a guideline. Figure 1 shows a micrograph of an AL6XN sample that has been etched with oxalic acid to test for sensitization. Sensitization is the formation of

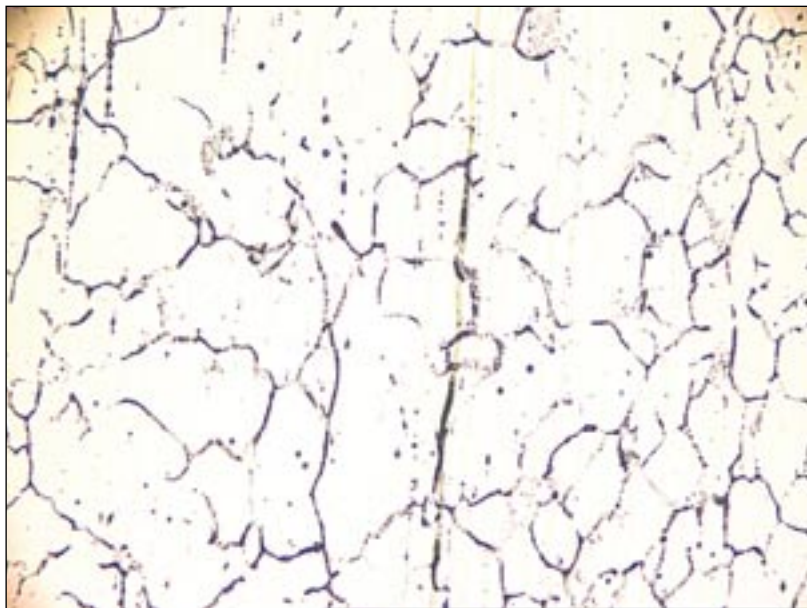


Figure 1. Micrograph of an AL6XN Sample Tested for Sensitization

chromium carbides along the grain boundaries, which weakens the material's ability to withstand certain corrosive environments and eventually leads to failure. When sensitization is present, it is revealed by the formation of a ditch structure as shown in Figure 2. The AL6XN micrograph in Figure 1 does not show the ditch structure that is representative of a sensitized sample.

Contacts: L.G. MacDowell (Louis.G.MacDowell@nasa.gov), YA-C2-T, (321) 867-4550; and Dr. L.M. Calle, YA-C2-T, (321) 867-3278

Participating Organization: USTDC (R.D. Vinje and J.J. Curran)

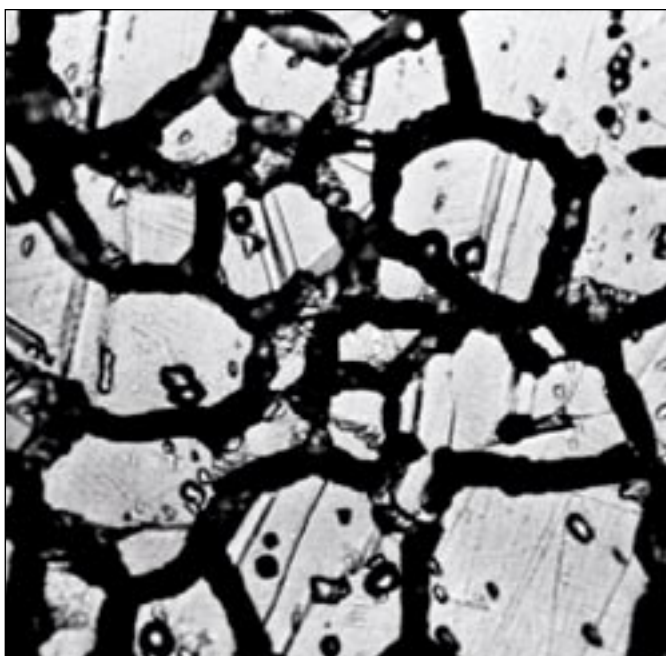


Figure 2. Ditch Structure (500X)
(One or more grains completely surrounded by ditches.)

(Reprinted, with permission, from A 262-02a Standard Practices for Detecting Susceptibility to Intergranular Attack in Austenitic Stainless Steels, copyright ASTM International.)

Electrochemical Characterization of Tubing Alloys in Simulated Space Shuttle Launch Pad Conditions

The 304L stainless-steel (304L SS) tubing is used in various supply lines that service the Orbiter at the KSC launch pads. The atmosphere at the launch site has a very high chloride content caused by its proximity to the Atlantic Ocean. During a launch, hydrochloric acid is produced as a by-product of the Solid Rocket Booster exhaust. The acidic chloride environment is aggressive to most metals and causes severe pitting in many common stainless-steel alloys.

The 304L SS tubing is susceptible to pitting corrosion that can cause cracking and rupture of both high-pressure gas and fluid systems. These failures can be life-threatening to launch pad personnel in the immediate vicinity. Furthermore, outages in the systems where the failure occurs can result in expensive delays in Shuttle operations. The implementation of a new tubing alloy will greatly improve safety and reduce maintenance costs, downtime losses, and the probability of failure.

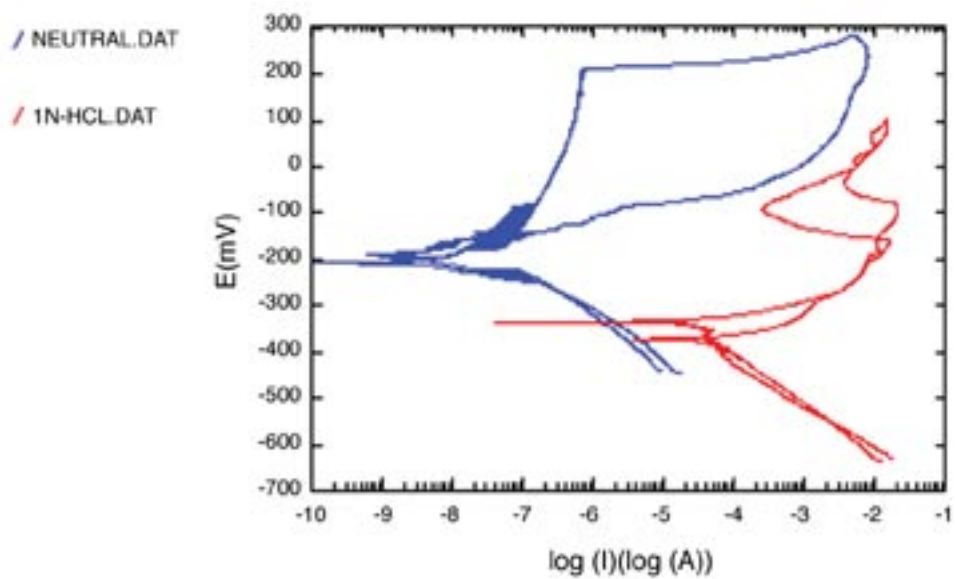
The objective of this investigation is to study the electrochemical behavior of 10 corrosion-resistant stainless-steel alloys to replace the 304L SS tubing at the Space Shuttle launch sites. The alloys included 317L, 316L, 2205, C-276, 625, 254 SMO, C-2000, AL-6XN, AL29-4C, and 2507. As a reference for the candidate materials, 304L SS was included in the study. The specimens were obtained from tubing that was cut and flattened prior to testing. Three electrochemical techniques were used to evaluate the performance of the materials: corrosion potential, polarization resistance, and cyclic polarization. The samples were placed in an electrochemical cell designed to expose a surface area of 1 square centimeter to the electrolytic solution. Electrolytic solutions were chosen to emulate conditions that are less aggressive than, similar to, and more aggressive than those found at the launch pads at KSC.

The figure shows the results from the cyclic polarization measurements for 304L SS alloy exposed to neutral 3.55% NaCl and 3.55% NaCl-1.0N HCl solution. The addition of hydrochloric acid results in a more aggressive environment, and the increased acidity of the solution is detrimental to the performance of the material. The position of the scans in the potential-current diagram shows that the corrosion performance of 304L deteriorated in the 3.55% NaCl-1.0N HCl solution.

A complete set of measurements is being collected using standard coupon samples under the same electrolytic conditions. Preliminary data suggest a strong correlation between the performance of the samples in the laboratory and similar specimens that were atmospherically exposed at the KSC Beach Corrosion Test Site.

Contacts: Dr. L.M. Calle (Luz.M.Calle@nasa.gov), YA-C2-T, (321) 867-3278; and L.G. MacDowell, YA-C2-T, (321) 867-4550

Participating Organization: USTDC (R.D. Vinje)



Cyclic Polarizations for 304L Stainless Steel in Neutral 3.55% NaCl and 3.55% NaCl-1.0N HCl

Advanced Multisensor for Electrolytic Characterization

This project investigated the feasibility of developing a sensing device for electrolyte characterization using an array of galvanic cells. The methodology needed to analyze and interpret the data is also being developed. The ultimate goal is to integrate the sensor into a subsurface explorer probe to determine the feasibility of grounding experimental devices on planetary soil, utilizing the soil as an electrical return path, and using the experimental data to select materials that will not corrode when in contact with the soil. While the focus of the research centers upon developing a device to study planetary surfaces, commercial applications are also feasible. These may include but are not limited to agricultural, biological, and geological analyses. The selection and optimization of galvanic cell electrodes to determine the corrosivity of solutions and soils are important to the investigation.

The first component of the multisensor (shown in figure 1) is an ion selective electrode (ISE) array for the qualitative and quantitative detection of individual ions. The second constituent of the device complements the first technique through the use of anodic stripping voltammetry (ASV) and cyclic voltammetry (CV). ASV is an analytical method in which analytes are preconcentrated on the surface of a working electrode for a specific duration. Through an anodic potential scan, the analyte is stripped from the working electrode and oxidized back to its original form, with a voltammetric signal indicating the ions present in solution. CV is a similar technique, except that it does not include the preconcentration step of the anodic stripping analysis. These components are being investigated with standard, well-characterized redox couples to determine the sensitivity of the electrodes and resistance to interfering signals.

The final element of the sensor is a galvanic cell array. The galvanic cell methodology is unique (developed at KSC) in that it attempts to analyze electrolytes based upon the corrosion rate and corrosion potentials exhibited by the metals. In essence, the galvanic cell concept (differing metals) is used to drive the system at a potential indicative of the corrosive processes taking place. This allows the electrochemical processes to occur without the application of external power, except for that needed to take measurements. While these open-circuit potential values indicate the corrosivity of the

system, they fail to provide information on the specific corrosion rates. These are often obtained from potentiodynamic polarization measurements.

For potentiodynamic determinations, the potential is scanned through a preset range of voltages near the open-circuit potential. Straight lines can be fit to the anodic and cathodic areas of the potentiodynamic polarization scans, which result in a Tafel plot. This plot gives the open-circuit potential of the system as well as the corrosion current.

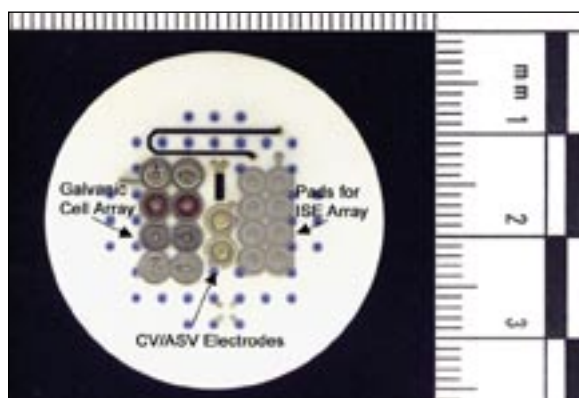


Figure 1. Multisensing Ceramic Substrate

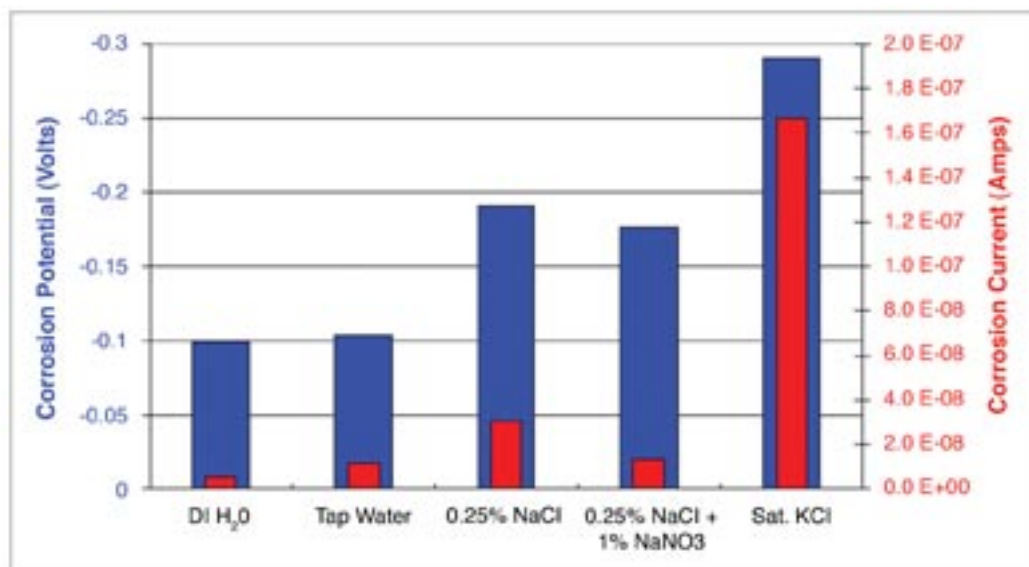


Figure 2. Corrosion Potentials and Corrosion Currents for Solutions of Different Corrosivities

Figure 2 shows the corrosion potentials and corrosion currents for a set of aqueous solutions. These were specifically chosen to illustrate a wide range of corrosivities. As shown, deionized (DI) water and tap water were the least corrosive. An addition of 0.25-percent sodium chloride (NaCl) to the DI water increases the corrosivity of the system as shown by the corrosion potential and corrosion current values. In contrast, an addition of 1-percent sodium nitrate (NaNO₃) to this solution shows a decrease in both values. This is indicative of the corrosion-inhibiting properties of the NaNO₃, which is a well-known corrosion inhibitor. Finally, the corrosion current of the saturated potassium chloride (KCl) solution clearly shows the greatly increased corrosivity of the system. These results are consistent with the known corrosivities of these solutions.

Key accomplishments:

- Completed cyclic voltammetry experiments with standard redox couples to investigate the response of the electronics and CV electrodes of the sensor.
- Integrated the sensing ceramic with commercial instrumentation to validate the response of the sensor.
- Gathered open-circuit potentials for the galvanic couples for a wide range of solutions varying in corrosivity.
- Obtained potentiodynamic polarization measurements for the individual galvanic couples exposed to solutions with a wide range of corrosivities.

Contact: Dr. L.M. Calle (Luz.M.Calle@nasa.gov), YA-C2-T, (321) 867-3278

Participating Organizations: USTDC (Dr. M.R. Kolody), NASA/JPL (Dr. M.G. Buehler), Tufts University (Dr. S.P. Kounaves), and YA-C (N.P. Zeitlin)

Chromate Coating Replacement for Military Aircraft

To enhance corrosion resistance of aluminum alloys, hexavalent chromium-based products are presently used. Unfortunately, tighter restrictions are being placed on the use of these coatings because of their carcinogenic effects and endangerment to the environment. The objective of this project is to expose 960 nonchromate-coated coupons to a harsh, outdoor marine environment at the KSC Beach Corrosion Test Site (BCTS) while tracking the deterioration of the surface pretreatments and coatings. This study is to determine the effectiveness of protection of environmentally compliant chromate replacement technology for chromate-inhibited coatings for aluminum materials on military aircraft.

The 960 coupons form a matrix of four aluminum alloys having nine pretreatments, each of which has five paint systems, all in sets of three or five coupons (see the table). Each coupon is scribed and was evaluated in accordance with ASTM D 1654, Standard Test Method for Evaluation of Painted or Coated Specimens Subjected to Corrosive Environments. This ASTM standard uses a rating system of 0 (worst) to 10 (best) depending on the distance of creepage from the scribe. The coupons were observed on a 6-week schedule and intensively evaluated on a 4-, 8-, and 12-month schedule using ASTM D 1654 ratings for blister sizes. All blisters were measured one-sided, that is from the scribe to the creepage front. All blister measurements were recorded for each coupon in millimeters. The maximum, minimum, and representative means were recorded along with each blister measured.

Alloys, Pretreatments, and Coating Systems

Alloys	Pretreatments	Primers	Topcoats
2024-T3 2219-T87 5083, H131 7075-T6	Alodine 1200S (immersion) TCP 10 (immersion) Alodine 5200 (immersion) Sanchem (spray) X-IT Prekote (wipe) Oxsilan AL-0500 (immersion) Chemdize 727ND (wipe) Bi-K Alkimate (immersion) Boegel (spray)	53022, carc solvent 53030, carc water 85582nc, nonchromated-water 85582c1, chromated-water 23377, chromate-solvent	53039, carc-solvent 82585, high solids

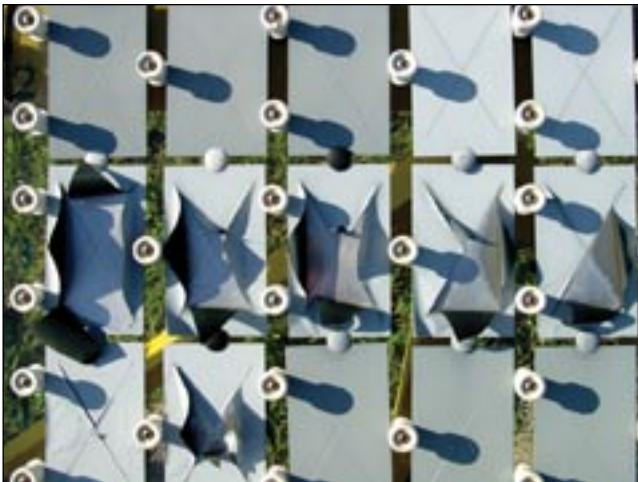
After 1 year, all coupons with an ASTM rating of 2 or less were considered failures, removed from the site, and sent back to the customer for evaluation. The remaining coupons that showed little or no degradation at the end of the 1-year period are being exposed for a longer period. There were 194 coupons that had an ASTM rating of 2 or below. All of the failures came from the coatings applied to the 2024-T3, 7075-T6, and 2219-T87 alloys. These failures consistently came from the 53030/53039, 53022/53039, and 85582nc/85285 paint systems. There were no fail rankings from the same coating systems applied to the 5083-H131 alloy.



Coupon Racks at the Beach Corrosion Test Site



Blistered Coupon, 8-Month Exposure



Coating Delamination Failure



Blistered and Coating Delamination Coupon, 8-Month Exposure

Key accomplishments:

- Built panels to hold 960 nonstandard-sized coupons.
- Installed approximately 960 coupons at the BCTS.
- Completed 1-year evaluations and photographic documentation.
- Developed a portable camera stand for taking consistent coupon photographs.
- Compiled a 6-month summary of results.
- Compiled a 12-month report of the test evaluation.

Contact: L.G. MacDowell (Louis.G.MacDowell@nasa.gov), YA-C2-T, (321) 867-4550

Participating Organization: USTDC (J.J. Curran and J.P. Curran)

Army Aircraft Alloys – Corrosion-Retardant Additive Testing

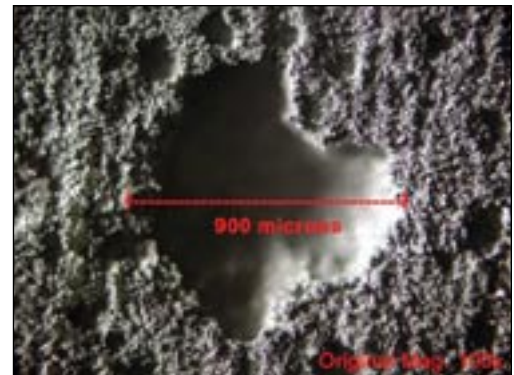
This project tested and evaluated commercially available chloride rinse agents (CRAs) for effectiveness of corrosion reduction by rinsing typical aviation metals. These metals are used in Army aircraft, missile, and ground vehicle systems and components. Four separate CRAs are being tested for their effectiveness in preventing or reducing corrosion of metals exposed to seacoast environments. Nine different metals specified by the U.S. Army have experienced a harsh, outdoor marine environment at the KSC Beach Corrosion Test Site (BCTS). Replicate alloy samples were exposed and rinsed weekly for periods of 1 and 2 years. CRAs and control solutions were sprayed onto metal coupons each week. Comparison testing of products and recommendations were reported at the 1-year and 2-year points. CRAs, numbered 1 through 4, were compared to seawater, demineralized water, and no-rinse as controls. The following materials/coatings were selected for testing:

- Aluminum 2024-T3 with 8625 coating.
- Aluminum 2024-T3 with 5541 coating.
- Aluminum 7075-T6, uncoated.
- Magnesium 4377 with 3171 coating.
- Steel 4340 carbon steel, uncoated.
- PH 13-8 molybdenum (Mo) high-strength steel, uncoated.
- AM-355 CRT high-strength steel, uncoated.
- C-250 maraging high-strength steel, uncoated.
- Titanium 6Al-4V, uncoated.

To establish CRA ranking, pitting characteristic ratings were applied to the aluminum and magnesium alloys. The results of this study showed that two of the chemical rinse agents tested, CRA 1 and CRA 3, were more effective in reducing corrosion on both aluminum and magnesium than the same exposure and rinsing with either demineralized water or tap water. These results contrast with the results for the other two commercial rinse agents tested. Rinsing with either CRA 2 or CRA 4 resulted in even more corrosion on aluminum or magnesium than rinsing with demineralized water or even with seawater. Because of the detrimental effects on the aluminum alloys, these two products are not recommended for use on military aircraft.



*Typical Pit, 7075T6 Aluminum Alloy -
Magnification $\times 100$*



*Typical Pit, Magnesium Alloy -
Magnification $\times 100$*

Corrosion ratings were based on weight loss for the 4340 steel and the C-250 maraging steel. The results of testing with the four rinse agents on these steels produced mixed results. Rinsing with CRA 3 produced the lowest corrosion rate, while rinsing with CRA 1 resulted in the highest corrosion rate. Rinsing with CRAs 2 and 4 produced similar results. The weight loss results are unclear due to the limited number of exposure samples for each alloy/exposure combination in this extensive study. The corrosion-resistant stainless steels and titanium alloys only showed superficial tarnishing and had no beneficial or detrimental effects.

Key accomplishments:

- Completed 1-year and 2-year exposures of coupons.
- Cleaned and evaluated all nine coupon material sets at the 1-year and 2-year points.
- Completed and delivered 1-year progress report.
- Presented 1-year data at Department of Defense Tri-Services conference.
- Presented 2-year data at National Association of Corrosion Engineers (NACE) 2003 corrosion conference.
- Developed and instituted a method to rate CRA effectiveness using ultrasound technology and image analysis software.

Key milestone:

- Prepare and deliver final report and associated coupons.

Contact: L.G. MacDowell (Louis.G.MacDowell@nasa.gov), YA-C2-T, (321) 867-4550

Participating Organization: USTDC (J.J. Curran and J.P. Curran)



*Detrimental Exfoliation Effects on
7075T6 Aluminum Alloy*



Coupon Exposure Stand and Rinse Setup

Electrochemical Analysis of Chloride Rinse Agents on Aircraft Alloys

NASA's Corrosion Technology Testbed is investigating the effectiveness of four chloride rinse agents (CRAs) to prevent or reduce corrosion of alloys commonly used in aircraft. The investigation included atmospheric exposure of rinsed samples of the alloys at the Beach Corrosion Test Site and electrochemical measurements at the Corrosion Laboratory. Both facilities are located at the Kennedy Space Center. Results from the atmospheric exposure investigation are the subject of "Army Corrosion-Retardant Additive Testing" (KSC Research and Technology 2002 Annual Report). The current report presents the results obtained using electrochemical techniques.

The alloys employed in this investigation are listed in the table. Electrochemical measurements are performed using an electrochemical cell to expose the aircraft alloys to four commercially available CRAs (CRA 1, CRA 2, CRA 3, and CRA 4), seawater, and deionized (DI) water. Seawater and DI water are included as reference electrolytes. The rinse agents are diluted according to the manufacturers' specifications. The electrochemical techniques being used include corrosion potential measurement, linear polarization, potentiodynamic scans, and cyclic polarization. The techniques used depend on the alloy being investigated.

Metal Alloys Used in the Electrochemical Analysis of Chloride Rinse Agents

Metal Alloys	UNS Alloy Designation	Designation This Study	Percent Composition
Aluminum	J9100	Al 2024-T3/5541	Al, 4.5 Cu, 1.5 Mg, 0.6 Mn
	A97075	Al 7075-T6	Al, Zn 5.6, 2.5 Mg, 1.6 Cu, 0.3 Cr
Steel Alloy	G43400	4340	Fe, 0.4 C, 1.8 Ni, 0.8 Cr, 0.25 Mo
High-Strength Steel	S13800	PH13-8Mo	Fe, 13 Cr, 8 Ni, 2 Mo
	S45850	C-250	Fe, 18 Ni, 7.5 Co, 5 Mo, Ti, Al
	S35500	AM-355	Fe, 15.5 Cr, 4.5 Ni, 3 Mo
Titanium Alloy	R65400	Ti-6Al-4V	Ti, 6 Al, 4 V
Magnesium Alloy	M11311	AZ31B-H24	Mg, 3 Al, 1 Zn

To date, data has been collected on Al 2024-T3 and Al 7075-T6 aluminum alloys. Open-circuit potential and cyclic polarization techniques were used to test the samples. Sample preparation involved cleaning the samples with ethyl alcohol, which served as a degreasing agent. This method was utilized to preserve the samples in a condition similar to the initial state of the panels placed at the Beach Corrosion Test Site.

Open-circuit potential measurements were monitored until a stable potential was achieved. Measurements were determined to be stable when the values of potential varied by no more than ± 5 millivolts (mV) for a period of 10 minutes. Once a stable potential was achieved, the cyclic polarization technique was used.

Analysis of the data shows that, of the four rinse agents, CRA 3 is the best and CRA 4 the worst for Al 2024-T3/5541. Seawater proved to be the most damaging electrolyte to this aluminum alloy. Figure 1 shows the results of cyclic polarization scans for Al 2024-T3 in CRA 3 and DI water. Plot 1 of figure 1 has a positive hysteresis loop, which is indicative of pitting, and a smaller corrosion current than plot 2, indicating that CRA 3 is better at reducing corrosion than DI water. Similar performance was revealed in the case of Al 7075-T6. CRA 3 performed best while CRA 4 proved to be the most aggressive rinse agent. Interestingly, CRA 4 proved to be more detrimental to the sample than seawater. Figure 2 shows the results of cyclic polarization for Al 7075-T6 in CRA 4 and DI water.

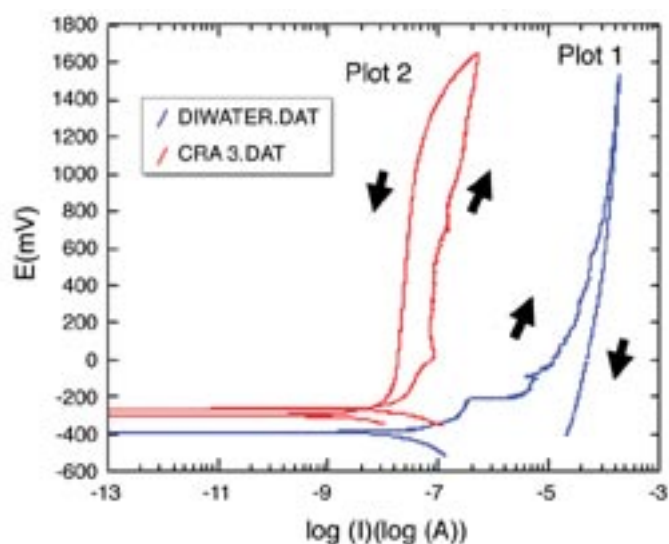


Figure 1. Cyclic Polarization Plots for Al 2024-T3 in DI Water and CRA 3

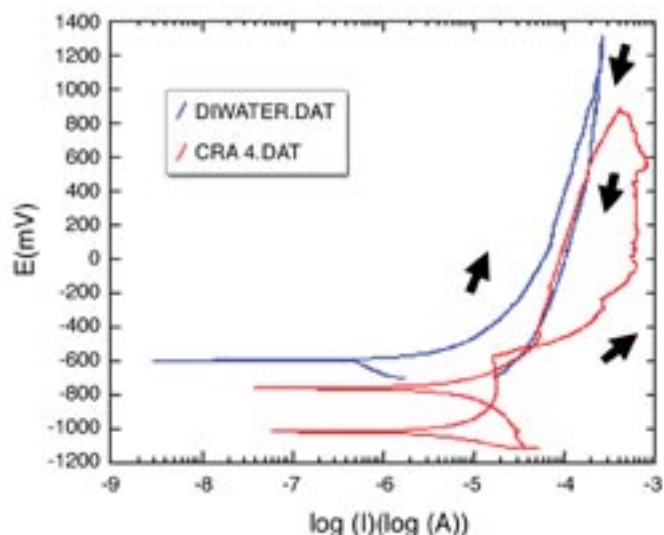


Figure 2. Cyclic Polarization Plots for Al 7075-T6 in DI Water and CRA 4

Contacts: Dr. L.M. Calle
(Luz.M.Calle@nasa.gov) YA-C2-T, (321) 867-3278; and L.G. MacDowell, YA-C2-T, (321) 867-4550

Participating Organization: USTDC (R.D. Vinje)

Development of Liquid Applied Coatings for Protection of Steel in Concrete

Corrosion of reinforcing steel in concrete is an insidious problem facing the NASA facilities at KSC, other Government agencies, and the general public. These problems include damage to KSC launch support structures, including transportation and marine infrastructures, as well as building structures. Because of these problems, the development of a galvanic liquid applied coating system would be a breakthrough technology having great commercial value for the following industries: transportation infrastructure, marine infrastructure, civil engineering, and construction.

Developing this type of system had several goals:

- Phase I concentrated on the formulation of coatings with easy application characteristics, predictable galvanic activity, long-term protection, and minimum environmental impact. These new coating features, along with the electrical connection system, will successfully protect the embedded reinforcing steel through the sacrificial cathodic protection action of the coating.
- Phase II improved on the formulations and included optimizing metallic loading as well as incorporating a humectant for continuous activation. In addition, development of optimum electrical connections continued.
- Phase III incorporated improvements from the previous phases to the test blocks.
- Phase IV incorporated the final upgrades onto large structures that are heavily instrumented (see figure 1).

Laboratory testing has demonstrated the commercial potential of this technology. Presently, testing is being conducted at the NASA/KSC Corrosion Technology Testbed Beach Corrosion Test Site with positive preliminary results. Figure 2 shows the correlation between weather and protection of steel in reinforced concrete. This demonstrates that protective current is available as needs arise. In addition, the data is being collected and remotely accessed from offsite locations.

Successful development and continued optimization of this breakthrough system would stimulate great interest in the NASA/KSC Corrosion Technology Testbed. Commercial patents on this technology would enhance KSC's ability to attract industry partners for similar corrosion control applications and establish the Corrosion Technology Testbed as a leader in solving corrosion problems.

Key accomplishments:

- Proved the feasibility of using liquid applied coatings for protection of embedded reinforcing steel in concrete.
- Determined the optimum mix ratio for specific liquid applied coatings.
- Determined that the addition of moisture attractors adds little or no benefit to coating performance.
- Developed improved electrical connectivity between the coating and the internal reinforcing steel.

- Added intensive embedded instrumentation in new simulated concrete structures for monitoring corrosion protection.
- Obtained patent.
- Successfully licensed product/technology to commercial partner.
- Coated Phase IV structures.

Key milestones:

- Analyze metallic loading.
- Install and evaluate embedded Ag/AgCl reference electrodes.
- Investigate coating-concrete interfacial resistance.
- Realkalinize carbonated concrete.



Figure 1. Closeup of One of the Phase IV Simulated Concrete Test Structures

Contacts: L.G. MacDowell (Louis.G.MacDowell@nasa.gov), YA-C2-T, (321) 867-4550; and Dr. L.M. Calle, YA-C2-T, (321) 867-3278

Participating Organization: USTDC (J.J. Curran, J.P. Curran, and Dr. R.G. Barile)

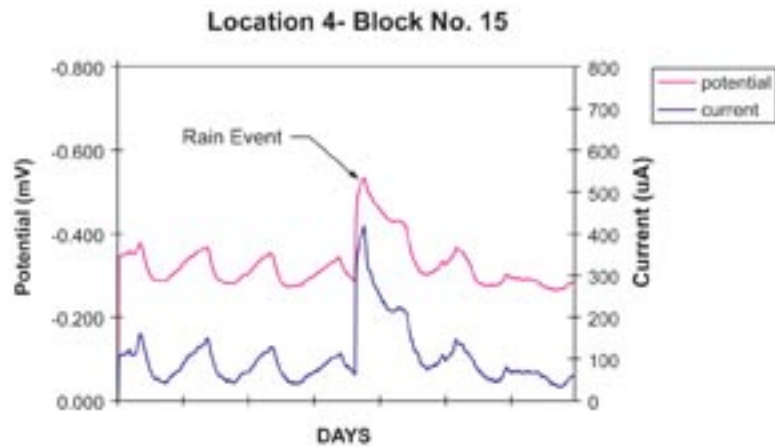


Figure 2. Current and Potential From Sample Block 15

Noise Mitigation of Ducted Supersonic Jets for Launch Exhaust Management Systems

The Launch Systems Testbed (LST) at KSC was created to support the development of clean launch pads for future launch vehicles, incorporating passive sound mitigation techniques to replace active noise reduction methods, such as water suppression systems. These launch pad designs focus on reducing cost while enhancing safety and quick turnaround times. The overall goal of the LST is to establish a capability to simulate a small-scale launch vehicle environment for use in testing and evaluation of launch pad designs for future space vehicles.

One of the LST's specific objectives is to develop launch exhaust management systems (LEMS) that effectively reduce the generated acoustic loads with innovative duct designs devoid of water injection systems. Scale-model testing, along with analytical methods, is helpful as a means of predicting the full-scale acoustic environment in designing such systems. A preliminary series of tests was designed to define the jet acoustic load environment for closed-duct and partially open-duct (upper duct wall removed) configurations. The LST has conducted cold-jet tests with nitrogen gas issuing from an ideally expanded small-scale nozzle of 1-inch exit diameter with an exit Mach number of 2.5. Tests were also conducted with free jets, jets passing through closed ducts, and jets passing through partially open ducts with an upstream J-type deflector.

With the use of a closed duct, the overall sound power of a Mach 2.5 supersonic jet is reduced by about 3 decibels (dB). The peak frequency is found to increase above the free-jet value as the angle from the jet axis is increased. These results also suggest that there is an optimum distance between the nozzle exit plane and the duct inlet for minimizing the sound power. The partially open duct results in increased sound levels near the duct axis relative to the free-jet case. Regarding the closed duct, larger reductions in sound power may be realized by increasing the

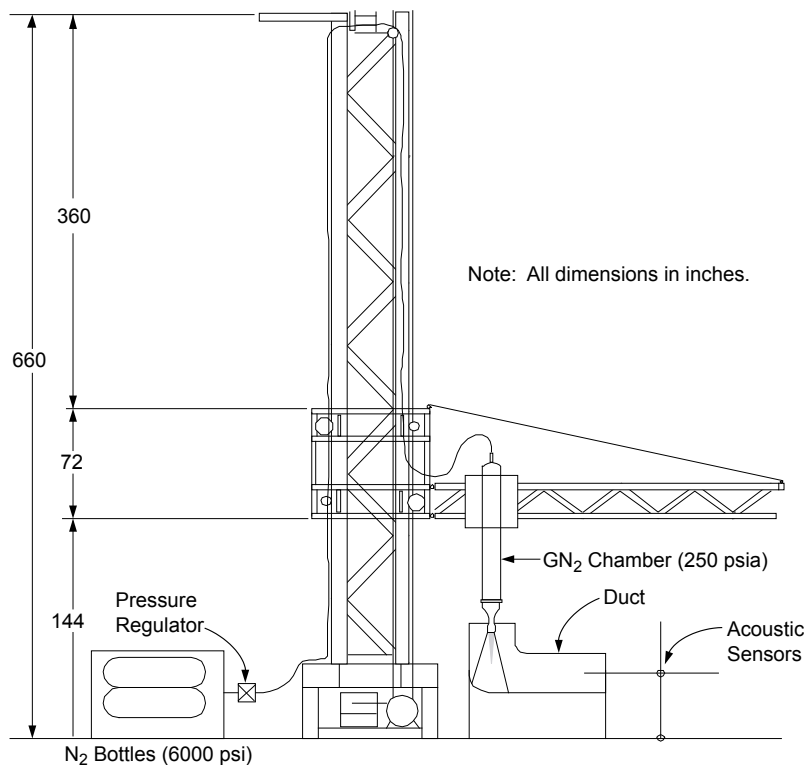
duct length, widening the duct cross section (adding a diffuser), and including absorbing liners on the duct walls.

Key accomplishments:

- Characterized the flow and acoustic environment of a free supersonic jet.
- Characterized the acoustic environment of a supersonic jet flowing through a covered duct with a J-deflector.
- Characterized the acoustic environment of a supersonic jet flowing through an open duct.

Key milestones:

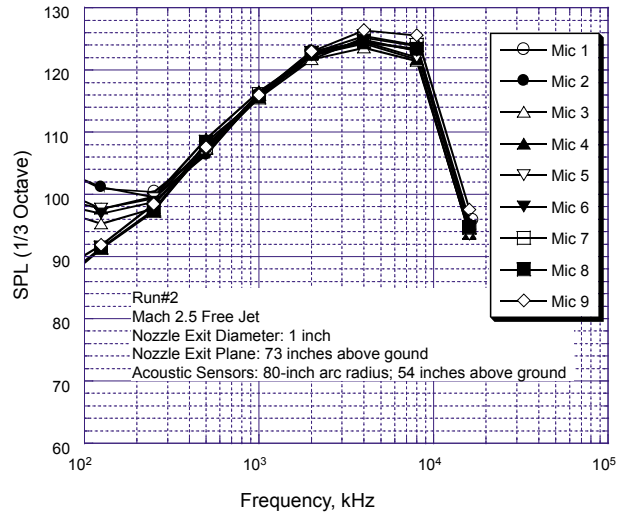
- Completed Phases I and II of Air Force Research Laboratory (AFRL) LEMS.



Overall Test Setup



Jet/Duct Configuration

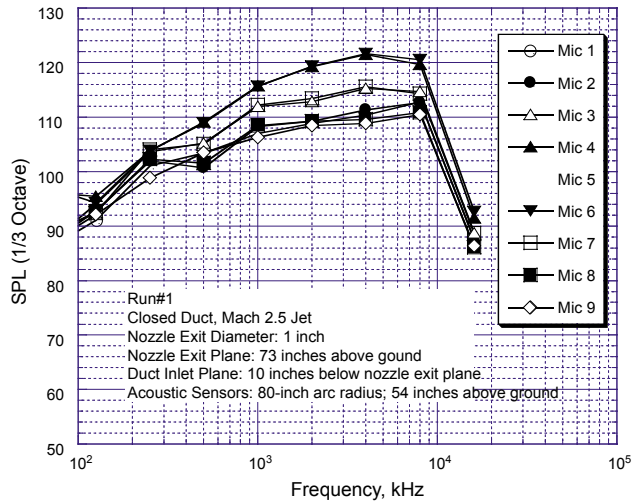


Spectral Sound Power for the Free Jet

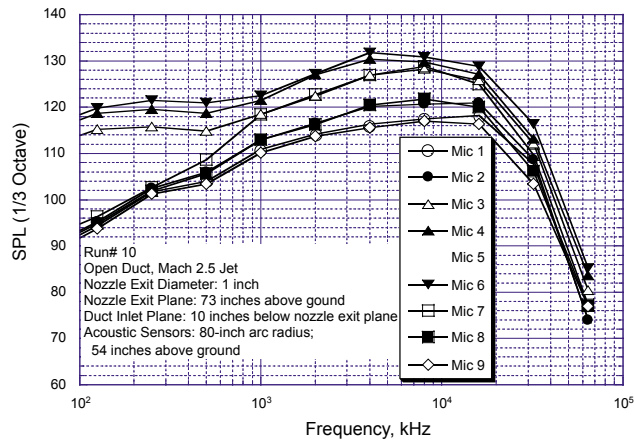
- Presented the study at Joint Army-Navy-NASA-Air Force (JANNAF) Conference and International Congress in Sound and Vibration (ICSV).
- Delivered test results to the AFRL Reusable Military Launch Systems (RMLS) team.

Contact: Dr. B.T. Vu
 (Bruce.T.Vu@nasa.gov), YA-C2-T, (321) 867-2376

Participating Organization: USTDC
 (Dr. M. Kandula)



Spectral Sound Power for the Jet Flowing in a Closed Duct



Spectral Sound Power for the Jet Flowing in a Partially Open Duct

Development of a Robust Finite-Element Method for Rocket Acoustics Problems

Launching space vehicles generates extreme vibration and acoustic conditions that can affect the launch pad, launch vehicles, and payloads. These acoustic loads result from the acoustic field generated by the rocket-engine exhaust stream with the ambient atmosphere and are the primary source of structural vibrations and internal loads during launch or static firings. Thorough knowledge and elimination of acoustic loads are critical to proper functioning of vehicle components and their supporting structures.

Problems that might arise from acoustic loading include (1) malfunction of electrical and mechanical components because of structural vibrations and internal acoustic loading, (2) fatigue failure of internal components and supporting hardware, (3) fatigue of lightweight exterior structures, such as antenna panels, (4) fatigue of lightweight spacecraft structures, and (5) unsuitable environmental conditions for the vehicle occupant. To manage and suppress the undesirable conditions, we must be able to accurately predict the acoustic and vibration levels by either analysis or testing.

The objective of the current project is to develop a user-friendly program to solve acoustic equations using the finite-element method (FEM). The method used is mixed-explicit implicit algorithm. This program will utilize the object-oriented program languages to create a unified environment for the preprocessor, the main solver, and the postprocessor. With this approach, the user can obtain the solution to the compressible Navier Stokes equations all in one environment, from the very raw data all the way to postprocessing and analysis of the results.

Key accomplishments:

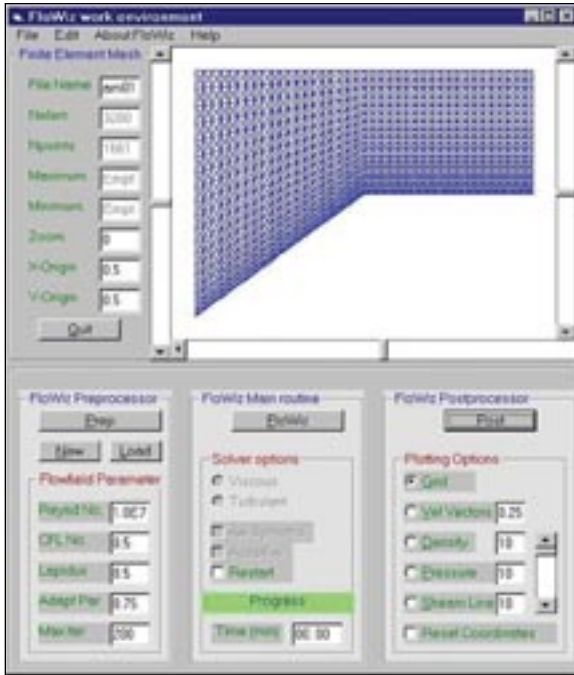
- Analyzed flow around complex geometry such as ramjets, scramjets, internal flow in a Space Shuttle main engine, and flow past cone-shaped objects.
- Developed a mixed-explicit implicit algorithm in finite elements.
- Conducted a seminar on FEM for rocket acoustics at NASA KSC.

Key milestones:

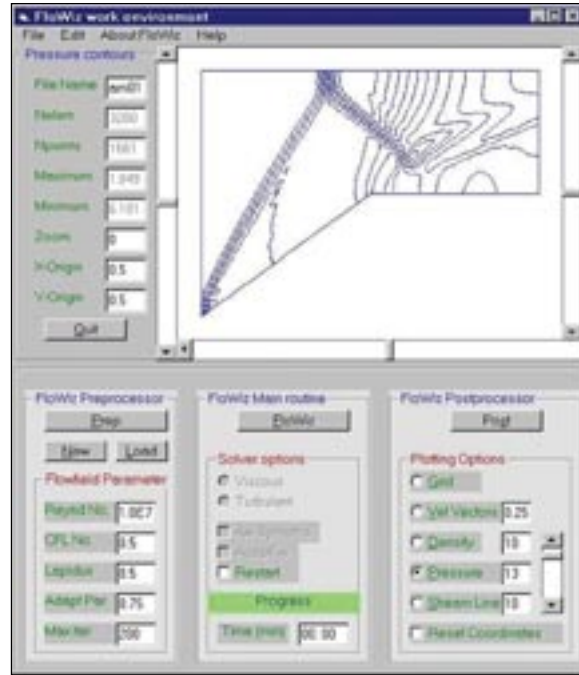
- Acoustic computation using Kirchhoff and Flowc-Williams Hawkings (FWH) codes.
- Presentation of study at the Thermal-Fluid Analysis Workshop (TFAWS), NASA-Langley Research Center.
- Software patent submission.

Contact: Dr. B.T. Vu (Bruce.T.Vu@nasa.gov), YA-C2-T, (321) 867-2376

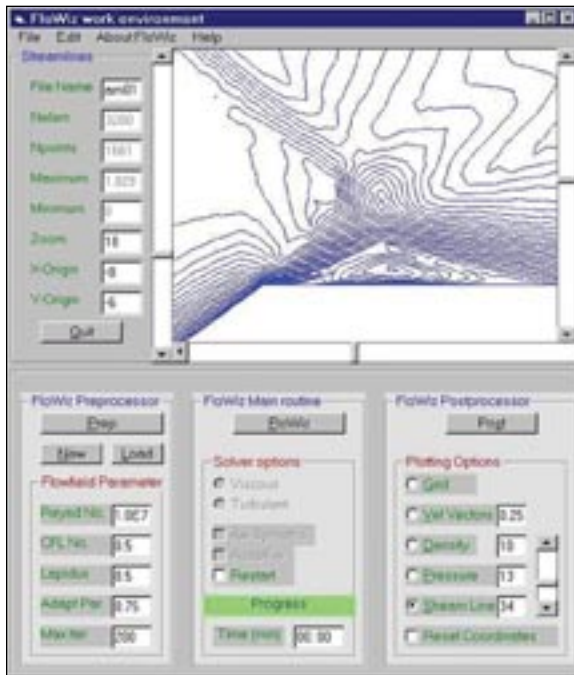
Participating Organization: Alabama A&M University (Dr. A. Mobasher)



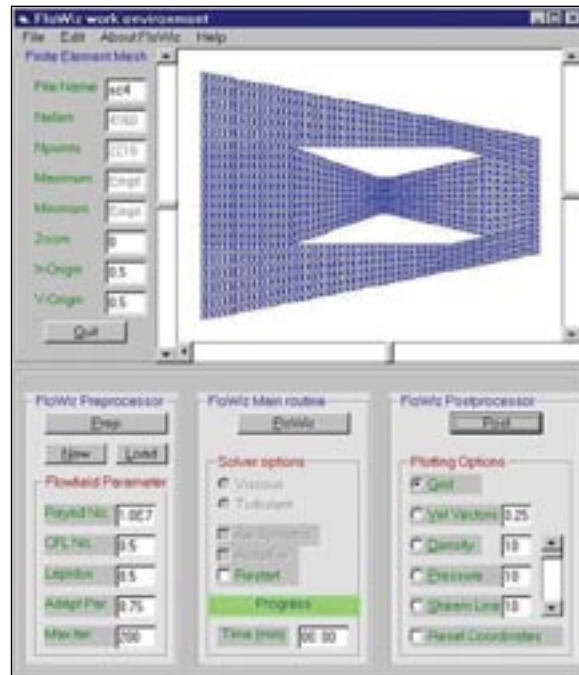
Computational Grid for Ramjet



Pressure Contours for Ramjet



Close-Up View of the Stream Line Contours Near the Position Where Shock Wave Interacts With the Boundary Layer (The recirculation zone is visible.)



Computational Grid for Scramjet

Tape Adhesion Testing Software

The Materials and Processes (M&P) Laboratory, located in the Vehicle Assembly Building (VAB), supports External Tank (ET), Solid Rocket Booster (SRB), and Orbiter operations with in-process testing for a variety of materials, including adhesives, foams, ablatives, and films.

The M&P Laboratory uses a Tinius-Olsen (T-O) 10,000-pound Universal Testing Machine to evaluate tape adhesion strength. Tape adhesion testing verifies tape for shelf life extension. The tape specimen is placed in the jaws of the T-O machine, which pulls 2 inches of tape from a steel test panel. The tape adhesion testing software makes over 500 measurements during the 2-inch pull. The software combines this data to determine the force required to remove tape from the panel. It then automatically reports the results on the tape adhesion testing input screen for inspection and storage in the tape adhesion database.

Previously, United Space Alliance (USA) laboratories at KSC did not have the ability to perform tape adhesion testing onsite. Performing this test onsite provides an obvious increase in processing efficiency.

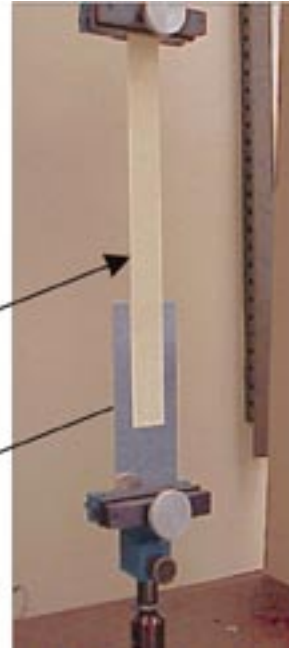
Another benefit is cost savings. Even though the primary use of this software is to test flight tapes, it also can be used to test ground support equipment (GSE)/nonflight tapes. Presently, we discard thousands of dollars' worth of tape with expired shelf life each year. This software gives USA the onsite ability to test tapes in the VAB M&P Laboratory and to create cost savings.

The software team and design team chose Oracle Forms and Reports running on a Microsoft Windows platform for the user interface. This combination of software application and operating system provided current database technology. However, Oracle Forms did not provide the special-purpose communication functions this effort required. In response, the software team embedded C++ function calls within the form. This allows the user to click an on-screen button to initiate two-way communication with the T-O via a serial port. This digital interface to an analog device allows the software to automatically direct the operation of the T-O machine, receive over 500 test values, average these values, store the data in a database, and report the results.

The C++ functions significantly extended tracking capabilities. These on-screen objects provide real-time display of T-O operational values and display dialog boxes for direct user interaction as required. Although it automatically initiates the T-O and



*Tinius-Olsen 10,000-Pound Universal Testing Machine
Performing an Adhesion Test*



Tape Adhesion Software Interface

starts testing, the software still preserves all manual backup capabilities.

Advances in communication technology make the direct interface of a test process and its tracking software both convenient and practical. The ability to take multiple measurements and mathematically manipulate the results prior to automatic storage in a database adds processing flexibility. It avoids the duplication of effort (and errors) involved when using a human being/key-board to interface an analog device to a database. In addition, it performs hundreds of calculations to provide the most accurate average possible, a process that would take hours to perform manually.

This contribution has been used in the Space Shuttle program. The tape adhesion testing software provides the M&P Laboratory with a convenient and accurate way to automatically record and report its tests. It provides better support to SRB/ET processing with automatic recording and mathematical manipulation of multiple values from the test-generating device

directly to the tracking and reporting software.

The concepts developed in this tracking system can be used in any manufacturing process requiring automated multiple recording, manipulation, and storage of analog information to a database.

Key accomplishment:

- Integration of C++ communications modules into Oracle Forms.

Key milestones:

- 2003: Program designed, coded, and fully implemented.

Contact: P.J. Bookman (Pamela.J.Bookman@nasa.gov), YA-C1, (321) 867-6381

Participating Organization: United Space Alliance (S.M. Schneider, A.M. Foderousky, G. Lebovitz, and A. Beckus)

Process and Human Factors Engineering Technologies

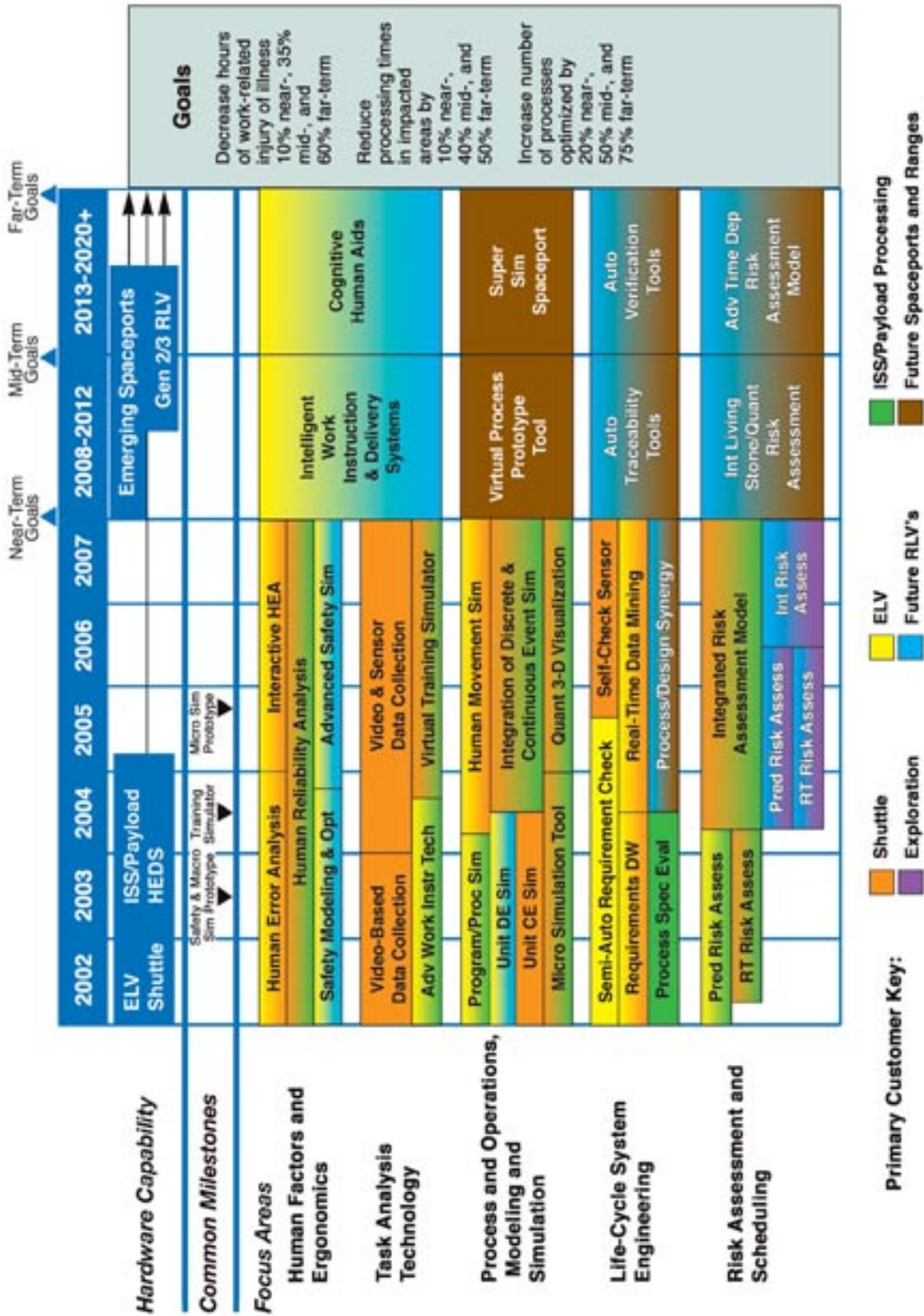
Process and Human Factors Engineering Technologies include research and development of innovative tools and technologies to improve process safety and efficiency. Spaceport and range systems have many unique aspects that require development of advanced process, human factors, and industrial engineering technologies. Process and Human Factors Engineering emphasizes the interfaces among people, processes, and hardware/software systems in specific work environments. Process and Human Factors Engineering focuses on the science of process improvement and optimization of the operational phases of complex systems, including current and future space transportation systems. The overall goal of Process and Human Factors Engineering Technologies is to develop highly effective technologies for designing, implementing, improving, and managing safe and efficient processes, systems, and work environments that can be quickly adapted to the changing needs of current and future spaceports and ranges.

Process and Human Factors Engineering Technologies directly support NASA's goals of achieving safe, reliable, and low-cost space access and exploration. Technology projects develop new concepts, methodologies, processes, and/or systems that advance the state of the art in one or any combination of the following technology focus areas:

- Modeling and Simulation
- Human Factors and Ergonomics
- Task Analysis Technologies
- Process and Operations Analysis
- Life Cycle Systems Engineering Tools
- Scheduling and Risk Assessment Technologies
- Management Support System Technologies

For more information regarding Process and Human Factors Engineering Technologies, please contact Tim Barth (Timothy.S.Barth@nasa.gov), YA-C, (321) 867-6230; or Dr. Gena Baker (Gena.H.Baker@nasa.gov), QA-C, (321) 867-4261.

Process and Human Factors Engineering Technologies Roadmap



Rev. Basic Oct. 2002

A Simulator Study of the KSC Shuttle Landing Facility Air Traffic Control Tower Design

The design of the new Shuttle Landing Facility (SLF) tower was well under way when personnel needed assurance that known problems would be mitigated by the new design. The best way possible was to “experience” the SLF from the new tower – a feat that could easily be accomplished by a high-fidelity, life-sized simulation. Fortunately, this technology was already in place at NASA’s Ames Research Center (ARC). KSC conducted the study in collaboration with Langley Research Center (LaRC) and ARC.

Modeling the KSC airspace required close interaction with the Master Planning Office to acquire specifications of land mass, latitude and longitude of the runway, existing structures, antennas, and other geographical mapping information. In addition, aerial photographs were taken of the terrain to model the topography of the airport and surrounding airspace. This task was accomplished by flying two helicopter missions over the SLF. Operations data were collected next. Through interviews with SLF operations personnel, documented procedures, and direct observations of landings, we gained a good understanding of the way business is done. Finally, all the data collected was modeled in FutureFlight Central – ARC’s 3-D Air Traffic Control (ATC) tower simulator. Its twelve 10-by-10-foot displays provided a 360-degree view of the SLF from the proposed tower, all before breaking ground.



New SLF Air Traffic Control Tower

The goal was to perform a human factors assessment of the proposed tower design. There were two main areas of concern – the cab interior layout and the location of the tower. This study was conducted to ensure that pertinent ergonomics considerations were taken to reduce fatigue while maintaining engagement. Special attention was paid to reducing errors due to misperceived affordances. The chosen site was evaluated to ensure that the controller in the new tower would no longer encounter the glare from the xenon lights at the ends of the runway experienced at the old tower. The height of the tower was also varied in the study to verify that controllers had an unobstructed view of both ends of the runway.

To date, all study objectives have been realized and construction of the new tower is ongoing. One of the biggest achievements is the opportunity SLF personnel had to operate in the tower environment and make recommendations before construction began. The study was completed in FY 2002.

In the future, with the model of KSC now available, a training environment will be developed where controllers at the Dryden Flight Test Facility and other alternate landing sites can practice. Other landing



Control Room Being Placed on Top of New SLF Air Traffic Control Tower by a Crane

operations such as convoy, security, and emergency medical will also benefit from this training environment. This model will be an invaluable resource to maintain the level of proficiency for all support personnel.

Key accomplishments:

- Modeled the KSC airspace.
- Started a library of landing support aircraft and ground vehicles.
- Determined the optimum tower height for unobstructed views of runway, taxiway, and apron.

Key milestones:

- Verified the adequacy of the tower design.
- Created the capability to simulate landing operations.

Contact: Dr. D.M. Elliott (Dawn.Elliott@nasa.gov), QA-D, (321) 867-2269

Participating Organizations: NASA Ames Research Center (Dr. B.G. Kanki and K.L. Christensen) and NASA Langley Research Center (G.W. Lohr)

Assessing Space Shuttle Launch Dates With Advanced Discrete-Event Simulation Technologies

This report documents the efforts to quantitatively assess the likelihood that the NODE-2 Space Shuttle mission (U.S. Core Complete) would launch on February 19, 2004. The Shuttle Program sought a tool for assessing how proposed changes might affect the chances of meeting the NODE-2 launch date and for identifying ways to increase the probability of on-time launch.

In response, a discrete-event simulation model was developed of the Space Shuttle manifest from STS-114 through STS-120 (NODE-2). The model was populated with planned processing times and the order of events from the baseline Space Shuttle manifest. Figure 1 shows the manifest that was modeled. Note that this was the manifest prior to the Columbia accident.

Probability distributions for delays to processing activities and mission durations were developed using empirical data. Such data was also used to assign event probabilities to launch scrubs and diverted landings to California. The model was further populated with these distributions and probabilities, but the occurrence of a fleetwide grounding (for example, because of a hydrogen leak or Orbiter wiring problem) or a major mishap was not factored.

Based on 1,000 replications of the discrete-event simulation model, it was determined that the NODE-2 mission had a .15 probability of launching on February 19, 2004 (see figure 2). The 95-percent confidence interval for that date ranged from .134 to .165. As time progresses, the probability of launching increases, as one would expect. For example, by March 25, 2004, there is greater than .8 probability that launch will have occurred.

Designating holidays as available processing days increased the probability of launch to .245. It was also theorized that the launch probability could be further improved by shifting margins within the manifest. When 6 days of reserve were shifted from the Orbiter Processing Facility to the launch pad for each of the seven Shuttle processing flows, the launch probability for February 19 increased to .31.

The discrete-event simulation model is ready for analysis of future Space Shuttle manifests.

Contacts: G.R. Cates (Grant.R.Cates@nasa.gov), PH-M3, (321) 861-9216; and A.L. Warren, PH-M3, (321) 861-9212

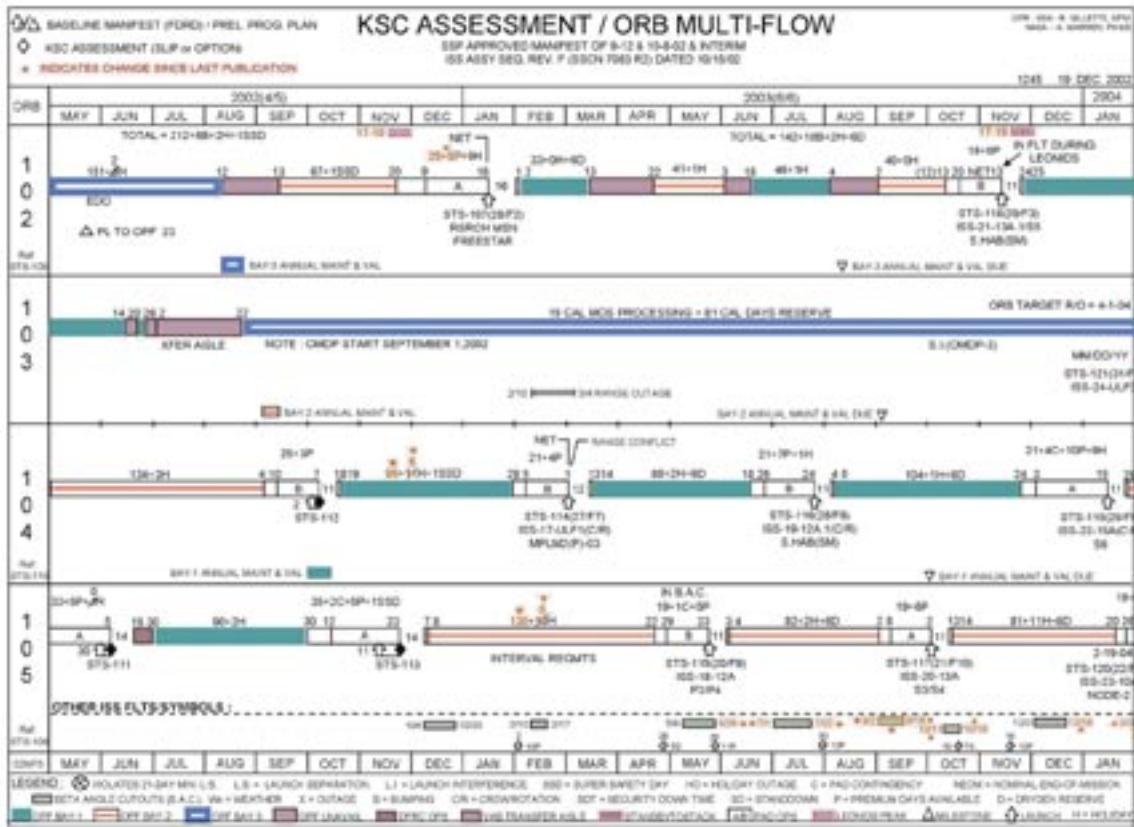


Figure 1. Manifest Used for Discrete-Event Simulation Modeling

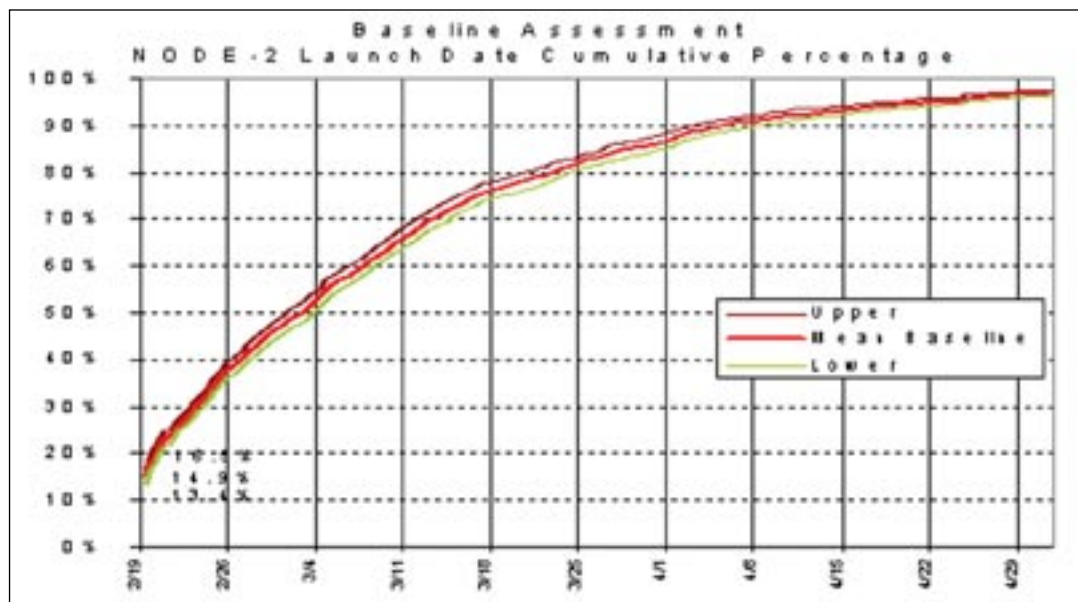


Figure 2. One-Thousand Replications of NODE-2 Mission Discrete-Event Simulation Modeling

Virtual Reality Simulations of Orbiter Temporary-Access Improvements

Various temporary platforms are used to gain access to the Orbiter and Orbiter Maneuvering Subsystem (OMS) pods during preflight processing through the Orbiter Processing Facility (OPF) and the Hypergolic Maintenance Facility (HMF). Temporary platforms consist of narrow, aluminum picboards installed by the High Crew using C-clamps and nylon roping. To improve preflight processing safety and efficiency, a cross-functional team was established to identify picboard temporary installations occurring for every processing flow. United Space Alliance (USA) Industrial Engineering and Shop personnel evaluated the process by comparing factors such as risk reduction, frequency of installation/removal, ease of completion, and project cost. Requests were then prioritized to have the top seven “temporary picboards” replaced with permanent, portable platforms designed to improve safety and access to the Orbiter/OMS pods.

To further enhance design efforts and aid future design reviews, NASA Industrial Engineering for Safety (IES) partnered with USA to simulate concepts in their respective processing environments. The virtual reality (VR) simulations were created by USA KSC Advanced Visualization Environment (KAVE) and Boeing KSC Design Visualization personnel using 3-D models generated by USA Design Engineering. The VR simulations provided the following benefits:

- Provided rapid prototyping without physical field modifications or models.
- Demonstrated feasibility of implementation.
- Provided easily grasped presentation of the concept to laymen (3-D versus 2-D).
- Refined design based on input from individuals with vested interest in the actual use of finished hardware.

Figure 1 shows the current temporary picboard setup for Engineering Support Request (ESR) K16997 (OMS Pod Leading Edge Access When Vertical at the 35-Foot Level) at the HMF east and west cells. The VR simulation depicted deployment, operation, and stowage of the conceptualized platform (figure 2). An avatar, a humanlike form, was also included to simulate and demonstrate a typical technician-to-platform and OMS pod relationship.



Figure 1. Temporary Picboard

The following ESRs were also selected for VR simulation:

- K17000, Elevon Fall Protection Barrier: Simulation included deployment and retraction motions of the proposed railing for OPF 3. An avatar was included in the simulation to demonstrate typical technician-to-railing relationship.
- K16964, Access to Engine Cavity 1: Simulation included installation and removal of the proposed access platform. An avatar was included in the simulation to



Figure 2. VR Simulation

demonstrate typical technician-to-platform relationship.

- K16993, Stinger/Up-Firing Thruster Access at the Y-Web Platform: Simulation suitable for OPFs 1 and 2 depicts deployment, operation, and stowage of the conceptualized platform. A 3-D model of the OMS pod and an avatar were included to show how a human operates and utilizes the conceptualized platform.
- K16994, Access Between the OMS Pod and Vertical Stabilizer: Simulation suitable for OPF 2 conceptualized platform was completed by Boeing.
- K16996, Access to Orbiter Forward Electrical Manifold in OPF 3: Simulation with an avatar included deployment, operation, stowage, and utilization of the conceptualized platform.
- K17001, OMS Pod Access to Flat Side When Vertical at 19-Foot Level (HMF): Simulation included deployment, operation, and stowage of conceptualized platform.

Key accomplishments:

- March 29, 2002: Received approval for Change of Partnering Agreement (CPA).
- May 22, 2002: Completed task list, platform requirements, and tools used.
- July 8, 2002: Created 3-D models for VR simulation development.
- September 18, 2002: Completed NASA deliverables (i.e., video and CDs).
- October 4, 2002: Presented final report to IES.

Key milestones:

- October 25, 2002: Control Configuration Board Directive (CCBD) issued to complete design, fabrication, and installation of K16964 and K16996.
- December 12, 2002: Design completed for K16997.
- February 28, 2003: Partnered fabrication/installation of K16997 and design of K17001 with NASA.

Contact: S.S. Wilkhu (Sandeep.S.Wilkhu@nasa.gov), YA-X, (321) 861-9085

Participating Organizations: KSA MA (J.M. Rozewski); PH-M3-A (D.B. Stambolian and M.M. Groh-Hammond); United Space Alliance (M.A. Sortman, E.J. Deremer-Cook, J.O. Moist, B.A. Lawrence, D.C. Larsen, W.C. Manley, C.J. Brown, B.R. Taylor, G.C. Atwood, B.C. Burns, K.P. Warren, P.A. Thomas, G.A. Farmer, E.E. Brindley, L.E. Hamilton, J.T. Noble, T.R. White, D.J. Luth, R.A. Butler, J. Lackascyck, P.A. Peabody, E.G. Rieck, S.G. Wachowski, and A.M. Rakofsky); and Boeing (R.P. Humeniuk)

Range Process Simulation Tool (RPST)

Robust and practical tools to quantitatively assess the impact of technology insertion on operational performance of space transportation systems are not currently available. In particular, new methods and tools are needed to quantitatively assess the impact of planned technology modernization/technology insertion on the operational performance of current and future spaceports and ranges.

This project designed, developed, and demonstrated the Range Process Simulation Tool (RPST), a decision support tool that facilitates quantitative change impact assessment. The technical approach involves defining change impact assessment requirements, designing and developing RPST software, developing baseline Range process models, defining focused test application scenarios, acquiring test application data, and testing and validating RPST. The RPST is intended for use by Range Planners and Range Technology Portfolio managers to quantitatively assess Range operational performance and assess the impact of Range technology changes/upgrades on operational performance. The RPST is an important first step toward deploying a realistic and robust Range operations change impact assessment capability. RPST also provides key enabling technology for modeling and analyzing future spaceports. The key RPST innovations are a novel, model-based approach for change impact assessment and a component-based, scalable, open-architecture approach that facilitates rapid tailorability and cost-effective deployment to varying spaceport application situations. The main RPST benefits are the ability to accurately and reliably predict impacts of technology changes on space transportation systems and the ability to reduce the Range operational and maintenance costs through improved change management decision support.

Key accomplishments:

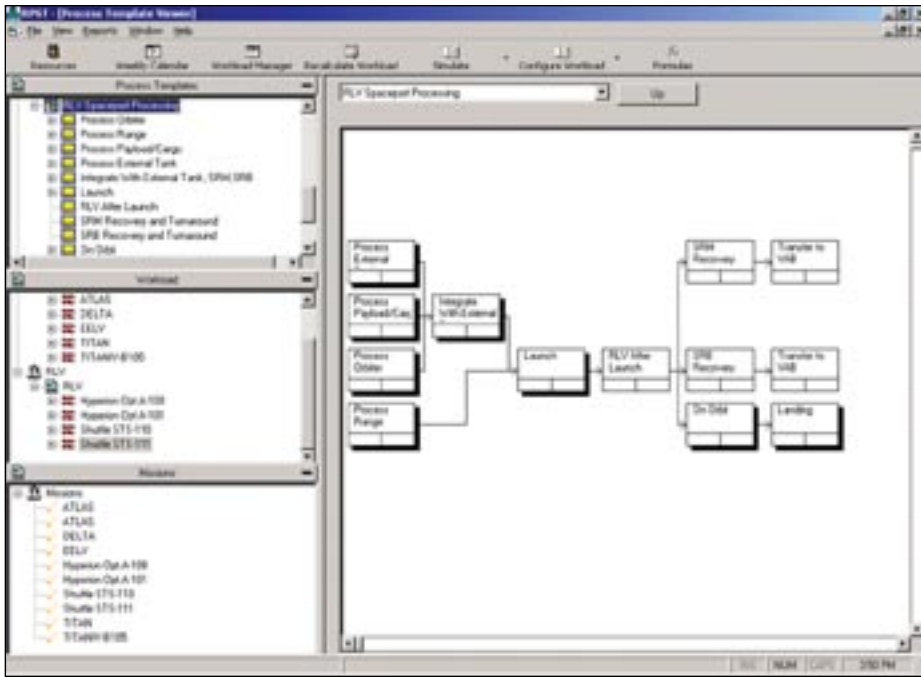
- 2001: Defined RPST requirements. Developed the preliminary RPST prototype. Identified RPST test scenarios. Defined a data collection and software testing approach.
- 2002: Completed a scalable RPST prototype and test scenario data collection. Completed initial RPST testing and validation and Phase II Final Report.

Key milestones:

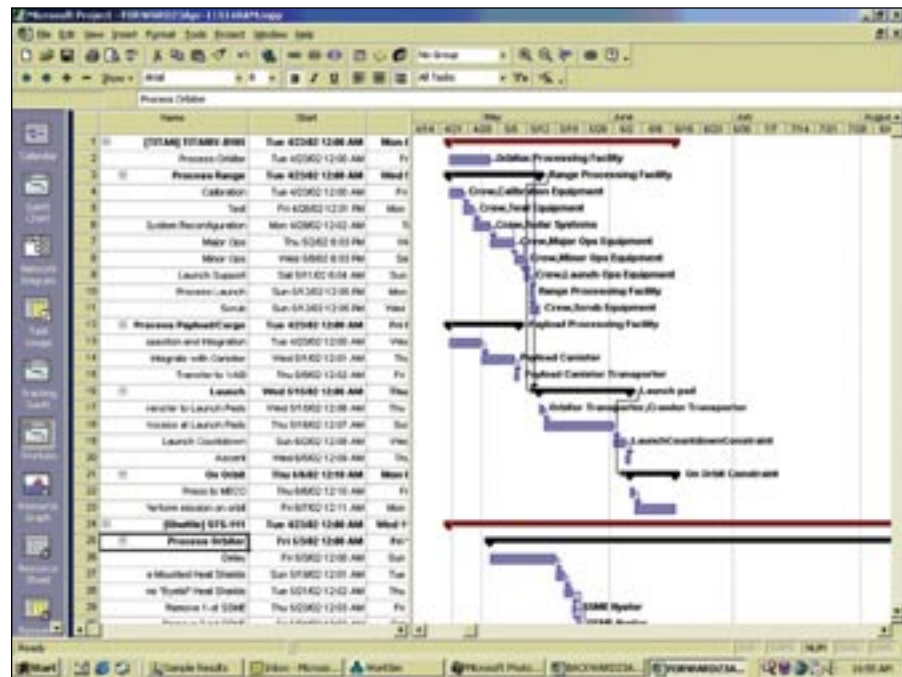
- 2003: Continue RPST testing and validation. Transfer RPST to other NASA, Air Force, and contractor organizations. Generalize RPST for commercial use.

Contacts: T.S. Barth (Timothy.S.Barth@nasa.gov), YA-C, (321) 867-6230; G.D. Phillips, TA-F-A, (321) 494-9167; and W.H. Haase, TA-F-A, (321) 494-9163

Participating Organization: Knowledge Based Systems, Inc. (Dr. P.C. Benjamin and M. Graul)



RPST Reconfigurable Process-Centered Analysis Concept



Example RPST Output

Spaceport Safety Modeling and Optimization

Many current and future NASA programs have invested heavily in simulation models to identify cost and schedule drivers. However, despite safety goals that are orders-of-magnitude more aggressive than cost performance goals, these programs have not invested heavily in simulation models to identify operations and maintenance safety drivers. Existence of a simulation modeling technology gap is part of the reason for the deficiency in safety modeling and optimization tools.

This research project explores the development of revolutionary new tools and technologies for macrolevel safety modeling and optimization. The goal is to develop a discrete-event simulation model that can be applied to any process to determine which tasks, systems, and maintenance actions have the greatest potential for causing personnel injury, hardware damage, and efficiency bottlenecks. With this information, a program can exercise control to mitigate these risk factors and thereby improve its operations. Developing a prototype tool will enhance the capability of preexisting (e.g., Shuttle, Atlas) or new (e.g., Orbital Space Plane) discrete-event simulation models already populated with typical task information (resource requirements and duration) by adding human factors and safety data.

The basic concept involves developing innovative analytical tools to help identify and quantify the critical, high-level safety drivers of a system, process, or product line. NASA/Kennedy Space Center's dual mission of space launch operations and spaceport and range technology development uniquely positions KSC to perform this research. KSC has established technology development capabilities and technology core competencies in industrial engineering. KSC's spacecraft processing facilities provide an ideal testbed for process and human factors engineering technology development.

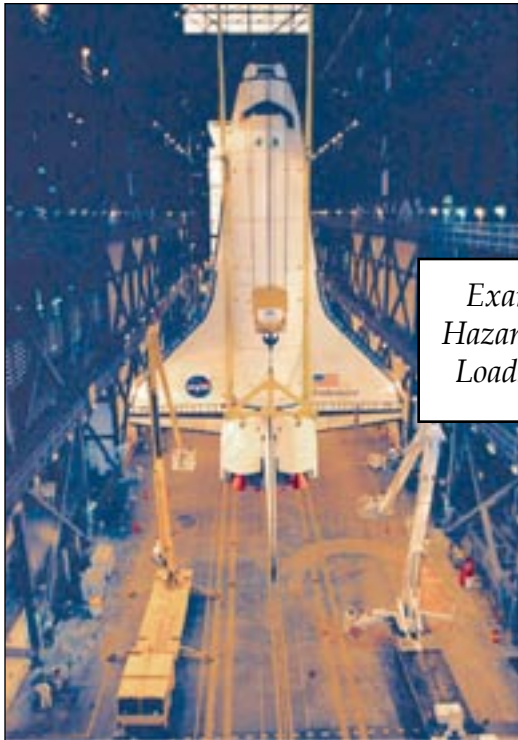
The research involves identifying relevant human factors safety data to accurately simulate the tasks affiliated with a process flow. The human factors safety data sample will include historical data (past health and safety incidents), human factors workforce safety data, human-error risk factors, etc. Developing the prototype tool will show proof of concept that human factors safety data can be combined with scheduling/resource data to more accurately determine safety and efficiency bottlenecks affiliated with a process flow.

Key accomplishments:

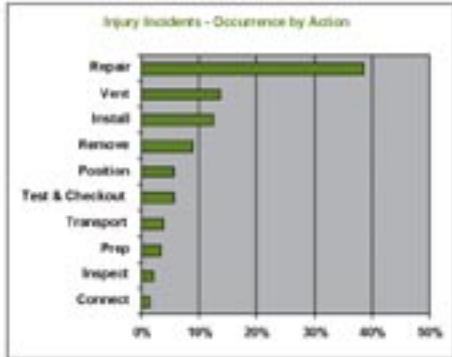
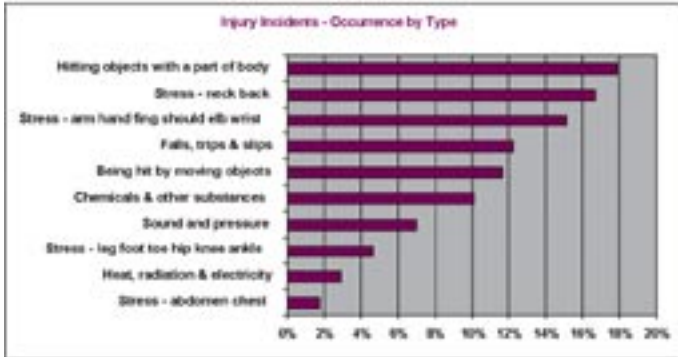
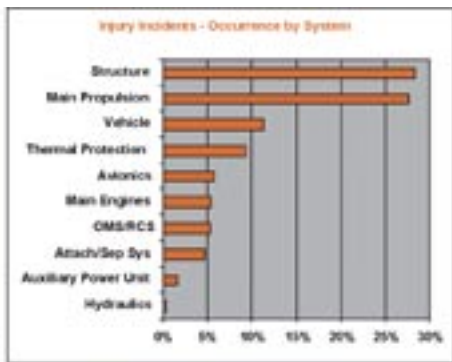
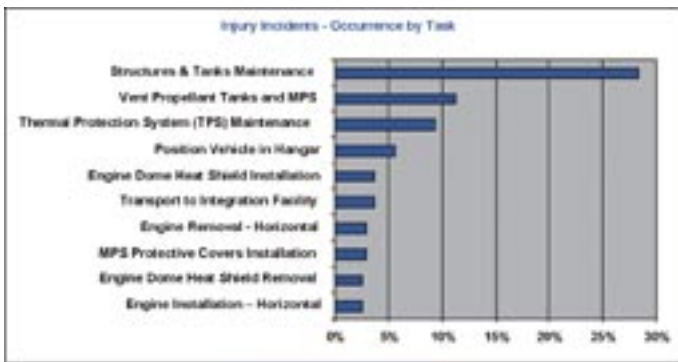
- 2002: Basic research was completed on schedule and within budget to explore the concept of using discrete-event simulation to model and optimize macrolevel safety drivers in spacecraft processing. An initial prototype was developed and tested with KSC data. The research results are encouraging.

Key milestones:

- 2003: Additional refinement of the concept based on testing with current Shuttle, Expendable Launch Vehicle, and potential future Reusable Launch Vehicle spacecraft processing flows. Based on the results of these tests, funding for developing this core enabling technology will be pursued from the Launch Services Program, Space Shuttle Program, and/or the Next-Generation Launch Technologies Program.



Example Spaceport Hazards — Suspended Loads, Heavy Panels



Safety Optimization Model Example Output — Quantification of Macrolevel Safety Drivers

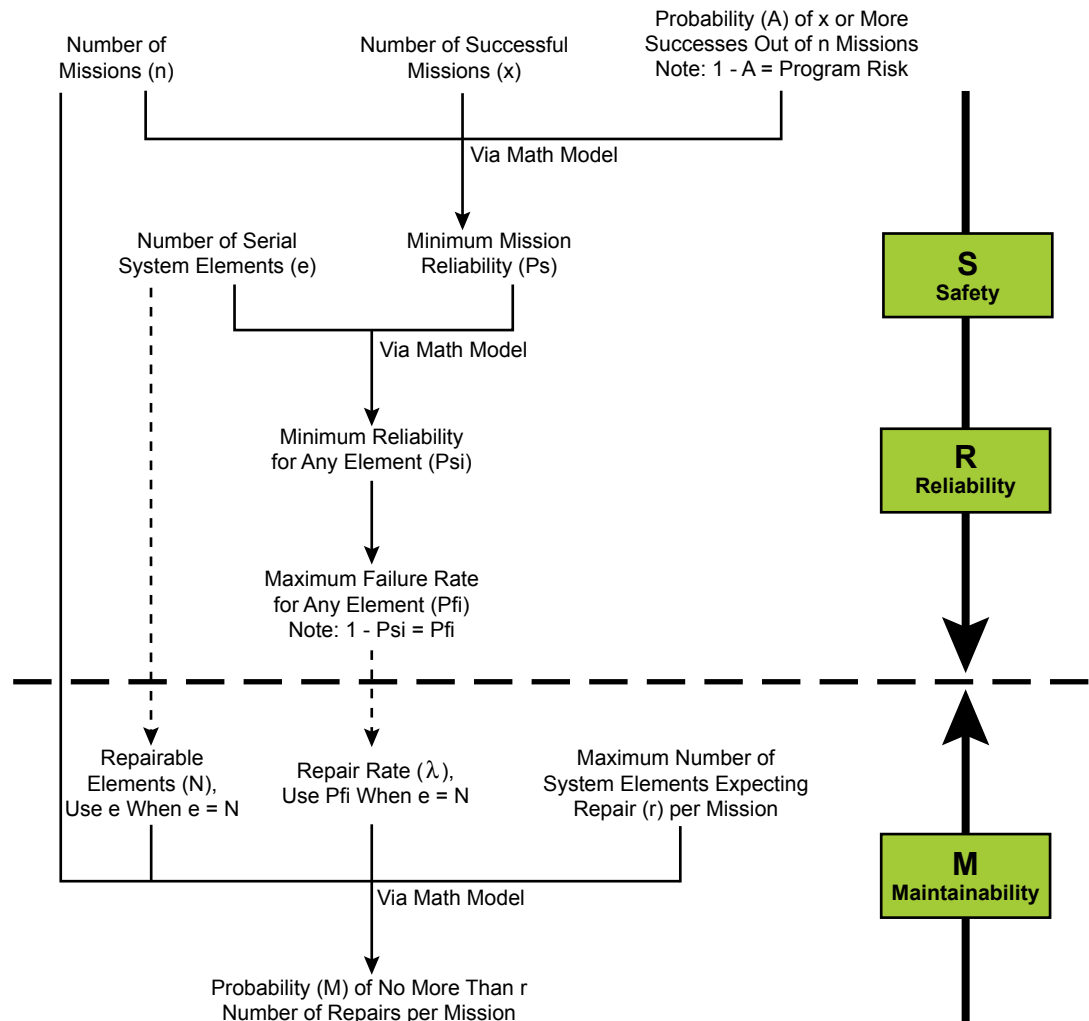
Contact: T.S. Barth (Timothy.S.Barth@nasa.gov), YA-C, (321) 867-6230

Participating Organizations: Lockheed Martin Space Systems Company (K. Brughelli) and Florida Institute of Technology (Dr. D.S. Carstens)

Advanced Process for Developing and Balancing Quantitative Safety, Reliability, and Maintainability Requirements

Because of the interrelationships between system maintainability and reliability, it is important to consider their integrated effects on system-, element-, and component-level design, development, test, and evaluation. Tradeoffs must be evaluated in establishing system reliability and maintainability requirements because of their impact on nonrecurring and recurring costs and the minimization of system life cycle cost. System dependability and responsiveness attributes are both heavily influenced by achieving an effective balance between reliability and maintainability design characteristics. These attributes then drive the safety, cost, and operation of the system.

The process established for developing and balancing quantitative requirements for safety (S), reliability (R), and maintainability (M) derives and integrates Level I requirements and the controls needed to obtain program key objectives for safety and recurring cost (see the figure). Being quantitative, the process conveniently uses common mathematical models. Even though the process is shown as being worked from the top down, it can also be worked from the bottom up. Two illustrations using this process are provided.



A Process for Developing and Balancing the Quantitative S, R, and M Requirements

This process uses three math models: (1) the binomial distribution (greater-than-or-equal-to case), (2) reliability for a series system, and (3) the Poisson distribution (less-than-or-equal-to case). The zero-fail case for the binomial distribution approximates the commonly known exponential distribution. Either model can be used. The binomial distribution was selected for modeling flexibility because it conveniently addresses both the zero-fail and failure cases. The failure case is typically used for nonhuman spacecraft as with missiles.

As the first step of the process, the Systems Engineering designer begins with three inputs: (1) the desired number of missions the program is planning (n); (2) the minimum number of successful missions for the duration of the program (x); and (3) the assurance (A) of obtaining x or more successes out of the n missions. In risk terms, $1 - A$ is the probability or likelihood of not obtaining x or more successes out of n number of attempts or not obtaining the desired level of safety and reliability over the life of the system's program. When these three inputs are used in the binomial distribution, the minimum mission reliability (P_s) is calculated. At this point of the process, the Level I safety requirement has been established.

The second step uses the minimum mission reliability (P_s) and an estimate of the number of serial line replaceable unit (LRU) elements (e) as inputs into the formula for reliability of a series system to calculate minimum element reliability (P_{si}). Maximum element failure rate (P_{fi}) is equal to $1 - P_{si}$. Without considering the maintainability burden, which has a very large influence on recurring cost, including the system's acquisition (fleet) size, the process at this point has established the safety and reliability requirements for the program.

The last step addresses the maintainability parameter, the parameter that provides a control for recurring costs resulting from maintenance and repair. Similar to assurance or program reliability (A), program maintainability (M) is a probability. The probability M is determined by the Poisson distribution and uses the following inputs: (1) the number of missions (n), (2) the number of elements (N , where $e \leq N$), (3) the LRU failure rate (P_{fi} or λ , where $\lambda \leq P_{fi}$), and (4) the maximum number of LRU repairs (r). Technically, M is the probability of

no more than r number of repairs occurring at a particular mission using e number of LRUs with an average failure rate of P_{fi} or λ .

To achieve the desired results in both M and the desired A , adjustments in e , P_{fi} , N , and λ must be made. These values become the enabling requirements to balance and achieve the desired key objectives of the program.

Illustration 1 ($e = N$ case): If $A = 0.99$ for 100 successes out of 100 attempts is required by program management and the current design concept calls for 100 serial systems ($e = 100$), then $P_{fi} \approx 1 \times 10^{-6}$ will satisfy the Assurance requirement. Additionally, if $N = e = 100$ and $P_{fi} = \lambda = 1 \times 10^{-6}$, then the probability of having no more than one repair per mission is 0.999999995. Thus, a Maintainability requirement desired at virtually any level for these management and system conditions is forecasted to be satisfied.

Illustration 2 ($e < N$ case): If $A = 0.99$ for 100 successes out of 100 attempts is required by program management and the current design concept uses 100 serial systems ($e = 100$), then $P_{fi} \approx 1 \times 10^{-6}$ will satisfy the Assurance requirement. Additionally, if each of the 100 serial systems contains an average of 1,000 subelements and each of the 100,000 subelements ($N = 1,000 \times e = 1,000 \times 100 = 100,000$) has an average repair rate of $\lambda = 1 \times 10^{-5}$, then the probability of having no more than one repair per mission is 0.7356 or about 74 percent. In other words, this design concept under a 99-percent level of assurance indicates there is a 26-percent chance of having two or more (up to N) repairs for each of the 100 missions. Thus, if the Maintainability requirement was targeted to be no less than 90 percent, the Maintainability requirement is forecasted not to be satisfied. Adjustments in the design parameters are required.

Contacts: T.C. Adams (Timothy.C.Adams@nasa.gov), IT-D1, (321) 867-2267; and R.E. Rhodes, YA-D4, (321) 867-6298

Human Engineering in Design and Modifications

Space Shuttle processing at KSC is envisioned to continue during the next 20 years and beyond in support of International Space Station activities, satellite repair and/or launches, and other key NASA objectives. During this timeframe, the Space Shuttle and ground support systems and hardware will continue to age. In an effort to maintain operational status, new engineering designs will be required to maintain, modify, upgrade, and incorporate changes.

These design changes require the integration of human engineering principles as described in MIL-STD-1472, Department of Defense Design Criteria Standard Human Engineering, the Department of Transportation/Federal Aviation Administration (DoT/FAA) Human Factors Design Guide, and other related standards and guidelines.

Results of KSC research and human factors investigations demonstrate the occurrence of undesirable events stemming from human-system interactions. These incidents were attributed to human factors issues such as industrial design and workplace design. The combination of these two contributing cause categories represents 28 percent of all contributing causes identified in Shuttle Processing human factors investigations. These contributing causes identified systemic issues that included misapplication or omission of basic human engineering principles identified in accepted standards and guidelines.

To ensure the human engineering principles are implemented by the design entities, training to understand the requirements in these standards is required. The primary training tasks include (1) a human factors awareness class, (2) use of a human factors design review checklist, (3) use of a human factors design quick-reference application guideline, and (4) a training module on the application of human engineering principles into the KSC design processes.

The training module consists of the following four main objectives:

1. Motivate the design community to consider human engineering principles early in the design development and modification stage. (The figures illustrate the practical improvements that can be realized when deliberate and early focus is placed on human engineering principles.)
2. Serve as an intermediate step or bridge between introductory human engineering principles and detailed scientific texts and scholarly research into human engineering principles.
3. Serve as an understandable source of human factors design information.
4. Provide current information on human-oriented design requirements.

Key accomplishments (2001 – 2003):

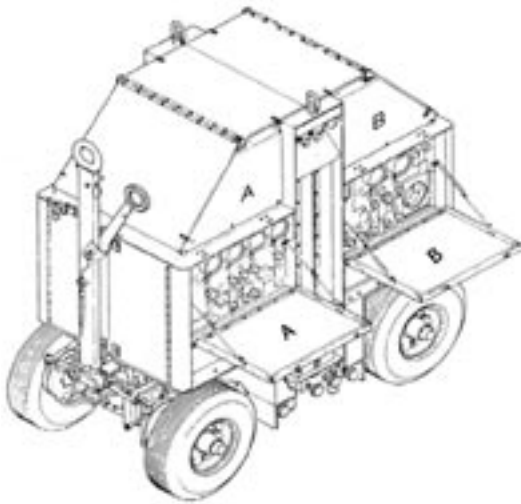
- Developed human factors and MIL-STD-1472 awareness overview.
- Developed the human factors design review checklist and quick-reference guideline.
- Developed the detailed MIL-STD-1472 training module concept.
- Delivered the human factors awareness overview and MIL-STD-1472 familiarization.

Key milestones:

- Complete development of detailed training course material on application of MIL-STD-1472.
- Deliver course to designers, design engineers, and “Train the Trainer.”

Contacts: T.L. O'Brien (Timothy.L.O'Brien@nasa.gov), PH-M3-A, (321) 861-0407; and M.M. Groh-Hammond, PH-M3-A, (321) 861-0572

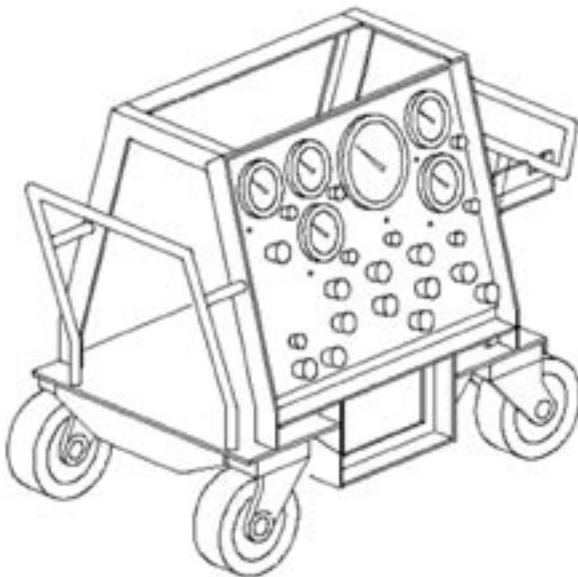
Participating Organization: United Space Alliance (H.W. Riley, Jr., J.R. Ewald, and G.P. Sweeney)



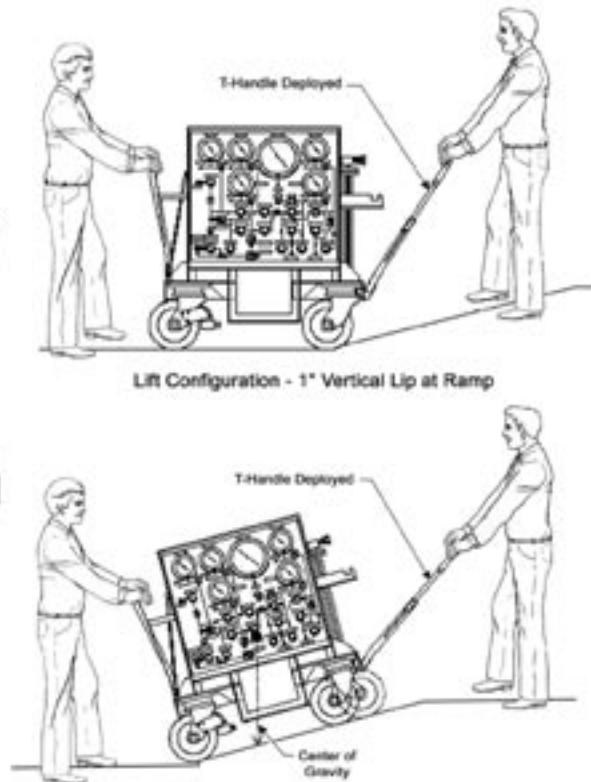
Existing Hydrazine Service Cart Drawing



Technicians Placing Existing 1,500-Pound Cart on MLP Deck



Proposed New Design of Hydrazine Service Cart Incorporating Human Engineering Principles



Task Analysis Technologies

This research effort focused on conducting task analyses on potential bottlenecks and hazardous processes identified at KSC. A task analysis is performed to identify specific improvement opportunities to mitigate or eliminate the risks associated with the potential bottlenecks. Task analysis is a generic term including work methods analysis, process failure modes and effects analysis (PFMEA), and other tools and techniques. The benefits of task analysis to spaceport operations on safety and cost performance have been demonstrated on specific tasks, and KSC seeks to perform many additional detailed task analyses. However, the relative complexity and infrequency of spaceport processing tasks make existing task analysis technologies expensive and time-consuming, require extensive training to adapt to the spaceport environment, and limit their use. This research produced a task analysis tool that enables a human factors analyst to perform a task analysis in days versus weeks because of the automated human-error taxonomies.

The steps involved in the Task Analysis Technologies project are as follows:

- Identification of hazardous tasks performed at KSC: Two current hazardous operations and two hazardous operations that will exist in near-term future operations were selected for analysis. Hazardous tasks are classified as any tasks that have resulted in close calls or actual incidents affecting (safety of personnel, collateral damage, etc.) or future tasks that have the potential to result in close calls or actual incidents.
- Task analysis training: Task analysis training was given to the team members by NASA Headquarters to ensure consistency.
- Performance of task analyses and development of recommendations for improvement: Different task analysis methodologies were performed based on the task being analyzed. A PFMEA was performed on the current operation of the Solid Rocket Booster blast shield installation (figure 1). A PFMEA is a procedure used to analyze the system's processes rather than a specific piece of equipment (NASA Human Factors [HF]-PFMEA Training, 2002). An HF-PFMEA was performed on the current operation of the Cargo Late-Access Task (figure 2). An HF-PFMEA is a systematic method to analyze each task in a process and identify human errors (failures) and the worst-case effect on the system (NASA HF-PFMEA Training, 2002). Both of the current operations analyses resulted in several recommendations to mitigate human error in task performance, enhancing the safety of both technicians and hardware. An HF-PFMEA was also performed for the future operation of the Advanced Technology Development Center LOX Pump Acceptance Test Procedure. This enabled the team to design the work procedure for the LOX Pump Acceptance Test with safety and human error in mind. A general task analysis was performed for the Payload Test and Verification System that resulted in the creation of the ideal process flow for future payloads that mitigates human-error-related risk factors and eliminates bottlenecks associated with current payload processing.
- Identification of technology barriers and challenges to performing better task analyses at KSC: It is important to identify current task analysis barriers and challenges to enable researchers to identify current technology gaps in this area, thereby revealing additional research opportunities. This

segment of the research focused on addressing such issues as how we become more efficient and effective in performing task analyses.

- **Task Analysis Tool Development:** The prototype tool (figure 3) was developed by automating the manual HF-PFMEA process, allowing an analyst to quickly identify actual improvement recommendations. This enables an analysis to be performed within days versus perhaps months, depending on the size of the task being analyzed.

Key accomplishments:

- 2002: Identified hazardous tasks performed at KSC, received task analysis training, conducted task analyses, developed recommendations for improvement, and identified technology barriers and challenges to performing better task analyses at KSC. Completed Task Analysis Tool and reports.

Key milestones:

- 2003: Conduct additional task analyses on KSC operations. Make task analysis tool available to end users.

Contacts: M.M. Groh-Hammond (Marcia.M.GrohHammond@nasa.gov), PH-M3-A, (321) 867-0572; and T.S. Barth, YA-C, (321) 867-6230

Participating Organizations: NASA YA, PH, and QA; Boeing; United Space Alliance; Florida Institute of Technology (Dr. D.S. Carstens); and USTDC



Figure 1. Technician Working on the 500-Pound Solid Rocket Booster Blast Shield Lifting and Installation Process

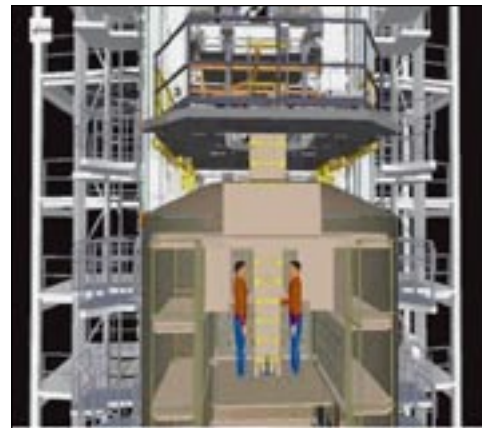


Figure 2. Cargo Late-Access Task Where Cargo Is Placed on the Payload at the Shuttle Launch Pad

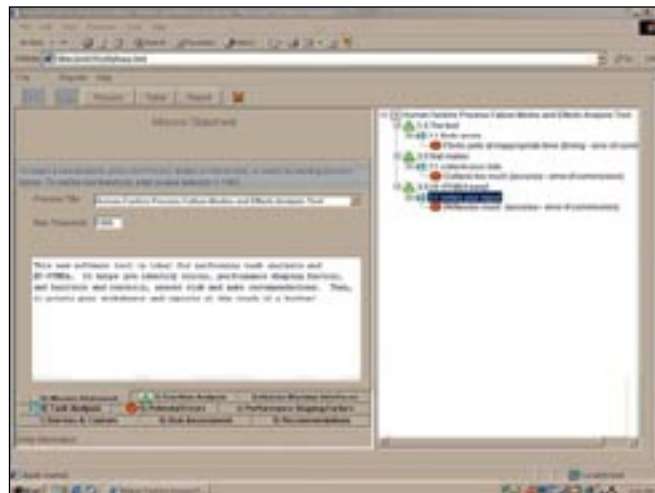


Figure 3. Task Analysis Prototype

Human Factors-Process Failure Modes and Effects Analysis (HF-PFMEA) Software Tool

The goals of HF-PFMEA are to identify factors that contribute to human error and either eliminate them or control them so their effects are manageable or acceptable. To that end, a new technology was sought to enable quick, user-friendly, and affordable HF-PFMEA; task-level analysis focusing on safety and performance issues; and the capability to analyze human factors issues such as health and safety risks. The HF-PFMEA Software Tool was developed to systematically analyze each task in a process to identify potential human errors, their respective worst-case effects on a system, and the factors that increase the likelihood of the human error. The HF-PFMEA Software Tool helps the user identify:

- Potential individual or team human errors.
- Factors contributing to or affecting the potential for human error occurrence.
- Barriers to prevent errors or inhibit the effect of errors.
- Risks associated with the human errors.
- Recommendations to reduce errors or mitigate their effects.

The tool consists of modules that allow the user to create a functional analysis and a hierarchical task analysis. With this information, the software then generates a dataset that interactively relates task action data to potential human errors, factors that can affect those errors, and barriers and controls that can prevent the errors or mitigate their effects. The database functions incorporated into the software develop HF-PFMEAs faster than the time-consuming manual method and create, print, and store reports, including HF-PFMEA tables that contain most of the analysis data. In addition, the tool provides the user a means to perform a risk assessment for the potential errors and their effects by determining the severity of the errors identified, the likelihood of their occurrence, and the probability of error detection prior to consequence. The software even provides suggestions for the development of recommendations to eliminate or reduce the risk of errors.

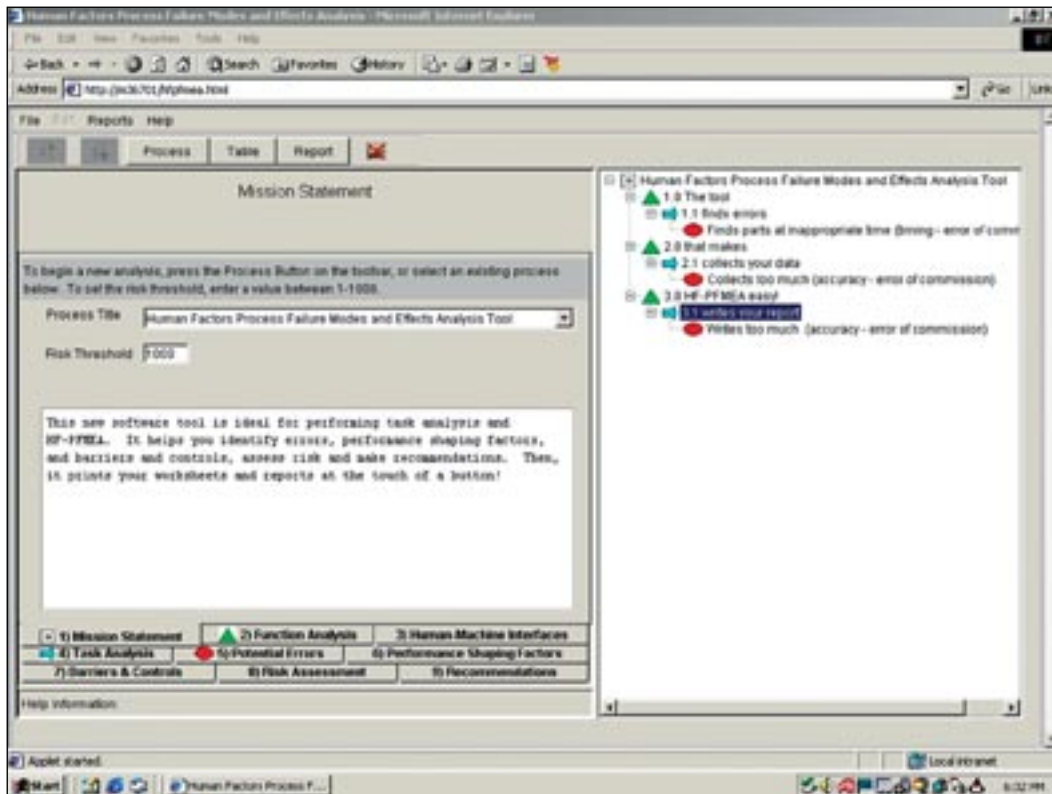
The HF-PFMEA Software Tool was developed from specific HF-PFMEA requirements and HF graphical user interface requirements. The code is written in Visual Basic and constructed with a program called J-Builder. The tool has three main interrelated components: analysis, task tree, and reporting. The application is very dynamic. All data entered and selected by the user is automatically saved and may be edited at any time. It allows users to build their own lists of data and can accept new missions, functions, tasks, subtasks (to any level), errors, performance-shaping factors, and barriers when necessary.

The program itself is written in Java, runs on a PC under the Windows operating environment (98, NT, or 2000), and can be accessed from the Internet. The program is compatible for data exchange with Microsoft Word, Excel, and Access.

The HF-PFMEA Software Tool is flexible enough to analyze a variety of operations, including maintenance. It can also be used to collect data on maintenance processing scenarios from a crew implementation and human factors perspective to enhance human performance and well-being. By doing so, the HF-PFMEA Software Tool promotes increased human capabilities to perform a variety of tasks while maintaining effectiveness and physical health.

Contacts: M.M. Groh-Hammond (Marcia.M.GrohHammond@nasa.gov), PH-M3-A, (321) 861-0572; and Dr. G.H. Baker, QA-C, (321) 867-4261

Participating Organizations: The Boeing Company (M. Philippart, Dr. K. Relvini, W.D. Valentino, and D.F. Baska) and Florida Institute of Technology (Dr. D.S. Carstens)



HF-PFMEA Graphical User Interface

Task Analysis of the Payload Test and Checkout System (PTCS)

In response to a request from the International Space Station Utilization Division, the KSC Process and Human Factors Engineering Working Group (PHFEWG) and The Boeing Company Human Factors/Industrial Engineers (HF/IE) performed a complete task analysis of the Payload Test and Checkout System (PTCS). The purpose was to use the insight gained to develop a Payload Test and Verification System (PTVS) for payload developers (PDs) and investigation developers (IDs) to use to test and check out their racks prior to delivery to KSC. Knowing how the racks are processed at KSC will help PDs develop racks that integrate more smoothly into the handling process. The working group selected the Microgravity Science Glovebox (MSG) rack as the test article and analyzed its progress from conception of requirements and documentation to testing and associated experiments in the PTCS at KSC.

The following seven steps were used to develop the MSG PTCS task analysis flow:

1. Collect and review documentation: general documents, mission-specific documents, lessons learned, mishap reports, and questionnaires and interviews with process owners.
2. Compile tasks and constraints: categorize in three areas - rack planning activities prior to delivery at KSC, customer off-line activities at KSC delivery, and on-line activities after delivery.
3. Design task analysis flow storyboard.
4. Convert storyboard to computer model.
5. Review automated task analysis flow.
6. Revise task analysis flow.
7. Complete deliverables: recommendations, lessons learned, and final report.

The MSG PTCS Task Analysis Flow identified potential and existing bottlenecks, interdependencies between processes and documents, and gaps in the process. The flow describes each task and document and illustrates its potential interaction with other processes by color and pattern. It clarified the complete process and identified the constraints that each participant represents in the process and the steps the hardware needs to follow for efficient end-to-end processing.

The PTCS task analysis of the MSG rack yielded the following recommendations that have broad application for rack processing:

- Require PDs to submit electronic drawings to KSC so equipment interference issues can be identified and prevented.
- Develop standard sets of common test equipment capable of supporting all types of racks to use when PD missions slip and the originally earmarked ground support equipment is obligated to other missions.
- Involve Human Factors/Industrial Engineering specialists at the beginning of design and throughout procedural reviews of processes requiring human-machine interface.



Microgravity Science Glovebox Payload

- Bridge documentation gaps to increase process understanding, eliminate redundant tests, track completion of tasks, and mitigate undocumented open items after turnover.
- Work toward an electronic hardware transfer log to reflect real-time rack configuration.
- Achieve more comprehensive and frequent communication between PDs/IDs and KSC.
- Refine definitions of effects on KSC integration and constraints on KSC operations and strengthen requirements for shipping instructions and for problem reports on late-stowage hardware to reduce open verification items after turnover.

The product of this endeavor was a Payload Test and Verification System that enables PDs and IDs to design and configure racks that integrate better into the Payload Test and Checkout System at KSC. The task flow analysis yielded a tool that can serve as a template for rack processors performing PTCS operations.

Contact: Dr. G.H. Baker (Gena.H.Baker@nasa.gov), QA-C, (321) 867-4261

Participating Organization: The Boeing Company (Dr. K. Relvini and J.G. Posada) and Florida Institute of Technology (Dr. D.S. Carstens)

Toolkit for Enabling Adaptive Modeling and Simulation (TEAMS)

As systems have become more complex, using quantitative operations analysis decision support tools, such as simulation, scheduling, activity-based costing, and optimization, has become increasingly important. These decision support tools, however, have several technical and pragmatic limitations. For example, systems simulation practice is afforded little automated support for the initial analysis, problem solving, and design tasks, which are largely qualitative in nature, and uses too much of both the domain expert's and the simulation analyst's time. It also requires significant investment of time and money to deploy and maintain simulations over extended periods of time and is not widely accepted by decisionmakers. Likewise, there is limited support for activity-based cost (ABC) model development and model maintenance. Similar problems exist for optimization modeling and scheduling. TEAMS targets these technical challenges associated with operations analysis, modeling, simulation, and cost analysis and will provide current and future spaceport designers with a knowledge-based infrastructure for quickly and easily developing, maintaining, and reconfiguring operations analysis models.

This project will design, develop, and demonstrate TEAMS, a decision support tool that promotes the quantitative process analysis of space transportation operations and maintenance. The technical approach involves the following tasks: (1) identify focused TEAMS application areas, (2) develop TEAMS applications, (3) test and validate TEAMS, and (4) generalize TEAMS for commercialization and technology transfer. Anticipated TEAMS products include a validated TEAMS software application, a reconfigurable spaceport operations modeling framework, and a scalable operations analysis knowledge repository. Key innovations include (1) a process-centered approach maximizing reuse of domain knowledge for rapid operations analysis model development; (2) open architecture and distributed plug-and-play architecture allowing for mass customization and rapid deployment; and (3) novel, simulation-based optimization mechanisms facilitating affordable risk minimization through exploration of a large number of spaceport designs.

Key accomplishments:

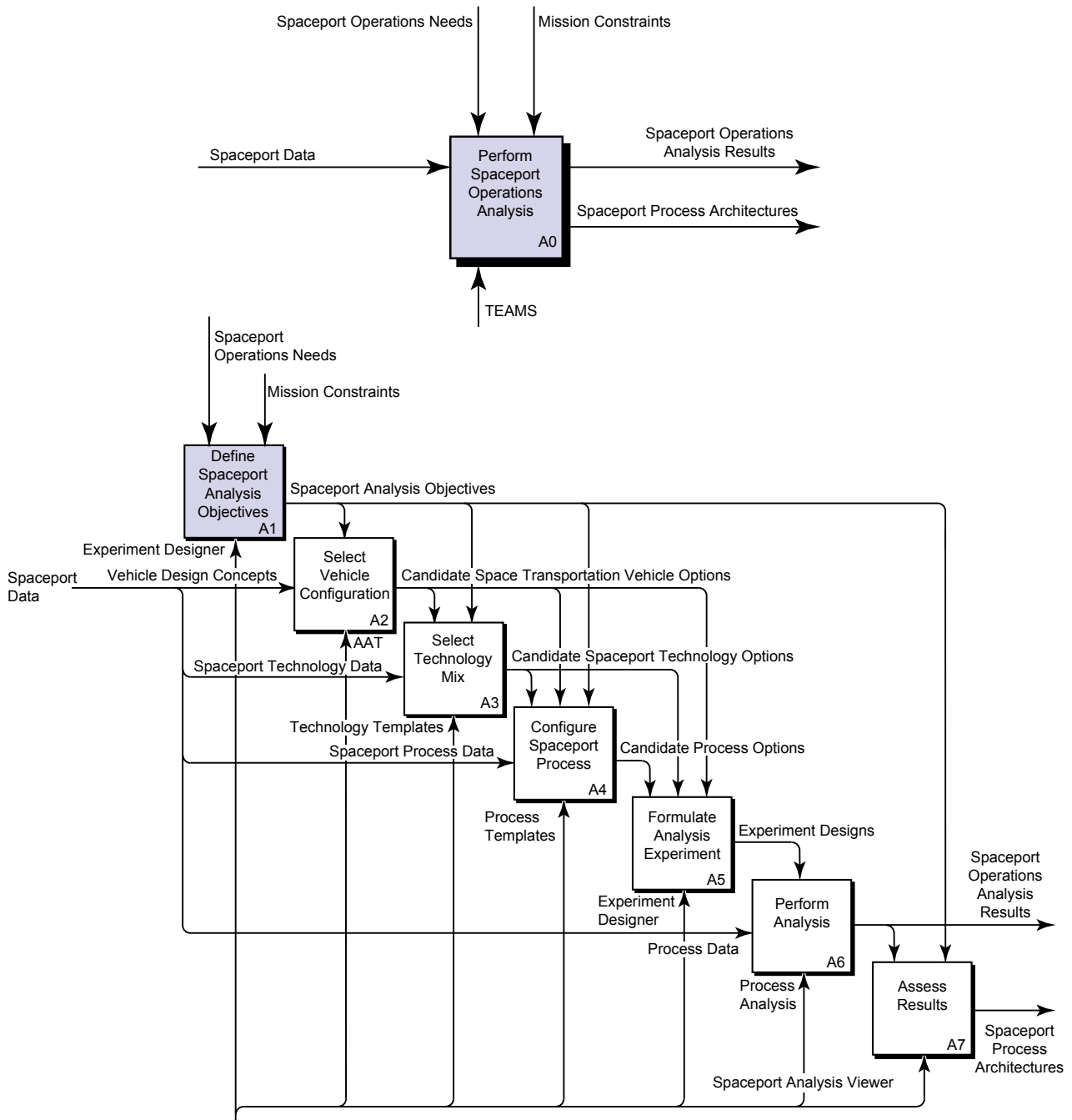
- 2001: Start of Phase I project and definition of TEAMS requirements.
- 2002: Completion of TEAMS prototype software and start of Phase II project.

Key milestones:

- 2003: Enhancement of TEAMS framework, refinement and hardening of TEAMS software, selection of KSC application areas, and development of KSC applications.
- 2004: Refinement of TEAMS framework, completion of TEAMS applications, and technology generalization for commercial use.

Contact: G.R. Rhodeside (Glenn.Rhodeside@nasa.gov), QA-C, (321) 867-7910

Participating Organization: Knowledge Based Systems, Inc. (Dr. P.C. Benjamin)

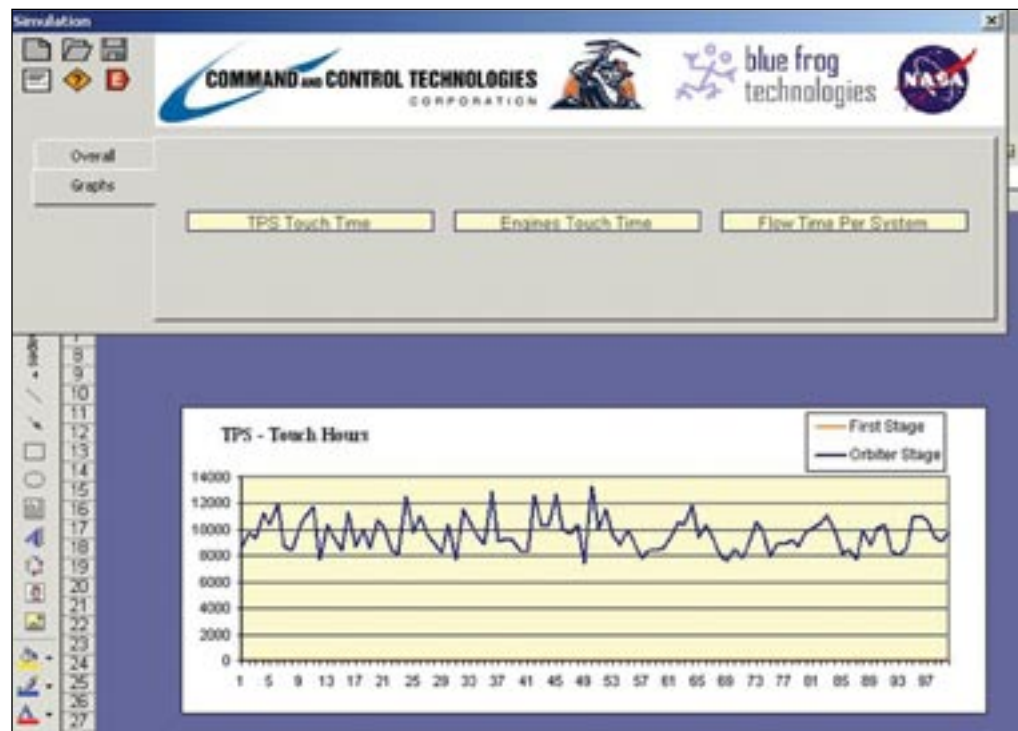


TEAMS Concept of Operation

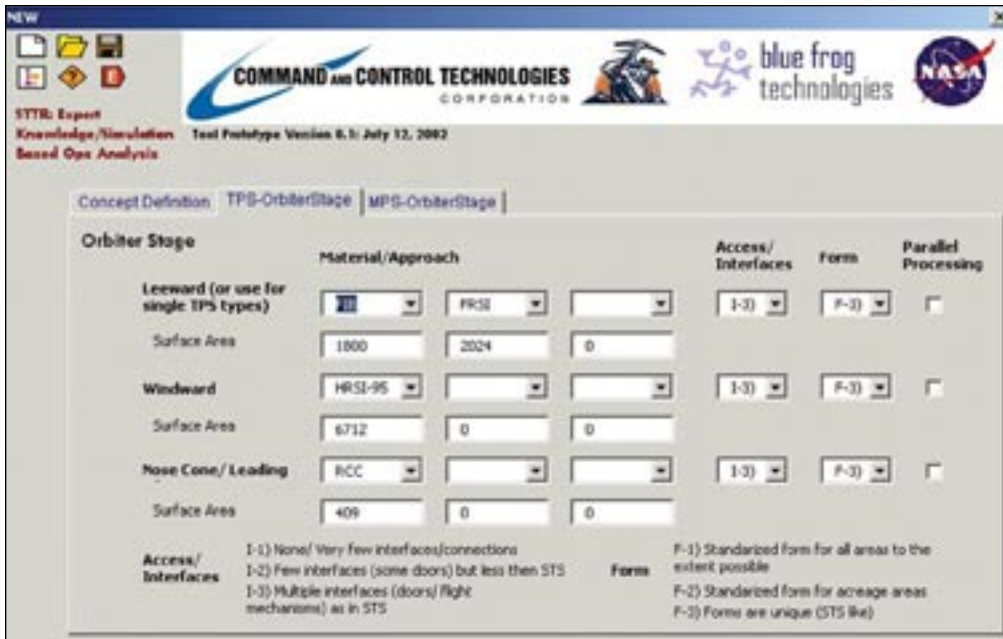
Activity-Based Costing and Simulation for the Operational Assessment of Future Space Transportation Systems

NASA's long-term goals include dramatically reducing the cost of space transportation. Achieving this goal requires innovative technologies and new approaches to vehicle design, development, manufacturing, and operations. Developing models that analyze all life cycle activities for space transportation system concepts, from development to operations, is one of the needed innovations.

Operations models (ground operations or spaceport operations) are an important part of the assessment of new reusable launch system architectures. Models are required to estimate significant portions of the system's life cycle cost, such as recurring and nonrecurring operations costs. Overall ground cycle time is also an important parameter to estimate because this will determine the system's yearly flight-rate capability per set of assets (flight and ground elements). This operational factor of turn-time will affect other up-front, nonrecurring costs, such as the number of vehicles, facilities, and equipment to acquire to meet a desired flight rate per year. Thus, downstream operations that seem far away actually affect up-front and immediate costs as well. The recurring costs and the flight rate are the result of tasks or activities that are required during ground operation, for example, the preparation of a payload for integration with the vehicle. Typically, the cost and task duration assessment of these processes is performed by experienced engineers who



Thermal Protection System (TPS) Labor Hours Estimation by Process Flows



Input Screen for Estimating TPS Labor Based on Such Drivers as Acreage Location, Material, Access/Interfaces, and Design Approach

employ their knowledge of production and operations technology, methods analysis, and engineering economics to predict the probable cost and production time of a product – in this case a ground operation activity.

This research focuses on developing and evaluating new techniques for automating the operations assessment of future space transportation systems by using a combination of activity-based costing and simulation modeling. The approach translates vehicle design parameters into a set of activities and a related process mapped in a domain (operations characteristics of future space vehicle concepts) where there is limited knowledge. This approach is innovative because it will, for the first time, combine activity-based cost modeling (which is known to work well in well-defined environments) with expert knowledge to estimate the activities, cost, and time characterizations associated with proposed space transportation concepts. A critical element of this research is gathering data and expert opinions to develop “knowledge engines” for major vehicle

subsystems. The knowledge engines capture existing and future approaches to a vehicle subsystem and link them to an activity set, time, cost, failure characterizations, and process map.

Key accomplishments:

- Created the initial framework for reusable launch system knowledge engines.
- Developed a preliminary knowledge engine (a spreadsheet, with a graphic user interface) for estimating operations factors, such as labor hours, for the thermal protection systems of future reusable launch systems.
- Documented the results of using activity-based cost modeling for future reusable launch systems.

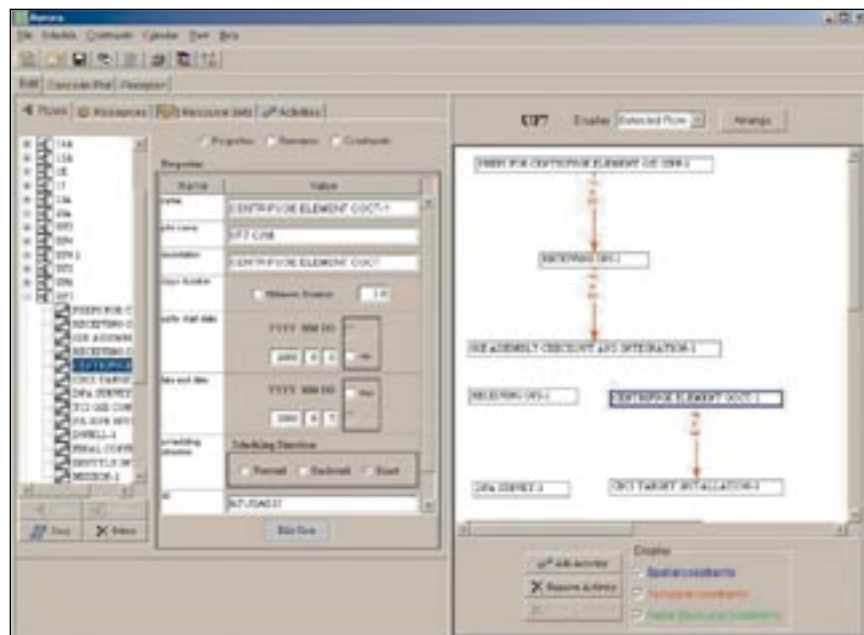
Contact: E.Z. Zapata (Edgar.Zapata-1@nasa.gov), YA-D4-A, (321) 867-6234

Participating Organization: Blue Frog Technologies, Inc. (Dr. A. Ruiz-Torres)

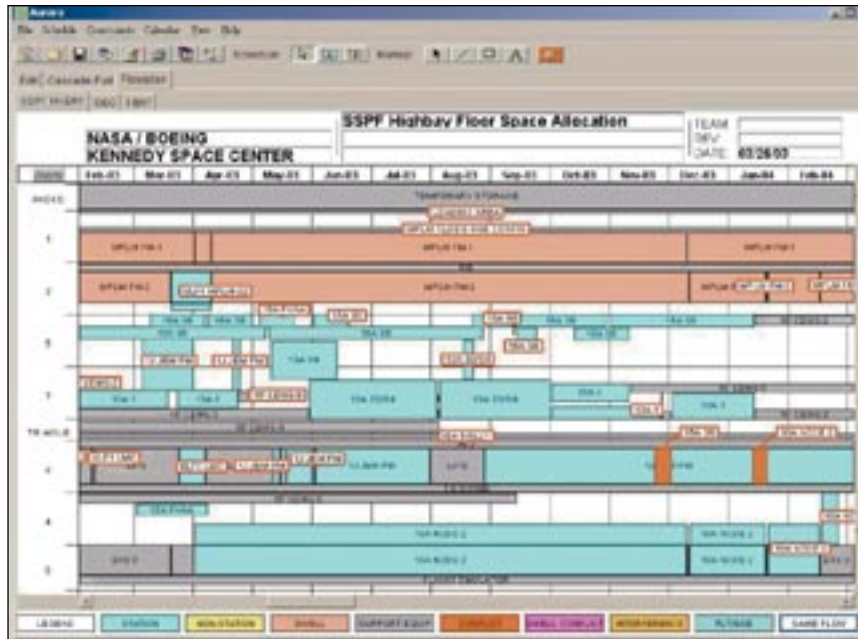
Artificial Intelligence Techniques for Payload and Vehicle Processing Scheduling

Preparing vehicles and payloads for launch is an extremely complex process involving thousands of operations for each mission. Each operation requires a variety of equipment and workspaces. Since several missions are in preparation simultaneously, they all compete for scarce resources. Furthermore, since many of these resources are extremely expensive and limited in number (often operating at or beyond their capacity), optimal assignment and efficient use are critically important. Ground rules, safety requirements, and the unique needs of processing vehicles and payloads destined for space impose additional constraints. These challenges are compounded by the endless changes to the schedule caused by late deliveries, delayed flights, and malfunctioning equipment. To resolve the many conflicts and to predict possible problem areas, operators must use a number of rules of thumb specifying where things should happen, whether they will happen on time, and whether the requested resources are actually necessary.

Although there are a number of commercially available scheduling systems, the degree of domain knowledge required for decisions and the unusual set of constraints make these of limited use. Stottler Henke solved these problems by applying a combination of artificial intelligence (AI) techniques to produce Aurora, a system capable of rapidly completing a near-optimal schedule. Aurora is unusual in that it combines sophisticated scheduling mechanisms with domain knowledge to solve the scheduling problem. Aurora's initial scheduling domain was Space Station Processing Facility (SSPF) scheduling support. This domain includes a number of problems unique to KSC, such as the need to schedule floorspace and maintain certain spatial relationships among the tasks and components. This complexity proved a good test of Aurora's scheduling potential.



Aurora Flow Editing and Display Window



Aurora Floorspace Resource Allocation Display and Editor

Aurora allows a range of informational access, graphically displaying resource usage, floorspace usage, and the spatial relationships among different activities. It also permits the user to create reports that can be analyzed in Excel. Scheduling experts can interactively modify and update the schedule and can request more information about specific scheduling decisions. This allows them to verify the system’s decisions and override them to resolve novel conflicts.

Stottler Henke has taken advantage of Aurora’s built-in flexibility to apply it to such disparate problems as Orbiter scheduling for USA and classroom and teacher scheduling for GE Medical Systems. The version of Aurora in use by KSC will be able to respond to changing scheduling needs in coming years by tracking personnel requirements and temporal relations, in addition to the more static resource requirements that are currently of central concern.

Key accomplishments and milestones:

- June 2001: Proof-of-concept prototype completed.

- April 2002: Released a scheduling system that provides support for spatial requirements and constraints as well as traditional scheduling needs for SSPF floorspace scheduling.
- December 2002: Released a refined version of Aurora with expanded support for the SSPF scheduling domain.
- March 2003: Completed development of temporally oriented Aurora for Orbiter scheduling.
- May 2003: Delivered completed Aurora scheduling system, featuring spatial and standard resource displays, temporal and resource-based scheduling, and import/export capabilities for interfacing with other planning systems.

Contact: S. Bigos (Steven.Bigos-1@nasa.gov), UB-C4, (321) 867-6166

Participating Organization: Stottler Henke Associates, Inc. (R. Stottler)

Design Root-Cause Analysis Knowledge Base

In pursuing NASA's goal to advance space transportation for anyone, anytime, and anywhere, knowledge of specific design shortfalls is greatly needed to more effectively develop launch vehicles and advanced spaceports. Knowing where the processing time is spent and where the operational infrastructure costs are incurred is a critical need in modeling the operations and the infrastructure of future concepts for both flight and ground systems. Acquiring information on specific operations functions and infrastructure elements will help in developing higher-fidelity operations models, as well as more effective flight and ground systems designs that are also more affordable, more responsive, and safer.

The Next-Generation Launch Technologies (NGLT) program is investing in the development of a design root-cause knowledge base to help meet this need. The design Root-Cause Analysis (RCA) Knowledge Base is made up of thousands of Space Shuttle maintenance tasks organized into three generic operations classes: operations modules, functions, and subfunctions. Further, the maintenance tasks are classified by the generic design discipline (flight and ground) that generates the work. In this manner, top-level knowledge of the experience gained by the Shuttle Program can be extracted to determine where the overall work content is concentrated. For example, the overall amount of unplanned troubleshooting and repair activity, versus servicing, versus assembly and handling, versus inspections and testing, can be determined and quantified. The RCA Knowledge Base then expands on this information by organizing design cause statements associated with why a specific operations subfunction exists, or why it takes a certain amount of time to perform. Currently (April 2003) the RCA Knowledge Base contains over 200 such cause statements. Associated with each design cause statement is at least one operational design need statement. It is expected that designers and technologists will quickly discover high-priority needs and more effectively develop new technologies and systems for the space transportation operator from a database of such statements.

Ongoing research and development include the following:

- RCA Knowledge Base support to development of the Schedule and Activity Generator/Estimator (SAGE). Specifically, identification of key system characteristics for SAGE concept definition and input, as well as report generation.
- RCA Knowledge Base support to a Design for Operations (D4Ops) space transportation architecture characteristics effort.

Key accomplishments:

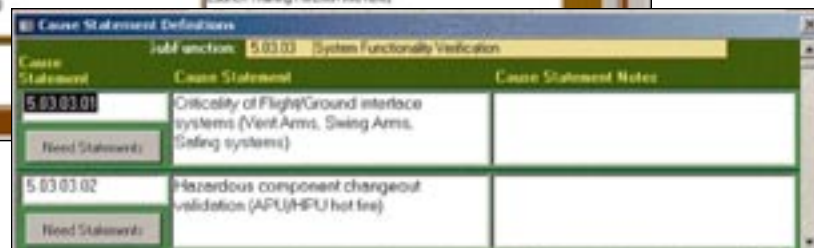
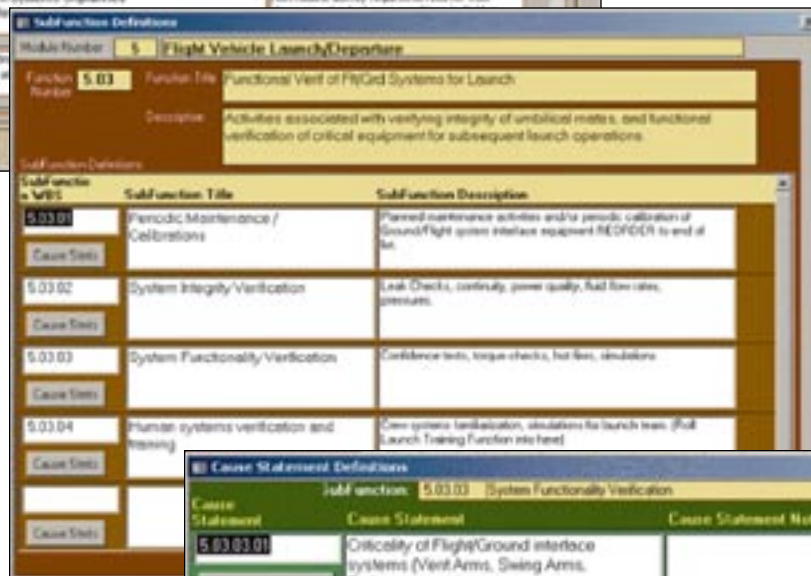
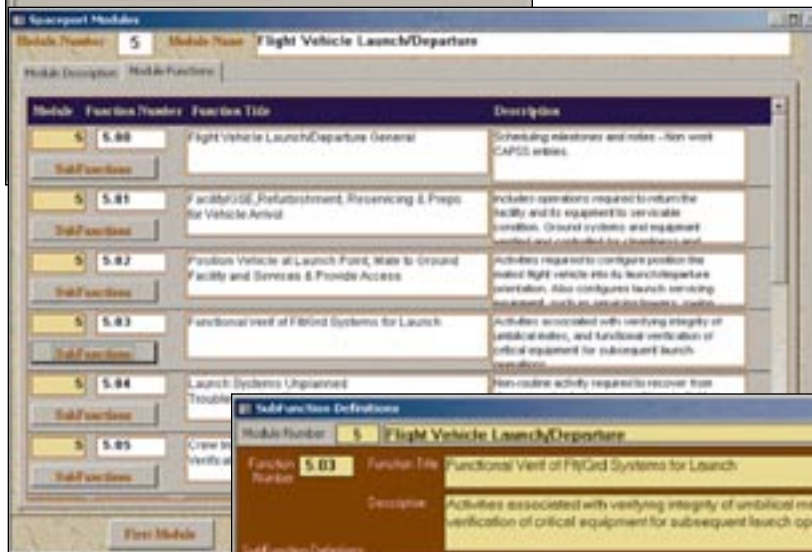
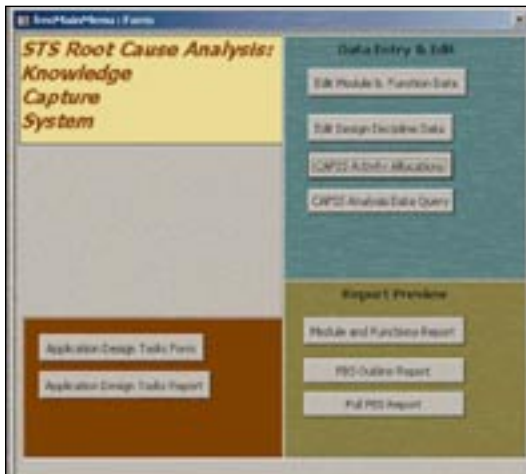
- Captured actual operations for eight Space Shuttle on-vehicle direct maintenance actions.
- Created an operations Functional Breakdown Structure (FBS) to three levels.
- Defined a set of generic design disciplines.
- Assigned a set of operations functions, subfunctions, and design disciplines for each maintenance task in a complete Space Shuttle processing flow (Space Shuttle Atlantis/STS-81).
- Developed algorithms for automatically mapping STS-81 applied knowledge to seven other processing flows.
- Analyzed and extracted information from the STS-81 analysis for the NGLT program and ongoing technology work in the field of space transportation operations modeling.

Key milestones:

- Completion of RCA Knowledge Base design.
- Completion of report generation capability.
- Engineering release of RCA Knowledge Base to the Space Transportation Information Network (STIN) for use by NASA and its NGLT contractors.

Contact: C.M. McCleskey (Carey.M.McCleskey@nasa.gov), YA-D4-A, (321) 867-6370

Participating Organizations: Lockheed Martin Space Systems (K.A. Ingoldsby) and USTDC (D.E. Johnson, Jr.)



Design Root-Cause Analysis Knowledge Base

Project Management Integration System (PMIS)

A commonly lacking yet critical component of successful application of project management concepts is the seamless integration of project management tools being used throughout the organization. Development and implementation of an integrated framework and system architecture for project management tools will result in optimized planning, cost estimating, risk management, and project control. NASA and KSC have designed a thorough system of well-defined policies and procedures based on traditional project management techniques. Investigation and analysis of project management strategies revealed that many different software applications are being used as project management tools. However, there was no integrated on-line system to assist project managers to efficiently use these applications to complete compliance requirements. Such a system would allow project teams to collaborate on project responsibilities while permitting project managers to spend more time managing project requirements rather than continually learning new project management tools. Therefore, the purpose of this work was to develop a framework for integrating project management tools used at KSC so they might be easily accessed and efficiently used from a central system architecture, administered through KSC's Systems Management Office (SMO). An additional goal of the project management framework was to reveal proven principles that establish the basis for project management success while integrating those principles to form a reliable system.

Prior to deciding on a particular project management tool, organizations must carefully evaluate the reliability of internal policies, procedures, and practices. Thus, initial developmental tasks for this architecture included investigating applicable policies, procedures, tools, and techniques. While many project management tools and techniques are integrated into project management software applications, many are also developed using other software such as Microsoft Access, Excel, Outlook, PowerPoint, and Word. The advantage of project management software is that it generally provides tools such as work breakdown structure (WBS), task list, Gantt chart, critical path analysis, and earned value analysis that help project managers and project team members accomplish scope, time, cost, and quality management. However, according to leading project management experts, quality is actually the fundamental goal of project success in accomplishing efficient integration of cost and schedule. Investigation of quality issues revealed that KSC SMO uses a diverse network of rationale-based metrics with specific goals developed around its mission to control quality.

Project management methodologies commonly used by industry experts were used to design the proposed interactive system. A well-integrated project management system with quick and easy Internet access was one of the primary objectives of PMIS. We used the experience of industry and academia to create an architecture for integrating the project management software applications in use at KSC. Research and analysis revealed that project managers at NASA KSC need the capability to (1) use project management software and systems without being an expert in the framework of the project management system and how it works, (2) access the project management system at any time from any place while maintaining organizational security, and (3) instantaneously and automatically notify team members that task requirements or action items have changed.

Furthermore, the desired architecture should eliminate redundancy by automating project team tasks to allow the transfer of data from forms, templates, and other required documentation into a knowledge base for integrated and distributed project management. Review of both Government and private-sector experiences resulted in a list of desirable

features for integrated project management in a Web-based environment that includes (1) simple, powerful processes, (2) form-based interfaces for easy connection to existing data sources and input/modification by nonproject management personnel, (3) well-organized, consistent data, (4) quick-scan dashboards, (5) in-depth reports, and (6) consistent and reliable security.

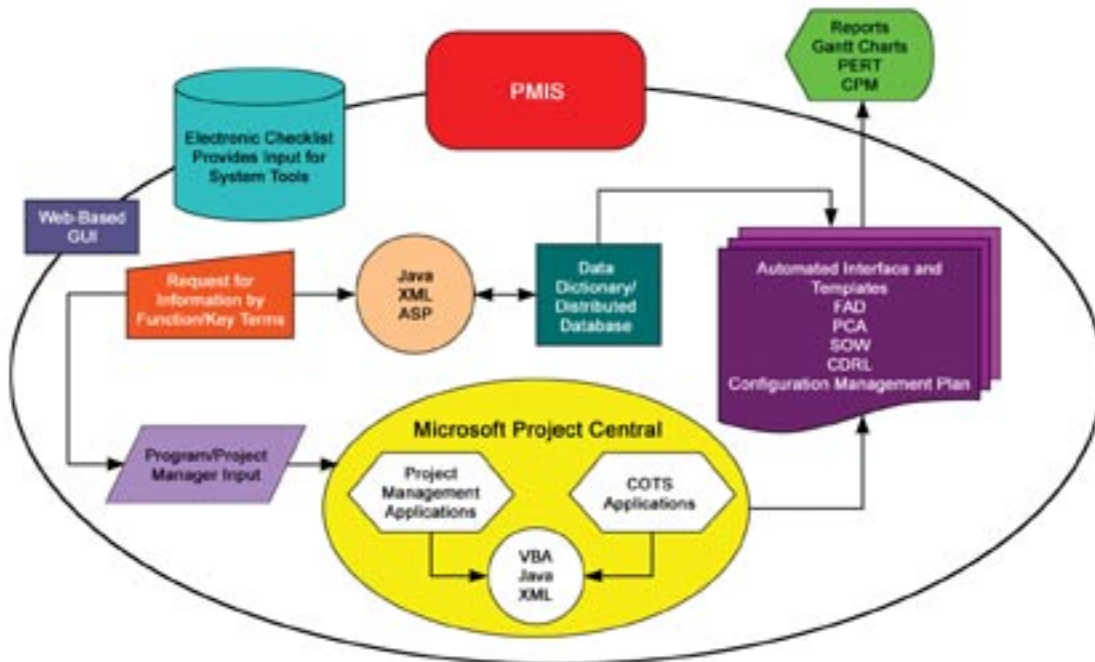
For large, complex organizations such as KSC, a system based on distributed project management concepts is the most feasible of the methods reviewed. Distributed project management offers the most versatile and effective solution to integration and automation for project management. This technology, while continuing to advance as a result of research and development in varied work environments, has shown significant benefits.

The proposed PMIS may be deployed using a Web-based graphical interface to integrate commercial off-the-shelf (COTS) software, application service provider (ASP) software, custom-designed software, or a combination

of these. The figure shows the proposed architecture of such an application. Review of the literature shows that Microsoft Project's custom programming language, Visual Basic for Applications (VBA), can be used to automate recurrent tasks and interact with other Windows applications. Java, XML, and VBA programming tools combine effectively to integrate these components into an interactive, on-line, distributed project management system. Unfortunately, research revealed that one of the most prevalent problems faced by organizations attempting to institute more efficient systems is the lack of implementation. Development of a KSC-wide project group to complete a prototype based on the PMIS architecture will facilitate deployment of the proposed solution.

Contact: T.E. Fredrickson (Tracey.E.Fredrickson@nasa.gov), QA-C, (321) 867-2770

Participating Organization: Miles College (C.D. Butler)



Proposed Project Management Integration System Architecture

Portfolio Analysis Tool (PAT)

A key characteristic distinguishing successful enterprises of the next millennium will be the ability to respond quickly, proactively, and aggressively to unpredictable change. Robust methods and tools to facilitate change management are therefore essential for the modern enterprise. This project targets the following key technology gaps and challenges associated with strategic change management:

- Lack of scientific methods for strategic change management.
- Lack of information-integrated software tools to support the change management process.
- Lack of knowledge management mechanisms that capture, store, and leverage corporate knowledge for strategic planning and control.

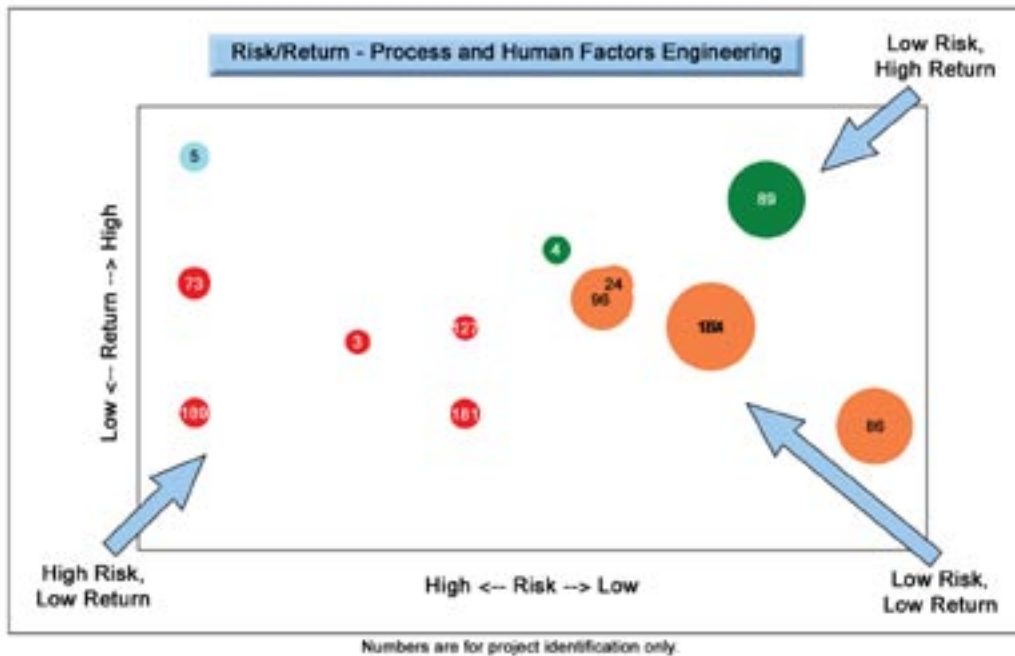
This project developed and demonstrated a Portfolio Analysis Tool (PAT), a Web-based software tool that facilitates strategic change management. Key functional requirements addressed by PAT include the following:

- Provide technology investment decision information: PAT provides decision-making information to facilitate strategic planning.
- Facilitate identification of technology gaps: A direct result of the portfolio analysis is to assist the precise identification of technology gaps.
- Promote technology roadmap development: The portfolio gap analysis results provide information to construct a time-phased technology development approach/roadmap.
- Facilitate decision making over distributed teams: PAT facilitates the collaborative, distributed decision-making processes associated with strategic planning and change management.

Intended PAT end users are strategic planners and technology portfolio managers. The PAT architecture includes a database server that provides storage of the information managed by PAT. PAT also provides a Web-based user interface that facilitates distributed capture of key information required to perform portfolio analysis. A central function of PAT is to facilitate sound project/technology investment decisionmaking as part of strategic change management. Different types of outputs and visualizations are generated by PAT to accomplish this function, including (1) Risk-Return Portfolio Analysis, (2) Gap Analysis, (3) Sensitivity Analysis, (4) Roadmap Generation,



Portfolio Analysis Tool Functional Architecture



Example Risk Return Analysis Output

and (4) On-Demand Reports. Key innovations include novel adaptation and application of portfolio theory for strategic decision support and a structured, knowledge-based method for strategic planning and change management.

Key accomplishments:

- 2001: Developed a prototype Web-based portfolio analysis tool. Completed change management method and initial test data collection and tool testing.
- 2002: Completed Phase II Final Report and PAT testing and validation. Completed PAT deployment at KSC and end-user training.

Key milestones:

- 2003: Expand PAT user base at KSC. Develop spreadsheet representations for Technology roadmapping. Refine PAT – roadmap linkages. Transfer technology to other NASA organizations and the U.S. Air Force.

Contacts: T.S. Barth (Timothy.S.Barth@nasa.gov), YA-C, (321) 867-6230; and E.Z. Zapata, YA-D4-A, (321) 867-6234

Participating Organization: Knowledge Based Systems, Inc. (Dr. P.C. Benjamin)

Biological Sciences

The Biological Sciences program at KSC conducts research and technology development in four basic life sciences areas:

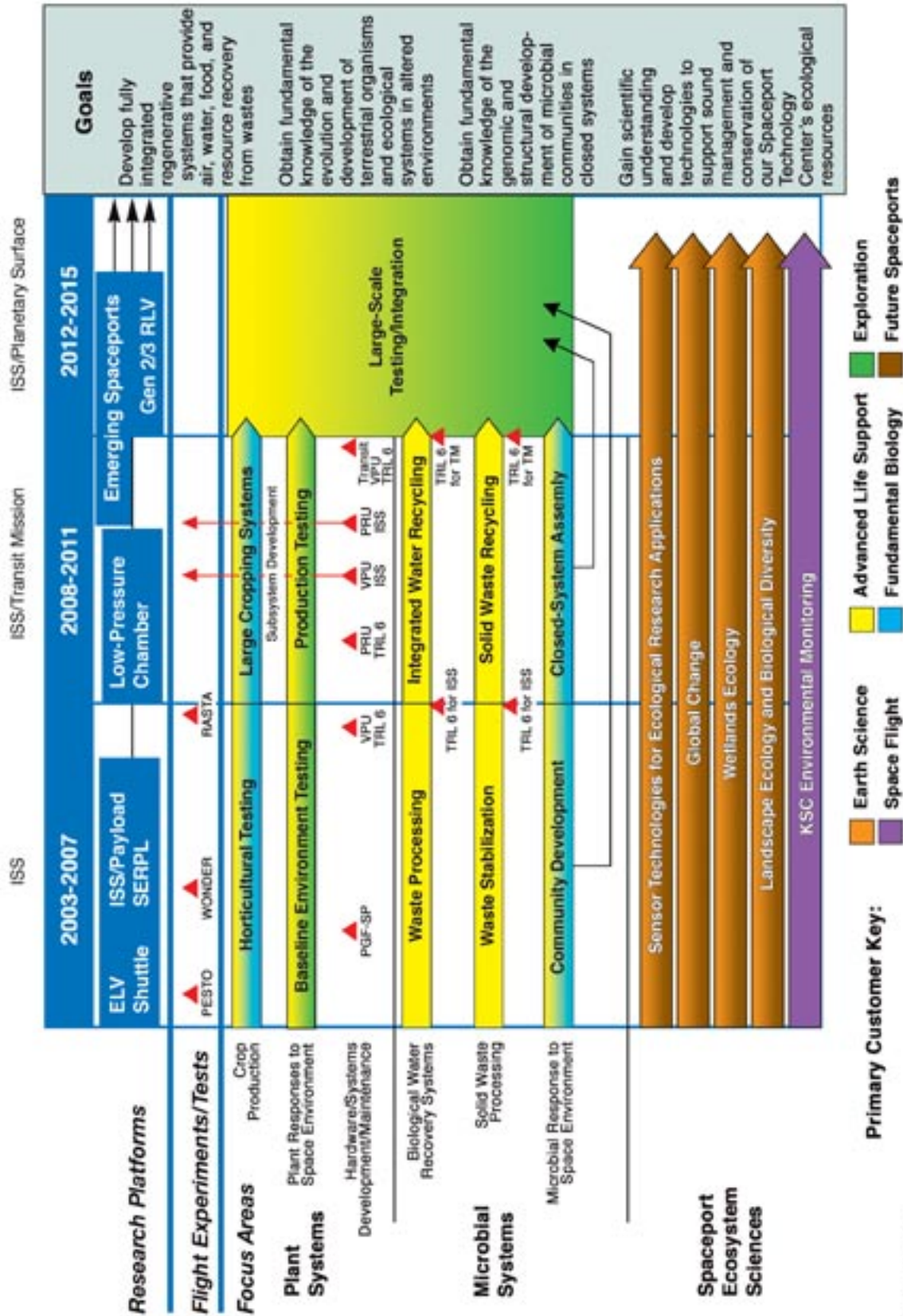
- Bioregenerative life support in closed biological systems.
- Metabolic response of plants to the space environment.
- Plant flight hardware development, design, construction, and validation.
- Application of results from this research and technology development to the management of agricultural and natural ecosystems on Earth.

Efforts in bioregenerative life support systems research for over 10 years have focused on crop growth and development with the primary emphasis on biomass production under closed conditions. In recent years, the focus has shifted toward the potential use of plants in recycling solid and liquid waste. Another goal for these studies was to determine the stability of microbial communities associated with the plant and recycling systems. The Biological Sciences program initiated significant efforts in understanding photosynthetic processes under spaceflight conditions. A series of studies was designed and initiated to determine the response of higher plants to microgravity and to determine if they would remain viable and useful components of a life support system. These experiments required adding new plant flight hardware and refurbishing older flight hardware that had been used for previous plant experiments. Plant flight hardware technology development efforts include investigating the use of light-emitting diodes and their effects on plant growth, using porous tube systems to deliver water and nutrients to the roots of plants, and developing both physical and biological sensors that could give a more complete understanding of the hardware operation and environment during spaceflight testing.

Studies to determine the stability of microbial communities with physiological profiling continued during the past year, and the use of molecular approaches to characterize these communities was expanded. Molecular and biological technologies that assist in determining the stability and functionality of microbial communities are essential for managing biological systems during long-duration spaceflights. The ultimate goal is to test the capacity of microorganisms to recycle solid and liquid wastes, including graywater and trash. The successful demonstration of bioregenerative life support technologies and the ability to support them in the spaceflight environment will permit NASA to estimate the resources needed to design, construct, and test life support systems for future missions. Ultimately, biological life support systems will be required to sustain autonomous human colonies in space. Understanding and optimizing both the biomass production and biological waste recycling concepts for life support, along with their associated reliabilities and costs, will be essential for future exploration of space.

For more information regarding Biological Sciences, please contact C.D. Quincy (Charles.D.Quincy@nasa.gov), YA-E4, (321) 867-8383; or D.W. Chamberland (Dennis.W.Chamberland@nasa.gov), YA-E4-B, (321) 867-6970.

Biological Sciences Roadmap



Rev. A, Aug. 2003

Demonstration of a Porous Tube Hydroponic System To Control Plant Moisture and Growth

Many areas of plant research can benefit from developing technologies to precisely control, alter, and monitor plant growth and physiological processes. The ideal test plant growth system would allow for control of (1) the spectral (the particular wavelengths of light) quality and intensity of the light environment, (2) the water and nutrient contact with the root system, (3) the temperature and humidity of the growth area, and (4) the concentration of gases in the atmosphere. Such a system would provide tremendous opportunities for plant research in areas such as remote sensing of plant stress, toxicology testing, tissue culture of plants, and plant physiology. Today's high-quality plant growth chambers can be used to address the atmospheric gas, temperature, and humidity concerns. Advances in lighting technology, such as light-pipe, light-emitting diodes, and other innovative light sources, are addressing issues associated with fine-control lighting. By accurately controlling the plant growth environment to minimize variance resulting from environmental responses, we can begin to accurately define treatment effects and minimum detectable differences in physiological characteristics as they relate to sampling strategies and procedures. In our work, we are exploring the possibility of creating a reliable and simple system for controlling the water and nutrients that are available to plant roots. This is the one characteristic of plant growth chambers that has not been adequately controlled. Specifically, we are evaluating configurations of the Porous Tube Plant Nutrient Delivery System (PTPNDS) (figure 1) as well assessing our ability to detect plant responses to the various configurations.

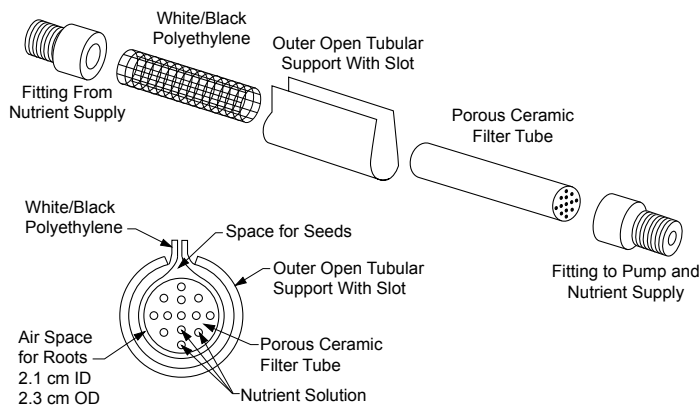


Figure 1. A Diagram of the Porous Tube Component of the PTPNDS

Eight porous ceramic tubes, 2 centimeters (cm) in diameter and 80 cm in length, were placed on each of three laboratory carts. These tubes were connected to a standpipe using a manifold at the upstream end and a peristaltic pump at the downstream end. The nutrient solution for each cart was contained in an 80-liter cooler and pumped to the standpipe using a submersible (magnetically coupled impeller) pump. Each cart can be moved independent of the others, allowing ready access to any of the plants being grown on the cart (figure 2).

Superdwarf wheat plants (*Triticum aestivum*, cv. Perigee) were grown for a complete life cycle. Planting was conducted on June 6, 2002, with solution flowing through each tube. The three variable nutrient solution pressures, henceforth referred to as applied water potentials, were established at the initiation of the study: -0.1 cm of water (-0.8 pascal [Pa]), -16 cm of water (-1,570 Pa), and -32 cm of water (-3,140 Pa).

It is important to note that these values are negative; the pressure is lower inside the tubes than outside. This is the pressure that controls the amount of water available to the plant roots. The main characteristics monitored at this stage are the progression of plant height, spectral reflectance, and fresh and dry weights of the plants.

The PTPNDS performed well, and wheat plants were cultured using the three applied water potentials in the rhizosphere. It was expected that the -0.1-cm treatment would exhibit superior growth compared to the other two applied water potentials. This was not the case. Instead these plants appeared to be oversaturated with nutrient solution early in their life cycles, and until the amount of leaf transpiration was sufficient to overcome this condition, the plant roots were oxygen-stressed. When the leaf transpiration rates were sufficient, the growth rate of the plants accelerated and matched or exceeded the growth rate of the plants grown with the other two applied water potentials. As expected, the percent plant moisture in the -32.0-cm treatment was significantly lower than the percent plant moisture of the other two treatments, which were not significantly different from each other. In addition, we found a strong correlation between percent leaf moisture and light reflectance signatures. While there was no significant difference found in the light reflectance signatures between the -0.1-cm and the -16.0-cm treatments, there was a significant difference between this pair and the -32.0-cm treatment.

Under water-stressed conditions, plants are expected to exhibit a decrease in photosynthesis and conductance while experiencing an increase in fluorescence at higher light intensities. No distinguishable trends were found for the parameters, with the exception of conductance. The -0.1-cm tray consistently had the highest conductance of the three treatments. Since photosynthesis was similar among all treatments, this indicates that plants on the -0.1-cm tray were the least water-use-efficient.

Key accomplishments:

- Developed hydraulic control systems for laboratory-scale crop tests.
- Collected experimental data on dwarf wheat.
 - Leaf moisture content with root water potentials controlled at -0.1, -1.6, and -3.2 kilopascals.
 - Collected percent moisture measurements along with spectral analysis for the three treatments.

Key milestones:

- Refine models defining relationships between moisture in components of the remote sensing scene and moisture in the plant canopy.
- Characterize and address individual species responses.



Figure 2. One of Three PTPNDS Units Used for the Study

- Incorporate the LI-COR photosynthesis system for measuring plant physiological responses.

Contact: Dr. T.W. Dreschel (Thomas.W.Dreschel@nasa.gov), YA-E4, (321) 867-2926

Participating Organization: Dynamac Corporation (C.R. Hall and T.E. Foster)

Atmospheric Management in Variable-Pressure Environments: A Step Toward Martian Greenhouses

Plants can be used for human life support in space because their photosynthetic process removes carbon dioxide (CO_2) from the air while producing oxygen (O_2). Plants can also be used as evaporators for purifying wastewater. The ultimate selection of life support technology for a particular space mission will depend on its cost and reliability. Because much of the cost for anything in space is linked to its mass, any reduction in mass will also reduce costs. By operating plant production systems at reduced pressures, structural mass and gas leakage can be reduced, and the potential for finding lighter transparent materials, such as clear plastics, to use as greenhouse covers can be increased. The goals of this project were to (1) establish a range of pressures that provide acceptable plant growth, (2) assess environmental monitoring and control capabilities across this range of pressures, (3) test psychrometric relationships as a function of pressure, and (4) construct a working preprototype of a deployable greenhouse for growing plants at low pressure.

The initial phase of the project involved testing lettuce plants in the hypobaric chamber to assess their tolerance and water balance at different pressures. Results from these plant tests and those published in the literature suggested that around 10 kilopascals (kPa) (1/10 atmosphere) is a likely minimum for vegetative crops, while around 25 kPa is a likely lower limit for crops that require flower, seed, and fruit development. In the latter case, a minimum partial pressure (pp) O_2 of around 15 kPa seems to be required.

A comparison of humidity sensors showed that capacitance devices were reliable across a wide range of pressures and easy to work with (figure 1). Commercial dewpoint devices were highly accurate but cumbersome. Wet/dry bulb (psychrometric) devices showed that wet bulb depression increased as pressure was decreased (at constant humidity) due to increased water vapor diffusion rates at the lower pressures.



Figure 1. Bell Jar System Used To Test Environmental Sensors at Different Pressures

Comparisons of infrared CO_2 analyzers showed a predictable change in sensor output with pp CO_2 but also a separate pressure effect depending on the sensor. This latter effect was likely related to pressure-induced band broadening of the infrared absorption lines for CO_2 . A hot-wire anemometer showed an expected drop in “apparent” velocity at reduced pressure due to reduced mass movement across the hot-wire. This was followed with a series of cooling tests using a brass “leaf” that was heated, and the rates of cooling were then monitored at different pressures. Results showed reduced cooling rates at reduced pressures. The findings were used to estimate boundary-layer thermal resistances to convective heat transfer, which could then be related to boundary-layer

resistances to gas transfer (e.g., CO₂ or H₂O) from leaves to air.

Related tests of water evaporation showed that saturation pressures at a constant temperature were independent of pressure (figure 2) and that evaporation rates at a constant vapor pressure deficit increase as pressures decrease (figure 3). The increased evaporation rates can be explained by increased gas diffusion rates at lower pressures.

Improvements to the deployable greenhouse prototype continued over the past year and the system is nearly complete (figure 4). Load cells for tracking the water used by individual plants and the condensate collection reservoir were installed and tested, and a series of solenoids and water pumps was installed for recycling the condensate to the plants. A chilled-water circulation system with a variable-speed pump was connected and tested for holding temperature and humidity set points. Two additional hemispherical Lexan domes were manufactured, and reinforcement ribs were added to one to accommodate low-pressure tests directly in the laboratory. Software routines were refined for controlling temperature, humidity, and CO₂ concentration and for rewatering the plants with condensate.

Contact: Dr. R.M. Wheeler (Raymond.M.Wheeler@nasa.gov), YA-E4-C, 476-4273

Participating Organizations: Dynamac Corporation, (Dr. P.A. Fowler) and University of Florida (Dr. V.Y. Rygalov)

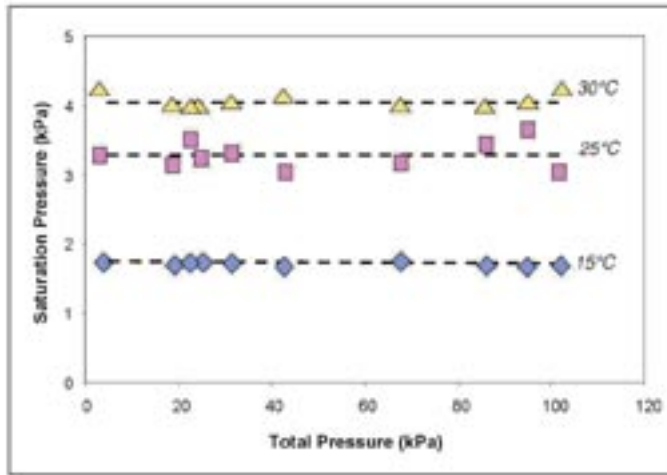


Figure 2. Test of Saturation Vapor Pressure for Water at Different Temperatures and Pressures

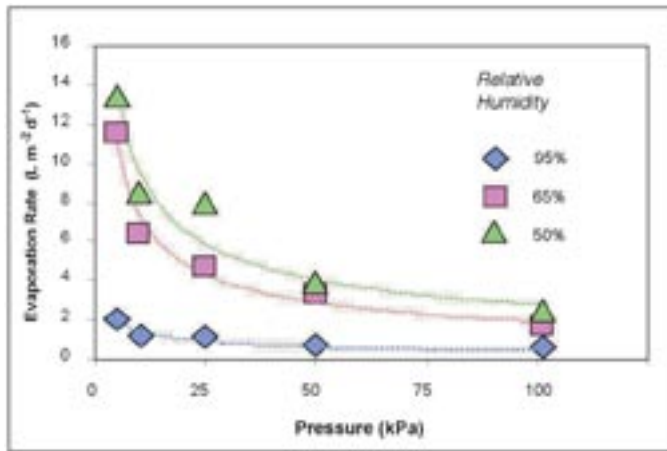


Figure 3. Water Evaporation Rates at Different Humidities and Pressures

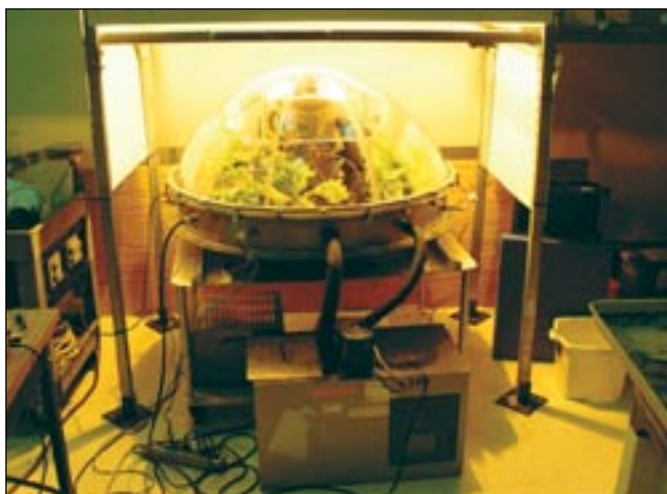


Figure 4. Reinforced Lexan Dome for Growing Plants at Low Pressure in the Laboratory

Advanced Life Support (ALS) Crop Testing

Through the processes of photosynthesis, plants (crops) could be used to provide oxygen (O₂) and food, while removing carbon dioxide (CO₂) in closed life support habitats. In addition, plants and their associated root-zone microflora can be used to purify wastewater where the transpiration is condensed as clean water. To effectively use plants for life support and understand the associated costs, information on their environmental requirements and responses is needed. The earliest opportunity for testing life support contributions of plants in space might involve small growth chambers flown on the International Space Station (ISS) or some related flight system.

ALS crop research activities at KSC over the past year involved (1) cultivar trials of radish (*Raphanus sativus*) and bunching onion (*Allium fistulosum*), (2) light spectral studies with radish and onion and photoperiod studies with potato (*Solanum tuberosum*), and (3) CO₂ studies with bean (*Phaseolus vulgaris*). Radish cultivars Sora and Cherry Bomb II performed well in hydroponic systems, even at 25 to 28 degrees Celsius (°C), temperatures that might be encountered in spaceflight. Yields of eight radish cultivars (grown for 21 days) and eight onion cultivars (grown for 42 days) were similar within a species under either cool white fluorescent or high-pressure sodium lighting at light levels of about 300 $\mu\text{mol m}^{-2} \text{s}^{-1}$ photosynthetic photon flux (PPF), which should be achievable on the ISS. Studies with potato showed that light levels as low as 2 to 4 $\mu\text{mol m}^{-2} \text{s}^{-1}$ PPF during dark cycles delayed tuberization. This suggests that “short-day” events in some plants, such as flowering and tuberization, may be perturbed by low levels of light during “night” cycles, as might occur in open- or mixed-crop production systems in space. CO₂ studies with bean showed that yields and water use efficiency were highest at CO₂ levels of 1,200 parts per million (ppm) (0.12 kilopascal [kPa]) compared to 400, 4,000, 8,000, and 16,000 ppm (0.04, 0.4, 0.8, and 1.6 kPa). CO₂ levels in space habitats with human crews (such as the ISS) commonly reach levels of 4,000 ppm, suggesting that CO₂ concentrations in spaceflight environments may be somewhat higher than optimal for certain plants.



*Twenty-One-Day-Old Hydroponically Grown Radishes (*Raphanus sativus* L. cv. Cherry Bomb II) Resulting From Cultivar Evaluation Tests*



*Forty-Two-Day-Old Bunching Onions
(Allium fistulosum) Growing in
Hydroponic Systems Under Cool
White Fluorescent Lamps*

Key accomplishments:

- Completed radish and onion cultivar evaluations under high-pressure sodium and cool white fluorescent lamps.
- Completed “light pollution” studies with potato.
- Completed super-elevated CO₂ studies with bean.

Key milestones:

- Initiate environmental tests with radish, onion, and lettuce to include typical ISS environments.
- Initiate mixed-cropping tests with radish, onion, and lettuce grown with solid media (arcillite) and hydroponics.
- Initiate cultivar evaluation tests with lettuce, tomato, and pepper.

Contacts: Dr. R.M. Wheeler (Raymond.M.Wheeler@nasa.gov), YA-E4-C, (321) 476-4273; and Dr. J.C. Sager, YA-E4-C, (321) 476-4270

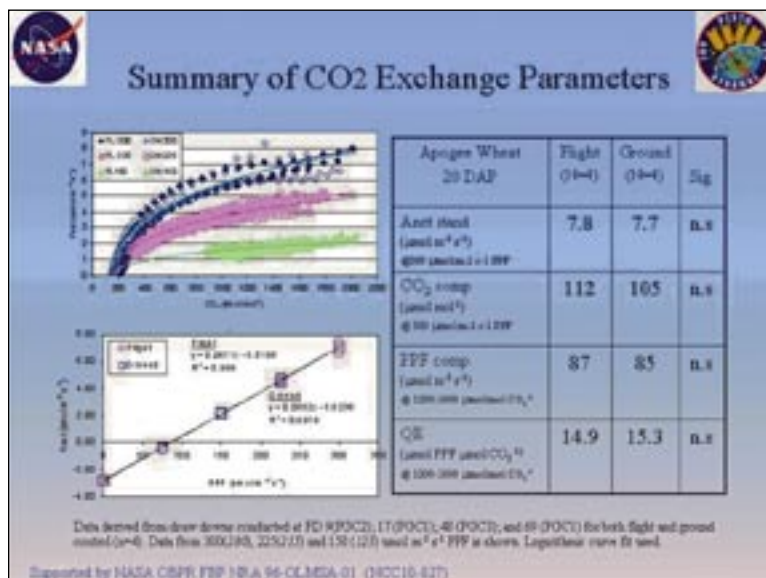
Participating Organization: Dynamac Corporation (Dr. G.D. Goins, N.C. Yorio, and Dr. G.W. Stutte)

Photosynthesis and Metabolism of Wheat in Microgravity

The photosynthetic rate of higher plants is a critical component of plant-based atmospheric regeneration systems being proposed for long-duration space missions. The Photosynthesis Experiment and System Testing and Operations (PESTO) experiment is designed to directly measure photosynthesis in microgravity so an informed decision on the feasibility and design of these systems can be made. The overall objective of this research was to determine the effect of microgravity on photosynthetic response of plant tissues developed in either gravity or microgravity. A specific objective of this research is to determine the effect of microgravity on (1) carbon dioxide (CO₂) and light response curves of wheat, (2) metabolism and electron transport processes associated with photosynthetic and respiratory gas exchange, (3) carbohydrate partitioning in wheat, and (4) gas exchange, including water, over a range of atmospheric vapor pressure deficits. Another objective is to use the knowledge gained to understand the response of plants grown under the elevated CO₂ conditions of commercial, controlled-environment crop production systems.

The PESTO experiment, which was conducted during Increment IV of the International Space Station (ISS), was one of the most complex plant experiments ever performed by NASA. The PESTO experiment was launched to the ISS onboard STS-110 (Atlantis) on April 8, 2002, and was returned to Earth June 19, 2002, onboard STS-111 (Endeavour), spending a total of 73 days in space. A ground-based control experiment was conducted on a 14-day delay and was harvested on July 3, 2002. During the flight period, there were seven harvests of PESTO wheat and priming of six wheat root modules on-orbit. Eighteen plants were fixed on-orbit for morphological and structural analysis, 4 plants were fixed for RNA and molecular genetic analysis, and more than 280 plants were frozen for biochemical analysis. The Biomass Production System (BPS) cameras collected 3,018 images during flight, and 3,640 images were obtained from the

ground-based controls. Sixty-five digital images of the wheat harvest were collected during flight, with 75 being collected from ground-based controls. In addition, crew members recorded approximately 50 images and over 3 hours of video of flight operations. Over 2 gigabytes of environmental data were obtained from the flight and ground-based control units. Activities have been directed to the preparation, maintenance, and return of the experiment from the ISS. The ISS experiment has produced a wealth of data that is currently being analyzed. There was excellent germination (greater than 95 percent) in each of the six root modules primed



Summary of Gas Exchange Characteristics, Including CO₂ and Light Response Curves Obtained Between Stands of Wheat Grown for 20 Days Onboard the ISS and on Earth

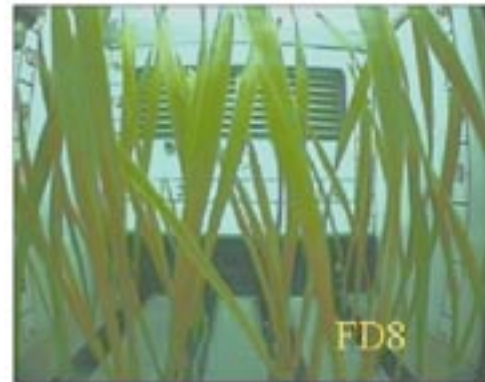
on-orbit, and growth rates between each replicate were comparable. Initial analysis of the data reveals no significant differences in either germination or growth rate between the flight and ground-based control treatments.

A primary objective of the flight experiment was to characterize gas exchange characteristics of the developing wheat canopy to differences in CO₂ and light. These CO₂ and light response curves were conducted at three stages of development on each chamber in orbit. The treatments consisted of obtaining CO₂ response curves at five different photosynthetic photonflux intensities. There were no statistically significant differences between the flight and ground-based control treatments in CO₂ response characteristics (including maximal photosynthetic rate and CO₂ compensation point) and in the light response characteristics of the developing wheat stands. Analysis of the morphological, structural, and biochemical processes associated with stand gas exchange measurements during the 73-day mission is ongoing.

A number of long-duration, preflight experiments were conducted in the BPS during FY 2002, including a high-fidelity ground-based control test and experiments to determine the effects of elevated root zone temperatures on wheat growth and development.

Key accomplishments:

- Completed 73-day mission during Increment IV onboard the ISS.
- Completed high-fidelity ground control experiment in the BPS.
- Completed five 24-day temperature experiments using ground control root modules.
- Published two manuscripts in peer-reviewed journals.
- Presented five talks at international scientific meetings.



Images of Wheat Growth at FD1 and FD8

Key milestones:

- Complete biochemical and biomolecular analysis of plant tissue.
- Complete ground control temperature experiments.
- Present results at international meetings and submit results for publication.

Contact: S.M. Quinn (Shawn.M.Quinn@nasa.gov), YA-E4, (321) 867-4721

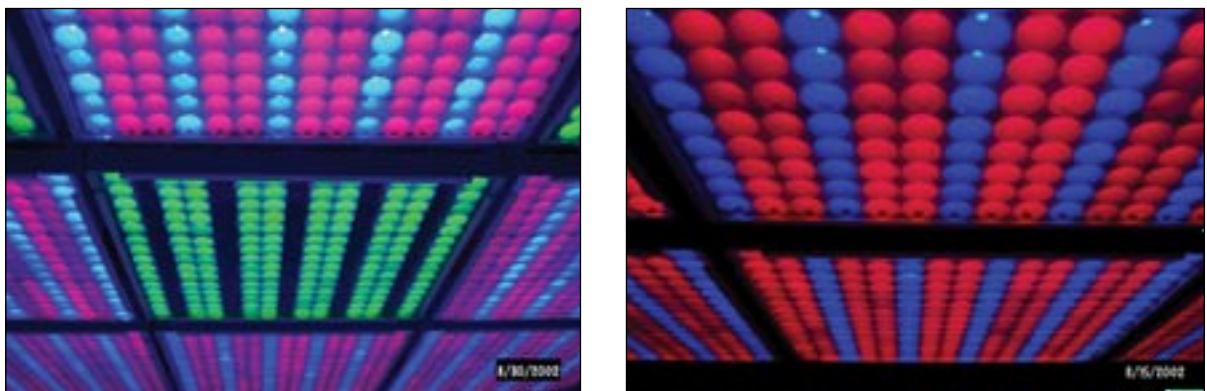
Participating Organization: Dynamac Corporation (Dr. G.W. Stutte)

Plant Lighting System

Plants can produce food, regenerate oxygen, and purify water for space inhabitants. A major challenge to growing plants in space will be controlling and supplying sufficient quantity and quality of light. Conventional lighting technologies would prohibit growing plants on a large scale in space due to low electric power conversion efficiencies. Current lighting research for space-based plant culture is focused on innovative lighting technologies that demonstrate high electrical efficiency and reduced mass and volume. Accordingly, light-emitting diodes (LEDs) are promising technologies being developed to efficiently generate photosynthetic radiation. LEDs can illuminate near the peak light absorption regions of chlorophyll while producing virtually no near-infrared radiation (which is not utilized in photosynthesis). The work in the KSC Life Sciences Support Facility, in association with NASA's Advanced Life Support (ALS)/Advanced Human Support Technology Project, is studying the use of LEDs as alternative light sources for plant production.

Within the ALS Project, salad-type plants represent crops that could provide a portion of fresh food as well as psychological benefits to the crew aboard future space transportation vehicles. Laboratory data generated with salad-type crops grown under various lighting sources could provide important information for modeling and developing future missions.

Work has been completed with Swiss chard, spinach, radish, and lettuce plants grown under different lighting sources for 28 days. Three lamp banks represented broad-spectrum white light sources (microwave, high-pressure sodium, and cool white fluorescent). Past tests also included separate LED arrays filled with a given peak wavelength of red (664, 666, 676, 688 nanometers) LEDs. Each LED array contained single rows of blue LEDs (474 nanometers) evenly distributed within the multiple rows of red LEDs. The relative stoichiometry of photosystem I and II reaction centers (which are responsible for the initial conversion of light energy in plants) was measured for each treatment. Additional measurements throughout growth, including plant chlorophyll fluorescence, accessory pigment concentrations, and responses of photosynthetic rate to light and carbon dioxide levels, were incorporated.



Arrays of Red and Blue LEDs With Green (left) and Without Green (right) Supplementation



Identical Lettuce Plants Under Arrays of Red and Blue LEDs With Green (left) and Without Green (right) Supplementation

The combination of red and blue light proved to be an effective lighting source for growing spinach, radish, and lettuce. However, the addition of green light may promote increased plant growth since green light penetrates the plant canopy better than red or blue light. Leaves in the lower canopy could use the transmitted green light in photosynthesis. For a space mission, highly optimized lighting systems are necessary to conserve power and maximize plant growth, so supplemental green light needs to be evaluated. Green light may also have additional psychological benefits for the crew. Plant leaves readily absorb red and blue light, so absorptance is high and reflectance is low. Therefore, even healthy plants grown under red and blue LEDs alone appear gray or black to humans. Hence, the addition of green LEDs to red and blue LED arrays makes plants appear green to the crew. Research has begun to evaluate the beneficial aspects of supplemental green light on salad crops in terms of increasing light penetration in the canopy and enhancing the aesthetic appeal of plants grown under LEDs.

Key accomplishments:

- 1999: Began experiments with growing salad-type plants with LEDs and microwave lamps.
- 2000: Completed initial salad-type plant growth studies with LEDs and microwave lamps. NASA NRA Solicitation 98-HEDS-01 grant to Dynamac Corporation was extended through 2001.
- 2001: Began experiments with mixtures of salad plant species to compare the growth of multiple crops in a common environment/hydroponics system. Testing included characterization of photosynthetic reaction center stoichiometry (photosystem I versus II) in response to light quality.
- 2002: Began experiments to evaluate the beneficial aspects of supplemental green light on salad crops in terms of increasing light penetration into the canopy and enhancing the aesthetic appeal of plants grown under LEDs.

Key milestone:

- 2003: Continue the evaluation of supplemental green light at different levels to determine the photobiological effects on salad crops.

Contacts: Dr. J.C. Sager (John.C.Sager@nasa.gov), YA-E4-C, (321) 476-4270; and Dr. R.M. Wheeler, YA-E4-C, (321) 476-4273

Participating Organizations: National Research Council (Dr. H.H. Kim) and Dynamac Corporation (Dr. G.D. Goins)

Effect of Microgravity on *Raphanus Sativus* L.

The objective of this experiment is to determine the effects of microgravity on the growth and development of radish (*Raphanus sativus* L.). Salad-type crops that have a short planting-to-harvest cycle may be used to supplement the primary diet of crews on short-to-medium-duration space missions. In addition to the life support applications, radish serves as a model system for evaluating the effect of microgravity on carbohydrate partitioning to the root.

Ethylene is a volatile plant hormone that has wide-ranging effects on radish growth and development. Accumulation of ethylene produced from both biogenic and anthropogenic sources may reduce plant productivity and alter growth. Experiments to determine the threshold of ethylene sensitivity in radish were conducted. Significant physiological and morphological changes occur with chronic exposure of 30-to-1,000-part-per-billion (ppb) ethylene. These concentrations are 7,500 times lower than the current guidelines for allowable spacecraft concentrations of ethylene. Research to develop techniques for removing ethylene is ongoing.

The Radish Assimilation in Spacecraft Testbed Atmospheres (RASTA) experiment will be conducted in space in a specialized plant growth chamber, the Plant Growth Facility-Split Plenum (PGF-SP) that is being built by Bionetics Corporation (Kennedy Space Center, Florida). Numerous tests were performed to optimize the conditions for plant growth in preprototype PGF-SP chambers, including types of watering systems, lighting systems, and rooting systems. Radishes grown in all tests undergo detailed morphological, developmental, and physiological analysis.

Key accomplishments:

- Completed experiments to determine dose response curve of radish to ethylene.
- Continued experiments to quantify production of volatile organic compounds from radish.
- Designed preprototype plant growth chambers for testing.
- Presented papers at two international conferences.
- Published three peer-reviewed manuscripts.

Key milestones:

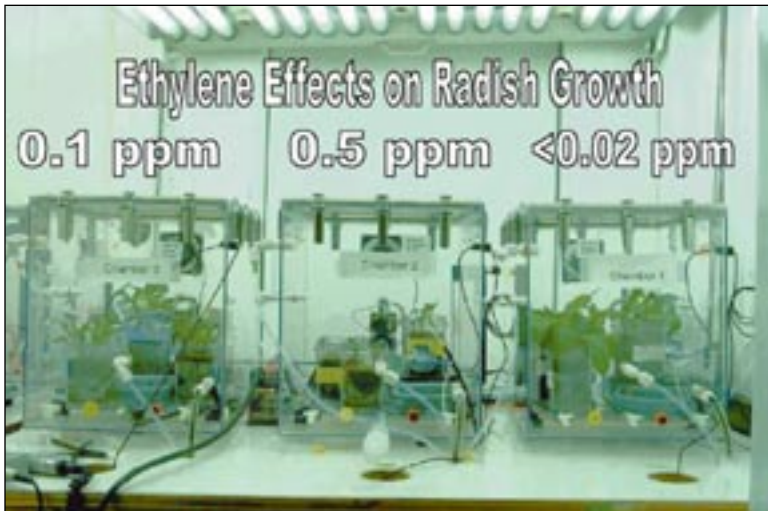
- Complete automated control system for continuous monitoring of biologically active volatile compounds.
- Determine developmental effects of starch partitioning in radish.
- Characterize morphological and physiological adaptations to light quality.
- Continue testing experimental protocols in prototype flight hardware.
- Present results at international scientific conferences.

Contact: S.M. Quinn (Shawn.M.Quinn@nasa.gov), YA-E4, (321) 867-4721

Participating Organization: Dynamac Corporation (Dr. G.W. Stutte)



Radish Plants Being Grown in Preprototype Flight Chambers Using Light-Emitting Diodes To Validate Methods for Growing Plants in Space



Closed Exposure Chambers Allow the Effects of Common Spacecraft Atmospheric Components on Plant Growth To Be Determined

INDEX

A

Adams, F.W., 35, 51
Adams, T., 63
Adams, T.C., 169
Allen, M., 81
Appleton, B., 68
Arkin, Dr. CR., 35, 51
Atwood, G.C., 163
Augustynowicz, Dr. S.D., 79, 81, 85
Azofiefa, Dr. J., 35

B

Baker, Dr. G.H., 155, 175, 177
Barile, Dr. R.G., 15, 147
Barth, T.S., 155, 164, 167, 173, 189
Baska, D.F., 175
Bastin, Dr. G.L., 105, 111
Bayliss, J.A., 129
Beckus, A., 153
Beil, R.J., 35
Benjamin, Dr. P.C., 164, 178, 189
Bigos, S., 183
Birr, R.B., 97, 99, 103
Blalock, N.N., 5, 35, 41, 43
Bonner, T., 74
Bookman, P.J., 153
Boyd, S.W., 103

Breakfield, R.A., 81, 85
Brindley, E.E., 163
Brown, C.J., 163
Brughelli, K., 167
Buehler, Dr. M.G., 121, 139
Buhler, Dr. C.R., 117, 119, 121, 123
Bull, J.B., 101
Bundick, S.N., 97
Burns, B.C., 163
Burns, B.M., 23, 37, 41, 43, 47, 49
Butler, C.D., 187
Butler, R.A., 163
Buttner, Dr. W.J., 7

C

Calle, Dr. C.I., 113, 117, 119, 121, 123, 125, 127, 129, 131, 133
Calle, Dr. L.M., 135, 136, 139, 145, 147
Carstens, Dr. D.S., 167, 173, 175, 177
Case, J.L., 27
Casteel, S., 97
Cates, G.R., 160
Chamberland, D.W., 191
Chang-Diaz, Dr. F., 35
Christensen, K.L., 159
Ciavarella, A.A., 19
Clements, G.R., 1

Coleman, A.M., 99
Cox, R.B., 9, 53
Crikis, A., 19
Cummings, K.R., 85, 86
Curley, C., 35
Curran, J.J., 71, 135, 141, 143, 147
Curran, J.P., 141, 143, 147
Czaban, S.K., 35

D

Davis, C.K., 25, 28, 30, 39
Denson, E.C., 97, 99, 103
Deremer-Cook, E.J., 163
Deyoe, R.T., 5, 47
Diaz, Dr. J.A., 35
Doctor, M.A., 83
Doesken, Dr. N., 9
Dominguez, J.A., 15, 25, 28, 30, 39
Dreschel, Dr. T.W., 195

E

Eckhoff, A.J., 5, 37, 41, 43, 49
Edelmann, J.J., 35
Elliott, Dr. D.M., 159
Erdogan, T., 101, 103, 105, 111
Ewald, J.R., 171

INDEX

- F**
Farmer, G.A., 163
Ferrell, B.A., 101
Fesmire, J.E., 79, 81, 83, 85
Floyd, D.P., 35
Foderousky, A.M., 153
Follistein, D.W., 35, 51
Foster, T.E., 195
Fowler, Dr. P.A., 197
Fox, J.J., 55
Fredrickson, T.E., 187
- G**
Gavura, J.M., 97
Gibbons, R.D., 16
Gibson, J.E., 85, 86
Gleman, S., 65, 73, 74, 77
Goembel, Dr. L., 131
Goins, Dr. G.D., 199, 203
Gompf, Dr. R.H., 129
Gordie, R.A., 63
Graul, M., 164
Greenfield, T.D., 16
Gribble, D.A., 133
Grier, R., 71
Griffin, Dr. T.P., 35, 51
- Groh-Hammond, M.M.*, 163, 171, 173, 175
Groop, E.E., 121, 125, 127
- H**
Haase, W.H., 164
Haberbusch, M.S., 59
Haley, S., 101
Hall, C.R., 195
Hallberg, C.G., 16
Hamilton; L.E., 163
Harlacher, M., 97
Harris, W.G., 105
Haskell, W.D., 9, 35, 51, 53
Heckle, Sr., K.W., 79, 81
Henderson, P.G., 35
Hickman, J.C., 101
Hoang, Dr. N., 99
Hodge, T.R., 45
Hogue, M.D., 123
Humeniuk, R.P., 163
- I**
Immer, Dr. C.D., 5, 9, 23, 27, 103
Ingoldsby, K.A., 185
- J**
Johnson, Jr., D.E., 185
- K**
Kandula, Dr. M., 61, 149
Kanki, Dr. B.G., 159
Kelly, A.O., 88
Kerios, C., 105
Kim, Dr. H.H., 203
Klinko, S.J., 25, 28, 30, 39
Klonowski, P.J., 86
Kolody, Dr. M.R., 139
Kounaves, Dr. S.P., 139
Kremer, S.E., 101
Kruhm, D.A., 1
- L**
Lackascyck, J., 163
Lane, Dr. J.E., 9, 23, 27, 33
Lanzi, R.J., 101
Larsen, D.C., 163
Lawrence, B.A., 163
Lebovitz, G., 153
Lippitt, T.C., 63, 73
Littlefield, A.C., 74
Lohr, G.W., 159
Lucena, A.R., 37, 41, 43
Luo, Dr. W., 123
Luth, D.J., 163

INDEX

M

MacDowell, L.G., 71, 135, 136, 141, 143, 145, 147
Madura, J.T., 107
Manley, W.C., 163
Manobianco, Dr. J.T., 27
Mantovani, Dr. J.G., 121
Marin, J.A., 101, 103
Mata, Dr. C.T., 37, 41, 43, 47, 49, 99, 103
Mazumder, Dr. M.K., 117
McCaskey, C.E., 86
McCleskey, C.M., 185
Medelius, Dr. P.J., 13, 37, 43, 107, 109
Merceret, Dr. F.J., 27
Merrill, T.W., 20
Michel, M.C., 20
Mobasher, Dr. A., 150
Moist, J.O., 163
Mueller, R.P., 15, 63, 65, 67, 68, 71, 73, 74, 77
Mundschau, Dr. M.V., 133
Murray, A.J., 99

N

Nagy, Z.F., 71, 85, 86, 91
Naylor, G.R., 35, 51
Nelson, R.A., 94, 97, 101, 105
Nguyen, C.T., 59

Nieten, D.A., 19
Nieves, R., 19
Noble, J.T., 163
Notardonato, W.U., 91
Nowicki, A.W., 121, 125, 127
Nurge, M.A., 11

O

O'Brien, T.L., 171

P

Parks, S.L., 45
Patterson, M.S., 101
Peabody, P.A., 163
Pelakh, B., 20
Perotti, J.M., 5, 37, 41, 43, 47, 49
Peters, J.W., 53
Philippart, M., 175
Phillips, G.D., 164
Polk, J.D., 16
Posada, J.G., 177
Poveda, G., 19
Powell, W.R., 101

Q

Quincy, C.D., 191
Quinn, S.M., 201, 204

R

Rakofsky, A.M., 163
Randazzo, J.J., 5, 13, 41, 43, 49
Rees, J.A., 13
Relvini, Dr. K., 175, 177
Rhodes, R.E., 55, 169
Rhodeside, G.R., 178
Richiuso, P.F., 129
Rieck, E.G., 163
Riley, Jr., H.W., 171
Robinson, G.F., 101
Rozewski, J.M., 163
Ruiz-Torres, Dr. A., 181
Rygalov, Dr. V.Y., 197

S

Sager, Dr. J.C., 199, 203
Sakahara, R.D., 97
Schneider, S.M., 153
Scholtens, B.E., 81, 83
Schultz, Dr. J.A., 51
Semmel, G.S., 20
Sierra, A., 111
Simpson, Dr. J.C., 99, 101, 103
Skaff, A.F., 59
Skelly, D.M., 94
Smith, E.C., 71
Sobchak, T.C., 97

INDEX

Sojourner, S.J., 91
Sortman, M.A., 163
Stalnecker, W., 67
Stambolian, D.B., 163
Stender, J., 91
Stottler, R., 183
Stout, S.J., 49
Stute, R.A., 16
Stutte, Dr. G.W., 199, 201, 204
Surma, J.M., 45
Sweeney, G.P., 171

T

Taylor, B.R., 163
Taylor, J.D., 13
Taylor, M.A., 133
Thomas, P.A., 163
Thompson, Dr. J.S., 133
Thompson, K.L., 113
Townsend, I.I., 73
Trautwein, J.K., 63, 73
Trout, D.H., 109

U

V

Valencia, L.M., 97
Valentino, W.D., 175
Van Sciver, S., 91
Vinje, R.D., 135, 136, 145
Vo, K.A., 20
Vu, Dr. B.T., 61, 149, 150

W

Wachowski, S.G., 163
Walls, L.K., 59
Warren, A.L., 160
Warren, K.P., 163
Waterman, R.D., 1
Wessells, R.L., 99
Wheeler, Dr. R.M., 197, 199, 203
White, T.R., 163
Whiteman, D.E., 97
Wicke, D., 67
Wilkhu, S.S., 163
Willard, D.E., 53
Williams, E.H., 105
Williams, Dr. M.K., 79, 83

X

Xie, Dr. X., 133

Y

Yorio, N.C., 199
Young, R.C., 7
Youngquist, Dr. R.C., 9, 11, 13, 23, 45, 53, 111

Z

Zapata, E.Z., 181, 189
Zeitlin, N.P., 139
Zoerner, R.D., 101, 103
Zysko, J.A., 33

REPORT DOCUMENTATION PAGE

Form Approved
OMB No. 0704-0188

Public reporting burden for this collection of information is estimated to average 1 hour per response, including the time for reviewing instructions, searching existing data sources, gathering and maintaining the data needed, and completing and reviewing the collection of information. Send comments regarding this burden estimate or any other aspect of this collection of information, including suggestions for reducing this burden, to Washington Headquarters Services, Directorate for Information Operations and Reports, 1215 Jefferson Davis Highway, Suite 1204, Arlington, VA 22202-4302, and to the Office of Management and Budget, Paperwork Reduction Project (0704-0188), Washington, DC 20503.

1. AGENCY USE ONLY (Leave blank)	2. REPORT DATE November 2003	3. REPORT TYPE AND DATES COVERED Technical Memorandum - 2003	
4. TITLE AND SUBTITLE Research and Technology 2003 Annual Report of the John F. Kennedy Space Center		5. FUNDING NUMBERS	
6. AUTHOR(S)		8. PERFORMING ORGANIZATION REPORT NUMBER NASA TM-2003-211190	
7. PERFORMING ORGANIZATION NAME(S) AND ADDRESS(ES) NASA, John F. Kennedy Space Center Kennedy Space Center, Florida 32899		10. SPONSORING / MONITORING AGENCY REPORT NUMBER	
9. SPONSORING / MONITORING AGENCY NAME(S) AND ADDRESS(ES) National Aeronautics and Space Administration Washington, D.C. 20546		11. SUPPLEMENTARY NOTES	
12a. DISTRIBUTION / AVAILABILITY STATEMENT Unclassified - Unlimited Subject Category 99		12b. DISTRIBUTION CODE	
13. ABSTRACT (Maximum 200 words) The John F. Kennedy Space Center (KSC) is America's Spaceport Technology Center. The KSC technology development program encompasses the efforts of the entire KSC team, consisting of Government and contractor personnel, working in partnership with academic institutions and commercial industry. KSC's assigned mission areas are space launch operations and spaceport and range technologies. KSC's technology development customers include current space transportation programs, future space transportation programs/initiatives, and enabling technical programs. The KSC Research and Technology 2003 Annual Report encompasses the efforts of contributors to the KSC advanced technology development program and KSC technology transfer activities. Dr. Dave Bartine, KSC Chief Technologist, (321) 867-7069, is responsible for publication of this report and should be contacted for any desired information regarding KSC's research and technology development activities.			
14. SUBJECT TERMS Research and Technology		15. NUMBER OF PAGES	
17. SECURITY CLASSIFICATION OF REPORT Unclassified		16. PRICE CODE	
18. SECURITY CLASSIFICATION OF THIS PAGE Unclassified	19. SECURITY CLASSIFICATION OF ABSTRACT Unclassified	20. LIMITATION OF ABSTRACT	